The roles of ChlI and ChlD, the AAA$^+$ subunits of Magnesium Chelatase

Nathan Bryce Porritt Adams

Department of Chemistry

The University of Sheffield

A thesis submitted for the degree of

Doctor of Philosophy

October 2012

Abstract

The protein magnesium chelatase consists of three subunits, ChlI, ChlD and ChlH. This protein lies at the branch point between heme and chlorophyll biosynthesis and has a regulatory role. It requires large amounts of energy to insert a magnesium ion into its substrate protoporphyrin IX. Two subunits, ChlI and ChlD are members of the AAA^+ ATPase super family of enzymes, and ChlI hydrolyses ATP to drive the introduction of magnesium into the porphyrin ring.

Magnesium chelatase (ChlIDH) will catalyse the exchange of radiolabelled ADP to ATP while the metal ion chelation reaction progresses in the forward direction. In isolation, the AAA^+ ATPase subunit, ChlI, also catalyses the same reaction. In contrast radiolabelled orthophosphate (Pi) cannot exchange to form ATP. This suggests a mechanism where either no E.ADP complex exists or it unable to react with free phosphate to give ATP.

Mutations in the putative conserved ATPase site in ChlI show $MgATP^{2-}$ is hydrolysed in a stochastic manner, while cooperativity between subunits promotes $MgATP^{2-}$ binding. Similar mutations in the putative ATPase site in ChlD reveal the first functional role of this enzyme in allosteric control of magnesium chelatase activity.

To Duncan

Acknowledgements

This work would not have been completed without the support and guidance of Dr Jim Reid, thank you.

Funding for this work was provided by the BBSRC, the Royal Society of Chemistry and the Biochemistry Society.

I wish to thank Dr Amanda Brindley for her wisdom in protein expression and molecular biology (specifically cysteine mutants of ChlI) as well as her ability to kick me into higher gear; Dr Rob Ducker for providing the surfaces used in microscopy work, allowing me to do some chemistry in a chemistry department; Dr Barbara Ciani and Dr Dave Finger for assistance in biophysical characterisation and other useful discussions; and finally Stewart Dods for proof reading.

Three years would not have been anywhere near as fun without: The housemates – Twin, Penny and Freyja; Burning Man – Matt, Jeff, Lucky, Rick, Robert, Charlie, Margaret, Brian, Maria, Flo, Nat, Sal and Jenae; Sheffield – Ruth, Hollie, Simon, Iain, Vicky, Stephen, Fiona, Leanne and Liz; and finally the Lab – Matt, Alexa, Iain, Mike, Ash, Esther and Jenny. Thank you.

To my parents, Ian and Suzanne, for their continuing support of their never ending student. One day I will get a 'proper' job.

Contents

List of Figures

List of Schemes

List of Tables

Abbreviations

ABA abscisic acid

ADP adenosine diphosphate

AMP adenosine monophosphate

ATP adenosine triphosphate

D_{IX} deuteroporphyrin IX

DTT dithiothetriol

EM electron microscopy

F5M fluoroscein-5-maleimide

LDH lactate dehydrogenase

MgD_{IX} magnesium deuteroporphyrin IX

MgP_{IX} magnesium protoporphyrin IX

MIDAS metal ion dependant adhesion site

MOPS 3-morpholinopropane-1-sulfonic acid

NADH nicotinamide adenine dinucleotide

PEP phosphoenol pyruvate

PK pyruvate Kinase

P_{IX} protoporphyrin IX

SAXS small angle x-ray scattering

TMR tetramethylrhodamine-5-maleimide

1

Introduction

1.1 Summary

Magnesium chelatase lies at the branch point between heme and chlorophyll biosynthesis. This multi-subunit complex requires large amounts of energy to insert magnesium into the chlorophyll precursor protoporphyrin IX (P_{IX}). Magnesium chelatase controls the level of a photosynthetic cofactor and as such has huge implications in the regulation of photosynthesis, and downstream production of energy in the form of biomass. It consists of three subunits, D, H and I.

This introduction covers the importance of the enzyme within the chlorophyll biosynthetic pathway, tetrapyrroles and their importance in biology and our current understanding of the structure and mechanism of magnesium chelatase.

1.2 Photosynthesis

Photosynthesis is the production of organic compounds from inorganic starting materials using sunlight, the primary energy source within the biosphere. It is the fundamental process from which all biomass, and hence food and fuel is derived from. All life ultimately derives its energy from the sun, except for a few specialized microorganisms.

Phototrophs such as algae, higher plants and cyanobacteria capture light energy to produce food. Chemotrophs such as animals and fungi, are dependent on phototrophs to supply sources of energy (3, 4). Fossil fuels are also a product of photosynthesis (5). The basic equation of photosynthesis is shown in scheme 1.1.

$$CO_2 + H_2O \xrightarrow[plants]{hv} (CH_2O)_n + O_2$$

Scheme 1.1: The chemical equation for photosynthesis.

The primary reaction in photosynthesis is the splitting of water to give the oxidant hydroxide and the reductant hydrogen. Hydrogen is used to reduce CO_2 to organic materials, and the hydroxide is converted to water and oxygen (4).

Low energy starting materials, carbon dioxide and water, are converted into high energy carbohydrates. This increase in energy comes from photons of energy captured by the photosynthetic machinery (3, 4).

Each year 56×10^{23} joules of energy hit the earth, half of which is reflected back by the upper atmosphere. Only 50 percent of the energy that is absorbed is in the required wavelength region, 40 percent of this compatible energy is reflected by the sea and desert which leaves 9×10^{23} joules of energy compatible with photosynthesis available to organisms (3).

1.3 Tetrapyrroles and porphyrins

Porphyrins (figure 1.1) are intensely coloured compounds with a central ring of 20 carbon atoms and 4 nitrogen atoms arranged as 4 pyrrole rings joined by single carbon bridges. They are often substituted at the α and β position carbons. They are either purple or red coloured, and often heavily fluorescent. The structure was deduced by Küster in 1912, and confirmed by the first synthesis of heme in 1929 by Hans Fischer (6, 7). Porphyrins are essentially planar but can distort significantly when bound to metal ions (6). They have an average diameter of 8.5 Å and a thickness of 4.7 Å. Porphyrins have a high degree of conjugation so are aromatic (7).

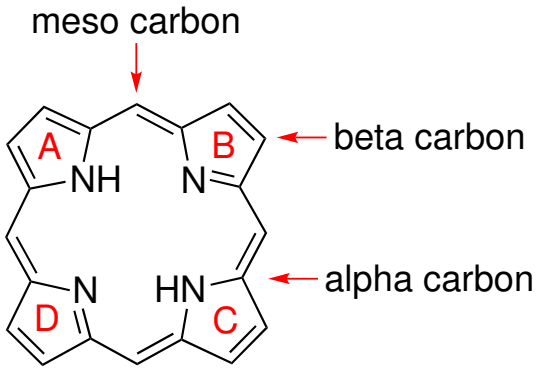

Figure 1.1: Generic porphyrin structure - highlighting the nomenclature of the rings and the description of carbons.

Similarities between biopigments highlight their conserved structures and function and point to a common evolutionary ancestry for living things. Their main function involves binding metals, the metal acts as a centre for biochemical processes. For example the iron in hemoglobin reversibly binds oxygen for transport. The porphyrin substitution and protein environment alter the redox potential of the metal centre, allowing the binding affinities of the metal to be finely tuned. Protein structure dictates the function of the reactive porphyrin centre (6).

The UV-Vis absorption of porphyrins is closely related to their physicochemical properties. An increase in the π electron density in the outer conjugated system by more electron withdrawing side chains leads to a more covalent bond character between the nitrogen and the metal ion, leading to longer wavelengths in both the absorbance and fluorescence bands. The substitution pattern on the porphyrins affects the spectra (7). The Soret band at around 400 nm, discovered in 1883, has an extinction coefficient of between 2 – 5 x 10^5 $M^{-1}cm^{-1}$, 10 to 20 times that of the bands found in the visible region. This band is found in all tetrapyrroles, chelated or not (7).

When irradiated with UV light porphyrins are highly fluorescent. The fluorescence is visible by eye at concentrations as low as 10^{-6} M and by spectroscopic methods at concentrations less than 10^{-8} M. The porphyrins have to be mono-disperse, as colloids of the porphyrins do not fluoresce. Mg^{2+}-porphyrins only fluoresce in polar environments (e.g. aqueous environments), suggesting that water is interacting with the metal centre as a source of electrons (7).

1.4 Chlorophyll and the photosynthetic apparatus

Chlorophylls are pigments that capture light, and are contained within chloroplasts. Chlorophyll was first isolated in 1817 by Pelletier and Caventou. In 1845 Mayer discovered that plants transform sunlight into chemical energy. Engelmann discovered that chloroplasts are the organelles in which photosynthesis occurs (3, 4).

Chlorophylls *a* and *b* are embedded in the thylakoid membrane within the chloroplast organelle (figure 1.2), where the conversion of light energy to chemical energy occurs. Chloroplasts are found in algae and higher plants, whereas in cyanobacteria photosynthetic membranes traverse the cytoplasm. Chloroplasts have thylakoid membranes arranged in stacks called grana, all within the stromal matrix enclosed within the chloroplast membrane. About 80 % of leaf cell volume is made up by chloroplasts, which are between 4 - 10 μm in diameter and 1 μm thick. There are between 1 and 100 per cell, and they are able to self replicate (3).

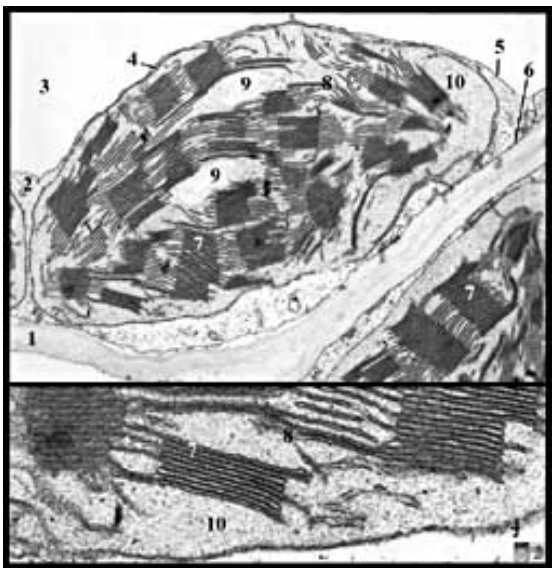

Figure 1.2: Transmission electron microscopy image of a chloroplast - 1, Cell Wall; 4, Chloroplast envelope; 7, Grana; 8, Thylakoid; 10, Stroma. Reproduced from Nijmegen 2003 (8)

The main green photosynthetic pigments are the chlorophylls *a* and *b*, which are aided by accessory pigments carotenoids and phycobilins which transfer energy to chlorophylls. Chlorophyll *a* is present in all organisms which evolve oxygen, while chlorophyll *b* is present in about one third of the concentration in higher plants and green algae (5).

Chlorophyll is a magnesium containing reduced porphyrin or chlorin. It captures

photons in the near UV and Red (400 and 650–700 nm) regions. The reduced macrocycle and conjugated double bonds are ideal for this frequency range (6).

Chlorophyll contains a polar porphyrin head and an apolar phytol tail (figure 1.3), and exists sandwiched between protein and lipid layers in the thylakoid membrane. Conjugation with lipid molecules allows the absorption profile (figure 1.4) of the pigment to be finely tuned, as well as allowing efficient transfer of energy within the reaction centre as the distance between molecules is optimised.

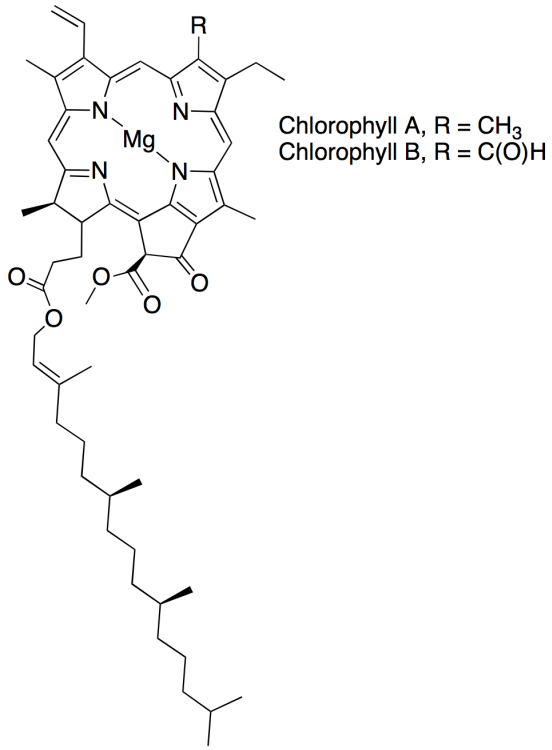

Figure 1.3: Chlorophyll *a* and *b* - Chemical structures of Chlorophyll *a* and *b*

Chlorophylls act together forming a photosynthetic system, transferring their energy from outer antennae molecules towards a reaction centre containing a pair of specialised chlorophyll molecules, which then trap and transfer the electrons away to be used in the biosynthesis of high energy intermediates (6). The energy of a photon absorbed by any one of the 300 chlorophyll molecules within a photosystem is ultimately transferred

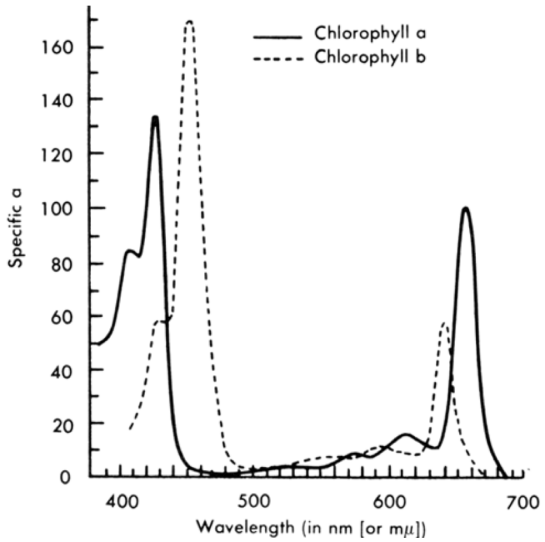

Figure 1.4: Absorption spectra of Chlorophylls *a* and *b* - Reproduced from from Hall and Rao (3).

to the reaction centre. For every eight photons absorbed there is the reduction of one CO_2 molecule and one O_2 molecule produced (3).

Chlorophyll absorbs energy within a region that other constituents of the cell do not. The absorption of a photon causes an excitation of a valence electron to a higher energy level. On relaxation the energy is used to split water (scheme 1.2) (3).

$$2\,H_2O + h\nu \xrightarrow{\text{Chlorophyll}} O_2 + 4\,H^+ + 4\,e^-$$

Scheme 1.2: The light mediated splitting of water by chlorophyll.

As well as producing organic molecules such as carbohydrates, photosynthesis also drives the production of the energy products (ATP and NAD(P)H) as well as the oxidised waste product oxygen. Protons released in the splitting of water produce a proton concentration gradient, which drives the formation of ATP, while electrons are used to reduce CO_2 (3).

1.5 Chlorophyll biosynthesis

Chlorophyll is synthesized from starting materials using glutamyl-tRNA or the condensation of succinyl coenzyme A (CoA) to produce 5-aminolaevulinic acid (ALA). Cyanobacteria and plants use the C_5 route (scheme 1.3) where ALA is derived from Glutamyl-tRNA (6, 9).

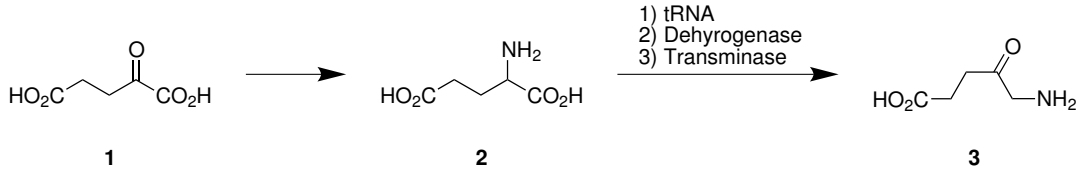

Scheme 1.3: Biosynthesis of ALA from 2-oxoglutarate (**1**) which is converted to glutamate (**2**) and via the C_5 pathway transformed into 5-aminolevulinic acid (ALA) (**3**).

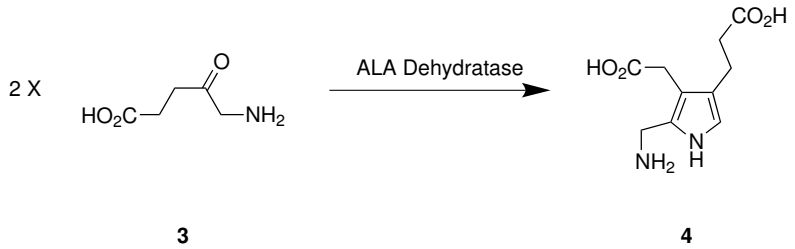

Scheme 1.4: The biosynthesis of porphobilinogen (**4**) is performed via the dehydration of ALA (**3**).

Two molecules of ALA are then condensed via ALA dehydratase to form the pyrrole ring of porphobilinogen (PGB) (scheme 1.4) (6, 10).

Four molecules of PGB are condensed via PBG deaminase and uroporphyrinogen III cosynthase (scheme 1.5) producing the reduced porphyrin uroporphyrinogen III. In this step, the four PGBs are linked head to tail, with the last pyrrole ring bound in a reverse fashion, forming bonds at the 2'–2' and 5'–5' positions rather than 2'–5' (see blue numbering in scheme 1.5). A cofactor consisting of dipyrryl-methane attached to PGB deminase acts as a substrate to which four PGBs are added, uroporphyrinogen

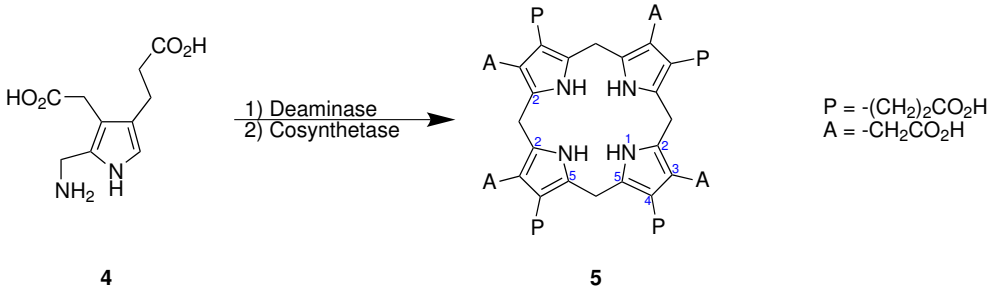

4 **5**

Scheme 1.5: Biosynthesis of uroporphyrinogen III (**5**) from the condensation of 4 molecules of PGB (**4**) mediated by the enzymes PBG deaminase and uroporphyrinogen III cosynthase.

III cosynthase is responsible for inverting the last pyrrole ring (6).

The four acetic acid side chains of uroporphyrinogen III undergo decarboxylation catalysed by uroporphyrinogen decarboxylase leaving the methylated product coproporphyrinogen III (scheme 1.6). This species then undergoes oxidative decarboxylation, catalysed by coproporphyrinogen oxidase, on rings A and B on the propionic acid side chains, converting them to vinyl groups forming the product protoporphyrinogen IX (**7**). The bridging carbon bonds between pyrrole rings are oxidised by protoporphyrinogen oxidase to give protoporphyrin IX (**8**) (6).

A magnesium ion is inserted into protoporphyrin by magnesium chelatase, forming magnesium protoporphyrin IX (MgP_{IX}) (11) (scheme 1.6, (**8**) to (**9**)). MgP_{IX} is further modified with S-adenosyl methionine (SAM) (scheme 1.6, (**9**) to (**10**)) in a reaction catalysed by magnesium protoporphyrin IX methyl transferase (MT) to methylate the propionic acid side chain on ring C forming magnesium protoporphyrin IX-13-methylpropionate. Reduction of the C8 vinyl group may also occur depending on species and time of day (6).

The C–13 propionic acid side chain on magnesium protoporphyrin IX-13-methylpropionate is converted into a β-keto ester which is then cyclised by oxidative cyclase, using oxygen and NADPH, forming protochlorophyllide (**11**). Protochlorophyllide is reduced to chlorophyllide (**12**) by protochlorophyllide reductase (6) (scheme 1.7). In some species

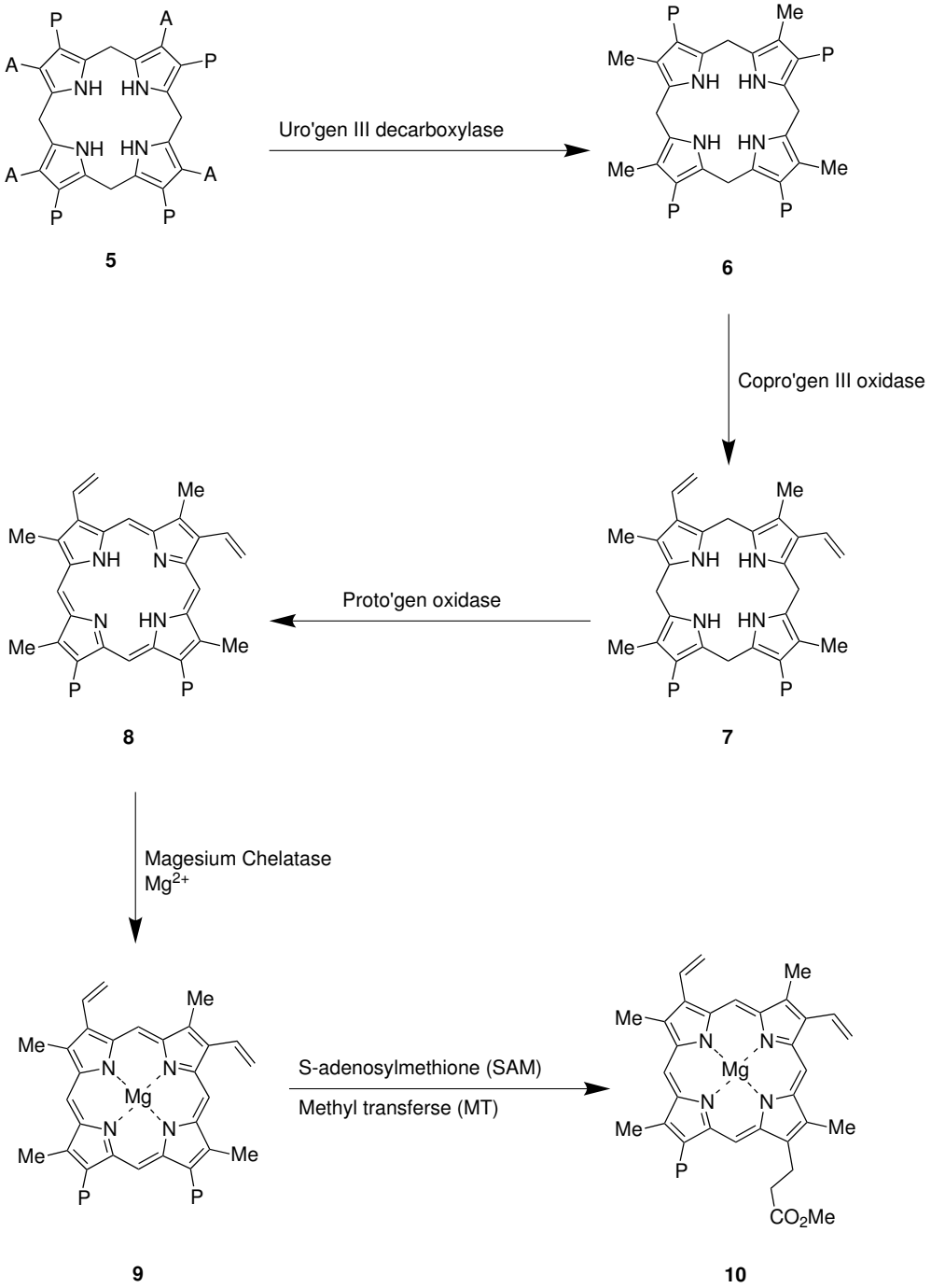

Scheme 1.6: Decarboxylation, metalation and methylation of uroporphyrinogen III (**5**) to magnesium protoporphyrin IX-13-methylpropionate (**10**).

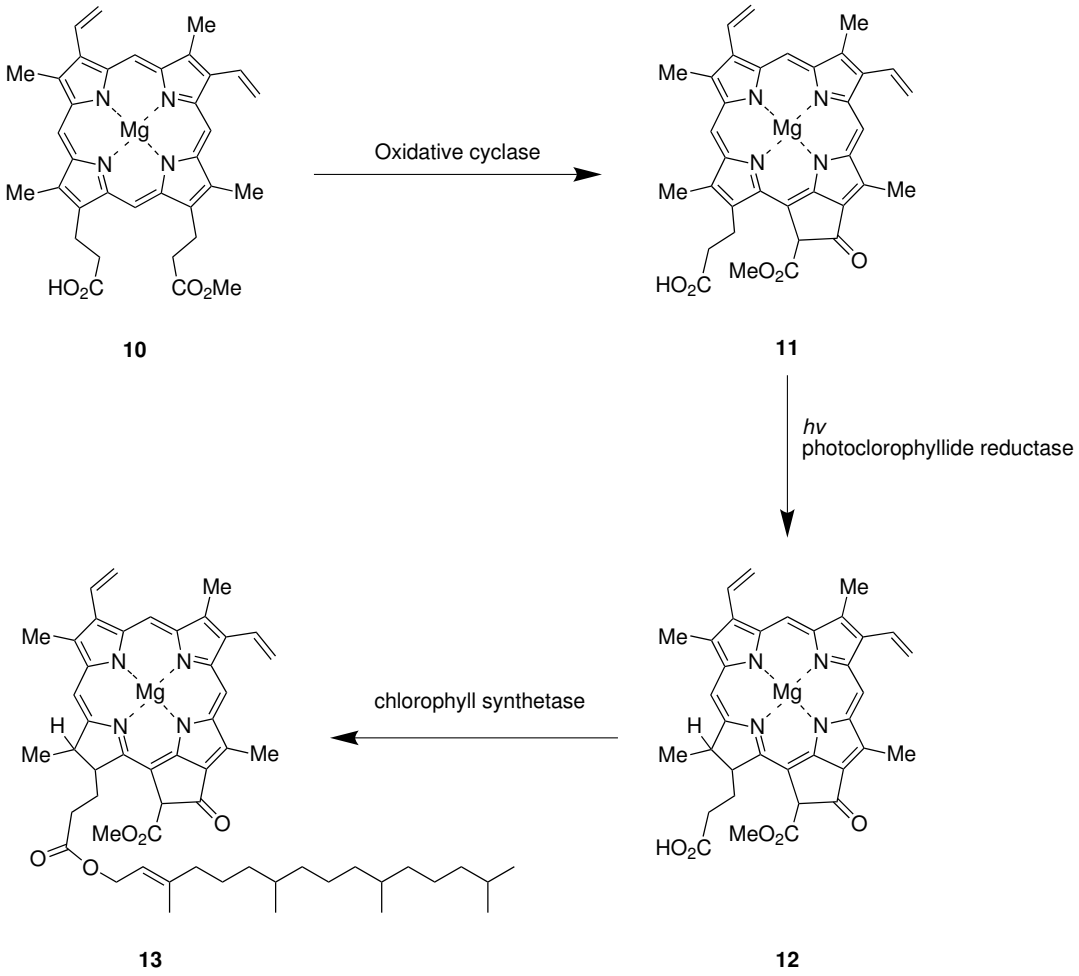

Scheme 1.7: Reduction of magnesium protoporphyrin IX-13-methylpropionate (**10**) to chlorophyll (**13**)

this is a photochemical reaction, while in others it is ATP dependant (12, 13, 14).

Chlorophyllide is then esterified with either phytyl diphosphate or geranyl diphosphate, and three double bonds in the phytol tail are reduced via chlorophyll synthetase, producing the final product chlorophyll (6, 9).

1.6 Metal ion chelatases

Metal ion chelatases insert divalent metals ions into tetrapyrroles during the biosynthesis of various cofactors and prosthetic groups. Four metal ions are involved, cobalt, iron, nickel and magnesium, all in the +2 oxidation state. Magnesium is in chlorophylls, iron in heme and siroheme, nickel in coenzyme F430 and cobalt in cobalamins, such as vitamin B12. Zinc(II) can also be inserted into protoporphyrin IX by ferrochelatases, but has no known function, although there have been reports of a bacterium which uses zinc instead of magnesium in its chlorophylls (1, 15).

Tetrapyrrole biosynthetic pathways branch at uroporphyrinogen III and at protoporphyrin IX (scheme 1.8). Uroporphyrinogen III is a precursor of cobalamines, coenzyme F430, sirroheme and protoporphyrin IX. Protoporphyrin IX is the last common intermediate in the biosynthesis of heme and chlorophyll (1, 16).

Metal ion chelatases are classified into two groups based on their structure and functional characteristics. Class I are structurally related metal ion chelatases including ferrochelatase which inserts Fe^{2+} into protoporphyrin IX to make heme, and sirohydrochlorin cobaltochelatase which can insert a cobalt ion into sirohydrochlorin (17). They utilize a single subunit that catalyses the ATP-independent insertion of metal ions into the tetrapyrrole substrate (1). Class II enzymes are multiprotein complexes with three required subunits and catalyse ATP-dependent metal ion insertion. Magnesium chelatase inserts Mg^{2+} into protoporphyrin IX in the chlorophyll biosynthetic pathway. This class also includes aerobic cobaltochelatase which inserts Co(II) into hydrogenobyrinic acid a,c-diamide in coenzyme B12 synthesis (1, 18).

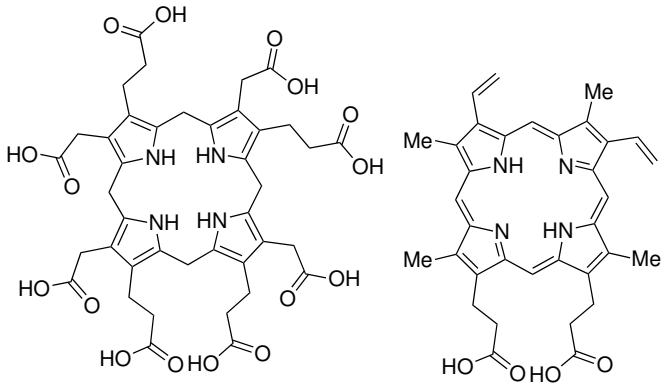

5 **8**

Scheme 1.8: The branch point molecules in tetrapyrrole biosynthesis uroporphyrinogen III (**5**) and protoporphyrin IX (**8**).

The rates of uncatalysed metal ion insertion into porphyrins are Cu(II) > Zn(II) > Mn(II) > Co(II) > Fe(II) > Ni(II) > Cd(II) ≫ Mg(II) (19). These rates are correlated to the abilities of these metal ions to lose their coordinated water molecule to create a naked ion. This observation lead to the early proposal that a function of magnesium chelatase may be to remove ligands attached to the magnesium ion to create the naked metal (20).

Plant chloroplasts can produce both heme and chlorophylls, and so contain magnesium chelatase and ferrochelatase, both of which require protoporphyrin IX as a substrate. There is a branch point within the chloroplasts with competing demands for the substrate (21). The biosynthesis of tetrapyrroles is under strict regulation since high concentrations are normally toxic to cells (1).

1.7 Magnesium chelatase

Magnesium chelatase consists of three subunits. In bacteriochlorophyll synthesizing organisms, they are referred to as BchI, BchD and BchH. In eukaryotic cells and cyanobacteria which produce chlorophyll, the subunits are referred to ChlI, ChlD and ChlH. For

convenience they are referred to here as I, D and H unless specified. Although identified as the enzyme required for magnesium insertion, the stoichiometry of magnesium chelatase subunits is yet to be fully determined (1), how the hydrolysis of ATP is coupled to ion insertion remains unknown, and no subunits from a chlorophyll producing organism have been crystallised.

1.7.1 Historical background to magnesium chelatase.

The first demonstration of an enzyme mediated magnesium ion insertion into protoporphyrin IX was demonstrated with *in vivo* studies of *R. spheroides* in semi-anaerobic conditions (22), where exogenous protoporphyrin IX was converted to magnesium protoporphyrin IX monomethyl ester. Gorchein was also able to demonstrate chelatase activity with spheroplasts, but not cell extracts, and demonstrated the requirement for ATP in the synthesis of magnesium porphyrins (23).

The earliest studies on magnesium chelatase made extensive use of cell extracts (24), such as intact cucumber chloroplasts (25). Magnesium chelatase proteins were extracted from thylakoid membranes from pea in two soluble extracts, which when mixed reconstituted magnesium chelatase activity (25, 26), revealing the multicomponent nature of the enzyme. The intact enzyme has yet to been purified from a photosynthetic organism. The majority of studies have been performed on recombinant expressed protein. The required substrates ATP, protoporphyrin IX and Mg^{2+}, were found when tobacco magnesium chelatase was expressed in yeast and reconstituted *in vitro* (27). The genes for magnesium chelatase, as well as recessive mutants, have been identified and partially characterised in barley (25, 28).

Recombinant proteins have been expressed and purified to homogeneity from *Rhodobacter sphaeroides* (29), *Rhodobacter capsulatus* (30, 31) and *Chlorobium vibrioforme* (32) as well as cyanobacterium *Synechocystis* PCC6803 (11) and the thermophilic *Thermosynechococcus elongatus* (33).

Magnesium chelatase activity is dependent on the formation of a complex between the I and D subunits. Complex formation requires $MgATP^{2-}$. This complex then binds to the H subunit, $MgATP^{2-}$, porphyrin and free Mg^{2+} to catalyse the insertion of magnesium into porphyrin. There is an absolute requirement for ATP hydrolysis as magnesium chelation is energetically unfavourable ($K_{eq} \sim 10^{-6}$) (1, 27, 31).

1.7.2 Subunit H - The porphyrin carrying moiety

ChlH and BchH bind protoporphyrin IX and are assumed to provide the environment for the insertion of magnesium into the porphyrin ring. The protein has multiple functions in regulation and catalysis, and may chaperone the cytotoxic product Mg-protoporphyrin IX to the next enzyme in the chlorophyll biosynthetic pathway (33). Within magnesium chelatase, the H subunit binds porphyrin before the insertion of a magnesium ion by forming a transient complex with a preformed ChlI–ChlD complex.

H is monomeric and soluble, found in the cytoplasm and is expressed throughout the tissues of higher plants, including seeds and roots (34). The H subunit directly interacts with porphyrin, seen initially by a reddish colour in the fractions from BchH during purification of the recombinant protein (35), and confirmed using tryptophan quenching binding studies which revealed a K_d of 1.22 μM for *Synechocystis* ChlH, 1.48 μM for *Thermosynechococcus elongatus* ChlH and 0.53 μM for BchH with the substrate analogue deuteroporphyrin IX (33, 36).

Single particle reconstruction of cryo electron micrograph images of ThrH from *T. elongatus* (33) and BchH from *Rhodobacter capsulatus* (37) reveal different tertiary structures (figure 1.5). ThrH is 148 kDa and has two domains, an open and asymmetrical cage like assembly with a 100 nm^3 internal space and globular N-terminal approximately 16 kDa (figure 1.5 **A** and **B**). This model is consistent with small angle x-ray scattering data (33, 38). The authors propose the cavity region may be the site for porphyrin binding. The crystal structure of ferrochelatase from *Bacillus subtilis* (figure 1.6) bound with transition state analogue *N*-methylmesoporphyrin shows a binding site which is much more packed (39), with the active site making ionic interactions, as well

as aromatic stacking to the pyrrole rings and steric interactions with protein. Although ferrochelatase is a very different enzyme from magnesium chelatase, the binding of porphyrins is likely to be similar, since the function is to control of the solvation state of a metal ion and provide an environment in which porphyrins can be deprotonated (40). The proposed binding site in ThrH does not appear to provide those conditions.

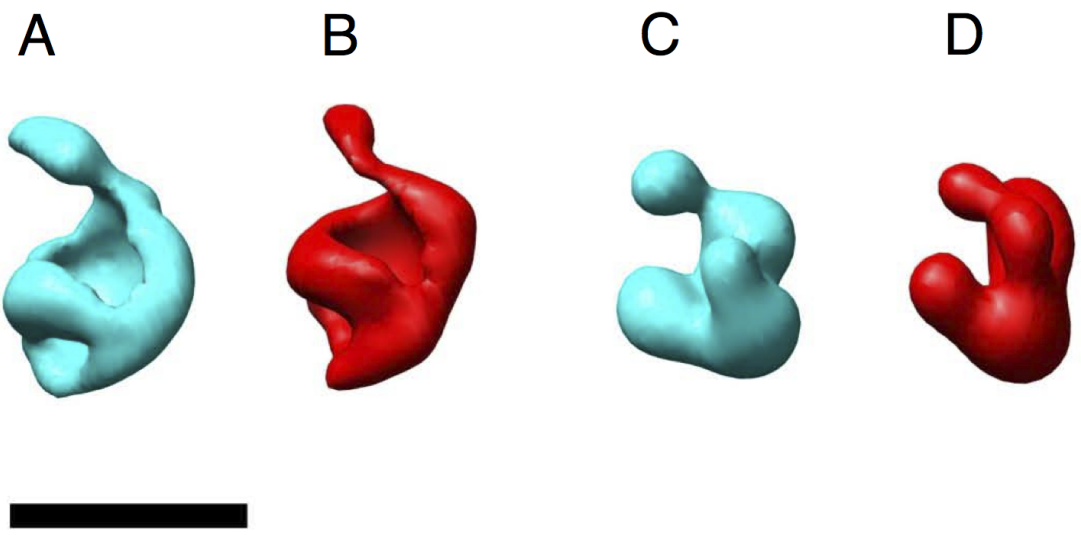

Figure 1.5: Single particle electron microscopy reconstruction of ChlH and BchH at 30 Å resolution - A and B – ChlH, C and D – BchH, blue unbound, red bound to porphyrin, scale bar = 10 nm, reproduced from Qian *et al* (33).

The N-terminal head region is highly charged and may be involved in protein-protein interactions, such as ChlM or allosteric activator Gun4. Deleting this region from the protein abolishes chelatase activity but not porphyrin binding. Movement of this head region on porphyrin binding (figure 1.5) appears to be quite substantial (33).

BchH appears to have three main domains, which on porphyrin binding (figure 1.7 **A** to **B**) join together in a thumb-finger style arrangement. Electron microscopy reconstructions of the protein reveal three major lobes of density. The lower half contains lobes II and III, while lobe I is perpendicular to lobes II and III. Lobe I has an additional finger attached which is flexible (37). Lobe I and II are within the N-terminal

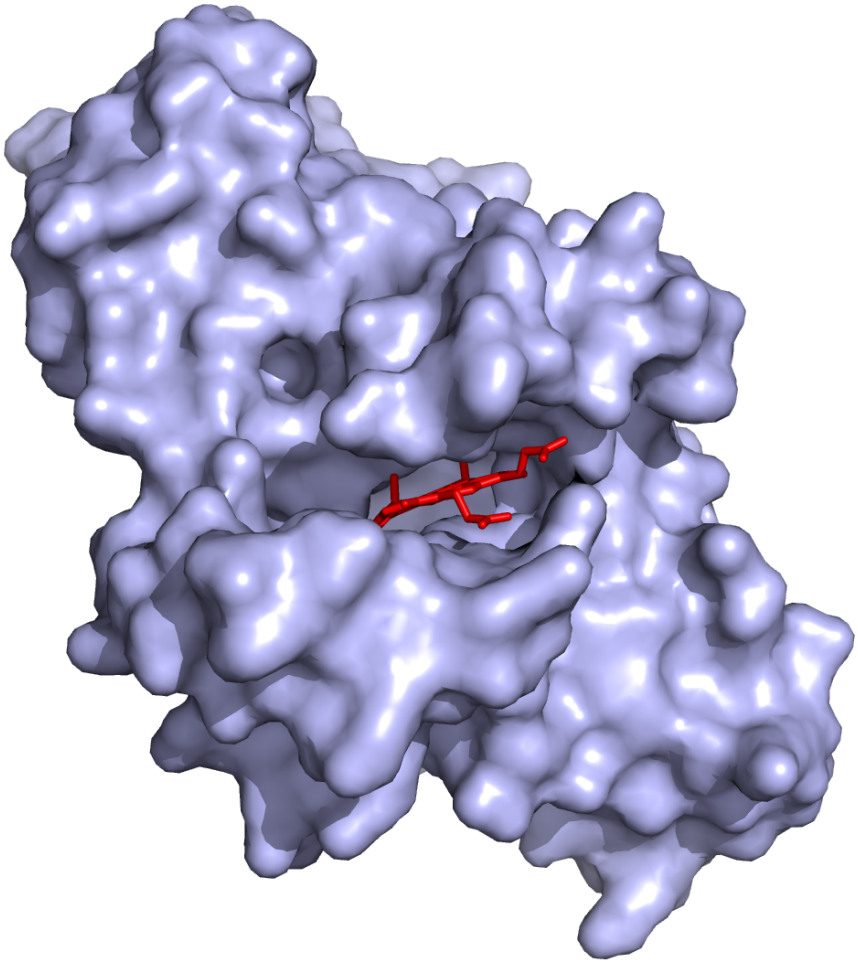

Figure 1.6: Crystal structure of ferrochelatase from *Bacillus subtilis* - Surface representation of the ferrochelatase (grey) with the transition state analogue *N*-methylmesoporphyrin (red sticks) showing close contacts between porphyrin and protein. PDB code 1C9E (39), structure rendered using PyMOL (41).

region, and retain porphyrin binding ability when lobe III is not present. Lobe III and the finger are contained within the C-terminal end of the protein. Porphyrin binding was suggested to occur between the two domains, clamping the substrate in place, potentially between the thumb and finger regions. On porphyrin binding, the structure becomes much more rigid, with the thumb and finger in direct contact (37).

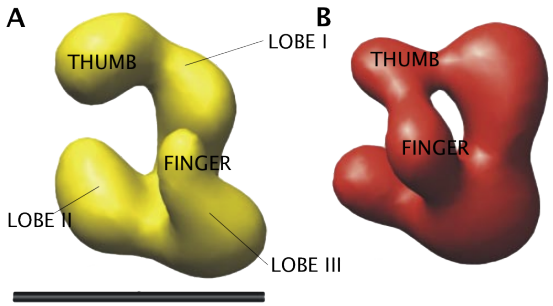

Figure 1.7: Low resolution structure of BchH - Single particle reconstruction of BchH **A** apo-BchH highlighting the three domain structure of the protein and the thumb and finger subdomains, which on binding of porphyrin **B** come into contact. Scale bar = 10 nm.

After chelation, free magnesium protoporphyrin IX is unlikely to be released into the cell as it is toxic. Too much pigment can cause photodamage to the cell and too little will result in a chlorophyll deficiency (33). It is thought that H regulates the next stage of chlorophyll biosynthesis. It is possible the ChlH-MgP_{IX} is the substrate for the next enzyme in the pathway *O*–methyl transferase (ChlM/BchM) (33, 37), or acts as a chaperone to channel MgP_{IX} to ChlM to ensure handover and prevent oxidation. One hypothesis is that once magnesium has been inserted, the ChlH-MgP_{IX} dissociates from the ID complex and binds to *O*–methyl transferase. There is evidence for this chaperone behaviour in *Synechocystis* and *Rhodobacter* systems (42, 43). The proteins BchM and divinyl protochlorophyllide *a* 8-vinyl-reductase (BchJ) shifts the mass action leading to 100% conversion to magnesium protoporphyrin IX, with a 1:1 ratio between BchJ or BchM, although BchM shifts the equilibrium faster than BchJ. The authors suggest that BchJ may mediate the delivery of BchH-MgP_{IX} to BchM (42).

Photosynthetic bacteria have a more complicated regulatory environment where they move between aerobic and anaerobic respiration and therefore must switch between anaerobic and photosynthetic growth mechanisms, during which the cellular products required will change (33). Within the chlorophyll biosynthetic pathway, ChlH stimulates the activity of *O*–methyl transferase in *Synechocystis* (43, 44, 45, 46), while Gun4 stimulates ChlH and regulates ALA-synthase at the very start of the chlorophyll biosynthetic pathway (scheme 1.3). Osanai *et al* (47) have found that ChlH interacts with Signalling factor E (SigE) as a repressor. SigE is a positive regulator for sugar catabolism, for example glycolysis. The interaction of the two proteins is mediated by the level of light, which may be related to the flux in magnesium concentration (47). The large number of roles ChlH appears to have in cells may explain the large structure.

ChlH from *Arabidopsis* is a putative abscisic acid receptor (ABA), acting as a positive regulator, specifically binding ABA. ABA mediates seed germination, post germination growth, and movement and aperture width of stomata (34, 48). ChlH is expressed ubiquitously in plant tissue, as it must be able to perceive ABA at the whole plant level. With increased levels of ABA, there is a decrease in the level of chlorophyll and protoporphyrin IX but an increase in the levels of ChlH and MgP_{IX}. ABA binds to the C-terminal of ChlH independently of protoporphyrin IX (34, 48), which may indicate that the signalling pathway is independent from magnesium chelatase activity. Mutants of ChlH that decrease the levels of chlorophyll synthesis have no effect on the levels of ABA regulation. ABA regulation is also separate from plastid to nucleus signalling role of ChlH (34). Müller and Hansson (49) could not reproduce the results of Shen (34), and the original method used by Shen has been retracted (50). More recent work by Wu has independently verified ABA binding to ChlH from *Arabidopsis*, barley and rice using three different assay techniques. Separately further study has shown that ChlH does have an effect on the ABA signalling in guard cells at the stomata, but Tsuzuki *et al* did not find direct binding between ABA and ChlH. Tsuzuki *et al* proposed that the entire magnesium chelatase protein, or MgP_{IX} may control the release of internal stores of Ca^{2+} in response to ABA (51).

1.7.3 Subunits I and D are AAA$^+$ ATPases.

The AAA$^+$ proteins (**A**TPases with **a**ssociated with various cellular **a**ctivities) are a super-family with a structurally conserved binding motif for ATP. They form active oligomeric systems that utilize ATP hydrolysis to drive their coupled biological activities. Members of this family have varied functions (52). They are involved in protein secretion and assembly, proteolysis, cell cycle control, DNA replication, transcription, membrane synthesis and fusion (53). They are thought to act by inducing conformational changes in protein substrates (54). Enzymes in this family contain a common domain of around 200 amino acids containing the Walker A and B nucleotide binding motifs (52, 54).

AAA$^+$ enzymes link ATP hydrolysis driven conformational changes to chemomechanical motion. This motion is then normally transduced throughout a multi-subunit complex. ATP binding and hydrolysis lead to at least two conformational states of the protein. Although the family show very conserved domains, their response to ATP hydrolysis varies from bimodal switching between on and off states, to a mixture of different conformations or to the situation where they do not actually hydrolyse ATP (52, 54).

1.7.4 The I subunit of magnesium chelatase

Sequence analysis of the I subunits reveal they belong to the AAA$^+$ family of proteins (55). BchI from *R. capsulatus* is the only essential subunit of magnesium chelatase with a high resolution crystal structure (2.1 Å PDB code 1G8P, (56)). The structure of BchI (figure 1.8) shows the characteristic fold expected of a AAA$^+$ family member. The conserved ATPase motifs can readily be seen in the structural model (figure 1.8), such as the location of the Walker A and B nucleotide binding motifs in the $\beta1/\alpha2$ and $\beta3/\alpha4$ respectively, and the sensor 1 motif at the interface of $\beta4/\alpha5$. When the crystal structure of BchI is superimposed on top of the structure of AAA$^+$ protease HslU, we see adenine and ribose may interact with a loop of 20 - 26 residues on α helix 5. Triphosphate interacts with Walker A and Walker B motifs with the β and γ

position on ATP. Lysine 58 forms a salt bridge with the β-phosphate group on ATP, serine 59 coordinates with a magnesium ion, and the sensor II arginine 289 is essential for protein activity (56).

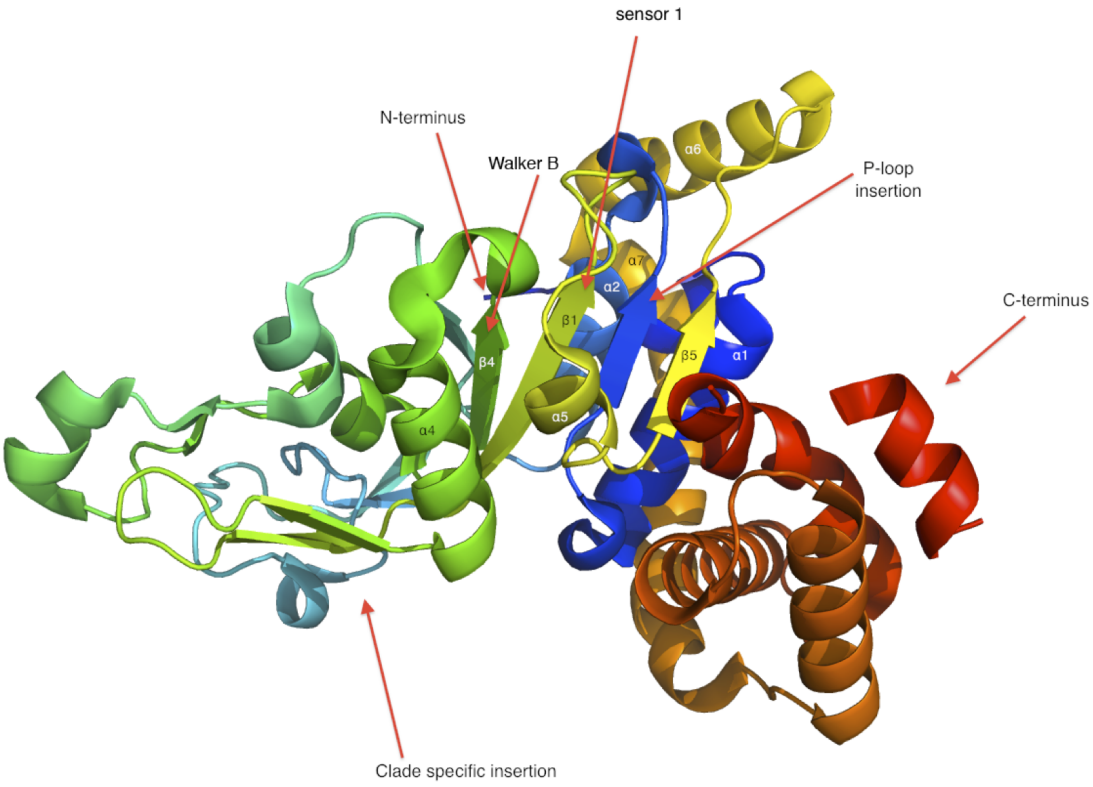

Figure 1.8: Cartoon representation of BchI crystal structure - important features of the AAA$^+$ highlighted, PDB code 1G8P (56), figure rendered using PyMOL (41)

The AAA$^+$ family can be split into 7 evolutionary clades, with differences being defined by insertion of secondary structure elements within and around the AAA$^+$ fold (52). Magnesium chelatase subunit I is part of clade 7 of the AAA$^+$ ATPase superfamily, also known as the PS-II insert clade, where a helical insertion after the 5th α helix repositions the sensor 2 motif. This clade has an unusual configuration of the C-terminal helical bundle. Instead of clamping over the ATP-binding site, it is located at the back of the protein, allowing it to interact with the ATPase site on an adjacent subunit. The helical insert and C-terminal maintain contact with the protein core. The lid on the binding site is obtained through interactions with neighbouring sub-

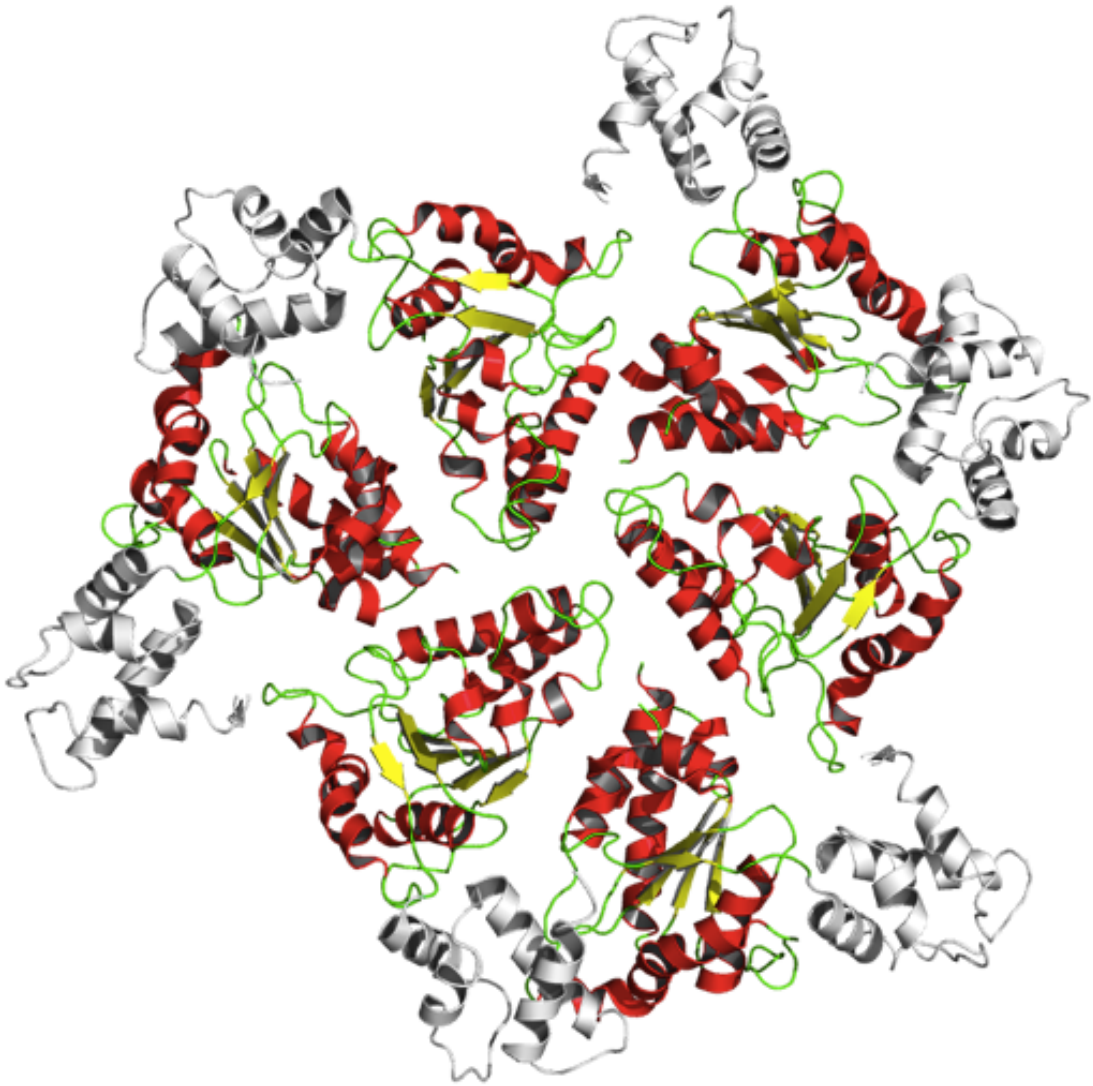

Figure 1.9: Modelled BchI hexamer - Cartoon representation of BchI hexamer modelled onto a hexamer of FtsH, using Swiss-Model (57) and rendered with PyMOL (41).

units, positioning the sensor II arginine into the correct place within the active site. This adaptation probably tunes the stability of the complex (52, 56). The N-terminal domain of BchI which contains the ATP binding site can be superimposed upon the N-terminal domain of the fellow AAA^+ proteins HslU and FtsH highlighting the similarity of ATPase active sites within this family. On superimposing BchI onto FtsH (figure 1.10) the flipped domain architecture of BchI is highlighted. The C–terminal helical bundle is shifted to make contacts with an adjacent subunit (56).

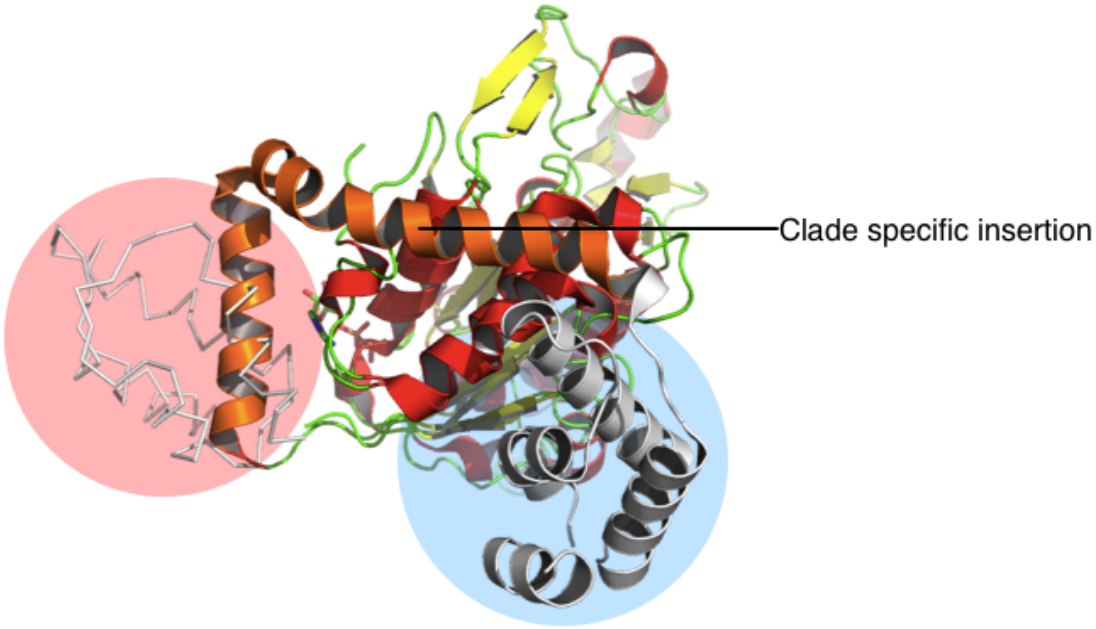

Figure 1.10: Flipped domain architecture of BchI - The crystal structure of BchI (cartoon) modelled onto structure of a subunit of FtsH (sticks) showing the differing locations of the Arginine finger domain from shaded red in FtsH to shaded blue in BchI. The orange helical insert shifts the location of the domain (56, 58).

ChlI contains one essential cysteine but it is not known whether it is involved with binding of nucleotide or involved with a conformational change in the presence of ATP. In the presence of the irreversible modifier of cysteines, N-ethylmaleimide (NEM), the ATPase activity of ChlI is abolished (59).

AAA^+ ATPases frequently show nucleotide dependant oligomerisation, and the I

subunit is no exception. The concentration of $MgATP^{2-}$ affects the ability of ChlI to self-assemble. ChlI binds $MgATP^{2-}$ which is essential for chelation activity and hydrolysis only occurs in the presence of free Mg(II) (35). In the presence of ATP, BchI forms oligomers of six subunits, approximately 110 – 120 Å in diameter, where there is an equilibrium between monomer and multi-subunit complexes. Published EM micrographs of ChlI showing heptameric oligomers do not reflect the dominant species in solution (*pers com* Pu Qian, The University of Sheffield), and latest hydrodynamic and EM data show a hexamer (56, 60).

The I subunit of magnesium chelatase is an ATPase (2, 60). ATPase activities vary between species, but a valid comparison is made difficult by the many measurements being taken at arbitrary substrate concentrations. The ATPase activity of BchI is low (table 1.1) compared when it is in the ID complex, where it reaches 0.24 nM min^{-1} (2). The rates of ATPase activity of BchI and BchID are 100,000 times lower than *Synechocystis* ChlI. The *Synechocystis* ID complex has a lower ATPase activity than ChlI alone (60, 61).

The I protein is able to exchange phosphate within the active site from ADP to ATP while powering chelation (62), indicating an enzyme-phosphate intermediate. Similar studies did not find the presence of an enzyme-ADP complex. No covalent enzyme–phosphate intermediate has been detected, while no adenosine monophosphate (AMP) is formed during the reaction (2, 62).

Table 1.1: ATPase and Phosphate exchange activity of subunits I and D adapted from Willows and Hanson (1), data from reference (2) and this thesis.

Organism	**Subunit**	**ATPase activity / nM $\mathbf{min^{-1}}$**	**ATPase exchange activity / pmol μg $\mathbf{protein^{-1}min^{-1}}$**
Synechocystis PCC6803	D	Trace	0.2
	I	8990	1.93
	I + D	2990	Not observed
R. sphaeroides	D	0.021	221
	I	0.092	576
	I + D	0.24	–

1.7.5 The D subunit of magnesium chelatase

Subunit D is also a member of the AAA^+ family of proteins (27, 61). In tobacco, the N-terminal shares 46% sequence homology with ChlI (figure 1.12) (63) but is missing a hairpin loop between $\alpha 2$–$\beta 2$ and a linker at $\alpha 7$, suggesting a common ancestral gene. Although the N-terminal AAA^+ domains share sequence identity, D is a much larger protein compared with I (ChlD is 75 kDa and ChlI is 39 kDa), and the extensive C-terminal domain suggests that ChlD may have a different function (27, 61). The C-terminal end of the AAA^+ domain in D shares a similar location as HslU C-terminal (56), in that it does not appear to have the flipped domain architecture of subunit I.

There is sequence homology between the amino acid sequence of the C-terminal region in BchD and integrin I domains. The integrin I domain is a region of approximately 200 amino acid residues present in many proteins which are involved in cell-cell and cell-matrix interactions. The integrin I domain binds to specific complimentary sequence motifs. Both BchH and BchI have these complimentary motifs, H has Leu-Asp-Glu and I either Arg-Gly-Glu in bacteria or Arg-Gly-Asp in plants (56).

ChlD contains no essential cysteines unlike ChlI and ChlH (59). Studies on truncated mutants have revealed that only a small section of ChlD is required for chelatase activity. The M_1LM_2 region of only 110 amino acids (figure 1.11) is required for protein-protein interactions between I and H and also for enzyme activity. M1 and M2 are predicted to be amphipathic helices. Removal of the N-terminal AAA^+ domain reduces chelatase activity, and it is thought that D might bind ATP, but there is no evidence to suggest that D binds ATP in isolation from the other subunits of magnesium chelatase. The C-terminal contributes more to chelatase activity than the N-terminal (63).

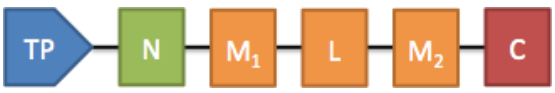

Figure 1.11: Schematic representation of ChlD - TP transit peptide, N N terminal, L poly proline linker, C C terminal, M peptide motifs.

Figure 1.12: Sequence alignment of I and D subunits from *Synechocystis PC6803* and *Rhodobacter capsulatus* - Key: **CHLISYNY3** – ChlI, **CHLIDSYNY3** – ChlD, **BCHIRHOCB** – BchI, **BCHDRHOCB** – BchD. Residues coloured blue are conserved either, with a darker blue indicating conservation between all 4 proteins. Alignment performed on UniProt and visualised using JalView 2.7 (64, 65)

Negative stain electron micrographs reveal that the BchD subunit forms stable oligomers independent of ATP and BchI (66). It is suggested that this produces a platform upon which I subunits can bind and construct the ID complex (56, 66). When the ratio of D to I exceeds 1:2, inhibition of activity occurs as there are possibly more D ring platforms than I units, allowing incomplete I oligomers to be formed (35, 66). Without the presence of I, the D subunit is degraded in vivo, suggesting the ID complex is required to prevent proteolysis (66).

1.7.6 The structure of the BchID complex

Single particle electron microscopy 3D reconstructions predict BchI has direct contact with BchD through interactions with the N-terminus and the β-hairpin insertion in helix $\alpha 2$ (this contrasts to the reports on tobacco ChlD (63)) characteristic of the PS-II clade of AAA^+ proteins. The N-terminal AAA^+ domains are arranged around a central core (figure 1.13). Modelling the sequence of BchD onto similar AAA^+ proteins predict the integrin I domain in BchD is near the arginine finger of BchI, and may prevent hydrolysis of ATP when the two subunits are complexed together, which may explain the reduction in ATPase activity of ChlID compared to ChlI in isolation. The structural analysis of the BchID complex shows I forming a trimer of dimers, allowing only three molecules of ATP to be hydrolysed at a time (67).

The conformation change that occurs on adenylyl-imidodiphosphate (AMP-PNP) binding leads to compression of the whole complex from 120 to 100 Å. On binding nucleotide, the integrin I domain is pulled up while BchD is pulled down towards the BchI monomer–monomer interface, leading to a contraction in the D ring. On ATP binding the complex becomes more contracted along the diameter, and stretched along the C3 axis. The BchD ring is more tightly packed on the outer edges, creating an opening in the centre, whereas with the BchI ring the pore is closed. This exposes the loop and hairpin insertions, which are normally involved in the binding of substrate and could be the productive state where BchH binds (67).

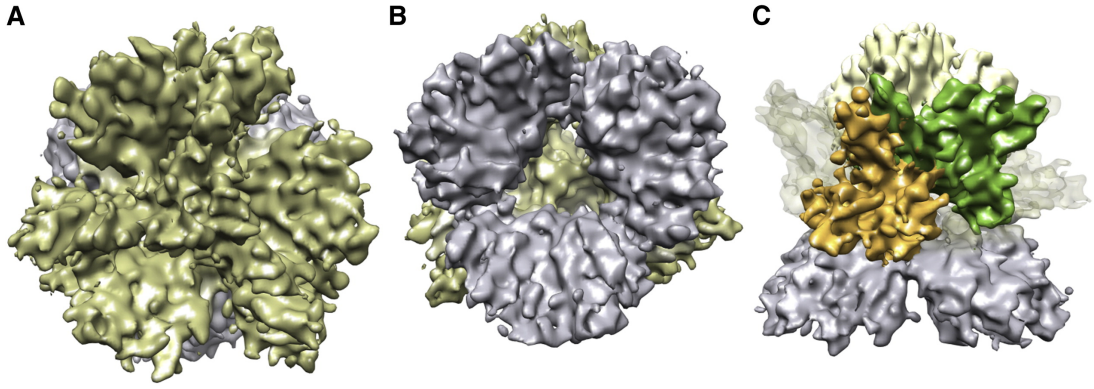

Figure 1.13: Structural model of BchID - Reconstructed model of the BchID ring structure in the presence of $MgADP^{2-}$ at 7.5 Å resolution. A) Top view of ID complex showing the BchD ring (gold), B) Bottom view of ID complex showing BchI ring (grey), C) Side view of ID complex, highlighting the proposed C-terminal domain of BchD with the integrin I domain and proline-rich region (green) and acidic residue-rich region (orange) of a BchD dimer. Image reproduced from Lundqvist *et al* (67).

ATP hydrolysis at the three ATP binding sites could disrupt dimer-dimer interactions, leading to dimer dissociations to allow ADP to ATP exchange. This suggests a complex alternating between nucleotide bound states with ATP bound to three alternative sites (66, 67).

The conformational changes in BchI lead to the movement of the integrin I domain in BchD, altering the conformation of the entire ring. The integrin I domain on D appears to interact with the complimentary RGE binding motif in BchI which is also assigned as the Sensor II arginine. This may explain the inhibitory effect of D on ATPase activity if sensor II is involved in interactions with D, preventing its role in binding and hydrolysing ATP (67, 68).

BchH is the substrate of the ID complex. Studies have shown that H undergoes a conformational change on the chelation of Mg^{2+} into protoporphyrin IX (69), which may be coupled with integrin I, it is speculated that the insertion in ChlI (H2, PS–I, PS–II and $\alpha 1$–$\beta 2$–β–hairpin) creates the BchH binding site which is exposed to solvent on ATP binding. H may also interact with D via the **m**etal **i**on **d**ependent **a**dhesion **s**ite

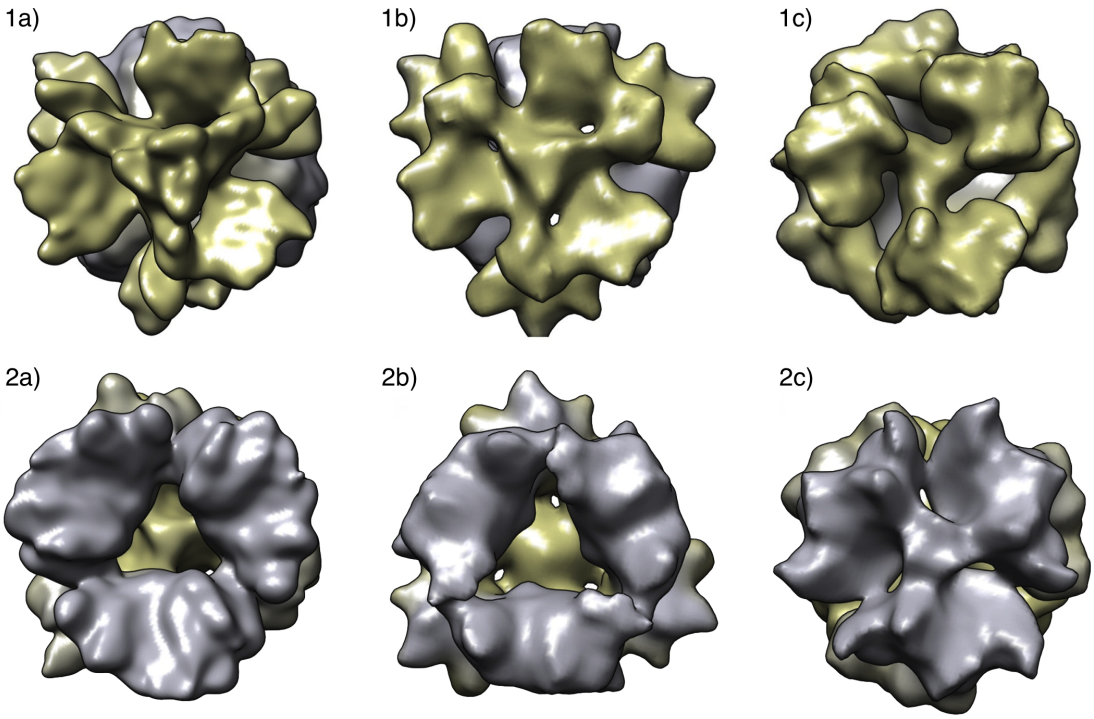

Figure 1.14: The flexible structure of the BchID complex in different nucleotide bound states - EM reconstructions of ID complexes at 13 Åresolution. 1) Top view of the BchD ring in gold 2) Bottom view of the BchI ring in grey. a) In the presence of ADP, b) AMPNP and c) ATP. Reproduced from Lundqvist *et al* (67).

(MIDAS) motif, with the complimentary motif LDV found. Mutations in the MIDAS abolish chelatase activity but not ATPase activity (67).

In the BchI ring the inserted PS-II helix is close to the integrin I domain of ChD, and interactions within this region regulate ATP-binding. Binding of H through its own complimentary motif to integrins may reduce any inhibitory effect leading to protein function (67).

1.7.7 Gun4 - The fourth subunit

A fourth protein involved with the magnesium chelatase reaction is Gun4 (**g**enome **un**coupled). The protein has been found to increase the rate of magnesium chelation while reducing the requirement for free magnesium, allowing chelation to occur at lower, physiologically relevant, concentrations of magnesium (70). Gun4 increases the second-order rate constant for the interaction between porphyrin and magnesium chelatase. Cyanobacterial and higher plant magnesium chelatases are stimulated by Gun4. The Gun4 protein binds ChlH, protoporphyrin IX, magnesium protoporphyrin IX and their more soluble analogues deutero- and magnesium deuteroporphyrin IX. *In vivo*, Gun4 is required for the production of chlorophyll (70, 71). It is located in the chloroplast as large multiunit complexes and as soluble monomers in the stroma (70, 71).

Pale phenotypes of *Arabidopsis thaliana* which contain the mutant gun5 have a lesion within the gene for ChlH. These mutants are still able to bind both P_{IX} and MgP_{IX}, and in mutant inhibition studies, it appears that the ChlH-gun5 mutant is a dead end complex which competes with wild type ChlH as a competitor for ChlID rings (72). On the addition of Gun4 the activity of the mutants is restored to levels seen in wild type without the presence of Gun4, which may explain how these mutant phenotypes still have small levels of chlorophyll (72).
Gun4 binds ChlH, protoporphyrin IX and magnesium protoporphyrin IX. MgP_{IX} represses transcription of the gun4 gene, implying a regulatory role for the protein (70). It is implicated in nucleus to plastid signalling, and binds magnesium porphyrins more tightly than free porphyrins, consistent with a role in regulating magnesium protoporphyrin levels *in vivo* (71). The highly helical Gun4 has two domains, with the proposed

protoporphyrin binding site conserved among species. The amino N-terminal has a helical arrangement, normally associated with protein-protein interactions (71).

1.8 Proposed model of magnesium chelatase reaction

Historically magnesium insertion into protoporphyrin IX has been viewed as a two step process. Initial experiments showed a lag phase (figure 1.15) followed by the rapid production of MgProto (21). These two steps were long thought to reflect firstly slow formation of the active chelatase complex giving a lag phase, followed by metal ion insertion into protoporphyrin IX. Each process is likely to be a complex, multi-step reactions.

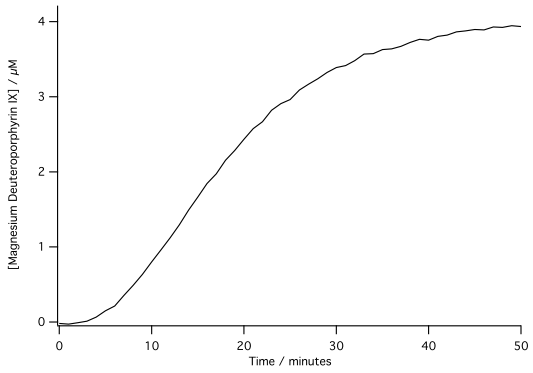

Figure 1.15: Typical progress curve of a magnesium chelatase assay - Using a continuous fluorometric assay detecting the product of the reaction magnesium deuteroporphyrin IX, the assays typically have a 10-minute lag phase, after which a steady state rate is quickly reached before $d[P]/dt = 0$ after about 40–50 minutes.

The hypothetical chemical process required for magnesium insertion into porphyrins consists of four steps (scheme 1.9). Firstly the nitrogens in the porphyrins core must be deprotonated, in conditions which favour metal ion insertion. The metal ion is then desolvated leaving a naked metal x^{2+} species, which is unfavourable, and possibly the rate limiting step. Metal nitrogen bonds then form. The process ends with the completion of the coordination sphere (19, 73).

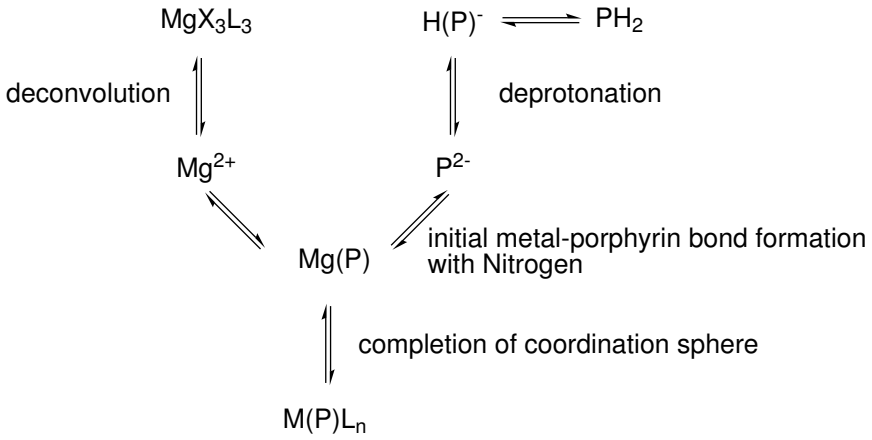

Scheme 1.9: For a magnesium ion to be inserted into a porphyrin, it must have the outer water or other ligands removed before bond formation with a deprotonated porphyrin.

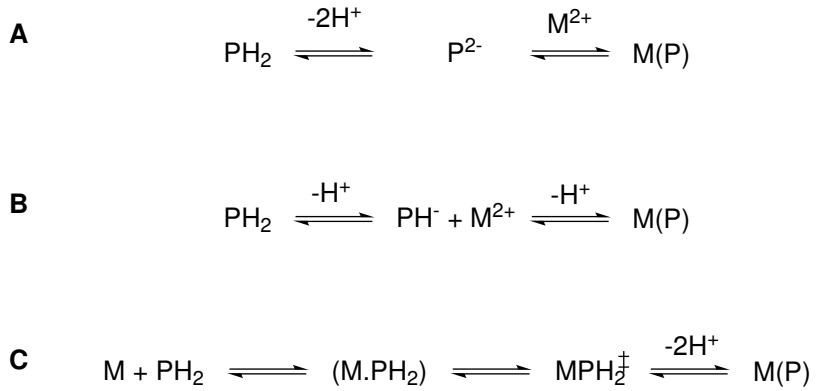

Scheme 1.10: Three different proposed mechanisms for metal ion insertion into porphyrin

There are three possible mechanisms for metal ion insertion (scheme 1.10). There is no evidence for mechanism **A** with a two proton dissociation mechanism (the pK_a 1 and 2 (scheme 1.11) is unknown for deuteroporphyrin, but deuteroporphyrin is in the free base form, PH_2, up to pH 14). The uncatalysed rate of magnesium insertion is inversely proportional to the concentration of hydrogen ions which suggests mechanism **B**. Nitrogenous bases such as pyridine and imidazole may act as catalysts in the insertion of magnesium, which suggests a pyridine-magnesium-porphyrin complex with the coordinated magnesium aiding the dissociation of hydrogen (73). The most likely

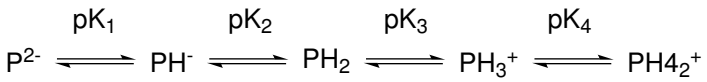

Scheme 1.11: The origin of porphyrin formal pK_a's, although the highly conjugated nature of porphyrins mean there are many tautomers present. The pK_a of a porphyrin nitrogen is a combination of the intrinsic basicity of the nitrogen and the partition coefficients of the species with the solvation environment.

is mechanism **C**, where the metal-porphyrin complex is formed after which metal then displaces both hydrogen ions giving the metalloporphyrin. This has been corroborated with observed intermediates and theoretical calculations (20, 74, 75).

The porphyrin binding site on the enzyme is likely to distort the planar nature of the ring (39, 40), and any deprotonated porphyrin species PH^- will likely be distorted by the three nitrogen lone pairs (74). This will lead to a highly complex sterically controlled process, with the outer sphere coordination of the metal ion also associated with porphyrin, with ligand dissociation from metal to allow the second porphyrin nitrogen to form a bond.

A suggested enzyme mechanism (scheme 1.12) for complex assembly is that the D subunit forms a hexameric complex, after which there is little or no exchange of subunits. After this, ATP and Mg^{2+} dependent construction of a two tiered ID complex occurs. ATP binding but not hydrolysis is required to form the ID complex (59). On the formation of the double ring structure, the ATPase activity of I is substantially reduced. The H subunit then binds to the ID complex, possibly through the integrin domain of D allowing metal ion insertion and ATPase activity.

The magnesium binding site is unknown, although there are possibilities such as the MIDAS motif (56, 66). There is a sigmoid relationship between the concentration of magnesium and the amount of activity in the enzyme from *Synechocystis* but not from *R. capsulatus* or *R. spheroides*. Magnesium is used in the reaction in three ways, as a substrate, in the co-substrate $MgATP^{2-}$ and to maintain protein-protein interactions (26, 76).

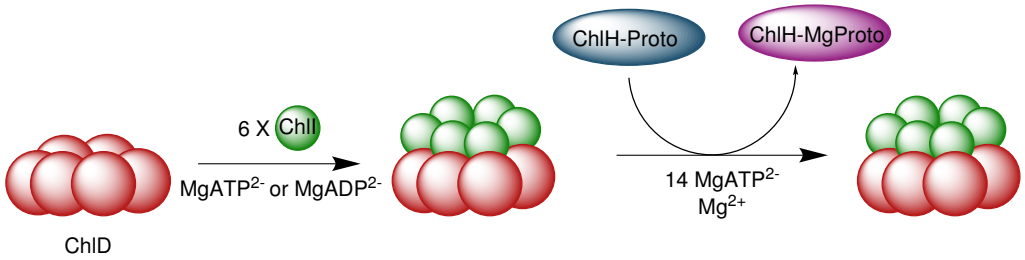

Scheme 1.12: Proposed mechanism of magnesium chelatase. ChlD forms a hexamer ring which acts as a platform upon which ChlI, in the presence of $MgATP^{2-}$ forms a hexamer. This hexamer binds a preformed ChlH-proto complex, and with the hydrolysis of $\sim$ 14 $MgATP^{2-}$ inserts a magnesium ion into protoporphyrin IX.

There is a lag phase in the production of MgD_{IX} and MgP_{IX}, which can be reduced if the reaction mixture is preincubated with ATP (21, 77). The lag is presumed to be due to the time taken to form the ID complex. The three proteins act as a loosely bound complex, and can be separated easily (26). A suggested model is that magnesium chelatase units must come together with an ATP dependent activation step before a reaction can occur. This is then followed by the catalysis step. $MgATP^{2-}$ is required for I and D to physically interact, although there is no requirement for ATP hydrolysis. This interaction occurs before H is involved in the complex (35). The ATPase activity of ChlI drives Mg^{2+} insertion into porphyrin (59, 78). BchI and the BchI:BchD complex have low ATPase activities which increases 33 fold on the addition of BchH (in *Synechocystis* the increase in activity is 16–20 fold) (2, 78).

Etiolated chloroplasts show the same lag occurs after exposure to light, with chlorophyll accumulated linearly after an initial lag. Heme is also only accumulated on exposure to light (25). Jensen *et al* found that subunits are only expressed after exposure to light, indicating the genes are controlled by the circadian clock (28).

ChlH can be viewed as a substrate with Michaelis-Menten kinetics (37). Titrating H against a fixed concentration of the ID complex produces hyperbolic curves for steady state rates, unlike the sharp titration curves expected with tight binding. There is no inhibition of activity on increasing the concentration of H present in the assay system,

suggesting that H-porphyrin can exchange with H in an IDH complex (37).

Reid and Hunter (76) give steady-state kinetic parameters for magnesium chelatase from *Synechocystis PCC 6803* as 3.20 μM for K_{DIX}, $K_{\mathrm{MgATP^{2-}}}$ as 0.45 mM, k_{cat} for chelation as 0.8 min^{-1} and $s_{0.5}$ (analogous to K_m in a cooperative system) for Mg^{2+} as 3.8 mM. The response to the concentration of $MgCl_2$ displays positive cooperative behaviour, and as Mg^{2+} must be in excess of the ATP concentration, this suggests that $MgATP^{2-}$ is the active form of the nucleotide (26, 35).

Both steps (activation and metal ion insertion) depend on ATP, but at different concentrations. Activation can take place without hydrolysis of ATP (determined by using thio-analogues of ATP) but not the chelation step (21, 78). ADP inhibits magnesium chelatase activity, while AMP has no effect. Chelation is not inhibited by elevated concentrations of magnesium protoporphyrin monomethyl ester, chlorophyllide or protochlorophyllide, but the ferrochelatase inhibitor N-methylmesoporphyrin IX a inhibits at millimolar concentrations (compared with nanomolar concentrations for ferrochelatase) suggesting an alternative mechanism of inhibition. Activity is inhibited by o-phenathroline and Co(III)-ATP-o-phenanthroline. Sodium fluoride inhibits chelation but not ATPase activity (2, 26).

1.9 Aims

This thesis aims to dissect the role of ATP binding and hydrolysis has on metal ion chelation in magnesium chelatase.

In chapter 3 the pathway of ATP hydrolysis is monitored using non-equilbrium isotope exchange to reveal the intermediates at the ATP binding site during metal ion chelation. While powering chelation, there is evidence for an enzyme-phosphate complex.

Chapter 4 provides a thermodynamic overview of the magnesium chelatase catalysed reaction, and how the protein uses free energy released from ATP hydrolysis to

shift the mass action ratio $[MgD_{IX}]/[D_{IX}][Mg^{2+}]$. This shift in mass action is characterised. The rate enhancement and catalytic proficiency of magnesium chelatase is calculated and the role of energy linkage discussed.

The role of the two AAA^+ proteins, ChlI and ChlD, is explored in chapters 5 and 6 respectively. Functional analysis of mutants in the ATPase site of the ChlI reveals the proposed hexamer of ChlI hydrolyses ATP in an unconcerted fashion, but cooperativly binds $MgATP^{2-}$. Similar mutations in ChlD show for the first time a role for ChlD in allosteric signalling between AAA^+ domains during the hydrolysis of ATP.

2

Methods and Materials

2.1 Materials

All chemicals were obtained from Sigma Chemical Company (Poole, Dorset) unless otherwise stated. Chelating sepharose and HiTrap columns were obtained from GE Healthcare (Little Chalfont, UK), porphyrins from Frontier Scientific (Logan, UT, USA). Chemicals for electrophoresis were purchased from Bio-Rad Ltd (Hemel Hempstead, UK).

2.2 Buffers, Reagents and Media

All buffers and culture media were prepared as described by Sambrook (79) unless otherwise stated. Growth media were prepared using deionised water. Solutions used in DNA, purification and kinetic work were prepared using distilled water which was further purified using a Milli-Q system (Millipore, Watford, UK). All reagents were of analytical grade. Media required for growing bacteria and DNA work was sterilised by autoclave at 15 p.s.i. 115 °C for 20 minutes, or for heat sensitive compounds via filtration through a 0.22 μm filter. Heat labile compounds were only added to solutions once they had reached $\approx$ 50 °C.

2.3 *E. coli* strains and plasmids

Escherichia coli used in this work are listed in Table 2.1. Strains were transformed and grown in Luria-Bertani (LB) medium (79) supplemented with neomycin (and chloramphenicol for Rosetta strains of *E. coli*), to a final concentration of 30 μgml^{-1} (34 μgml^{-1} for chloramphenicol).

Transformed cells were stored as glycerol stocks at -80 °C (LB media, supplemented with 20% (w/v) glycerol).

2.4 Production of chemically competent *E. coli* cells

All *E. coli* strains were treated as described by Hanahan (80). Untransformed cells were streaked onto a non-antibiotic plate and grown overnight at 37 °C. Ten colonies

Table 2.1: *E. coli* strains used for transformation and expression of recombinant proteins.

Strain	**Relevant Properties**	**Supplier**
JM109(DE3)	endA1 glnV44 thi-1 relA1 gyrA96 recA1 mcrB$^+$ Δ(lac-proAB) e14$^-$ [F' traD36 proAB$^+$ lacI^q lacZΔM15] hsdR17($r_K^-m_K^+$) (F^- ompT rB^- mB^-) + bacteriophage DE3	Sigma-Aldrich
BL21(DE3)	(F^- ompT rB^- mB^-) + bacteriophage DE3	Sigma-Aldrich
JM109	endA1 glnV44 thi-1 relA1 gyrA96 recA1 mcrB$^+$ Δ(lac-proAB) e14$^-$ [F' traD36 proAB$^+$ lacI^q lacZΔM15] hsdR17($r_K^-m_K^+$)	Sigma-Aldrich
Rosetta	F^- ompT $hsdS_B(R_B^- m_B^-)$ gal dcm λ(DE3 [lacI lacUV5-T7 gene 1 ind1 sam7 nin5]) pLysSRARE (Cam^R)	Novagen

Table 2.2: List of plasmids used for protein growth and mutagenesis experiments

Plasmid	Relevant Properties	Reference
pET9a-His$_6$ChlD	pET9aHis plasmid containing Synechocystis chlD gene sequence cloned between the NdeI and BamHI sites	Jensen, 1996 (11)
pET9a-ChlI	pET9a plasmid containing Synechocystis chlI gene sequence cloned between the NdeI and BamHI sites	Jensen, 1996 (11)
pET9a-His$_6$ChlI	pET9aHis plasmid containing Synechocystis chlI gene sequence cloned between the NdeI and BamHI sites	Jensen, 1996 (11)
pET9a-His$_6$ChlH	pET9aHis plasmid containing Synechocystis chlH gene sequence cloned between the NdeI and BamHI sites	Jensen, 1996 (11)

were inoculated into 200 ml 2xYT medium and grown at 37 °C 250 RPM until the culture had reached an OD_{550} of between 0.35 and 0.5. The cells were pelleted by centrifugation (10 minutes, 12,000 RCF), gently re-suspended in 67 ml RF1 buffer (0.1 M RbCl, 50 mM $MnCl_2$, 30 mM potassium acetate, 10 mM $CaCl_2$, 15% (w/v) glycerol, pH 5.8) and incubated on ice for 15 minutes. The cells were centrifuged once more and the pellet resuspended in 15 ml of RF2 buffer (10 mM RbCl, 75 mM $CaCl_2$, 10 mM MOPS, 15% (w/v) glycerol, pH 6.8). The competent cells were flash frozen in liquid nitrogen in 200 μl aliquots and stored at -80 °C.

2.5 Transformation of competent *E. coli* cells

An aliquot of competent cells was thawed on ice for 10 minutes before 1-2 μL of plasmid DNA was added to 200 μl of cells. After incubation on ice for 30 minutes, the cells were subject to a heat shock for 90 seconds at 42 °C, then placed on ice for a further 2 minutes. 800 μl of sterile LB was added and the cells were incubated at 37 °C, 200 RPM for 1 hour, harvested by centrifugation (1 minute, 4000 RPM) and re-suspended in approximately 100 μL of LB and spread on a pre-warmed LB-agar plate with appropriate antibiotic. Colonies grew overnight at 37 °C.

2.6 Nucleic Acid Manipulation

2.6.1 Small scale purification of plasmid DNA (mini-prep)

Plasmid DNA was prepared by a Plasmid Mini Prep DNA purification kit (QIAgen, Crawley, UK) according to the manufacturers instructions. Transformed *E. coli* were grown overnight in 10 ml of LB medium with appropriate antibiotic selection at 37 °C, 250 RPM. Cells were harvested by centrifugation at 12,000 RCF, 4 °C. The yield was typically 5 μg plasmid DNA per mini-prep.

2.6.2 Site directed mutagenesis

Site directed mutagenesis of DNA plasmids was achieved using the Quickchange method (Aglient Technologies, Wokingham, UK). Reactions were performed in a total volume of 50 μl using 10× reaction buffer supplied, 125 ng of each primer, 2 mM dNTPs and 2.5

units of Pfu Ultra polymerase. Primers were produced by Invitrogen (Paisley, UK) and re-suspended in water to 100 ngμl^{-1}. 100 ng of DNA from either ChlI (pET9a-ChlI) or ChlD (pET9a-His$_6$ChlD) was used as template. Reactions were carried out with a modified cycle program from the manual. Primers were denatured for 30 seconds at 96 °C, followed by 20 cycles of amplification (96 °C, 30 sec; 55 °C, 1 min; 68 °C, 10 mins) with a final extension at 68 °C in a Techne TechGene thermal cycler. Following PCR, parental DNA was digested using dpn1 for 1 hour at 37 °C. Table 2.3 and Table 2.4 detail the primers used to make mutants of ChlI and ChlD.

Table 2.3: List of oligonucleotide primers used in site directed mutagenesis of ChlI

Mutation	Forward oligonucleotide	Reverse oligonucleotide
K53A	GCGATCGGGGAACCGGGGCATCCACTACCATTAGAG	CTCTAATGGTAGTGGATGCCCCGGTTCCCCGATCGC
E154Q	GCATTCTCTATGTGGACCAAGTTAACCTGTTGGAC	GTCCAACAGGTTAACTTGGTCCACATAGAGAATGC
R210A	GGCCTCAATTGTTGGATGCATTCGGCATGCATGCTG	CAGCATGCATGCCGAATGCATCCAACAATTGAGGCC
R210E	GGGAATTGCGGCCTCAATTGTTGGATGAGTTCGGCATGCATGC	GCATGCATGCCGAACTCATCCAACAATTGAGGCCGCAATTCCC
R291A	GCAGAACTTGATGTGGACGGGTTAGCGGGAGATATTGTTAC	GTAACAATATCTCCCGCTAACCCGTCCACATCAAGTTCTGC
R291M	GCAGAACTTGATGTGGACGGGTTAATGGGAGATATTGTTAC	GTAACAATATCTCCCATTAACCCGTCCACATCAAGTTCTGC
C121S	AACGGAAGACCGGGTGTCCGGCACCATCGACATCG	ATGTCGATGGTGCCGGACACCCGGTCTTCC
C244S	ATCCCCATCCTTTCTCTGACCAATATCAAACG	TTTGATATTGGTCAGAGAAAGGATGG
C282S	TGAAAGTATCGGAAGTCTCTGCAGAACTTGATGTGG	ACATCAAGTTCTGCAGAGACTTCCGATACTTTCACC
C324S	AGTAATTGTGCTTTCTTTACGCCATCG	ATGGCGTAAAGAAAGCACAATTACTCG

Table 2.4: List of oligonucleotide primers used in site directed mutagenesis of ChlD

Mutation	Forward oligonucleotide	Reverse oligonucleotide
K49A	GGCGGGGCACAGCCGCATCGGTCATGGCTA	TAGCCATGACCGATGCGGCTGTGCCCCGCC
E152Q	GGGGTGCTGTACATTGACCAGTTGAATTTACTGGATG	CATCCAGTAAATTCAACTGGTCAATGTACAGCACCCC
R208A	GTCGCCATTTATTGGACGCCATTGCGATCGCCTTGA	TCAAGGCGATCGCAATGGCGTCCAATAAATGGCGAC
R208E	GCGTCGCCATTTATTGGACGAGATTGCGATCGCCTTGAG	CTCAAGGCGATCGCAATCTCGTCCAATAAATGGCGACGC
R289A	CGGCCTCCAGGGCCATGCGGGAGAATTGTTT	AAACAATTCTCCCGCATGGCCCTGGAGGCCG
R289M	GCGGCCTCCAGGGCCATATGGGAGAATTGTTTG	CAAACAATTCTCCCATATGGCCCTGGAGGCCGC
C73S	AACCGTTACCAATCCGATCCAAAAAATCC	ATTTTTTGGATCGGATTGGTAACGGTTGC
C186S	TTTCAGCATCCCTCCCAGCCTTTATTAATTGC	AATTAATAAAGGCTGGGAGGGATGCTG
C550S	AAACTTTGCCCTCTGGCGGTGGTTCTCC	AGAACCACCGCCAGAGGGCAAAGTTTCC

2.6.3 Agarose gel electrophoresis of DNA

PCR and purified DNA fragment were routinely analysed by electrophoresis in 0.6% agarose gels in 1× TAE (40 mM Tris-acetate, 1 mM EDTA) running buffer containing SYBR Safe stain (Invitrogen). 6× gel loading buffer (New England Biolabs) was added to DNA samples, and between 10 - 500 ng of DNA was typically loaded per lane. 200 ng of 1 kb DNA ladder (New England Biolabs, Hitchin, UK) was run as a marker to estimate the sizes of DNA fragments. DNA was visualised using a blue safe light through an orange filter.

2.6.4 DNA Sequencing

Plasmid DNA required for sequencing was transformed into *E. coli* JM109 cells and DNA purified as above. Samples of 10 ngμl^{-1} were sequenced by the University of Sheffield Core Genomics facility in the Medical School. Custom primers required for sequencing were supplied by Invitrogen. Results were analysed using FinchTV (Geospiza, Seattle, WA, USA) and Serial Cloner (Serial Basics, France) software.

2.7 Protein concentration

2.7.1 UV absorbance

The concentration of protein by UV was determined by entering the sequence into the Prot Param program (65) and using the calculated extinction coefficient at A_{280}. If the protein solution was heavily contaminated with nucleotide (peak at 260 nm), then a Bradford assay as detailed in section 2.7.2 was used to confirm protein concentration.

2.7.2 Bradford assay

Concentrations of proteins were also determined using the Bradford assay (Sigma-Aldrich) in accord with the manufacturers instructions. Bovine serum albumin (BSA) was used to obtain a standard curve.

2.8 Protein Expression in *E. coli*

2.8.1 Standard Auto-inducing Protein Expression (ChlH, ChlI, BchI)

Plasmid DNA containing the pET9a-based vectors were transformed into *E. coli* strain BL21(DE3). Resulting transformants were grown initially in starter cultures overnight at 37 °C, 250 RPM and then in 500 ml of ZYM-5052 (81) at 200 RPM, 25 °C for 20 hours. Cells were harvested by centrifugation (14,000 RCF, 4 °C, 20 minutes) and stored at -80 °C.

2.8.2 Protein overexpression in Rosetta strain (ChlD, ChlI mutants, ChlD mutants)

Plasmid DNA containing the pET9a-based vectors were transformed into *E. coli* Rosetta strain. Resulting transformants were grown initially in starter cultures overnight at 37 °C, 250 RPM and then in 500 ml of 2xLB (20 gl^{-1} Tryptone, 10 gl^{-1} Yeast extract, 10 gl^{-1} NaCl) at 250 RPM, 37 °C for 6 hours (OD_{600} generally 0.8-1 at this point). Induction was achieved by the addition of Isopropyl -D-1-thiogalactopyranoside (IPTG) to a final concentration of 0.4 mM and cells grown for a further 10 hours at 18 °C, 200RPM. Cells were harvested by centrifugation (14,000 RCF, 4° C, 20 minutes) and stored at -80 °C.

2.9 SDS-polyacrylamide gel electrophoresis (SDS-PAGE)

Protein samples were separated by SDS-polyacrylamide gel electrophoresis using the buffer system of Laemmli (82), and the protocol as detailed in Sambrook *et al* (79). A 5% stacking gel and 8, 10 or 12% separating gel were used unless stated otherwise. All samples were heated to 75 °C for 10 minutes with β-mercaptoethanol. 1 – 10 μl were loaded per well. Protein bands were visualised with Invitrogen Safety Stain (Invitrogen). Precision Plus Protein Standards 20 – 250 kDa (Bio-Rad) were used as molecular weight markers.

2.10 Protein Purification

2.10.1 Purification of His_6-tagged proteins

1 l of cell culture was combined and harvested by centrifugation at 14,000 RCF for 20 minutes and cells resuspended in 10–20 ml chilled binding buffer (50 mM Tricine/NaOH, 0.5 M NaCl, 0.3 M Glycerol, 10 mM imidazole, 1 mM AEBSF, pH 7.9). Cells were disrupted on ice with sonication for 3 × 15 seconds with 1 minute gaps (Soniprep 150, MSE), and cell debris removed by centrifugation at 40,000 RCF for 40 minutes at 4 °C. The supernatant was then filtered through 1.2 μM and .22 μM syringe filters, and loaded at 0.5 mlmin^{-1} onto a Ni(II) HisTrap HP HiTrap column (GE Healthcare) pre-equilibrated with 3 volumes of binding buffer. The column was washed with 10 volumes of 15 mM imidazole, and an elution gradient of 15 to 250 mM imidazole run over 20 column volumes. Eluted proteins were detected via UV at 280 nm and fractionated. Fractions containing protein were checked by SDS-Page. Protein was further purified by anionic ion exchange chromatography (see section 2.10.2).

2.10.2 Purification of non-tagged proteins

Anionic ion-exchange chromatography using a 10 cm^3 Q-sepharose column was performed as described by Reid (76) using gradient elution between two buffers: Buffer A, 50 mM Tricine/NaOH, 0.3 M Glycerol, 1 mM DTT, pH 7.9; Buffer B, 50 mM Tricine/NaOH, 0.3 M Glycerol, 1 M NaCl, 1 mM DTT, pH 7.9. Each subunit was loaded onto the column pre-equilibrated in buffer A and washed until the UV peak had decreased to approximately baseline levels. Bound proteins eluted using a linear gradient of 0 – 80% B over 150 ml. ChlI, ChlD and ChlH all elute at approximately 0.4M NaCl. Protein elution was monitored at 280 nm using the UPC-900 on an Äkta FPLC. Protein was further purified as in section 2.10.3.

2.10.3 Further polishing purification by anion-exchange

Proteins to be monitored with regards to the intrinsic ATPase activity were further purified to remove any potential highly active ATPase contaminants. Protein fractions from section 2.10.2 were diluted with an equal volume of buffer A and applied to a 5 cm^3 Source15Q column pre-equilibrated in 25 ml of buffer A. The column was washed

with 20 ml of buffer A and then a linear gradient applied over 60 ml from 0 – 80 % buffer B. Proteins eluted at approximately 0.3M NaCl.

2.10.4 Further purification by gel filtration

ChlI subject to EM, X-ray crystallography study and ChlI subject to steady state kinetic analysis were further purified by gel filtration. Approximately 2 ml of protein was applied to a 320 ml Sephadex 200 column pre-equilibrated with buffer A and eluted at 0.5 mlmin^{-1}. Protein fractions eluted at *ca.* 180 ml were aliquoted and stored at -80 °C.

2.11 Substrate preparation

2.11.1 Porphyrin preparation

Approximately 5 mg of deuteroporphyrin IX (D_{IX}) or magnesium deuteroporphyrin IX (MgD_{IX}) was dissolved in chelatase buffer (50 mM MOPS/KOH, 0.3 M Glycerol, 1 mM DTT, pH 7.9). This solution was vortexed for 1 minute and centrifuged at 13,200 RCF for 1 minute to remove insoluble aggregates. This photosensitive solution was transferred to a black microcentrifuge tube. Porphyrin concentration was determined by instantaneous conversion to free base in 0.1 M HCl using the extinction coefficient (ε_{399} =433000 $\mathrm{M}^{-1}\mathrm{cm}^{-1}$) from Falk (7).

2.11.2 ATP and ADP preparation

Approximately 300 mg of adenosine 5'-triphosphate disodium salt (ATP) or adenosine 5'-diphosphate disodium salt (ADP) were dissolved in 10 ml of Milli-Q water and the pH adjusted to 7 using NaOH. The concentrations of solutions were determined in water using the extinction coefficient (ε_{259} =15400 $\mathrm{M}^{-1}\mathrm{cm}^{-1}$) from Engel (83).

2.12 Steady-state assays of Magnesium Chelatase

Assays were carried out in chelatase buffer (50 mM MOPS/KOH, 0.3 M glycerol, 1 mM DTT, pH 7.7) at 34 °C and fixed ionic strength $I = 0.1$ with KCl, in a total volume

of 100 μl. A BMG LabTech Fluostar Optima microplate reader (Aylesbury, UK) with excitation through a 420± 5 nm and emission 580± 5 nm filter was used to detect the production of product MgD_{IX} over a period of one to two hours. Protein concentrations used were 0.1 μM ChlD, 0.1 μM ChlI, 0.4 μM ChlH and substrate concentrations were 5 mM $MgATP^{2-}$, 10 mM free Mg^{2+} and 8 μM D_{IX}, except where stated otherwise. The maximum rate observed was taken as the steady state rate, which occurred approximately 10 minutes after an initial lag phase. Known concentrations of MgD_{IX} in chelatase buffer and containing enzyme were analysed to produce a second order polynomial calibration curve.

Steady state rates (ν_{ss}) were calculated from the chelatase progress curves using Optima MARS data analysis suite (version 2.20) included with the microplate reader, fitting to a linear slope over 10 minutes after the initial lag period. All kinetic constants were plotted against substrate concentrations and these data fitted to equations through unweighted nonlinear regression using Igor Pro 6.2 (Wavemetrics Inc. Lake Oswego, OR, USA).

2.13 Steady-state assays of ATP hydrolysis

Assays were carried out in chelatase buffer (50 mM MOPS/KOH, 0.3 M glycerol, 1 mM DTT, pH 7.7) at 34 °C and fixed ionic strength I =0.1 with KCl, with 2 U of Pyruvate Kinase (PK) and Lactate dehydrogenase (LDH), 2 mM phosphoenolpyruvate (PEP) and 200 μM NADH, in a total volume of 200 μl. A BMG LabTech Fluostar Optima microplate reader in absorbance mode with a 340± 5 nm filter was used to detect the decrease in absorbance of NADH. Protein concentrations used were 1 μM ChlD, 1 μM ChlI and substrate concentrations were 5 mM $MgATP^{2-}$ and 10 mM free Mg^{2+}, except where stated otherwise. The maximum rate was taken as the steady state rate after ATP injection. Known concentrations of NADH within chelatase buffer were analysed to produce a linear calibration curve.

Steady state rates (ν_{ss}) were calculated from the ATPase progress curves using Optima MARS data analysis suite (version 2.20) included with the microplate reader, fitting the linear decrease in absorbance observed after the addition of ATP to the

system. All ν_{ss} were plotted against substrate concentrations and these data fitted through unweighted non-linear regression using Igor Pro 6.2.

2.14 Data analysis methods

All data analysis was performed using Igor Pro 6.2.

The Michaelis-Menten equation (equation 2.1), where ν_{ss} is the steady state rate, ν_{max} the maximum rate, [S] the concentration of substrate under investigation and K_m the Michaelis constant for the substrate.

$$\nu_{\mathrm{ss}} = \frac{(\nu_{\mathrm{max}} \cdot [\mathrm{S}])}{(K_m + [\mathrm{S}])} \tag{2.1}$$

The Hill Equation where n is the Hill coefficient and $s_{0.5}$ is the substrate concentration where half maximal activity is observed (equation 2.2).

$$\nu_{ss} = \frac{(\nu_{max} \cdot [S]^n)}{(s_0.5^n + [S]^n)} \tag{2.2}$$

Errors in fitted parameters were propagated using equation 2.3.

$$\left(\frac{\sigma_f}{f}\right)^2 = \left(\frac{\sigma_A}{A}\right)^2 + \left(\frac{\sigma_B}{B}\right)^2 - 2\frac{\sigma_A \sigma_B}{AB}\rho_{AB} \tag{2.3}$$

2.15 Non-equilibrium Isotope Exchange assays on Magnesium Chelatase

Assays were carried out in 50 mM MOPS/KOH, 0.3 M glycerol, 1 mM DTT, pH 7.7 at 34 °C and fixed ionic strength I =0.1 with KCl, in a total volume of 100 μl. A cellulose

TLC plate was used to separate nucleotides using 0.8 M LiCl as the development solvent. Developed plates were exposed to phosphor imaging plates for time depending on the activity of the radioactive material present (from 10 minutes to 3 weeks), and visualised on a Fuji Film Phosphoimager (Bedford, UK) and data analysis performed using MultiGauge software package (version 2.2, Fuji). Protein concentrations were 0.1 μM ChlD, 0.2 μM ChlI, 0.4 μM ChlH and substrate concentrations were 5 mM $MgATP^{2-}$, 10 mM free Mg^{2+} and 8 μM DIX, except where stated. Samples were taken at 1– and 2– minute intervals up to 12 minutes and quenched with an equal volume of 100 mM EDTA, pH 10.0.

2.15.1 PnP/MES Assay

Standard magnesium chelatase assays were doped with 1 mM ADP, approximately 1 nM $^{32}P_{\alpha}ADP$ (40 μCi), 2U purine nucleotide phosphorylase (PNP) and 200 μM 7-methylguanosine (MES).

2.15.2 PK/LDH Assay

Assays were doped with 5 mM PO_4^-, approximately 1 nM $^{32}PO_4^-$ (40 μCi), 2 mM PEP, 200 μM NADH, 1 U pyruvate kinase (PK) and 2 U of lactate dehydrogenase (LDH).

2.16 Circular Dichroism Spectroscopy

CD spectra of proteins (0.1 $mgml^{-1}$) were recorded on a Jasco J-810 spectropolarimeter (Great Dunmow, UK) at 25 °C. All samples were in 50 mM Potassium phosphate buffer, pH 7.4. Buffer only measurements showed that this buffer did not mask the protein signal. Temperature ramps were run to determine melting temperature of proteins (T_m, from 5 – 95 °C monitoring CD at 222 nm, and the first derivative of the curve taken using the included software (Spectra Manager 2, version 2.09.01).

2.17 Pull Down assays

15 μM ChlD and ChlI were mixed with 40 μl Ni(II) chelating sepharose in the presence and absence of 5 mM ATP, 15 mM $MgCl_2$ in a total volume of 200 μl of 50 mM Tricine,

0.3 M Glycerol pH 7.9 at room temperature for 30 minutes. The resin was washed three times with their respective binding buffer and then 40 μl 2× SDS-PAGE loading buffer added directly to the resin and heated to 95 °C for 15 minutes. A 10 μl of sample was loaded onto SDS-PAGE for analysis.

2.18 Dynamic Light Scattering of Proteins

Proteins were concentrated to 10 mgml^{-1} using 30,000 MWCO spin concentrators (GE Healthcare) and then diluted into buffer A in the presence or absence of 5 mM ADP, 15 mM $MgCl_2$ to a final protein concentration of 5 mgml^{-1} and total volume of 100 μl. Samples were incubated at room temperature for 10 minutes then analysed using a Malvern Instruments Zetasizer Nano (Malvern, UK) assuming that water is a valid reference and settings set to automatic. Results were reported as particle size compared to intensity.

2.19 Conformational change detection via tryptophan fluorescence quenching

1 μM of protein in 50 mM MOPS/KOH, 0.3 M glycerol, 15 mM $MgCl_2$, 11 mM KCl, pH 7.7 34 °C was excited at 295 nm ± 1 nm, and emission monitored at 338 nm ± 5 nm using a Fluoromax 3 fluorometer (Horiba Jobin Yvon, Stanmore, UK) as the concentration of nucleotide was increased from 100 nM to 3 mM. Change in fluorescence was normalised to protein concentration and plotted against nucleotide concentration, and fitted to the single site binding equation 2.4 to obtain values for K_d for nucleotide.

$$f(s) = \frac{B_{\max} \times s}{K_\mathrm{d} + s} \tag{2.4}$$

2.20 Labelling proteins with fluorescent dyes

2.20.1 Large volume labelling with maleimide dyes

ChlI was equilibrated into thiol modification buffer (50 mM Tricine, 0.3 M Glycerol, 150 mM NaCl, pH 7.4) using G-25 resin. 5 mM ADP and 15 mM $MgCl_2$ were added

and incubated at room temperature for 5 minutes. 25 molar equivalents of maleimide dye dissolved in dimethylformamide was added to the solution and stirred for 2 hours at room temperature in the dark. The reaction was quenched with the addition of 10 mM DTT and then the mixture was loaded onto a G25 HiTrap column and equilibrated into standard binding buffer removing unreacted dye (50 mM Tricine, 0.3 M Glycerol, 1 mM DTT, pH 7.9). Further dialysis against standard binding buffer did not reduce or alter the absorbance spectrum of the protein. ChlI mutants (K53A, E154Q, R210A) were treated essentially the same as in section 2.20.1 but were conjugated with 25 molar equivalents of fluorescein-5-maleimide.

2.20.2 Small volume labelling

Protein (ChlI, ChlD) was re-equilibrated into thiol modification buffer using 30,000 MWCO spin concentrators. 20 μM of protein was incubated in buffer containing 5 mM ADP and 15 mM $MgCl_2$ for 10 minutes at room temperature before the addition of 10 molar equivalents of maleimide dye and incubated with nutating mixing for 2 hours before the reaction was quenched with the addition of 1 mM DTT and a further 5 minutes of incubation. Excess dye was removed via 7,000 MWCO Seba Spin Desalting columns (Thermo Scientific, Erembodegem, Belgium) following the manufacturers instructions.

2.21 Förster Resonance Energy Transfer

Assays were carried out in chelatase buffer (50 mM MOPS/KOH, 0.3 M glycerol, 1 mM DTT, pH 7.7) at 34 °C and fixed ionic strength I =0.1 with KCl, in a total volume of 1 ml using a Fluoromax 3 fluorescence spectrometer.

2.21.1 Interactions between ChlI WT and ATPase mutants

The emission spectra of approximately 1 μM of fluorescent-dye tagged mutant (K53A, E154Q, R210A) were measured in the presence of 1 μM ChlD, 5 mM ATP and 15 mM $MgCl_2$ with excitation at 470 nm and a 2 nm band gap. The concentration of fluorescently tagged mutant was held at $\sim$ 1 μM while the concentration of fluorescently tagged ChlI WT was increased in $\sim$ 1 μM amounts. Each preparation was incubated at 34 °C for 5 minutes before spectra were recorded.

2.21.2 Peak Fitting

Peaks in the emission spectra from FRET experiments were fitted using an exponentially modified gaussian curve (a convolution of a gaussian with an exponential decay) using the Multipeak 2.0 fitting routine in Igor Pro 6.2 (Wavemetrics). The equations are summarised (equations 2.5 and 2.6), where t is the gaussian mean, s is gaussian sigma and r is the Regularised gamma function $r = \Gamma_p(t)$:

$$f(t) = \frac{(1+r)}{2} \tag{2.5}$$

$$y = r \cdot e^{\left(-r \cdot t + s^2 \cdot \frac{r^2}{2}\right)} \cdot f(t) \cdot \left(\frac{t}{s} - s \cdot r\right) \tag{2.6}$$

2.22 Analytical Size exclusion chromatography

2.22.1 Preparative Scale

Chromatography was performed in 50 mM Tricine/NaOH, 0.3 M Glycerol, 1 mM DTT, 5 mM ADP, 15 mM $MgCl_2$ pH 7.9 at room temperature using a Superdex 200 column (GE Healthcare) coupled to a DAWN EOS Multi-angle Light Scattering instrument and Optilab rEX refractive index detector (Wyatt Technologies, Santa Barbara, CA, USA).

2.22.2 HPLC scale

Samples were purified on a Biosep S4000 HPLC gel filtration column using gel filtration buffer (50 mM Tricine/NaOH, 0.3 M glycerol, 1 mM DTT, pH 7.9 34 °C) on an Agilent 1200 HPLC system with multi-diode array UV detection and single wavelength fluorescence detection. Fractions were taken of peaks and used for electron microscopy and SDS-Page analysis.

2.23 Analytical Ultra centrifugation

Sedimentation velocity analytical ultra centrifugation was performed in 50 mM Tricine/NaOH, 0.3 M Glycerol, 1 mM DTT, 5 mM ADP, 15 mM $MgCl_2$ pH 7.9 at room temperature

using a XL-A Analytical Ultracentrifuge (Beckman, High Wycombe, UK) detecting protein labelled with fluorescein-5-maleimide at 497 nm. The sample was centrifuged at 27,000 RPM with 200 scans taken at 4– minute intervals. Data were analysed using Proteomelab XL-A (Beckman).

2.24 Surface modification with Ni-NTA

A glass coverslip was prepared for modification by cleaning with Piranha solution (3:1 concentrated sulfuric acid : 30 % Hydrogen Peroxide), rinsed with water, followed by the RCA (Radio Corporation of America) cleaning process (84), rinsed with water and finally dried *en vacuo* under heat. The substrate was immersed in a 0.1% solution of (3-aminopropyl)triethoxysilane for 30 minutes and then washed with toluene, a 50:50 solution of toluene and ethanol, ethanol and then sonicated in ethanol. The substrate was then dried *en vacuo* for 30 minutes. The surface was functionalised with a 12% solution of glutaraldehyde for 20 minutes, and rinsed with ethanol. A 200 μM solution of Ni-NTA conjugate in water was applied to the substrate for 2 hours and then washed with ethanol. Unreacted glutaraldehyde was blocked with 0.5 mM n-butylamine in ethanol for 1 hour and then washed with ethanol and dried with nitrogen.

2.25 Binding Proteins to a surface

Ni-NTA surfaces were charged with Ni^{2+} using 100 mM $NiSO_4$ and washed three times with d.d. distilled water. Three volumes of non-thiol containing surface buffer (50 mM MOPS/KOH, 0.3 M Glycerol, 5 mM nucleotide (ADP or ATP), 15 mM $MgCl_2$, was washed onto the surface three times to equilibrate the surface. Proteins solutions of $\sim$ 0.1 μM were incubated in surface buffer for 10 minutes then rapidly diluted to concentrations of between 10 and 0.1 nM and washed onto the surface for 30 seconds.

2.26 Confocal Microscopy of Proteins

Images were obtained using a Zeiss LSM 510 Meta inverted confocal microscope (Cambridge, UK) and 40x/1.30 Oil Immersion lens, with a pixel dwell time of 27.2 μs. Pixel size was 0.11 μm.

Tetramethylrhodamine-5-maleimide was excited using a laser wavelength 543 nm laser (80% transmission) and emission detected between 565 – 615 nm of light detected as a result of filter used.
Fluorescein-5-maleimide was excited using a laser wavelength 488 nm laser (6% transmission) and emission detected between 500 – 550 nm of light detected as a result of filter used.

3

The ATPase cycle of magnesium chelatase proceeds through an Enzyme-phosphate complex.

3.1 Introduction

Isotope exchange techniques use isotopically labelled substrates or products to follow enzyme catalysed reactions; the benefit of these techniques is that the flux through a segment of the reaction can be isolated from the rest of the reaction pathway. Isotopic flux can be followed even when unlabelled components are at equilibrium or when the flux of unlabelled and labelled component are moving in alternative directions.

In group transfer reactions, isotope exchange can be used to measure the flux between all substrates of an enzyme, explaining in detail the order of substrate binding and release (85). In simple kinetic mechanisms, the order of substrate binding and product release can often be revealed through initial rate experiments in the forward and backward directions. In complex systems, steady-state kinetics can be ambiguous and in cooperative systems, uninterpretable. Isotope exchange offers independent evidence for specific enzyme-intermediate complexes (86). Analysis of exchange at equilibrium is well established (86), but these methods are not well suited to enzymes, like magnesium chelatase, that operate far from equilibrium.

3.1.1 Non-equilibrium isotope exchange

The isotope flux equations for reactions far from equilibrium are exceptionally complicated, so the method is not suited to determining rate constants. Isotope exchange under non-equilibrium conditions remains useful as the method offers an approach to reveal specific enzyme-product complexes.

Non-equilibrium exchange from labelled product to substrate can be used to determine the order of product release and provides evidence that specific enzyme product complexes exist on the reaction pathway. If in an ordered release mechanism (scheme 3.1) radiolabelled **P*** is introduced in the absence of **Q** (removed from the system using auxiliary enzymes), the two pathways can be distinguished.

If the enzyme follows route 2 then radiolabelled **P*** can react with the **EQ** complex to produce radiolabelled substrate. However if the enzyme releases **Q** as the first prod-

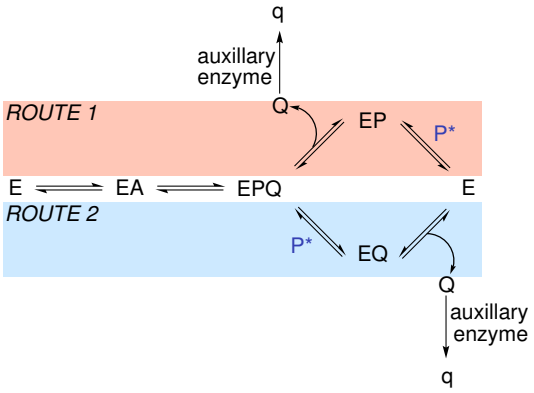

Scheme 3.1: A reversible fragment of an enzyme reaction where the product **P** is radiolabelled (**P***), and the auxiliary enzyme converts all product **Q** to a compound **q** which is unable to bind to the EP complex.

uct, then no radiolabelled **A** will be detected as there is no reversible path connecting **P*** to **A**.

As both mechanisms allow products in solution to react to give substrate, the unlabelled product has to be removed from the system to prevent the in solution back-reaction. This can be conveniently achieved through the use of auxiliary enzymes to remove the unlabelled product.

Previous examples of non-equilibrium isotope exchange to determine product release order in enzyme pathways are described in the following references (87, 88, 89, 90).

3.1.2 The mechanism of ATP hydrolysis catalysed by ChlI.

ATP hydrolysis catalysed by ChlI drives magnesium ion insertion. The rate of magnesium ion insertion with respect to the concentration of $MgATP^{2-}$ has been reported (76), and the nucleotide bound states are likely to be intimately involved in the coordinating events that lead to magnesium ion insertion.

Non-equilibrium isotope exchange allows us to detect the formation of short-lived complexes or difficult to detect species, showing the path of ATP hydrolysis in the

active site of magnesium chelatase.

ADP to ATP exchange has previously been shown to be catalysed by *Synechocystis* ChlI (61) but in this work the auxiliary enzyme purine nucleotide phosphorylase (PNPase) was not present to remove free phosphate. As a consequence, this experiment could not distinguish between the reaction of Pi from solution and reaction of an enzyme-phosphate complex; they came to no conclusion on the origin of the observed exchange. The authors results also showed no exchange was catalysed by ChlH or ChlD, consistent with the data presented here. They did not assess the exchange in the presence of a complete set of subunits and a functioning magnesium chelatase assay. They concluded that phosphate transfer was unlikely to be related to a covalent phosphoenzyme intermediate because ChlI did not incorporate ^{32}P when incubated with ^{32}PγATP (2).

Isotope exchange studies on the AAA$^+$ protease Lon attempted to observe ^{18}O incorporation into phosphate found that ATP hydrolysis was irreversible (91). Lon is a hexamer, with an ATPase and protease domain in each subunit. In this protein, ATP hydrolysis is used to power the unfolding of protein substrates. ATP hydrolysis may be irreversible as it is tightly coupled to protein unfolding and hydrolysis.

Other AAA$^+$ enzymes including MgsA (92) and Dyenin (93) have been crystallised with tetrahedral anions within the AAA$^+$ active site (figure 3.1). In the MgsA structure the ion is assigned as phosphate, while in dyenin the anion is assigned as sulfate due to the high sulfate concentration used in the crystallisation conditions. The radius of the two ions is very similar (218 pm for sulfate compared to 230 pm for phosphate (94)), so the anion within dyenin may be phosphate. Alternatively, sulfate could be binding as a phosphate mimic. In both cases these tetrahedral anions are bound to the lysine in the Walker A motif. Crystallographic evidence supports enzyme-phosphate complexes in the ATPase sites of AAA$^+$ enzymes.

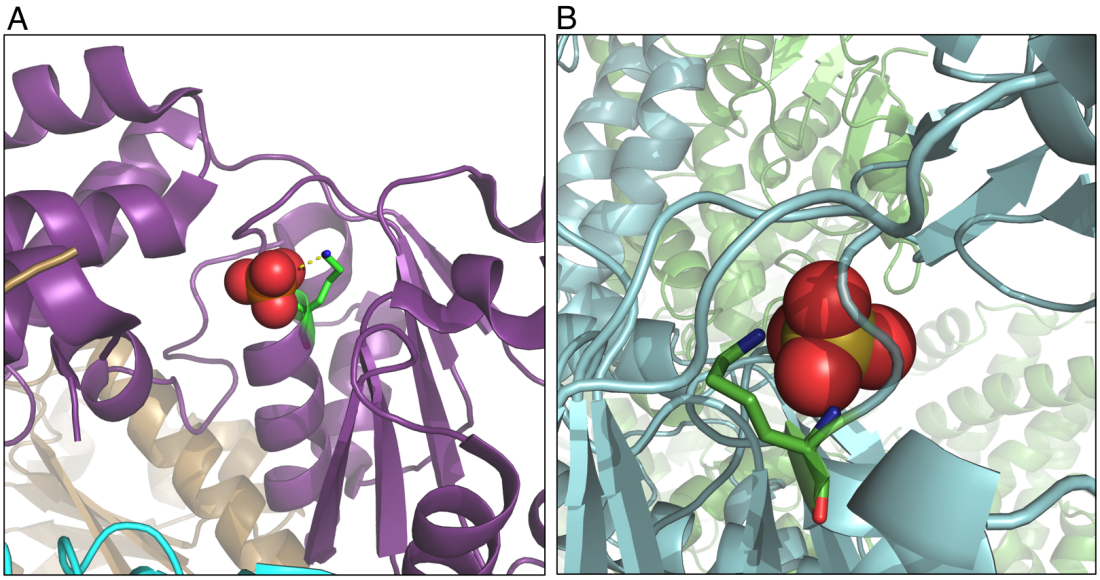

Figure 3.1: Tetrahedral anions in non-covalent interactions with Walker A lysine - A) Walker A motif of the AAA^+ protein MgsA (PDB code 3PVS, resolution 2.5 Å) showing gross protein structure in cartoon, Walker A lysine in sticks and PO_4^- in red spheres. **B)** Walker A motif of the AAA^+ protein Dyenin (PDB code 4AI6, resolution 3.4 Å), presentation as before. Structures were rendered using PyMol (41).

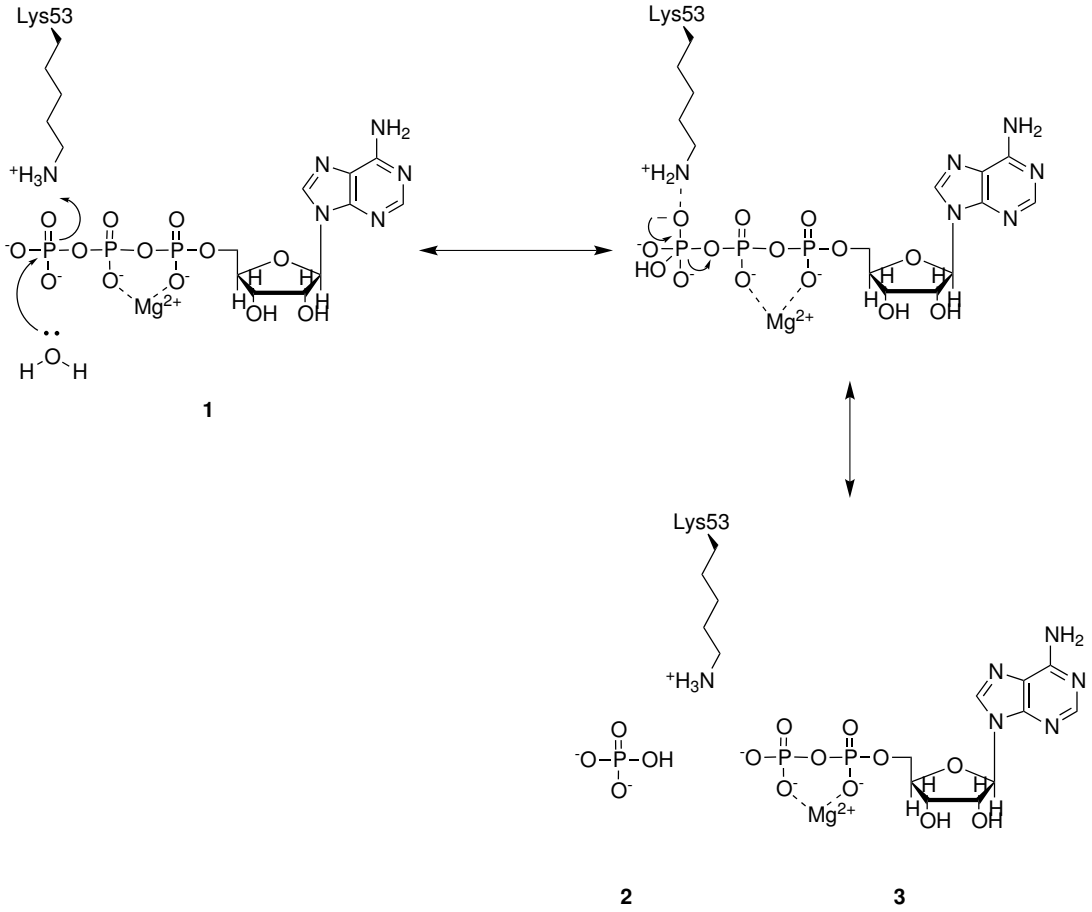

.

Scheme 3.2: A proposed mechanism for the hydrolysis of ATP (**1**) proceeds via a nucleophilic water molecule in the active site attacking the γ–phosphorus, with the transition state stabilised by the Walker A Lysine. On the collapse of the high energy intermediate, the γ–phosphate (**2**) is released, leaving radiolabelled ADP (**3**). As proposed by Thomas *et al* (91)

3.2 Results and discussion

3.2.1 Detecting an enzyme-phosphate complex in the ATP hydrolysis pathway of magnesium chelatase

To determine if an enzyme-phosphate complex exists, we added product (radiolabelled ADP) to an assay, in the presence of auxiliary enzymes to remove free phosphate. If labelled ATP is detected we can conclude that the enzyme follows an E.Pi pathway (scheme 3.3).

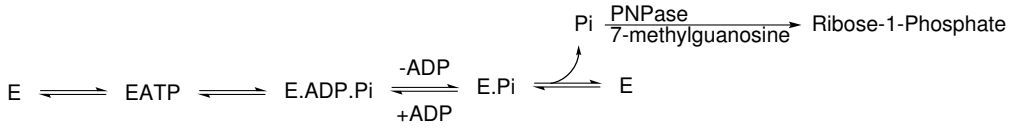

Scheme 3.3: ATP pathway of magnesium chelatase (**E**) where it moves through a **EPi** complex. By adding radiolabelled ADP and formation of radiolabelled ATP will indicate the presence of the EPi complex.

Assays were performed in the presence of purine nucleotide phosphorylase (PNPase) and 7-methyl guanosine (MEG) (reaction scheme 3.4). This auxiliary enzyme removes free phosphate from solution, preventing reaction with the ^{32}PαADP. Any radiolabelled ATP has to be formed by the reaction of an enzyme-phosphate complex and not via the reaction of ADP and Pi from solution.

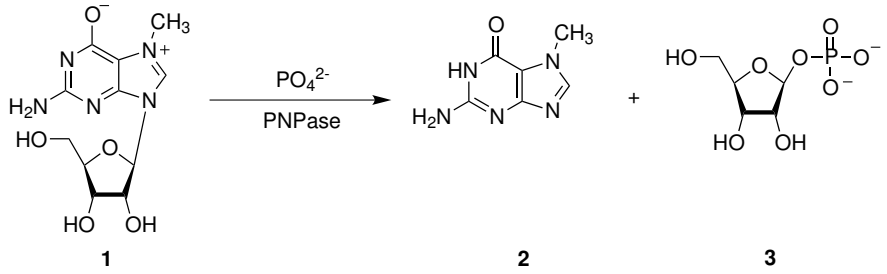

Scheme 3.4: Reaction catalysed by PNPase in the presence of free phosphate and 7-methylguanosine (**1**) leading to the products 7-methylguanine (**2**) and Ribose-1-Phosphate (**3**).

A chelatase assay (5 mM ATP, 15 mM $MgCl_2$, 50 mM MOPS/KOH, 0.3 M glycerol pH 7.7 34 °C) was doped with 40 μCi of $^{32}P\alpha$ADP. Radiolabelled ATP synthesised during the assay was detected and quantified using densitometry of cellulose thin layer chromatography (TLC) plates using a solvent system (0.9 M LiCl) which separates nucleotides. Table 3.1 summarises the results. The rate of exchange was taken from the linear progress curve during the first 15 minutes of the reaction. There was no change in rate when the amount of coupling enzyme was doubled.

Table 3.1: ADP to ATP exchange catalysed by magnesium chelatase in 50 mM MOPS/KOH, 0.3 M glycerol, 5 mM ATP, 1 mM ADP, 15 mM $MgCl_2$ 2 mM KCl 2U PNPase, 200 μM MES pH 7.7 (Assays with porphyrin were 8 μM (deuteroporphyrin IX (D_{IX})) Enzyme concentration was 2 μM ChlI, 2 μM ChlD, 4 μM ChlH for assays 1 – 4, and 1 μM ChlI, 1 μM ChlD, 4 μM ChlH for assays 5 and 6. Rates normalised by concentration of ChlI

Assay	**Protein**	v_i / **[ChlI]** $[\alpha$-$^{32}P]ADP \rightarrow [\alpha$-$^{32}P]ATP
1	ChlI	0.52 ± 0.09 min^{-1}
2	ChlD	not observed
3	ChlH	no observed
4	ChlID	0.19 ± 0.04 min^{-1}
5	ChlIDH	0.96 ± 0.15 min^{-1}
6	ChlIDH + porphyrin (D_{IX})	1.44 ± 0.05 min^{-1}

Exchange studies can be compromised by low concentrations of highly active contaminating proteins, in the case of nucleotide exchange, the protein adenylate kinase (ADK) (95, 96, 97) can provide an alternative pathway for the synthesis of radio-labelled ATP and AMP via two molecules of radio-labelled ADP. The use of the alpha labelled ADP meant that any AMP formed by adenylate kinase would also be radio-labelled and thus observed. No AMP was detected. The addition of the adenylate kinase inhibitor P^1,P^5-di(adenosine-5') pentaphosphate (AP_5A) (98) did not alter the rate of radio-labelled ATP formation.

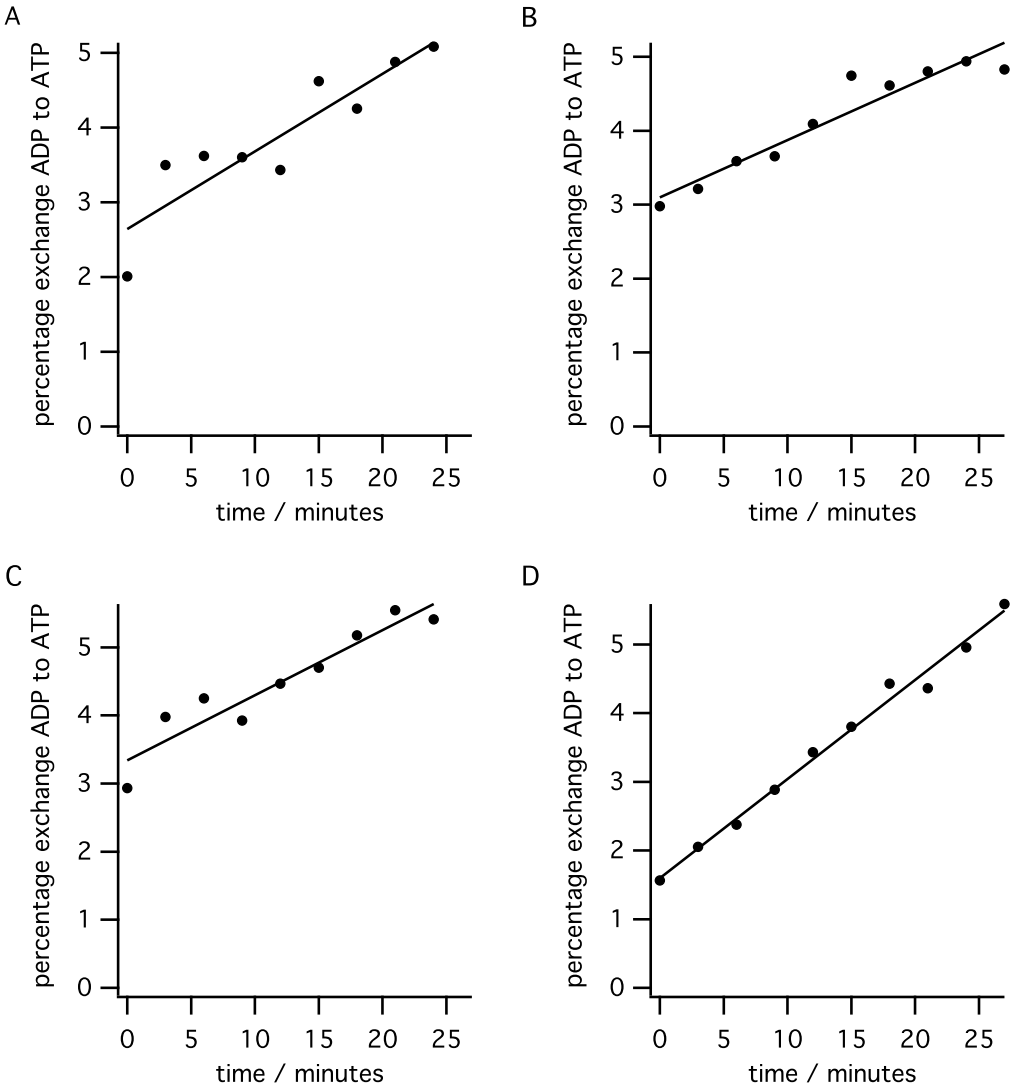

Figure 3.2: Time course of isotope exchange from ^{32}PαADP to ^{32}PαATP - A, ChlI; **B**, ChlID; **C**, ChlIDH - D_{IX}; **D**, ChlIDH + D_{IX}. Conditions shown in table 3.1

The conclusion drawn is that the radio-labelled ATP detected must be formed via enzyme-phosphate complex.

3.2.2 MgADP binds to magnesium chelatase, and inhibits magnesium ion insertion

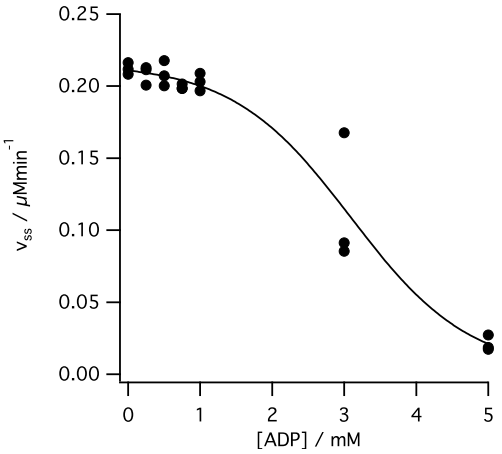

Figure 3.3: ADP Inhibition of steady state rates of Mg^{2+} chelation. - Assays performed in 5 mM ATP, 10 mM free Mg^{2+}, 50 mM MOPS/KOH, 0.3 M glycerol, 1 mM DTT , $I = 0.1$, 8 μM D_{IX}, pH 7.7, 34 °C, with 0.1 μM ChlD, 0.2 μM ChlI and 0.4 μ ChlH. The line is empirical.

In steady state assays ADP inhibits the magnesium chelatase activity (figure 3.3).

Binding titrations between ChlI and nucleotide found that both ATP and ADP bind to the enzyme with similar K_d. The ATP binding titration should be treated with caution as ATP will be hydrolysed, and as such a mixture of ATP and ADP will be formed on ChlI. The binding titration data was fitted to the one site binding model shown in equation 2.4.

The inhibition studies show that $MgADP^-$ binds the chelatase. ChlI is known to bind $MgADP^-$ and this binding has been used to characterise interactions with ChlD (59), low resolution structural work (67) and within this work (see sections 5.2.2.1 and

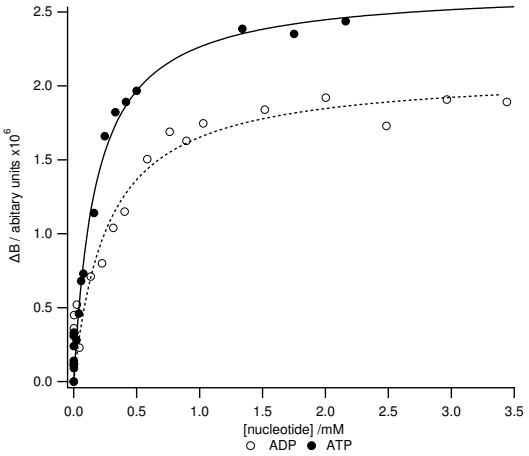

Figure 3.4: Binding titration of nucleotide with ChlI - Binding titration monitoring tryptophan fluorescence quenching (λ_{ex} = 295 ± 1 nm, λ_{em} = 388 ± 5 nm) with 1 μM ChlI in 50 mM MOPS/KOH, 0.3 M glycerol, 1 mM DTT, 15 mM $MgCl_2$ pH 7.7 34°C. Closed circles - ATP, K_{d} = 0.18 ± 0.03 mM; Open circles - ADP K_{d} = 0.27± 0.06 mM. Line is theoretical, and described by the single site binding model equation 2.4.

5.2.6.2). This Enzyme-ADP complex may be a dead end complex unable to chelate magnesium ions, and not on the pathway for ATP hydrolysis required for activity of the enzyme.

3.2.3 No catalytically competent enzyme-ADP complex is detected on the ATP hydrolysis pathway.

Magnesium chelatase catalyses ATP hydrolysis through an enzyme-phosphate complex. If the enzyme releases products in a random order, then an enzyme-ADP complex could also feature on the hydrolysis pathway. Isotope exchange experiments were performed with ^{32}Pi to detect catalytically competent enzyme-ADP complexes.

To measure magnesium chelatase catalysed exchange of radiolabelled Pi to ATP, a magnesium chelatase assay (5 mM ATP, 15 mM $MgCl_2$, 50 mM MOPS/KOH, 0.3 M glycerol pH 7.7 34 °C, 8 μM D_{IX}, 10 mM Potassium Phosphate, with 2 units of PK and LDH and 200 μM NADH and 2 mM Pyruvate) was doped with 40 μCi of ^{32}Pi. The PK/LDH system prevented free ADP and Pi in solution forming radio-labelled ATP.

Table 3.2: Pi to ATP exchange catalysed by magnesium chelatase in 50 mM MOPS/KOH, 0.3 M glycerol, 5 mM ATP, 1 mM ADP, 15 mM $MgCl_2$ 2 mM KCl 2U PK/LDH, 200 μM NADH, 2 mM PEP pH 7.7 (Assays with porphyrin were 8 μM (deuteroporphyrin IX (D_{IX})), protein concentrations of 0.2 μM ChlI, 0.1 μM ChlD, 0.4 μM ChlH.

Protein	v_i / **[ChlI]** ^{32}Pi – [γ-^{32}P]ATP
ChlI	Not quantifiable (< 1%)
ChlD	Not observed
ChlH	Not observed
ChlID	Not observed
ChlIDH + porphyrin	Not observed

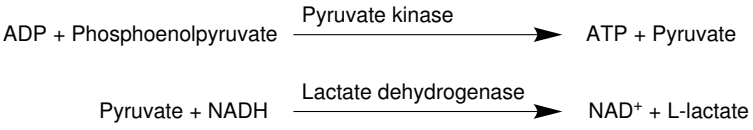

Scheme 3.5: The reaction of PK/LDH for sequestering free ADP

ATP formed from radiolabelled phosphate was quantified via densitometry. There was no quantifiable exchange (table 3.2). ChlI catalysed an unquantifiably small exchange. No other enzyme complexes catalysed a phosphate to ATP exchange.

ChlI can hydrolyse ATP via a pathway allowing formation of an unquantifiable amount of radio-labelled ATP, through a reaction between radio-labelled phosphate and ADP on enzyme. Magnesium chelation requires all three proteins (ChlI, ChlD and ChlH) be present. The full chelatase system does not produce radio-labelled ATP from ^{32}Pi. When ATP hydrolysis is coupled to metal ion insertion there is no detectable enzyme-ADP complex.

Phosphate does not inhibit magnesium chelatase (figure 3.5). Lack of inhibition by phosphate suggests that phosphate binding is weak, and therefore, it would be difficult

to see exchange with an enzyme-ADP complex.

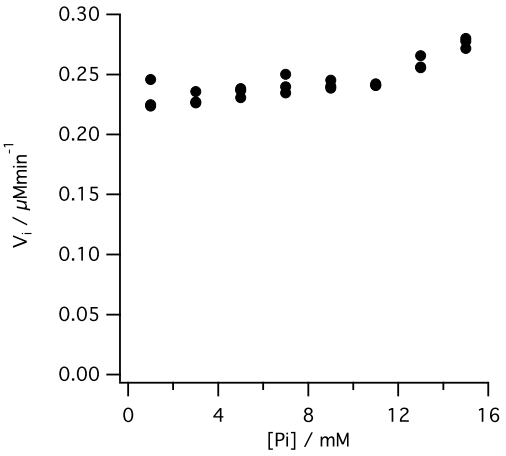

Figure 3.5: Pi inhibition of magnesium chelatase - An increasing concentration of free phosphate does not inhibit the initial rate of magnesium chelatase.

3.3 Conclusion

Magnesium chelatase couples ATP hydrolysis with magnesium ion chelation into the porphyrin ring. The primary route via an enzyme-phosphate complex is proposed.

Although this work provides no evidence for a catalytically significant E.ADP complex, this does not mean the complex does not exist. Two conditions could prevent ADP to ATP exchange occurring. Firstly, if the product binds too weakly, the exchange may not proceed at any appreciable rate. This condition may apply to magnesium chelatase as phosphate in the assay solution up to 16 mM does not inhibit the reaction (figure 3.5), demonstrating that phosphate binding to the enzyme is weak.

Secondly, there may be an irreversible conformational change occurring between the E.ATP to E.ADP complexes, so that even in the presence of excess phosphate, ATP is not formed. This could occur due to a large conformational change in the ATPase reaction cycle. For example if the phosphate binding residue moves away from the ADP binding site during the large conformational changes observed through the sequence of

ATP binding and hydrolysis as seen in the ChlI subunit of *R. sphaeroides* magnesium chelatase (67). There is a large body of evidence to suggest that ADP does bind to ChlI and causes conformational change (60, 67, 78).

These experiments provide evidence that the ATPase sites in magnesium chelatase proceed through an enzyme-phosphate complex and provide no evidence for an enzyme-ADP complex (scheme 3.6). The exchange results for ChlI demonstrates a AAA^+ protein forming this enzyme-phosphate complex under *in vitro* catalytic conditions.

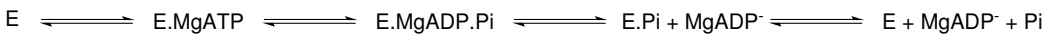

Scheme 3.6: Potential sequence of ATP hydrolysis on ChlI - The ordered release of products from an enzyme catalysed ATP hydrolysis proceeding via an enzyme-phosphate complex with ADP acting as a dead end inhibitor. The reaction of enzyme-ADP to enzyme-ATP has not been detected.

4

The catalytic power of Magnesium Chelatase

4.1 Introduction

Enzyme catalysed reactions can have rate constants approaching the rate of diffusion, while the equivalent uncatalysed reactions can show half lives of over 1 million years. The uncatalysed rate constants of biological processes span a range of 19 orders of magnitude, whereas catalysed reactions fall within a 10^4 range for k_{cat}. A recent survey of single-substrate enzymes shows that overall second order rate constants ($k_{\mathrm{cat}}/K_{\mathrm{m}}$) vary between 10^9(the limit of diffusion) and10^4 $\mathrm{M}^{-1}\mathrm{s}^{-1}$ (99).

Many of the studies on enzyme catalytic power have dealt with single substrate enzymes. To extend this work with complicated multi-substrate enzymes such as magnesium chelatase, requires a careful choice of rate constants to compare with the uncatalysed reaction. Magnesium chelatase presents another problem as an ATPase coupled system, the precise equivalent uncatalysed reaction does not exist.

4.1.1 How to quantify the catalytic power of an enzyme.

Comparing the rate constants for catalysed and uncatalysed processes provides a quantitative view of enzyme effectiveness.

All enzyme mediated reactions have a larger number of associated rate constants than the equivalent uncatalysed reactions due to the increased molecularity. In general, the effectiveness of enzymes with any number of substrates can be assessed, but initially the single substrate case will be discussed and then extended.

The ratio $k_{\mathrm{cat}}/k_{\mathrm{uncat}}$ describes the relative rates between the active site environment and solution (100, 101) . The reaction coordinate shown in figure 4.1 highlights the rate constants used to determine the catalytic proficiency of an enzyme, these are shown again on the reaction scheme (scheme 4.1).

The rate enhancement compares turnover of the enzyme-substrate complex to product and the uncatalysed reaction in solution (figure 4.2) (101). As k_{uncat} varies much more than k_{cat}, the level of rate enhancement provided by an enzyme depends primarily

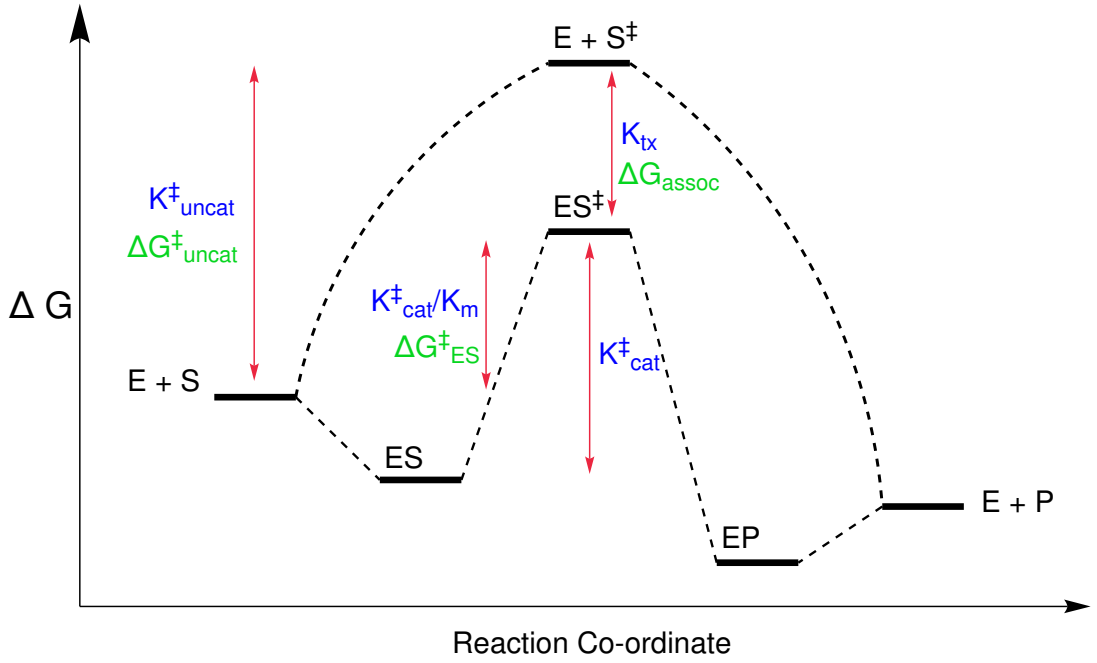

Figure 4.1: Free energy diagram of an uncatalysed and enzyme catalysed reaction - Showing the origin of constants described in section 4.1 and in equations 4.1 and 4.2.

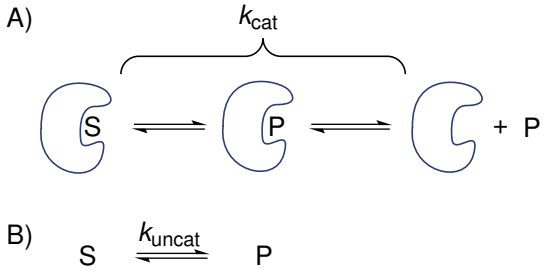

Figure 4.2: Rate enhancement compares the enzyme solubilised reaction compared to the equivalent in solution reaction - A) On enzyme solubilisation and the origins of the value for k_{cat}, **B)** The in solution origin of the value for k_{uncat}.

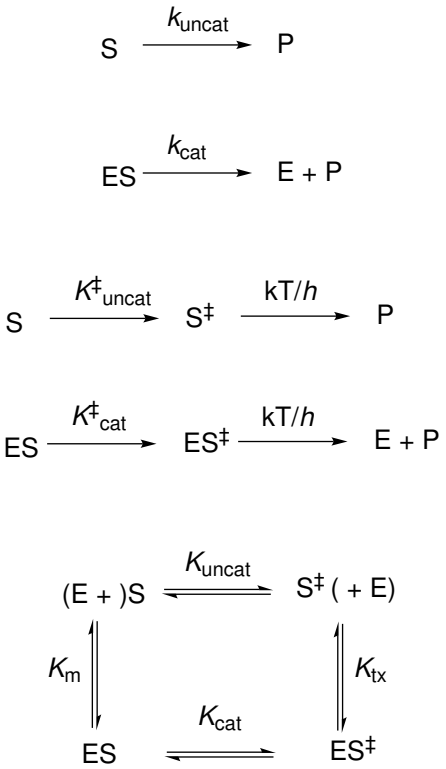

Scheme 4.1: The origins of the kinetic constants used to describe enzyme proficiency.

on the uncatalysed rate. The amount of rate enhancement provided varies dramatically, with $k_{\mathrm{cat}}/k_{\mathrm{uncat}}$ varying by 10^{14} within a sample of enzymes (100, 102).

Rate enhancement may not provide a true representation of how good a catalyst an enzyme is, as k_{cat} represents the slowest step of a reaction. Although k_{cat} may represent bond making and breaking on enzyme, in many systems it may reflect a conformation change, and therefore provide only a lower limit on the rate constants for bond making or breaking in the active site. Even if k_{cat} reflects bond making and breaking this is still not a valid measure of catalysis, as the ES complex is a different species from EP. In the best case, k_{cat} provides the rate constants for chemical transformations in the active-site. These transformations are only part of the catalytic cycle, however, and a true measure of catalysis needs to reflect the transformation of substrate in solution to product in solution.

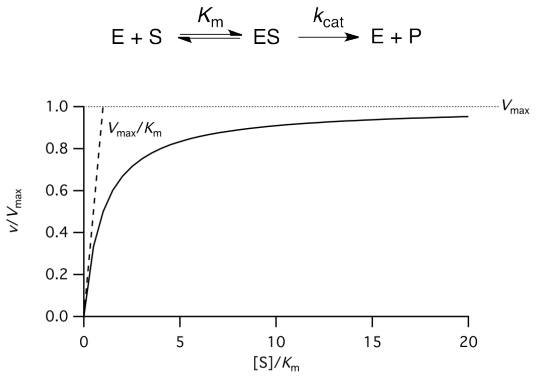

Figure 4.3: The origins of the second order rate constant $k_{\mathbf{cat}}/K_{\mathbf{m}}$ - An idealised enzyme displaying non-covalent binding with substrate produces a hyperbolic line describing the Michaelis-Menten rate constants. $k_{\mathrm{cat}} = V_{\mathrm{max}}/[\mathrm{E}]]$

Enzyme efficiency is represented by the overall second order rate constant $k_{\mathrm{cat}}/K_{\mathrm{m}}$ (figure 4.3), which reflects the free energy difference between $\mathrm{E} + \mathrm{S}$ and the transition state complex $\mathrm{ES}^{\ddagger}$. The value takes into account all the rate constants in a reaction which follow Michaelis-Menten characteristic hyperbolic behaviour with respect to substrate concentration, and can be used to define the specificity of an enzyme, either for different substrates for an individual enzyme, or the the specificity of a class of enzymes

for one substrate.

The ratio $(k_{\mathrm{cat}}/K_{\mathrm{m}})/k_{\mathrm{uncat}}$ can describe the catalytic proficiency of an enzyme. The value relates energy differences of transition state in solution and the enzyme-bound transition state (figure 4.1, equation 4.1) (100, 102). This value is unaffected by non-productive binding, as any non-productive binding will have an equal and opposite effect on both k_{cat} and K_{m}.

Equation 4.1 is logarithmically related to equation 4.2 if the temperature is known, allowing calculation of enzyme proficiency using readily available rate constants. The term $k_{\mathrm{cat}}/K_{\mathrm{m}}$ describes different processes occurring on the enzyme and is treated as a second order constant.

$$\Delta G^{\ddagger}_{\mathrm{ES}} = \Delta G^{\ddagger}_{\mathrm{uncat}} - \Delta G^{\ddagger}_{\mathrm{assoc}} \tag{4.1}$$

$$K_{\mathrm{A}} = (k_{\mathrm{cat}}/K_{\mathrm{m}})/k_{\mathrm{uncat}} \tag{4.2}$$

This method can be extended for multi-substrate enzymes, where there are multiple Michaelis constants for multiple substrates (figure 4.4 highlights a third order rate constant $(k_{\mathrm{cat}}/K^{A}_{\mathrm{m}}K^{B}_{\mathrm{I}})$). The problem with multiple substrate systems is that $k_{\mathrm{cat}}/K_{\mathrm{m}}$ is defined at saturating concentrations of the other substrate, so $k_{\mathrm{cat}}/K^{A}_{\mathrm{m}}$ reflects the reactions of $\mathrm{EB} \longrightarrow \mathrm{E} + \mathrm{P}$ (scheme 4.2). So, in the case of a two substrate reaction, the overall third-order rate constant reflects the reaction $\mathrm{E} + \mathrm{A} + \mathrm{B} \longrightarrow \mathrm{E} + \mathrm{P}$ and is the most appropriate measure of catalysis.

4.1.2 Energy coupling and the shift in mass action.

Many enzymes can couple the energy gained from nucleotide hydrolysis to useful work. Enzymes that directly transfer phosphate to produce activated products are distinct from enzymes that use the energy of ATP hydrolysis to drive conformation change in

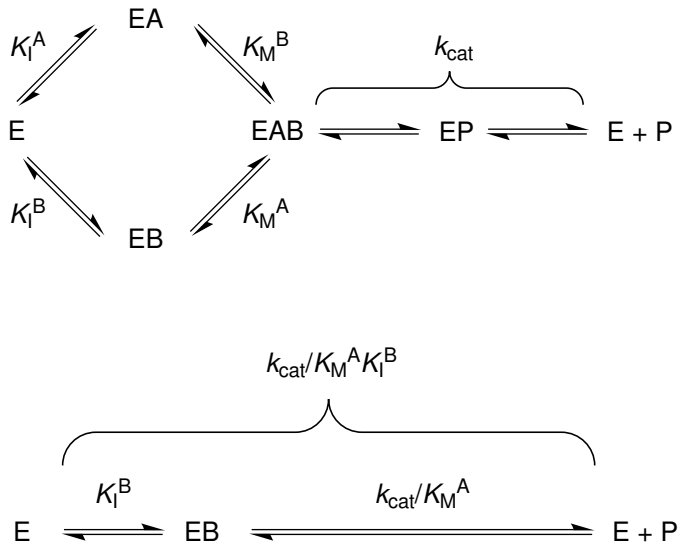

Scheme 4.2: Rationalisation of multiple substrates in quantifying enzyme proficiency.

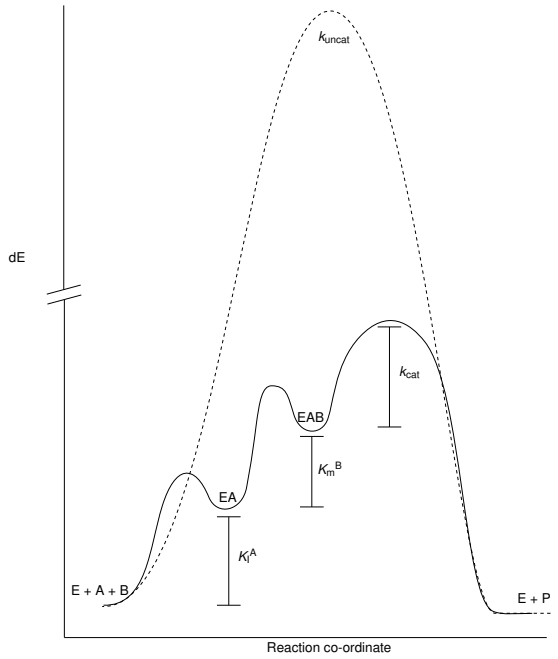

Figure 4.4: Reaction co-ordinate of catalysed and uncatalysed magnesium chelation - Representing the steps diagrammatically shown in Scheme 4.2 through the top route.

a separate active site. The mechanism of energy coupling via allosteric interactions during the reaction can be described as *conformational coupling* (103).

4.1.3 Mechanisms of conformationally coupled ATPases.

For an enzyme to couple two reactions, concerted events must occur in each active site. These events must be linked by allosteric interactions. A conformationally coupled mechanism (scheme 4.3) relies on the enzyme having different affinities for substrate and product depending on the nucleotide bound state of the ATPase domain. Events in one active site are controlled by events in the linked site. This mechanism can also be described in a series of barrier diagrams (figure 4.5).

$$E \overset{ATP}{\rightleftharpoons} E^{ATP} \overset{S}{\rightleftharpoons} E^{ATP}.S \rightleftharpoons E^{ADP}.S \rightleftharpoons E^{ADP}.P \rightleftharpoons E.P \rightleftharpoons E$$

Scheme 4.3: A conformationally coupled enzyme mechanism - Free enzyme **E** does not bind either substrate **S** or product **P**. Binding of nucleotide produces the $\mathbf{E^{ATP}}$ state which only binds **S**. $\mathbf{E^{ATP}S}$ induces ATP hydrolysis to produce the $\mathbf{E^{ADP} \cdot S}$ form, which is able to complete the reaction of S $\longrightarrow$ P. Although **P** can bind to $\mathbf{E^{ADP}}$, the only acceptable route to this conformation is via $\mathbf{E^{ATP} \cdot S}$. On formation of **P**, the enzyme collapse to the ground state releasing **P**.

In the model shown in figure 4.5, the energy barriers (red or green lines) are altered via allosteric interactions from the binding of substrate or the production of product leading to an increase or decrease in respective energy barriers, altering the free energy of different transition states as barriers move.

With the model in figure 4.5, no reaction occurs if only ATP is bound (state **2**). On binding S, the energy barrier for transformation of ATP lowers (state **3**), promoting formation of ADP (state **4**). ADP remains tightly bound, but its formation alters the barrier for S allowing formation of P rather than dissociation of S (state **5**). Formation of the E.P complex resets the energy barrier for the ATP/ADP active site, allowing the release of ADP which then resets the enzyme to state **6** allowing the release of P,

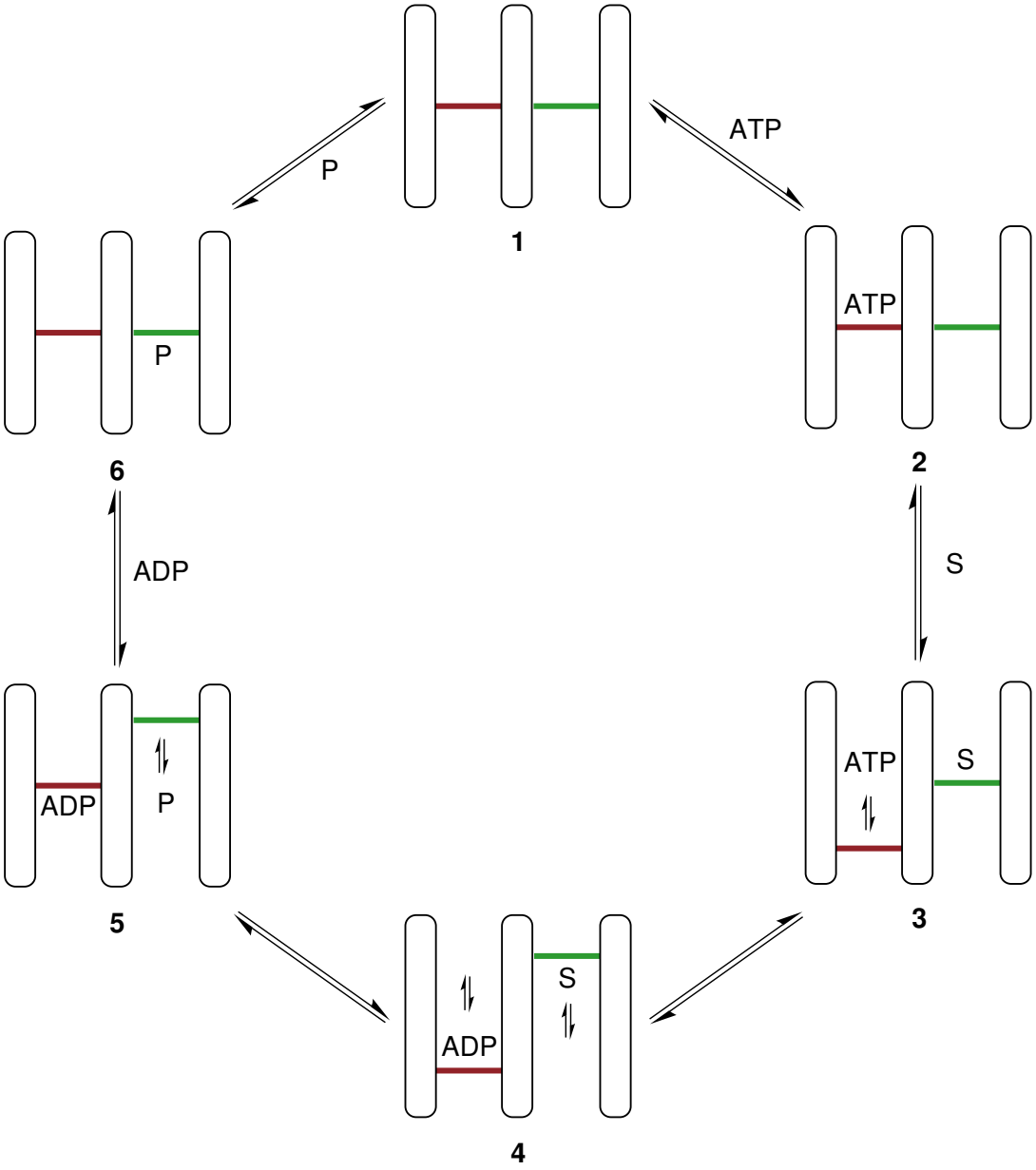

Figure 4.5: A theoretical model for conformational coupling for an enzyme with two active sites - An enzyme with two active sites as shown in red and green, with energy barriers as indicated by their respective heights. Barriers indicate an unfavourable transition-state or ground state equilibrium, with internal double arrows representing the equilibrium that is established following the removal of the barrier for that step. Reproduced from Leyh (104).

returning the enzyme to the beginning of the catalytic cycle (state **1**) (104).

Perfect coupling, where there is no uncoupled ATP hydrolysis or futile conversion of P to S, would require infinite thermodynamic barriers, which is impossible. Intrinsic ATPase activity in the absence of substrate is common and allows a pathway for ATP hydrolysis to occur in absence of substrate. As the concentration of substrate increases, the ATPase activity also increases (figure 4.6). A leak pathway implies a non-productive species (e.g. EADP · S in scheme 4.3), which can loose nucleotide without converting substrate to product.

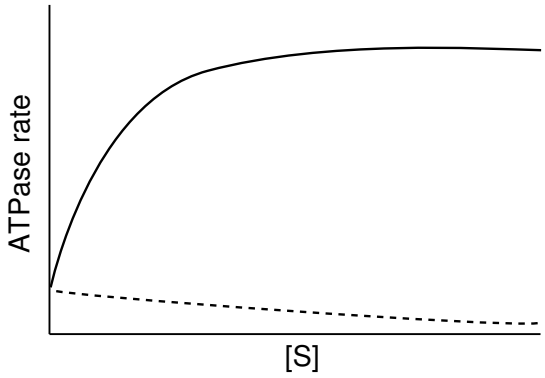

Figure 4.6: Intrinsic ATPase activity as an indication of a leak pathway - Solid line is the ATPase rate in response to [S], dashed line is the level of intrinsic ATPase activity which contributes to the total activity of the protein.

For an ATPase to discriminate between the different complexes present in the pathway, enzyme-nucleotide intermediates must not decompose, but provide conformational change that allows a second process to occur, in effect molecular discrimination (103).

Within magnesium chelatase, the ATPase stoichiometry has been previously determined for *Synechocystis* as 15 ATP to 1 MgD_{IX} (76), and in *Rhodobacter* it is even higher. By calculating the temporary change in mass action ratio that magnesium chelatase can achieve on $[MgD_{IX}]/[D_{IX}][Mg^{2+}]$ allows us to calculate the change in free energy of the reaction, and therefore the level of energy titration occurring on enzyme.

This work details the first characterisation of an AAA^+ enzyme with respect to its rate enhancement (k_{cat}/k_{uncat}) and enzyme proficiency ($(k_{cat}/K_m)/k_{uncat}$). The enzymes ability to alter the mass action ratio of $[MgD_{IX}]/[D_{IX}][Mg^{2+}]$ by coupling the energy of ATP hydrolysis to magnesium chelation is determined, and reasonable mechanisms for energy coupling discussed.

4.2 Results

4.2.1 Accurately determining absolute porphyrin concentration in the presence of magnesium chelatase subunits.

To determine how magnesium chelatase alters the mass action ratio, there is a requirement to measure accurately the differences between initial and steady state concentration of porphyrin. Porphyrin concentrations estimated from a linear calibration curve in the absence of enzyme were unrealistic with negative concentrations calculated at $t = 0$. The problem arises as magnesium chelatase subunits very slightly quench the fluorescence emission from MgD_{IX}. This can be resolved by building a calibration curve in the presence of chelatase subunits. The resulting curve can be described by second order polynomial (figure 4.7).

4.2.2 The steady state concentration of magnesium deuteroporphyrin.

Magnesium chelatase catalysed insertion of Mg^{2+} into a deuteroporphyrin IX (D_{IX}) has a characteristic progress curve showing a rise and fall in product concentration (figure 4.8). In the presence of 5 mM $MgATP^{2-}$, a steady-state in product concentration (where $d[P]/dt \sim 0$) is reached after 80 minutes. At this point conversion of substrate to product is incomplete.

To determine if the exhaustion of available ATP leads to the steady state in product concentration, an ATP regenerating system (PK/LDH, see scheme 3.5, page 69) was introduced into the assay system.

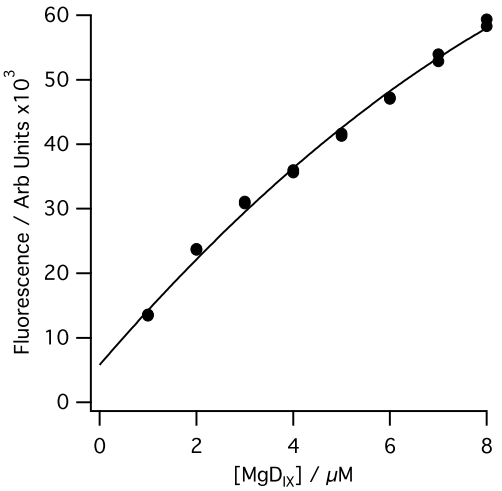

Figure 4.7: Sample calibration curve of known magnesium deuteroporphyrin - Calibration curve with 2$^{\text{nd}}$ order polynomial fitted, $k_0 = 5800$ (held constant in the fitting procedure at the fluorescence of the blank), $k_1 = 15814 \pm 820$, $k_2 = 1213.9 \pm 163$. Gain on the plate reader was set to 2076. Calibration was performed in standard chelatase buffer (50 mM MOPS/KOH, 11 mM KCl, 1 mM DTT, pH 7.7, 34 °C) containing 0.1 μM ChlI, 0.1 μM ChlD, 0.4 μM ChlH.

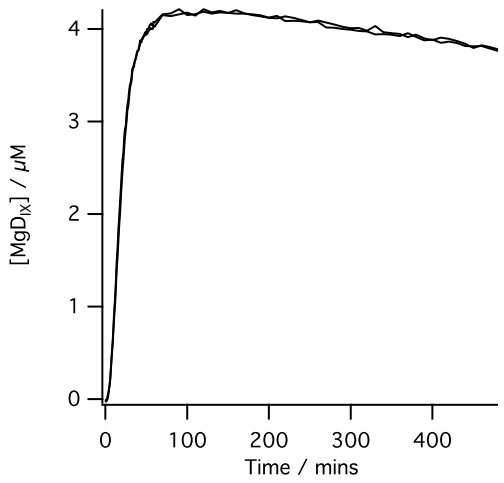

Figure 4.8: Time course of a standard magnesium chelatase assay - Magnesium chelatase assay progress curves show a characteristic rise and fall of product magnesium deuteroporphyrin (0.1 μM ChlI, 0.1 μM ChlD, 0.4 μM ChlH in the presence of 5 mM $MgATP^{2-}$. All reactions were performed at 34 °C, 50 mM MOPS/KOH, I = 0.1, pH 7.9, 1 mM DTT and contained 8 μM D_{IX} and 10 mM free Mg^{2+}.

On addition of the PK/LDH ATP regenerating system, the turnover number, k_{cat}, was the same (0.52 min^{-1}) while the K_m varied (from 0.82 mM without to 0.43 mM with the PK/LDH system) (figure 4.9). This change in K_m is probably due to an increase in the availability of $MgATP^{2-}$ at lower concentrations. The maximum ratio of $[MgD_{IX}]/[Mg^{2+}][D_{IX}]$ is the same at saturating concentrations of ATP in the presence and absence of PK/LDH, with approximately half of the available D_{IX} being converted to MgD_{IX}.

4.2.3 The steady state change of magnesium deuteroporphyrin.

The steady state concentration of MgD_{IX} depends on the initial concentration of $MgATP^{2-}$ (figure 4.10A). The steady state concentration of magnesium deuteroporphyrin exceeds the number of active sites present, demonstrating product is released from the enzyme. The enzyme catalysed conversion of substrate to product is incomplete and there are substantial amounts of deuteroporphyrin substrate present in

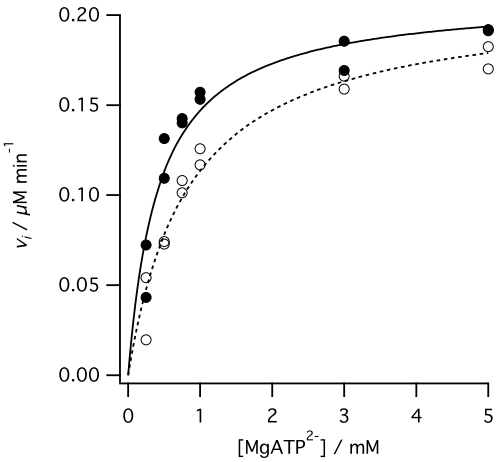

Figure 4.9: Initial rate of magnesium chelatase with respect to $MgATP^{2-}$ concentration - Conditions: 50 mM MOPS/KOH, 0.3 M glycerol, 1 mM DTT, 8 μM D_{IX}, 15 mM $MgCl_2$, I = 0.1 with KCl; open circles standard experiment, filled circles include 2 U of pyruvate kinase (PK) and 2 mM phosphoenolpyruvate (PEP). Lines are theoretical and are described by the Michaelis-Menten equation. Standard experiment kinetic parameters $k_{cat} = 0.52 \pm 0.01$ min^{-1}, $K_m = 0.84 \pm 0.12$ mM; +PK/PEP values $k_{cat} = 0.52 \pm 0.01$ min^{-1}, $K_m = 0.43 \pm 0.07$ mM.

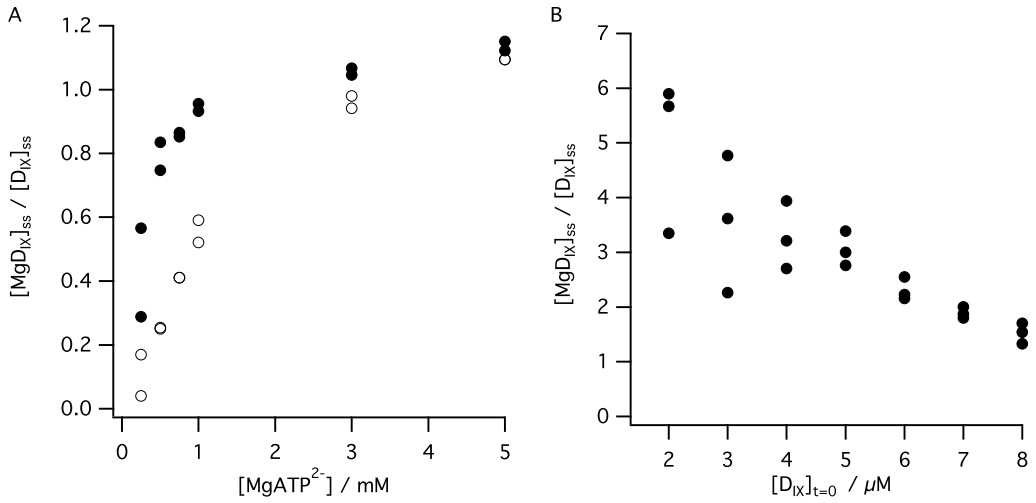

Figure 4.10: Steady state magnesium deuteroporphyrin concentration to deuteroporphyrin - A) With respect to $MgATP^{2-}$ concentration with 8 μM D_{IX}, open circles control experiment, filled circles include 2 U of pyruvate kinase (PK) and 2 mM phosphoenolpyruvate (PEP). **B)** with respect to initial deuteroporphyrin concentration. Conditions: 0.1 μM ChlI, 0.1 μM ChlD, 0.4 μM ChlD, 50 mM MOPS/KOH, $I = 0.1$, 0.3 M glycerol, 1 mM DTT, 10 mM free Mg^{2+}, pH 7.9, 34 °C.

solution. At high concentrations of $MgATP^{2-}$ the ratio $[MgD_{IX}]/[D_{IX}]$ tends towards 1, which is not changed on addition of an ATP regenerating system.

The steady state ratio of $[MgD_{IX}]/[D_{IX}]$ achieved also depends on the initial concentration of deuteroporphyrin (figure 4.10B). At low concentrations of D_{IX}, the system is capable of converting effectively all D_{IX} to MgD_{IX}, with a $[MgD_{IX}]/[D_{IX}]$ ratio of 5 ± 1.4, whereas at higher concentrations the ratio is 1.5 ± 0.19. All experiments were performed in the presence of 10 mM free Mg^{2+}, and correspond to $[MgD_{IX}]/[D_{IX}][Mg^{2+}]$ ratios of 500 and 150 respectively.

4.2.4 The rate of uncatalysed dechelation of magnesium deuteroporphyrin.

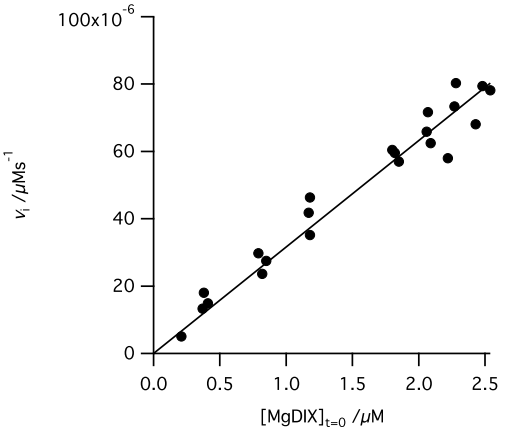

Figure 4.11: Initial rates of magnesium deuteroporphyrin dechelation - rates taken at 34 °C in 50 mM MOPS/KOH, $I = 0.1$, 1 mM DTT, pH 7.9. Data fitted to a straight line with a slope of $31.7 \times 10^{-6} \pm 0.9 \times 10^{-6} s^{-1}$.

$$MgD_{IX} \underset{k_{+1}}{\overset{k_{-1}}{\rightleftharpoons}} Mg^{2+} + D_{IX}$$

Scheme 4.4: Magnesium Deuteroporphyrin dechelation

The equilibrium constant (K_{eq}) for magnesium chelation is 10^{-6} (76), this was

determined by following the spontaneous loss of Mg^{2+} from MgD_{IX} over 24 hours. The initial rates of this process are shown in figure 4.11 and allow the determination of the first order rate constant for the demetallation of MgD_{IX} to Mg^{2+} and D_{IX}. Within the examined concentration range, the first-order rate constant for the decay was $31.7 \times 10^{-6} \pm 0.9 \times 10^{-6} s^{-1}$. This implies a second order rate constant for magnesium chelation of deuteroporphyrin IX *ca.* 30×10^{-12} $M^{-1}s^{-1}$.

As magnesium porphyrins are exceptionally photolabile, to prevent photolysis of MgD_{IX} care was taken to limit illumination time with the flash lamp. Over the 20 hour course of the experiment, the porphyrin was illuminated with 1800 flashes. When this number of flashes was repeated over a 5 minute period, no appreciable decay occurred.

4.3 Discussion

The spontaneous formation of magnesium deuteroporphyrin is a slow process. Magnesium chelatase catalyses the reaction (scheme 4.5). Magnesium chelatase uses the free energy of ATP hydrolysis to produce far more MgD_{IX} than predicted from the equilibrium constant. Spontaneous magnesium chelation is difficult as the there is a large energy barrier to overcome during the exchange of water oxygen ligands for porphyrin nitrogen ligands (75).

A proposed chemical mechanism for magnesium chelation is summarised in scheme 4.6. The start of the process begins with the deformation of porphyrin. The rate limiting step in the reaction has been calculated as the removal of a water molecule from the coordination sphere of magnesium with a ΔG of 77 $kJmol^{-1}$ (breaking a hard-acid hard-base interaction) (75). Magnesium-nitrogen bond formation on porphyrin follows, and then completion of the coordination sphere (1, 75).

The ligand exchange on magnesium from water to nitrogen on the porphyrin may be a concerted process as shown in scheme 4.6 or may occur via a protein intermediate, either through a protein–oxygen–magnesium or protein–nitrogen–magnesium complex. It is unknown whether all these processes occur within the H subunit of magnesium

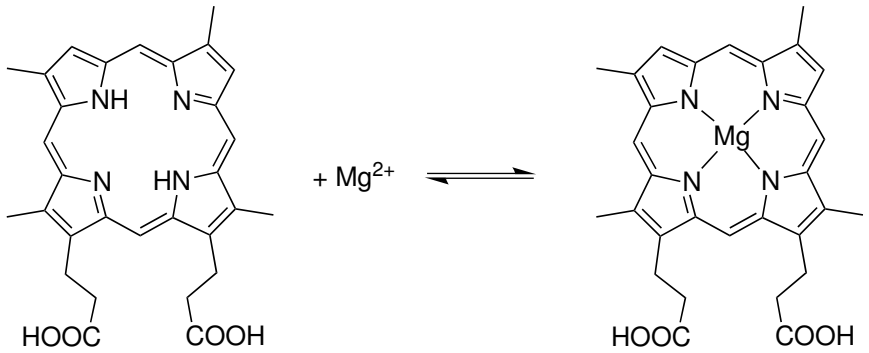

1 2

Scheme 4.5: Biochemical equation showing the insertion of Mg(II) into the ring of deuteroporphyrin

chelatase, but from studies in solution, metal ion insertion into deuteroporphyrin can be catalysed by the presence of nitrogenous bases, such as pyridine (73). The activation energy for insertion falls from 153 kJmol^{-1} for an uncatalysed reaction to 66 kJmol^{-1} for a pyridine catalysed insertion (73), which is similar to the uncatalysed activation energies for insertion of Zn^{2+}, Co^{2+} and Mn^{2+}.

Within the protein, loss of water ligands on magnesium might be promoted by a histidine ligand either in the active site or at another location. The protein may provide a mechanism to remove the metal ion in the same manner as suggested with ferrochelatase, where histidine and glutamine residues remove a water molecule from iron before the reaction with porphyrin commences (105).

4.3.1 Magnesium chelatase shifts the mass action ratio by 8 orders of magnitude

Magnesium chelatase couples ATP hydrolysis with magnesium porphyrin formation, which allows it to generate a product-substrate ratio far from the equilibrium position. This is seen in the rise and fall of product over time (figure 4.8) as ATP is hydrolysed. At saturating concentrations of ATP and porphyrin the mass action ratio $[MgD_{IX}]/[Mg^{2+}][D_{IX}]$ is 150 rather than 10^{-6}, 8 orders of magnitude different, a free

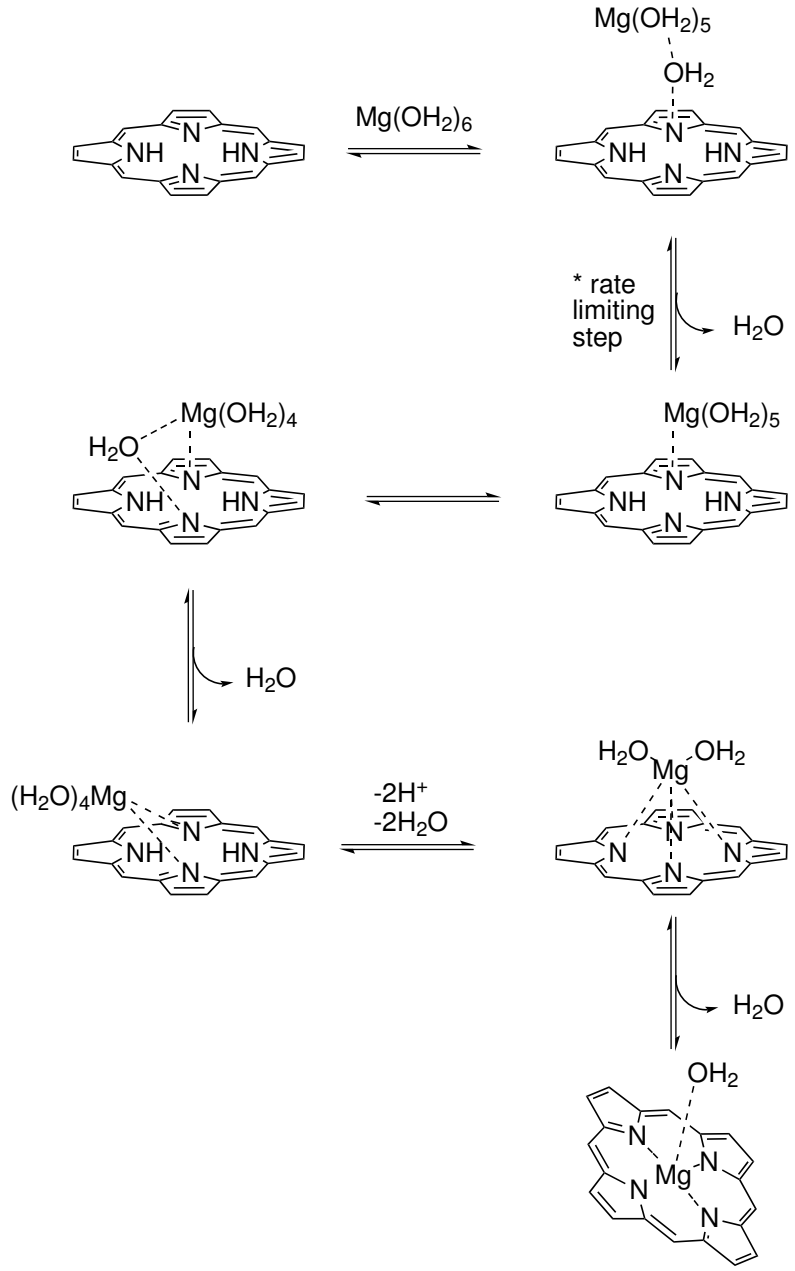

Scheme 4.6: Proposed uncatalysed mechanism for magnesium insertion into a porphyrin, adapted from Buchler (19) and Shen (75). The proposed rate limiting step is the movement of a water molecule from the internal coordination sphere to the outer coordination sphere with replacement by nitrogen on porphyrin, according to DFT calculations (75).

energy change of +53 kJmol^{-1}. The free energy of hydrolysis ($\Delta G'$) of ATP hydrolysis is –60 kJmol^{-1} at cytoplasmic concentrations of ATP (106), which would suggest that one metal ion could be chelated per ATP hydrolysed, but the actual stoichiometry have been determined to be 15 ATP per 1 chelation in *Synechocystis* (76) and 40 in *R. capsulatus* (107). The large amount of ATP required remains to be explained, but the level of ATP hydrolysis per mole of MgD_{IX} formed is far larger than required.

ATP may not just be used as thermodynamic driving force, but also to accelerate the reaction. Magnesium chelatase is not a fast enzyme with a turnover of 0.013 s^{-1} (76), ATP is not an accelerant on kinetic grounds. The reaction may simply fail the majority of times, and only succeed on average one in fifteen hydrolysis events.

Perhaps ATPase activity is also used to regulate the action of the chelatase, as the product magnesium protoporphyrin is toxic. Binding of ATP and hydrolysis could control inter-conversion of active and inactive forms of the complex, with similar processes seen in many GTPases (108, 109). If the ATPase action of magnesium chelatase was conserved so that all energy was transferred for metal ion insertion, then all energy available from the donor reaction would be available to the acceptor. Not all the energy may be required, and the enzyme may need to alter the level of product by titrating the energy down to decrease the amount of cytotoxic product produced. There may be an initial coupling efficiency of 100% where there is complete conversion of D_{IX} to MgD_{IX}, as seen at low concentrations of starting material in assays (*ca.* 1 μM D_{IX}). As the concentration of porphyrin increases, there is a decrease in the percentage conversion which may indicate a decrease in coupling efficiency.

The ATP stoichiometry may be reduced *in vivo* with coupling to one or more enzymes. The presence of Gun4 increases the rate of the reaction, but does not alter the ATP stoichiometry (71). In *R. capsulatus* the presence of the downstream protein BchM also increases the amount of magnesium porphyrin produced, but whether the ATPase stoichiometry is altered is not known (42). The high ATP stoichiometries are reproducible *in vitro* but their biological and mechanistic significance is still unknown.

Magnesium chelatase's ability to link ATP hydrolysis to magnesium insertion relies on successful energy linkage which in turn is related to the relative energy barriers between conformations. Jencks (103, 110) proposed coupled systems must link macromolecular discrimination with ATP hydrolysis, where there must be signalling steps to indicate successful conversion of substrate to product. This signal would allow an enzyme form activated by ATP hydrolysis to collapse back to the original state, rather than proceed with catalysis. Endogenous product rather than product from enzyme turnover may cause the E' discharge, leading to ATP super-stoichiometries, or the enzyme may hydrolyse ATP to form the E.Pi form without coupling that process to product formation. A proposed energy coupling pathway for magnesium chelatase is shown in figure 4.7. To determine if product uncouples ATPase, the ATPase activity of the system needs to be monitored as a function of magnesium porphyrin concentration at a constant concentration of deuteroporphyrin.

Models for conformationally coupled enzymes and the closely related models for active transport across membranes (ref. (110)) show tight coupling between the two reaction pathways. As discussed above, this tight coupling requires that we have a high barrier to steps in the ATP hydrolysis pathway when not productively linked to metal ion chelation. One plausible model for the high ATPase stoichiometry is shown in scheme 4.7. In this case, ATP hydrolysis and ADP release activate the chelatase active site and in the productive pathway magnesium is inserted. If the barrier to phosphate release is low and it disassociates, then the enzyme falls back to an inactivated conformation, leading to futile ATP hydrolysis. The leak pathways may be controlled by allosteric signals or simple product inhibition in one of the active sites, allowing regulation of energy transfer and therefore the level of product.

4.3.2 A qualitative assessment of the rate enhancement of magnesium chelatase

Magnesium chelatase shifts the product : substrate ratio of $[MgD_{IX}]$: $[D_{IX}\ ][Mg^{2+}]$ by 8 orders of magnitude (from 10^{-6} without enzyme to 150 with enzyme), as well as

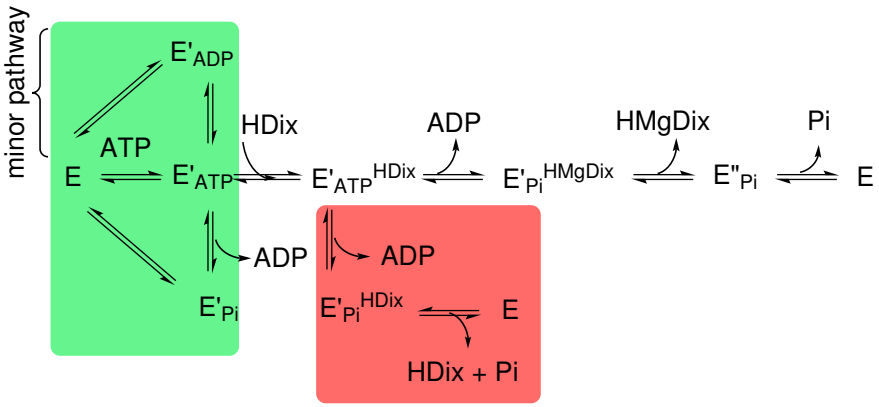

Scheme 4.7: Proposed energy coupling pathway for magnesium chelatase, where E is the ChlID complex, and excess of MgD_{IX} product will cause the the ID complex to collapse back to the ground state without having completed a productive cycle. The green box is the intrinsic ATP hydrolysis pathway as discussed in chapter 3, and the red box is a hypothetical unproductive leak pathway.

accelerating the rate of metal ion chelation ($k_{cat}/k_{uncat} \approx 400 \times 10^6$ M).

For a pseudo first order reaction (scheme 4.8) the half-life can be calculated, assuming a reasonable concentration of magnesium *in vivo* is 1 mM. The half-life is around 0.7 million years.

$$Mg^{2+} + D_{IX} \longrightarrow MgD_{IX}$$

Scheme 4.8: The second order reaction of magnesium and deuteroporphyrin to form magnesium deuteroporphyrin.

This is within the range half-lifes of uncatalysed biological reactions compiled by Wolfenden (101). Ferrochelatase, sirohydrochlorin cobaltochelatase and a zinc chelating antibody are examples where there is no coupled nucleotide hydrolysis with metal ion chelation (111, 112, 113). Many other enzymes achieve comparable rate enhancements without the need for nucleotide hydrolysis, suggesting that magnesium chelatase catalysed ATP hydrolysis is not needed to break some high kinetic barrier.

4.3.3 A quantitative assessment of the rate acceleration.

Previously determined rate constants for magnesium chelatase (76) allow for a quantitative analysis of the rate enhancement and proficiency of magnesium chelatase.

Uncatalysed metal ion insertion is not coupled to ATP hydrolysis, and there is no known equivalent of such a coupled, but uncatalysed reaction. The enzymes main function is magnesium insertion into porphyrin in the chlorophyll biosynthetic pathway. As such, this description of the catalytic power of magnesium chelatase focuses on the chelation reaction at saturating ATP. The rate enhancement ($k_{\mathrm{cat}}/k_{\mathrm{uncat}}$) for Mg^{2+} insertion is approximately 400 $\times 10^6$ M. In theory this value estimates the effectiveness of the active site at accelerating the chelation reaction, but magnesium chelation is not the rate determining step. The rate determining step occurs before magnesium insertion into porphyrin, therefore k_{cat} does not reflect metal ion chelation (69). The value is a lower estimate of the rate enhancement of the enzyme and does not take into account any major structural shifts that occur in solution, or that magnesium ion insertion involves two substrates.

Calculating an enzymes proficiency ($(k_{\mathrm{cat}}/K_{\mathrm{m}})/k_{\mathrm{uncat}}$) (101) for a single substrate system (comparing the two routes shown in scheme 4.9) is relatively straight forward. The case for magnesium chelatase is more complex as this enzyme has two substrates, and is also cooperative with magnesium concentration. Scheme 4.9 can be modified to take into account two substrate systems (scheme 4.10) using the parameter $(k_{\mathrm{cat}}/(K_{\mathrm{M}}^{\mathrm{A}}K_{\mathrm{I}}^{B}))/k_{\mathrm{uncat}}$. A reaction coordinate for a two substrate enzyme is shown in figure 4.4, as the enzyme proceeds through two binding steps before it reaches the transition state, the constants from these two steps are combined. In the case where the order of binding steps is unknown, the two potential routes of binding for this idealised enzyme are shown in scheme 4.11.

This ratio $k_{\mathrm{cat}}/(K_{\mathrm{M}}^{\mathrm{DIX}}s_{0.5}^{M}g)/k_{\mathrm{uncat}}$ best describes the enzyme catalysed production of magnesium porphyrin from free magnesium and porphyrin and is approximately $30 \times 10^{15}\mathrm{M}^{-1}$. This ratio has units of M^{-1} and is equivalent to $\frac{1}{K_{\mathrm{TX}}}$, where K_{TX} is a measure of the dissociation constant of the enzyme transition state complex. A low

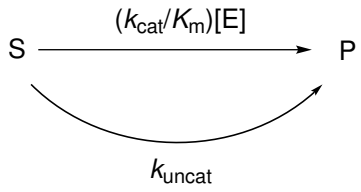

Scheme 4.9: Single substrate (S) to single product (P) model of enzyme for determining rate enhancement

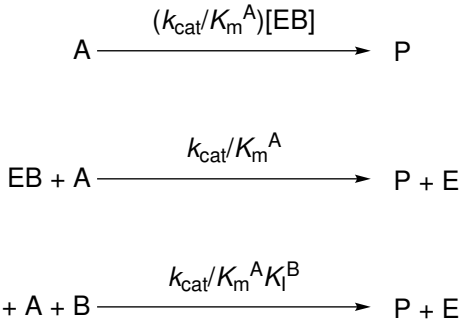

Scheme 4.10: Derivation of kinetic values to calculate enzyme proficiency for a two substrate enzyme

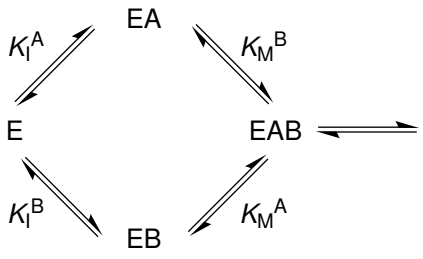

Scheme 4.11: The two possible binding routes for a two substrate enzyme such as magnesium chelatase.

value of K_{TX} implies a high affinity. For magnesium chelatase the transition state is in the attomolar range (equation 4.3), indicating a high affinity for the transition state.

$$K_{\mathrm{TX}} = \frac{1}{30 \times 10^{15}\mathrm{M}^{-1}} = 33 \times 10^{-18}\mathrm{M} \tag{4.3}$$

Magnesium chelatase is able to temporarily maintain equilibrium far from expected mass action ($[\mathrm{MgD_{IX}}]/[\mathrm{D_{IX}}][\mathrm{Mg}^{2+}]$) by coupling ATP hydrolysis with magnesium insertion.

In conclusion there are two distinct methods for assessing the effectiveness of an enzyme that catalyses a conformationally coupled reaction. The kinetic approach compares the n^{th} order rate constant for an uncatalysed reaction with the $(n+1)^{\mathrm{th}}$ order rate constant for the catalysed reaction. The second approach directly compares the shift in mass action ratio that the enzyme can produce with the equilibrium constant. Using the kinetic approach we see that magnesium chelatase provides a substantial catalytic rate acceleration over the uncatalysed reaction. Magnesium chelatase provides a good environment for catalysis, with a catalytic profiency equivalent to attomolar affinity for the transition state. Magnesium chelatase achieves a substantial shift in the mass action ratio (*ca.* 10^8). The kinetic and thermodynamic problems faced by magnesium chelatase have now been quantified. The rate enhancement provided by magnesium chelatase is substantial, but not extraordinary compared to the normal range of enzyme catalysis, while the shift in mass action ratio is formidable, does not explain the high ATP stoichiometry.

5

Probing cooperativity in the AAA$^+$ domain of ChlI

5.1 Introduction

The magnesium chelatase subunits, ChlI and ChlD, are both members of the AAA^+ ATPase family (55, 56). AAA^+ proteins are molecular motors involved in many processes throughout the cell, from DNA repair (114), cellular transport (115), proteolysis (116, 117) and chlorophyll biosynthesis. ChlI and the N-terminal of ChlD show sequence similarity, (figure 5.1) with 33 % identity between ChlI and the N terminal AAA^+ domain of ChlD in *Synechocystis*; while Tobacco I and D subunits share 46 % identity. ChlI drives chelatase activity by using the chemical energy obtained from the hydrolysis of ATP (60, 78).

It is of interest to determine how ATP hydrolysis in ChlI is linked to the insertion of magnesium into porphyrin in ChlH. The molecular motor part of the enzyme is presumed to act with ChlH and ChlD, providing energy for the chelatase reaction. The ChlI hexamer may act in a cooperative manner, with each active site communicating the presence of different nucleotide forms, promoting activity. Or it may simply use the hexamer form as a structural role, and provide mechanical energy via a probabilistic interaction with ATP, independent of internal conformational changes or cooperative action.

AAA^+ proteins have a number of conserved motifs in the ATPase active site which are normally vital for their activity (figure 5.1) (54). These are the Walker A and B nucleotide binding motifs, the Arginine Finger and Sensor II Arginine.

The Walker A motif (GxxxxGK[T/S] where x is any residue) contains a conserved lysine. This lysine is presumed to bind ATP and when mutated to an alanine usually abolishes nucleotide binding (115, 118). For example, the Walker A lysine in the AAA^+ protein N-ethylmaleimide sensitive factor (NSF) is essential for ATP binding (118). Mutating the Walker A lysine can also prevent the formation of the active oligomeric form of the protein, and has also been associated with protein-protein interactions (115, 119).

The Walker B motif (hhhhDE where h is a hydrophobic residue) (54) when the glutamic acid is mutated to a glutamine frequently locks AAA^+ proteins into a nucleotide

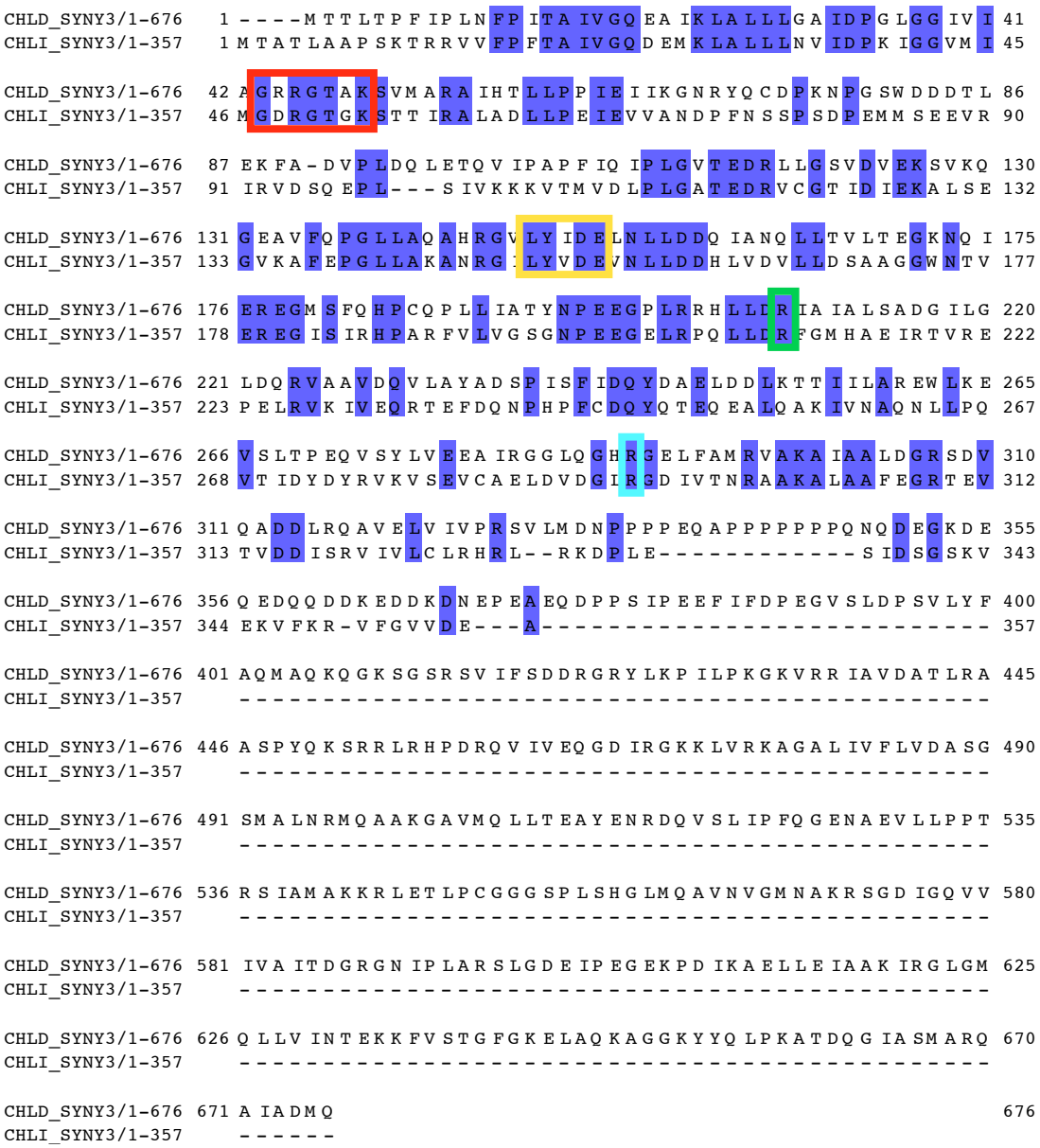

Figure 5.1: Sequence alignment of ChlI and ChlD - Regions highlighted show the conserved AAA$^+$ domains of the two proteins: Red - Walker A motif, Yellow - Walker B, Green - Arginine Finger, Blue - Sensor 2 (54), blue shaded residues are conserved between the two proteins. Alignment performed on UniProt (65) using the software Clustal Omega program (120).

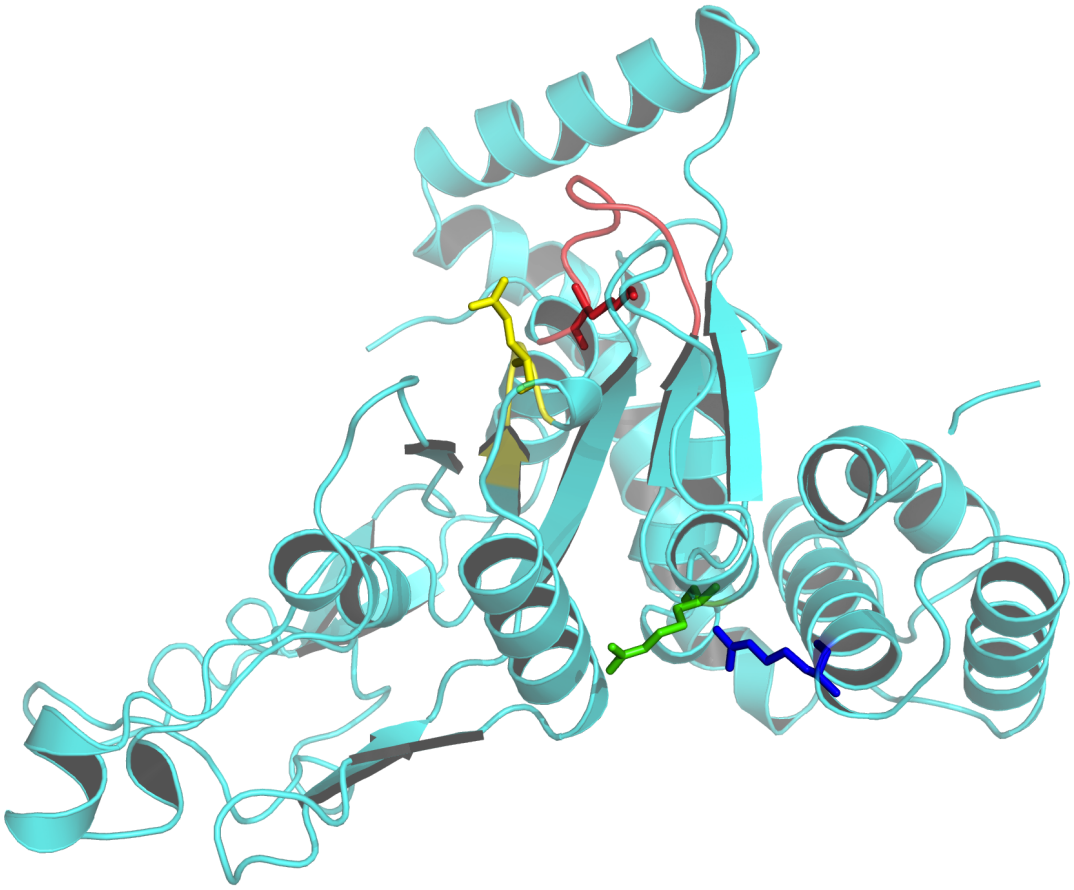

Figure 5.2: Homology model of ChlI - Cartoon representation of ChlI with the conserved ATPase features highlighted in sticks. Walker A lysine in red, Walker B glutamine in yellow, arginine finger in Green and the Sensor 2 arginine in blue. The homology model was produced using SWISS-MODEL (121) and rendered using Pymol (41).

bound state (119, 122, 123, 124, 125). ATP binds but is not hydrolysed; in this state complex assembly appears to be allowed (119, 126). This locked state may promote adjacent sub-units into binding nucleotide (117), assisting in revealing cooperative action between subunits.

Mutation of the arginine finger to an alanine achieves two objectives. Arginine, with a planar positive guanidine group is able to form multidentate interactions with phosphate via either hydrogen bonds or electrostatic interactions. The long side chain enables long range interactions between multi-domain complexes, such as members of the AAA^+ family. The arginine finger is highly conserved in the AAA^+ family, and is suspected to interact with the γ-phosphate of ATP in the binding pocket of an adjacent subunit (127). While normally essential for ATP hydrolysis, it is not required for binding (128, 129). In some cases it is thought to sense hydrolysis and contribute to structural changes communicated through the system. It also has been found to stabilise subunit-subunit interactions (130). Mutations of this arginine have been found to force the protein ClpX to adopt a post-hydrolysis 'relaxed' conformation (131).

Hansson *et al* (132) made the sensor II mutant in BchI, as well as two other mutants in the BchI subunit corresponding to chlorophyll deficient barley strains which contained mutations in the barley I subunit (the *Xantha-h* gene product). All mutants were still able to form oligomeric structures as determined by analytical size exclusion chromatography and surface plasmon resonance. While still being able to bind nucleotide, as shown by the formation of oligomers in the presence of nucleotide, the mutants were all impaired ATPase and inactive chelatases. Eqimolar mixes of mutant and wild type had 52 % activity of wild type, indicating that the hexamer does not power chelation through simultaneous coordinated action. The data provided further evidence that binding and not hydrolysis is required for the formation of the ID complex. This work looked at a single mutant to wild type ratio at an arbitrary substrate concentration. For a more rigorous analysis of the mutants, full characterisation at multiple mutant to wild type ratios is required.

The Walker A (K53A), Walker B (E154Q) and arginine finger (R210A) mutants have been made in *Synechocystis* ChlI from and the resulting proteins are impaired

ATPases and inactive chelatases. These mutants provide tools to probe site site interactions within the hexamer of ChlI. Mixtures of mutant and wild-type ChlI assemble to form hybrid magnesium chelatase complexes with both active and inactive subunits. These hybrid complexes allow us to investigate subunit interactions. If subunits interact to drive the chelatase reaction, then increasing the proportion of inactive mutant in hybrid complexes will cause a steeply non-linear loss of activity. For all the mutants examined, this is not observed when $MgATP^{2-}$ is saturating; k_{cat} decreases linearly with increasing concentration of mutant. In contrast, when ATP is limiting a non-linear loss of activity is seen on increasing mutant concentration. Taken together these results show that ChlI subunits work independently when bound to nucleotide but binding is cooperative. This suggest a mechanism where the interactions between the subunits change on moving through a reaction cycle.

Initial work has begun on labelling active protein onto a surface, and the implications of this work will be discussed.

5.2 Results and Discussion

Six mutants of ChlI were prepared with mutations in the Walker A (K53A), Walker B (E154Q), arginine finger (R210A, R210E) and sensor II (R291A, R291E) motifs. Table 5.1 details the mutants produced for this work and their level of characterisation.

5.2.1 Initial characterisation of ChlI ATPase mutants.

5.2.1.1 Cloning, over-expression and purification of ChlI mutants.

Mutagenesis was achieved using the oligonucleotides mutant primers shown in table 2.3, with the pET9a-ChlI vector used as a template for mutagenesis.

The identity of mutants was confirmed by sequencing. Mutant proteins expressed in Rosetta cells. Mutant protein was produced to at least the level of wild-type, with

Table 5.1: Summary of characterisation of ChlI AAA^+ mutants

Mutant	DNA Sequenced	Transformed/Expressed	Purified	CD Spec	Melting Temperature / °C	Relative ATPase / Percentage	Magnesium chelatase activity
K53A	✓	✓	✓	✓	47	12.5	none
E154Q	✓	✓	✓	✓	47	6	none
R210A	✓	✓	✓	✓	47	5	none
R210E	✓	✓					
R291A	✓	✓	✓	✓	34	n.d.	n.d.
R291E	✓	✓					

SDS-PAGE showing the appearance of intense bands at the same mass as ChlI. Mutants were purified as wild type ChlI.

5.2.1.2 Secondary structure of ChlI mutants.

Circular dichroism spectra were taken to determine if the mutations had altered the secondary structure of ChlI (figure 5.3). No major differences in spectra were recorded for mutants in Walker A (K53A), Walker B (E154Q) and Arginine Finger (R210A). Therefore differences in activity cannot be attributed to altering of the secondary structure of the protein. The sensor II mutant, R291A, has an altered CD spectra compared to wild type, lacking a minima at 208 nm.

5.2.1.3 Global stability of the ChlI mutants.

The molar ellipticity of ChlI wild type compared to mutants at 222 nm (the major trough for alpha helix absorbance) was observed while increasing the temperature from 20 to 80 °C. The first derivative of the data was taken and the steepest gradient was deemed to be the melting temperature (T_m) of the protein. No major changes of T_m were found for mutants in the Walker A (K53A), Walker B (E154Q) and Arginine Finger (R210A) motifs, all of which had a melting temperature indistinguishable from wild-type at 47 °C (figure 5.4). The mutation in the Sensor II motif (R291A) had an altered T_m of 34 °C. As such, no further work was performed with this mutant.

5.2.2 Assembly characterisation of ChlI mutants.

CD spectroscopy and stability analysis demonstrates that these mutant proteins are folded. For any activity assay to be meaningful, mutants not only need to be folded, they also need to assemble into the intact wild type complexes. A series of assembly assays to determine the behaviour of these mutants was carried out. Firstly, ChlI will self-assemble into a hexamer, although this species is likely to not be on the reaction pathway. We tested the self assembly behaviour of these ChlI mutants using dynamic light scattering (section 5.2.2.1). ChlI will also form a stable complex with ChlD; this

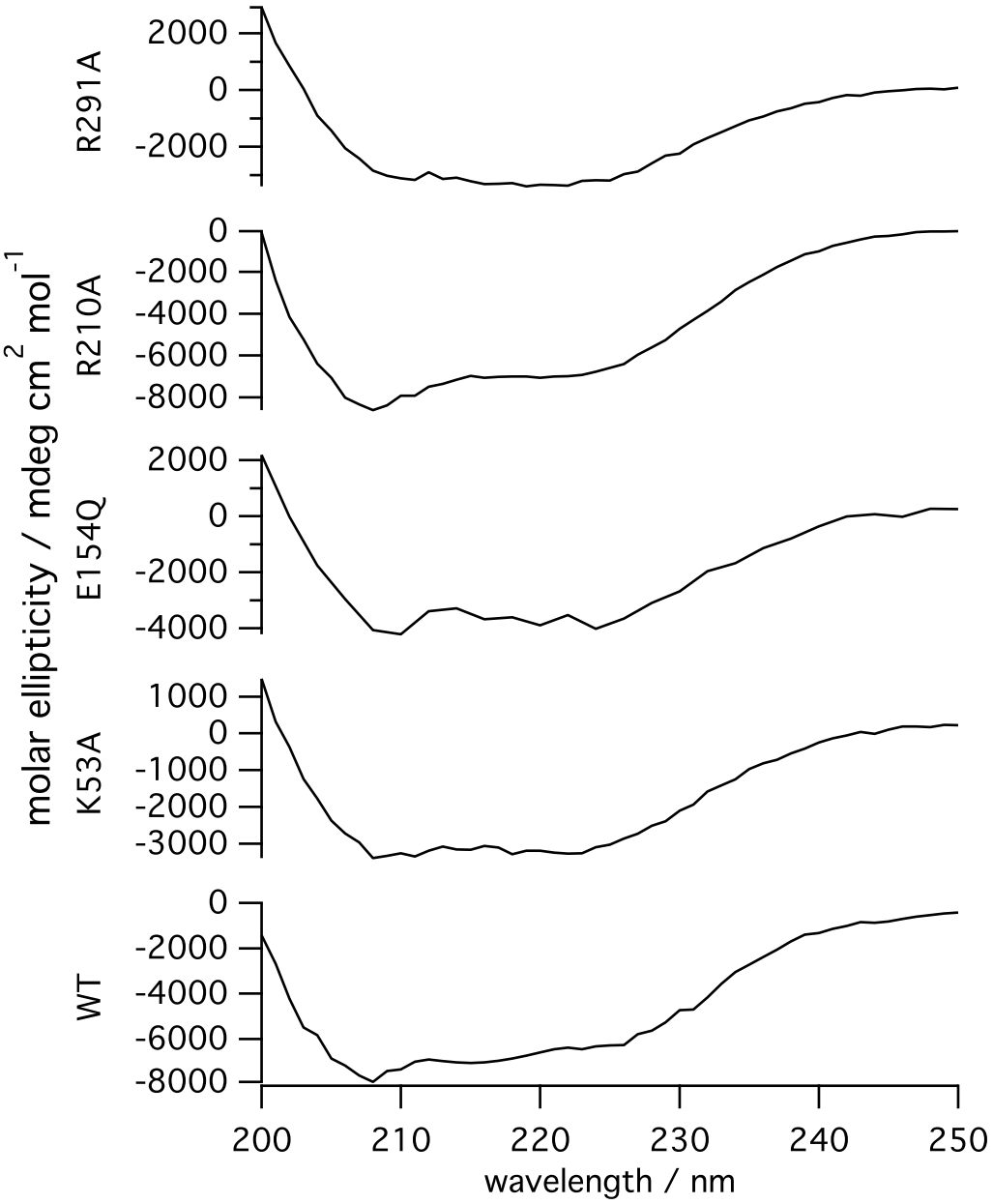

Figure 5.3: Far UV CD spectra of ChlI mutants - CD spectroscopy of protein secondary structure reveals no major differences in between WT and mutants. Protein concentrations were 0.1 mgml^{-1}, in 50 mM potassium phosphate, pH 7.4, 25 °C.

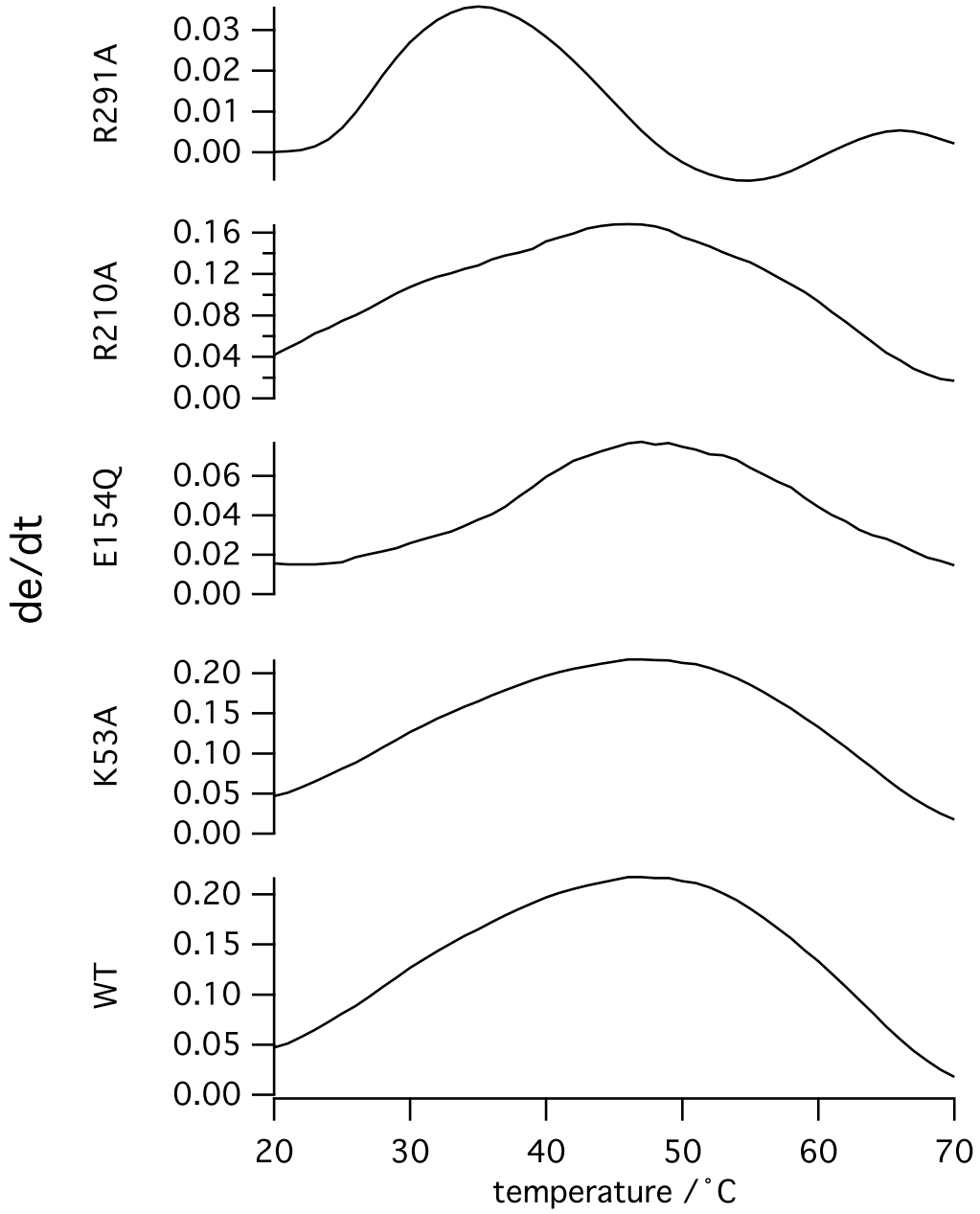

Figure 5.4: Melting temperatures of ChlI - T_m was determined by taking the first derivative of the slope while monitoring the CD of 222 nm while increasing temperature. Protein concentrations were 0.1 $mgml^{-1}$, in 50 mM potassium phosphate, pH 7.4. The temperature was increased at a rate of 1 $°Cmin^{-1}$.

complex is thought to be biologically relevant. The simplest assay for formation of a ChlID complex is analytical chelating sepharose chromatography when only one of the two subunits is His-tagged. The results of these co-purification (or pull-down) experiments is given in section 5.2.2.2. Probing cooperativity through mutant mixing requires that the mutant proteins can form mixed complexes with the wild type. One way of assaying such mixed complexes is to fluorescently label both the wild type and mutant proteins with different dyes and measure energy transfer (FRET). The results of these FRET experiments are given in section 5.2.2.3. Taken together, our assembly experiments show that the K53A and R210A mutants do not self-assemble into a ChlI only ring, but form a ChlID complex and also form a mixed ChlID complex. The E154Q mutant is indistinguishable from wild-type as it forms all of these complexes.

5.2.2.1 Monitoring the ability for ChlI WT and mutants to form larger complexes using dynamic light scattering.

Dynamic light scattering (DLS) is a technique that monitors time dependant fluctuations in the scattering intensity of incident laser light. This allows the calculation of an apparent hydrodynamic radius. For protein and biological macromolecules, this techniques allows for the calculation of the radius for a hypothetical hard sphere and gives an apparent particle size. While this value is not an accurate reflection of particle size, changes in the apparent radius give a convenient measure of a complex assembly.

Wild type ChlI, along with the series of mutants were analysed by DLS in the presence and absence of nucleotide and 10 mM free Mg^{2+}. The results indicate that wild type and the Walker B mutant (E154Q) (figure 5.5A and C) are able to form oligomers of a higher radius in the presence of nucleotide, while K53A and R210A do not increase the hydrodynamic radius in the presence of nucleotide (Graphs B and D, figure 5.5).

Mutations in Walker A motifs often prevent nucleotide binding (54), and as a consequence prevent nucleotide dependant self assembly. As the K53A mutant is an ATPase (table 5.1), it must be able to bind ATP. This mutation must have an alternative influence on the self-assembly of ChlI. Arginine finger residues act across subunit-subunit interfaces, so it is reasonable to expect them to stabilize the ChlI assembly. Mutating

this residue clearly impairs the self-assembly of ChlI. In contrast, as mutants in the Walker B motif are often proposed to stabilize bound nucleotide states, these mutants are likely to still assemble into ChlI rings. Assembly of Walker B mutants was observed.

The failure of the K53A and the R210A mutants to self-assemble suggests that they do not show wild-type assembly behaviour. However, the ChlI hexamer is probably not an assembly intermediate on the path to the intact chelatase. The critical test is assembly of a mutant ChlI: ChlD complex.

5.2.2.2 Mutant ChlI proteins can form ChlID complexes.

The interaction between ChlI and ChlD is essential for chelatase activity. Mutants in either subunit that cannot form the ChlID complex would not be mechanistically informative. To probe whether the series of mutants expressed are able to interact with ChlD, a series of pull down assays were performed in the presence and absence of nucleotide. Pull down assays are a simple method of probing protein protein interactions, but do not give the dissociation constant, K_d. In order for ChlI to interact with ChlD, $MgATP^{2-}$ and free Mg^{2+} must be present (59). It was found that the mutants K53A, E154Q and R210A all direct interacted with ChlD in the presence of ATP (figure 5.6).

The Walker A mutant (K53A) maintains interactions with ChlD, which is expected as it is an ATPase (see section 5.2.3). The Walker B mutant (E154Q) while able to bind ATP is not expected to catalyse hydrolysis. Formation of this complex is expected, as Jensen previously showed binding but not hydrolysis of ATP is required for the interaction between ChlI and ChlD (78). The Arginine Finger mutant (R210A) maintains interactions with ChlD. R210A is expected to be able to bind nucleotide, and as such will be in the correct conformation to allow an interaction with ChlD.

5.2.2.3 Monitoring complex assembly with fluorescently labelled ChlI.

The inactive AAA^+ mutants of ChlI provide a resource to probe coordinated action within the hexamer of ChlI. Previous studies have demonstrated the power of substitut-

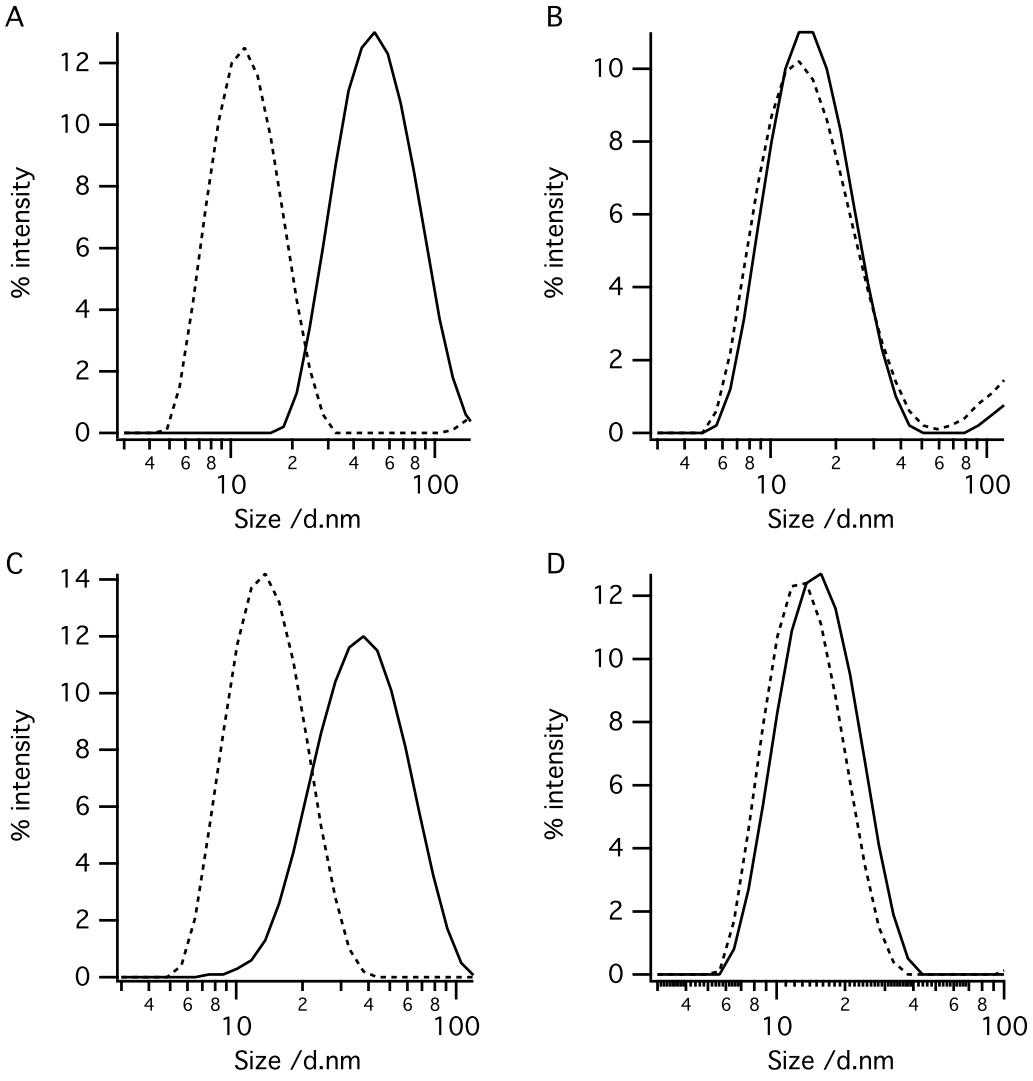

Figure 5.5: Dynamic Light Scattering of ChlI WT and ATPase mutants - A: Wild Type ChlI, B: K53A-ChlI, C: E154Q-ChlI, D: R210A-ChlI. Dashed traces no nucleotide, solid traces 5 mM ADP, 15 mM $MgCl_2$. DLS was performed on 45 μM protein samples in 50 mM MOPS, 1 mM DTT, pH 7.7. A total of 3 runs with 20 readings per run were performed with results averaged by the software (Malvern Instruments NanoSizer).

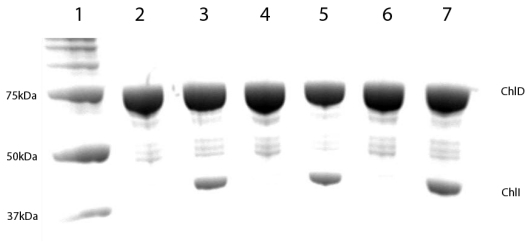

Figure 5.6: Pull down to monitor interactions between ChlD and ChlI WT and Mutants. - Interactions between the two proteins only occur in the presence of 5 mM ATP, 15 mM $MgCl_2$ in 50 mM tricine/NaOH, 0.3 M glycerol, 0.5 M NaCl, pH 7.9. Lane 1: Markers, 2: K53A $MgATP^{2-}$, 3: K53A + $MgATP^{2-}$, 4: E154Q - $MgATP^{2-}$, 5: E154Q + $MgATP^{2-}$, 6: R210A - $MgATP^{2-}$, 7: R210A + $MgATP^{2-}$. Band at 75 kDa is ChlD, Band at 39 kDa is ChlI mutant. ChlD was His_6 tagged and allowed to bind to charged Ni(II) chelating sepharose with the respective ChlI protein in the presence and absence of 5 mM $MgATP^{2-}$ and 10 mM free Mg^{2+} in 50 mM tricine/NaOH, 0.3M glycerol pH 7.8, 20 °C . Interactions were detected using SDS-PAGE stained with Safety Stain (Invitrogen).

ing wild type for mutant within AAA^+ proteins in revealing allosteric communication between adjacent and distant subunits within this family of enzymes (116, 117, 131). An elegant solution to reveal subunit interactions has been reported by Martin *et al* (131), where multiple subunits were coexpressed on one vector with each subunit linked by flexible linkers. Individual subunits were mutated, and these proteins assayed for activity. This approach often produces insoluble concatenated proteins, so a statistical mixing approach has been used in this study.

Wild type and mutant subunit complexes are essential to probe mixed hexamers. To monitor this interaction, the proteins were labelled with either an acceptor or donor fluorescent dye and studied in a FRET experiment. Thiol modification of ChlI with N-ethylmaleimide, in the presence of ATP, does not remove ATPase or chelatase activity (59). Similar maleimide chemistry was used to label ChlI wild type and mutants with fluorescent dyes (scheme 5.1). The thiol from a cysteine adds across the double bond of a maleimide to form a thioether very selectively at a pH lower than 8 (44, 133).

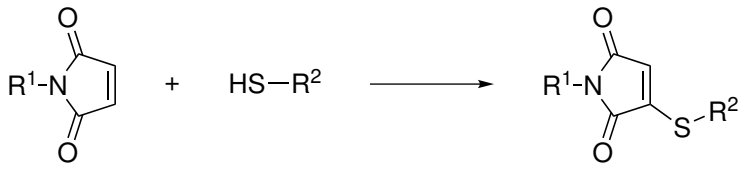

Scheme 5.1: Reaction of a thiol (**2**) with a maleimide (**1**).

5.2.2.4 Labelling wild type ChlI with tetramethylrhodamine-5-maleimide

Wild type ChlI was labelled with the fluorescent dye tetramethylrhodamine-5-maleimide (scheme 5.2) using standard methods (133). After desalting and dialysis, fluorescence excitation and emission spectra were recorded and compared with the free dye (figure 5.8). Both λ_{em} and λ_{ex} were red shifted by approximately 5 nm on conjugation with protein. This red shift is consistent with successful labelling of the protein, and can been visually seen on a gel (figure 5.7), the lower intensity apparent in the wild-type lane arises from the different excitation spectra of this dye.

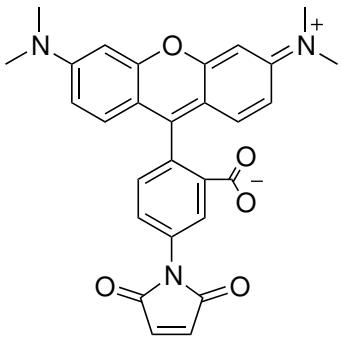

Scheme 5.2: Tetramethylrhodamine-5-maleimide

5.2.2.5 Labelling mutant ChlI with fluorescein-5-maleimide

Mutants were labelled with fluorescein-5-maleimide as before. Figure 5.9 shows the absorbance and emission spectra of labelled E154Q. Labelled R210A and K53A gave identical spectra (not shown). The slight redshift to λ_{ex} = 497 nm from 495 nm indicated successful labelling. SDS-PAGE analysis of labelled protein demonstrates that

the proteins have been covalently modified with dye (figure 5.7).

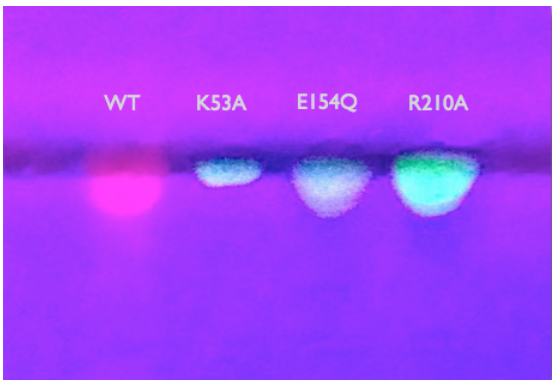

Figure 5.7: Fluorescently labelled protein - 8 % SDS-PAGE illuminated with UV light and photographed in colour. The presence of fluorescent bands indicates successful labelling of the protein. The protein is labelled above its respective band on the photograph. Wild-type was labelled with tetramethylrhodamine-5-maleimide and mutants with fluorescein-5-maleimide.

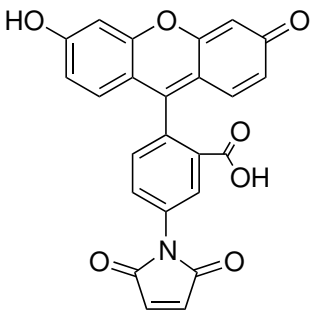

Scheme 5.3: Fluorescein-5-maleimide

5.2.2.6 Labelled ChlI interacts with ChlD.

Fluorescently labelled ChlI can still form a complex with ChlD. A pull down assay demonstrates that labelled ChlI still binds unlabelled ChlD in the presence of $MgATP^{2-}$ (figure 5.10).

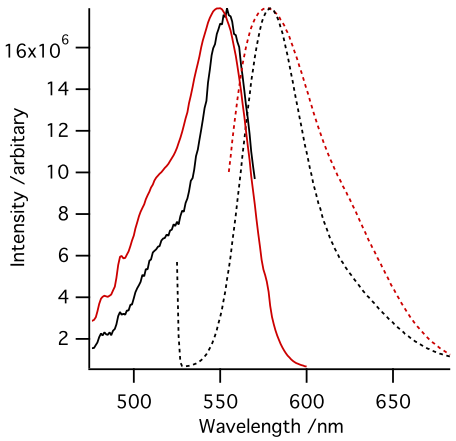

Figure 5.8: Fluorescence spectra of Tetramethylrhodamine-5-maleimide and labelled ChlI WT - Red: Tetramethylrhodamine-5-maleimide solid line, excitation spectra, λ_{max} ex = 549 nm; dashed line, emission spectra, λ_{max} em = 576 nm (λ_{ex}=549 nm); black: labelled ChlI WT solid line, excitation spectra λ_{max} ex = 554 nm; dashed line, emission spectra λ_{max} = 578 nm. Spectra recorded in 50 mM tricine-NaOH, 0.3 M glycerol, 1 mM DTT, pH 7.7, 34 °C.

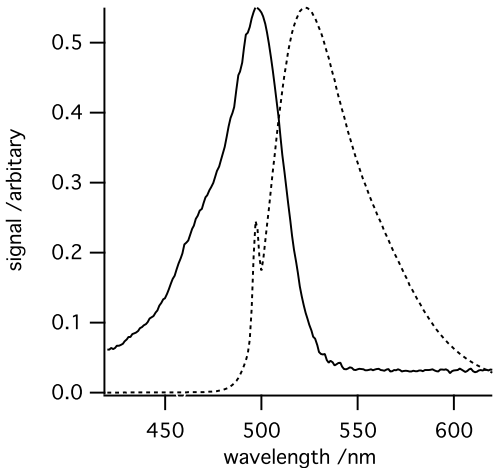

Figure 5.9: Excitation and emission Spectra of ChlI-E154Q labelled with fluorescein-5-maleimide - Excitation (solid) and emission (dashed) spectra of ChlI-E154Q labelled with fluorescein-5-maleimide, λ_{max} excitation = 497 nm; λ_{max} emission = 523 nm (λ_{max} = 497 nm). Spectra recorded in 50 mM tricine-NaOH, 0.3 M glycerol, 1 mM DTT, pH 7.7, 34 °C.

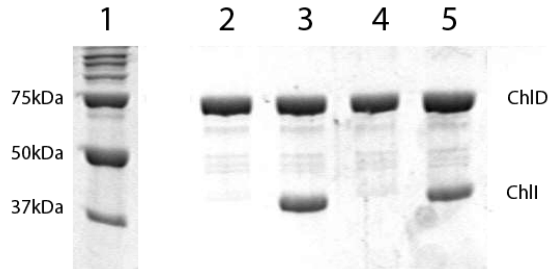

Figure 5.10: Protein interactions between ChlD and unlabelled and labelled ChlI. - Lane 1: Marker; 2: ChlI WT unlabelled - $MgATP^{2-}$; 3: ChlI WT unlabelled + $MgATP^{2-}$; 4:ChlI WT labelled with fluorescein-5-maleimide - $MgATP^{2-}$; 5: ChlI WT labelled with fluorescein-5-maleimide - $MgATP^{2-}$. ChlD was tagged with a His_6 tag while ChlI was untagged, allowing for interactions to be monitored using Ni(II) chelating sepharose. Pulldowns were performed in 50 mM tricine/NaOH, 0.3 M glycerol pH 7.9 25 °C.

5.2.2.7 Wild type and mutant ChlI are able to form a complex.

To determine if wild-type and mutant ChlI can form mixed complexes, labelled wild-type (tetramethylrhodamine) and mutant (fluorescein) ChlI was introduced to ChlD in solution (figure 5.11). When excited at 470 nm, emission is only observed from fluorescein (figure 5.11, solid line). When $MgATP^{2-}$ and Mg^{2+} were introduced, FRET was observed to an additional peak at 580 nm, characteristic of tetramethyl-rhodamine (figure 5.11, dotted line). These spectra demonstrate that there is $MgATP^{2-}$ dependant formation of a complex between ChlD and both wild-type and mutant ChlI. For FRET to be achieved, fluorophores normally need to be within *ca.* 10 nm of each other (134). In the presence of ChlD, $MgCl_2$ and ATP, with increasing concentration of wild type protein labelled with an acceptor fluorophore, the emission of donor fluorophore from mutant at 523 nm was increasingly quenched with a shoulder peak forming at 576 nm. This shows that mutant and wild type protein are able to interact with each other and form complexes in the presence of ChlD (figure 5.12).

In order to quantify the changes in FRET seen on increasing acceptor concentration, the peaks shown in figure 5.12 were fitted to an exponentially modified Gaussian distribution in Igor Pro (Wavemetrics, OR, USA) using the Multi-peak 2.0 package

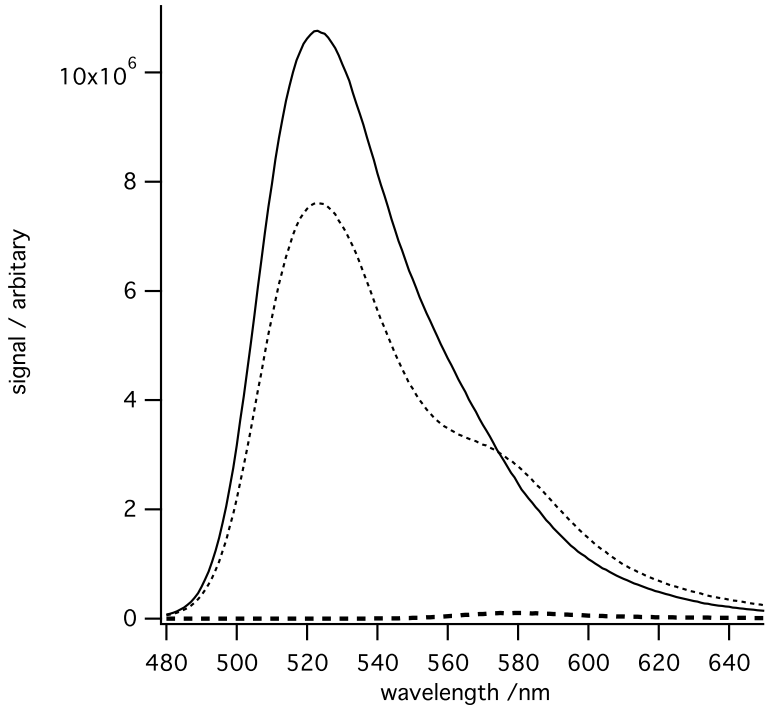

Figure 5.11: ChlI WT and mutant emission spectra in the presence and absence of ATP - 1 μM ChlI WT labelled with tetramethylrhodamine-5-maleimide mixed with 1 μM ChlI E154Q labelled with fluorescein-5-maleimide in the presence of 1 μM ChlD with: Solid - no ATP present; dots 5 mM $MgATP^{2-}$, dashes emission spectra of ChlI WT labelled with tetramethylrhodamine-5-maleimide when excited at 470 nm, without the presence of ChlI-E154Q mutant labelled with fluorescein-5-maleimide. Concentrations of protein are approximate.

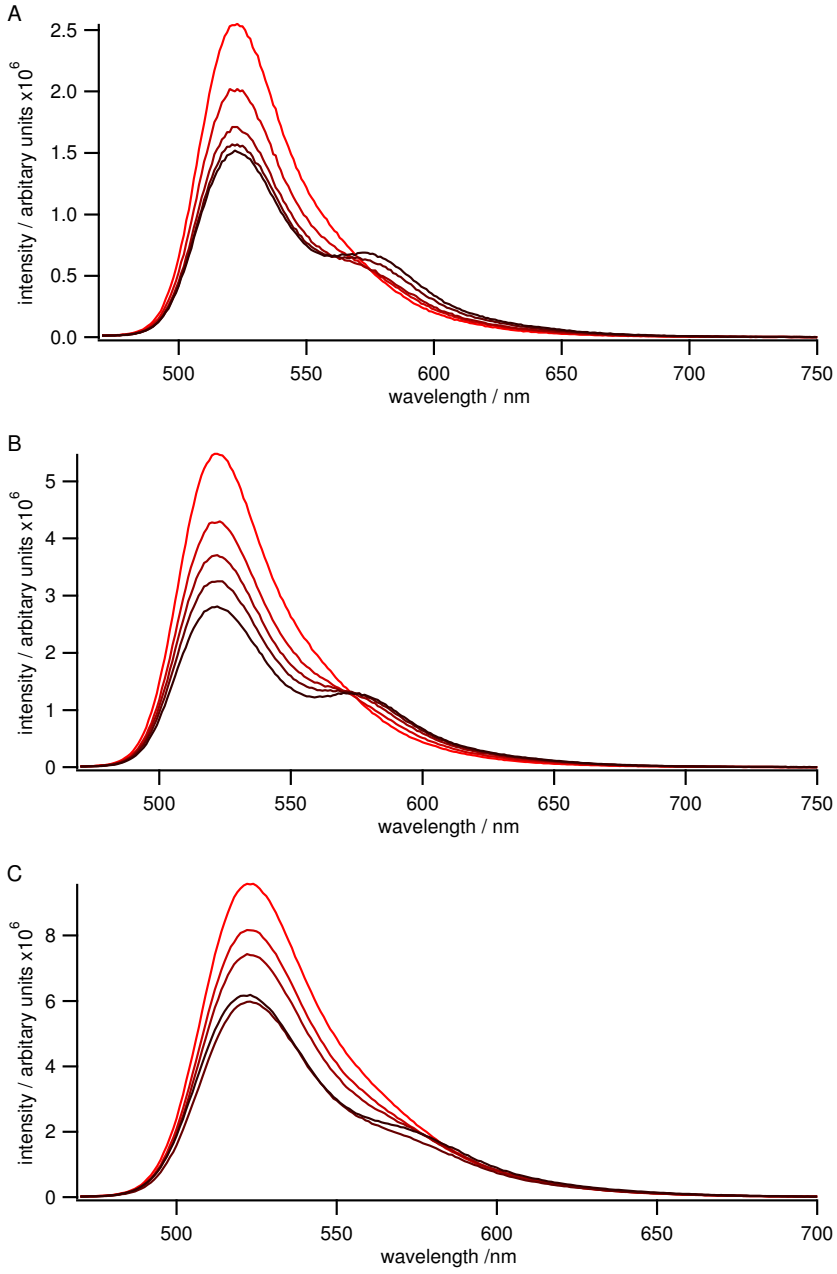

Figure 5.12: Emission Spectra of fluorescent labelled mixes of ChlI wild type and A, Walker A (K53A); B, Walker B (E154Q); C, Arginine Finger (R210A) - with increasing concentration of WT in 50 mM MOPS, 0.3 M glycerol, 5 mM ATP, 15 mM $MgCl_2$, pH 7.7, excitation at 470 ± 5 nm, emission spectra recorded between 480 and 650 nm with 2 nm band gap. As wild type concentration increases (increasingly dark coloured lines) the shoulder at 576 nm becomes more apparent while the emission of donor mutant at 523 nm decreases.

(see section 2.21.2) , normalised for total peak area and plotted against approximate concentration of ChlI WT added to a mixture of mutant ChlI and ChlD, (figure 5.13) and shows that for K53A and E154Q there were approximately the same change in fluorescence signal on increasing acceptor concentration. With R210A, less FRET is observed. This may be due to changed labelling efficiency, or to poorer complex formation.

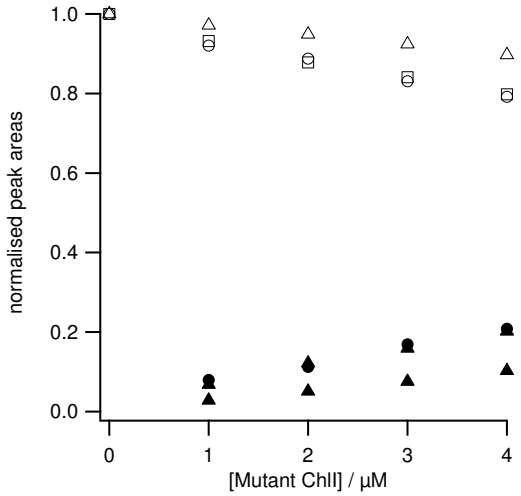

Figure 5.13: Peak areas of FRET titration of WT ChlI with ATPase mutants - Circles - K53A; Squares - E154Q; Triangles - R210A. Open - donor peak size; filled - acceptor peak size.

The data from the FRET titration (figure 5.12 and pulldown assays (figure 5.6) provide evidence of a concentration dependant formation of ChlID complexes at saturating nucleotide concentrations. Significantly, there is clear evidence in the FRET titrations that mixed complexes of wild type and mutant ChlI assemble in the presence of ChlD. These data do not provide information on complex assembly at limiting nucleotide concentrations.

Table 5.2: The steady state rates of ATP hydrolysis catalysed by ChlI mutants

Enzyme	$k_{\mathbf{cat}}$ **/ min**$^{-1}$	$K_{\mathbf{m}}$ **/ mM**
WT	7.23 ± 0.72	0.16 ± 0.03
K53A	0.90 ± 0.14	0.26 ± 0.10
E154Q	0.17 ± 0.05	0.01 ± 0.02
R210A	0.16 ± 0.06	0.02 ± 0.04

5.2.3 ChlI AAA$^+$ mutants have impaired ATPase activity and no chelatase activity

Mutations in the AAA$^+$ domain are expected to reduce ATPase activity. Using the Pyruvate Kinase / Lactate Dehydrogenase (PK/LDH) coupled enzyme assay, the ATPase activity of mutants of ChlI (table 5.2, figure 5.14) was characterised with respect to the concentration of $MgATP^{2-}$.

All the mutants had severely impaired ATPase activity compared to wild type. The Walker A mutant had the highest activity of these mutants. This mutant is clearly still able to bind nucleotide, so it is reasonable that is still interacts with ChlD (figure 5.6).

All the mutants were unable to catalyse magnesium chelation (see figure 5.17). This shows that the effect of mutagenesis is more significant on the chelatase than the ATPase. One explanation for this observation is that multiple ATPase subunits interact to drive the chelatase, so the effect on the chelatase is a substantial multiple of the effect on the ATPase.

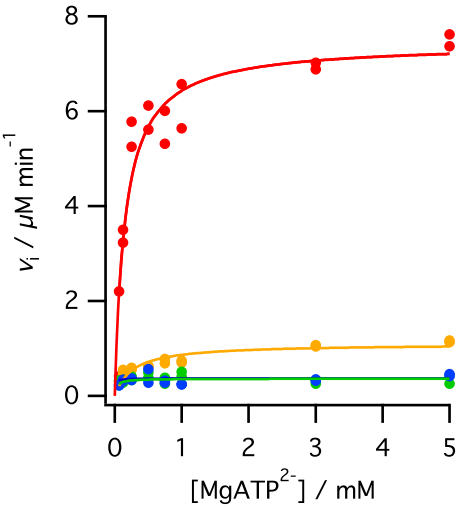

Figure 5.14: The dependence on $MgATP^{2-}$ of the rates of ATP hydrolysis catalysed by mutants of ChlI. - Red, Wild Type; yellow, Walker A (K53A); green, Walker B (E154Q); blue, Arginine Finger (R210A). Assays were performed in 50 mM MOPS/NaOH, 0.3 M glycerol, 1 mM DTT, 10 mM free Mg^{2+}, 2 mM PEP, 200 μM NADH, pH 7.7, 34 °C. Lines are theoretical and described by the Michaelis–Menten equation with characterising parameters in table 5.2.

5.2.4 Using AAA$^+$ mutants of ChlI to probe site–site cooperativity within a ChlI ring

5.2.4.1 Probing site–site interactions within the ChlI hexamer

Electron microscopy of BchID predicts that ChlI forms a hexamer within the ID complex, with EM reconstructions revealing a trimer of dimers like structure (67, 135). As the ATPase active site is formed at the interaction between these two sites, these mutants are prime candidates to probe site–site interactions.

Wild type–mutant mixing titrations, where the proportion of mutant to wild type is varied while maintaining total ChlI concentration yields a mixture of heterohexamers containing both mutant and wild type. Communication between subunits can be detected by comparing the activities of heterohexamers against a control.

The distribution of mutant and wild type subunits within the ChlI hexamer was simulated using the binomial distribution. This model assumes that mutant and wild type have a similar likelihood of being incorporated into a hexamer and there is random distribution of substitutions into the hexamer. Subunit distributions are described by equation 5.1 and plotted in figure 5.15A in a similar manner to Werbeck *et al* (116), where P is the probability that an hexamer contains i mutant subunits, n is the total number of subunits (for a hexamer $n = 6$) and p is the proportion of mutant present as shown in equation 5.2.

$$P(i) = \binom{n}{i} p^i (1-p)^{n-i} \tag{5.1}$$

$$p = \frac{[\text{ChlI Mutant}]}{[\text{ChlI WT}] + [\text{ChlI Mutant}]} \tag{5.2}$$

If the subunits in the ring function independently we expect a linear relationship between proportion of wild type protein and activity. Losing an active subunit from a ring will decrease activity in proportion. If subunits are coupled with each other

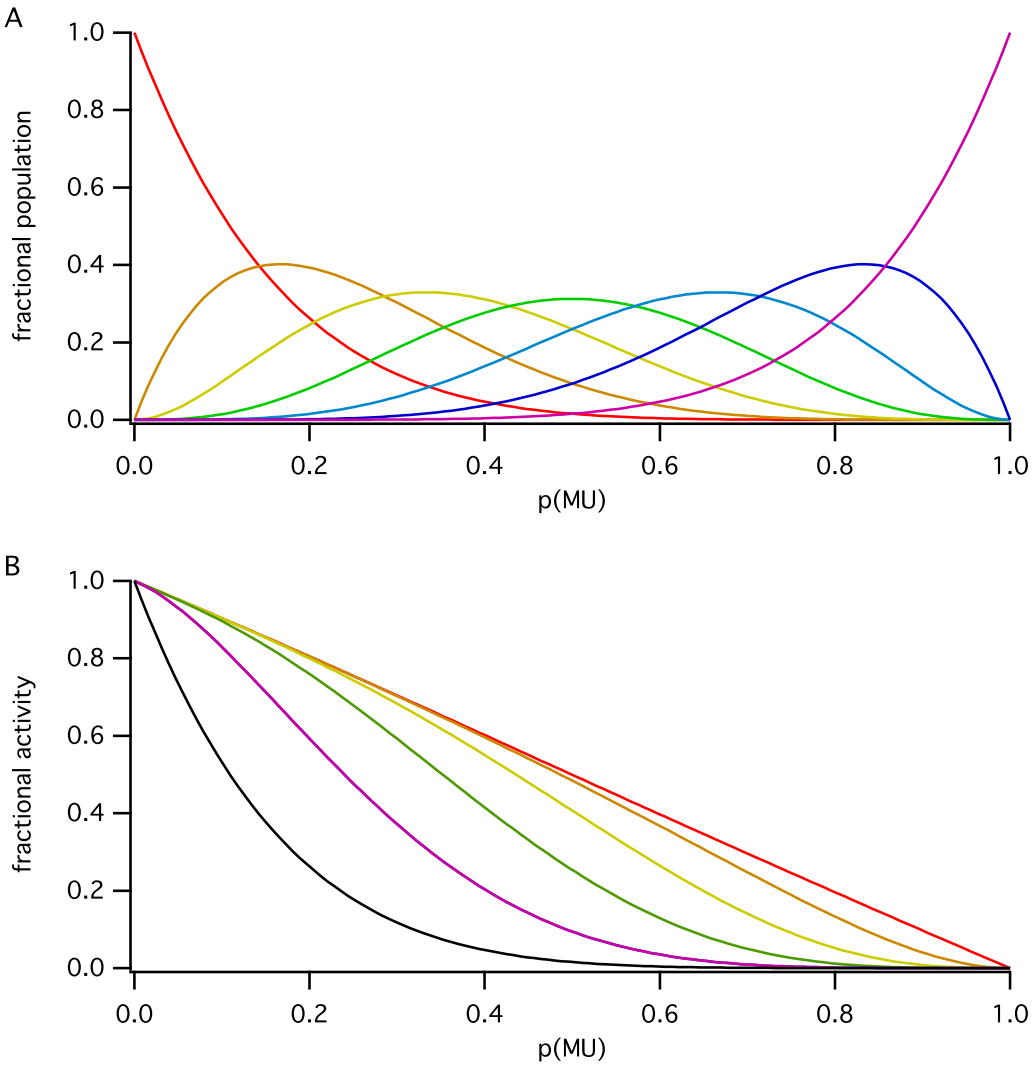

Figure 5.15: Models of hexameric ring populations and activities - A) Populations of substituted hexamers present on increasing concentration of mutant. Red - 0 substitutions, Orange - 1 substitution, Yellow - 2 substitutions, Green - 3 substitutions, Light Blue - 4 substitutions, Dark Blue - 5 substitutions, Purple - 6 substitutions. **B)** Lines indicating the affect on activity of the ring depending on vital number of subunits required for activity to occur. Black - 1 substitution totally destroys ring activity, Purple – 2 substitutions, Green - 3 substitutions, Yellow - 4 substitutions, Orange - 5 substitutions, Red - 6 substitutions (i.e. extreme case where each subunit act independently of each other).

however, activity will decrease in a steeply non-linear fashion. If for example the entire hexamer functions as a single unit, then a single substitution will produce an inactive complex (figure 5.15B black line). We can model the number of subunits needed within a ring for chelation. Figure 5.15B shows the affect on fractional activity depending on the number of substitutions required to deactivate the ring.

5.2.4.2 A working model for the stoichiometry of the ID complex

The minimal requirements for enzyme catalysed magnesium chelation activity are the ChlI, ChlD and ChlH subunits (61). The AAA^+ mutants of ChlI were all inactive in chelatase assays. This result confirmed that hydrolysis of ATP within the ChlI subunit is required for chelatase activity.

For these mutant mixing experiments in a multi-subunit enzyme, it is important to establish reaction conditions where the enzyme activity depends on the concentration of the varied subunit. Mutant mixing experiments are not readily interpretable if the ratio of mutant to wild type is varied when the subunit is present in large excess.

Previous kinetic experiments showed an optimum activity with a ratio of 2:1:4 for ChlI:ChlD:ChlH (35). These conditions ensure that ChlI saturates ChlD, but if a 1:1 stoichiometry is correct, this ratio is inappropriate when performing mutant substitution experiments. The effect of ChlI concentration on the magnesium chelation rate displays behaviour indicative of a 1:1 relationship between ChlI and ChlD at saturating ATP (figure 5.16A). If the I and D subunits form a double ring, as has been proposed (67), a 1:1 ratio in the complex would be expected. This discrepancy from the previously described 2:1 ratio may arise from improvements in the assay system for this enzyme (stopped vs. continuous) or from improved protein purification.

A tight binding relationship (equation 5.3, where k is the rate constant of interest) is displayed between the two subunits with respect to k_{cat}, with an inflection point at approx 0.08 μM, which suggests a 1:1 relationship (figure 5.16A). At limiting nucleotide concentration ($k_{\mathrm{cat}}/s_{0.5}$), weaker binding between the subunits is observed.

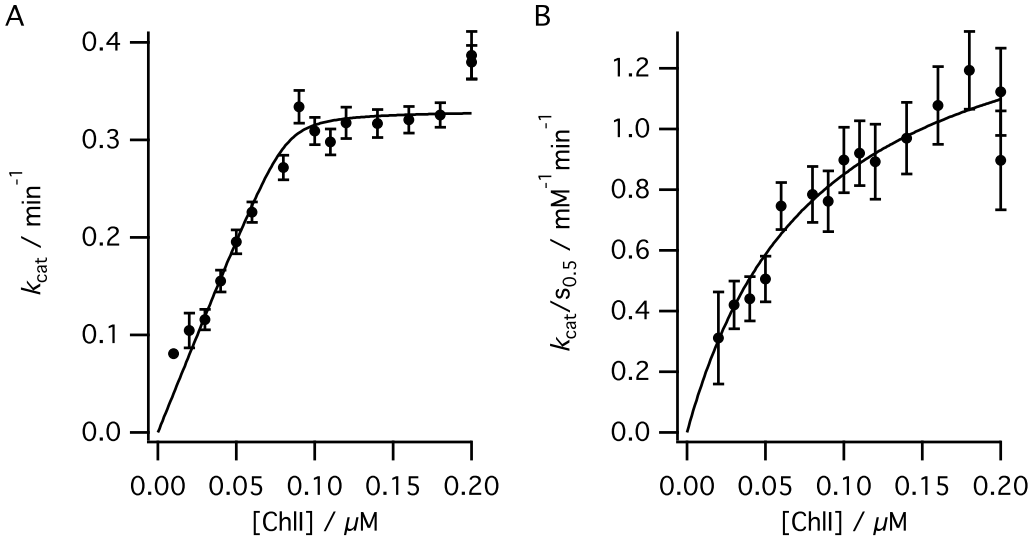

Figure 5.16: Binding titration of ChlI into a constant concentration of ChlD and ChlH - A) ChlI titrated into constant concentration of ChlD (0.1 μM). Values for k_{cat} obtained from the concentration of ChlH (0.3 μM) after fitting to the Hill equation. Line plotted is theoretical and described by the tight binding model (equation 5.3). E = 0.078 $\pm$ 0.006 μM, $K_d = 1.7 \pm 2.1$ nM. **B)** Second order rate constant $k_{\mathrm{cat}}/s_{0.5}$ plotted against concentration of ChlI. Line plotted is theoretical and described by equation 5.3. E = 0.056 $\pm$ 0.04 μM, $K_d = 0.03 \pm 0.03$ μM. Assay performed in 50 mM MOPS/KOH, 0.3 M glycerol, 0.5 – 5 mM ATP, 10 mM free $MgCl_2$, 8 μM D_{IX}, 34 °C, pH 7.7.

Table 5.3: Comparing the variance of experimental results of k_{cat} to predicted results based on the models in figure 5.18A-C using the sum of squares of the difference between experimental and modelled results. *Modeled number of subunits that can be substituted before failure to power chelation.

Protein	Comparison Model*					
	independent	five	four	three	two	one
K53A	0.0037	0.0023	0.0058	0.0262	0.0739	0.1606
E154Q	0.0023	0.0014	0.0041	0.0200	0.0581	0.1312
R210A	0.0037	0.0034	0.0090	0.0324	0.0838	0.1753

$$k^{obs} = k^{max} \times \frac{[I]_T + [D]_T + K_d - \sqrt{([I]_T + [D]_T + K_d)^2 - 4[I]_T[D]_T}}{2[D]_T} \tag{5.3}$$

5.2.4.3 Steady state kinetic analysis of mixed mutant complexes

The steady state rate (ν_{ss}) of magnesium chelation was recorded with respect to $MgATP^{2-}$ concentration at different ratios of mutant to wild type, at a constant total concentration of ChlI. ν_{ss} was calculated as the maximum slope of the change in fluorescence over ten minutes, and plotted against [$MgATP^{2-}$] and the data fitted to the Hill equation (figure 5.17).

As the proportion of mutant increases, chelatase activity is inhibited. 100 percent mutant traces show no activity (trace 8 in figure 5.17). For k_{cat}, comparing a linear decrease in turnover against the control (figure 5.18A-C) is the most appropriate model, as in the control there is a linear decrease in k_{cat} as the concentration of ChlI is lowered. The data from mutant mixing and the control shows little difference from linearity, except at high concentrations of mutant. Analysis of the variance of experimental results from modelled behaviour (table 5.3) shows little difference between the linear model and one or two essential subunit models, but large differences favouring the linear model over three or more essential subunit models.

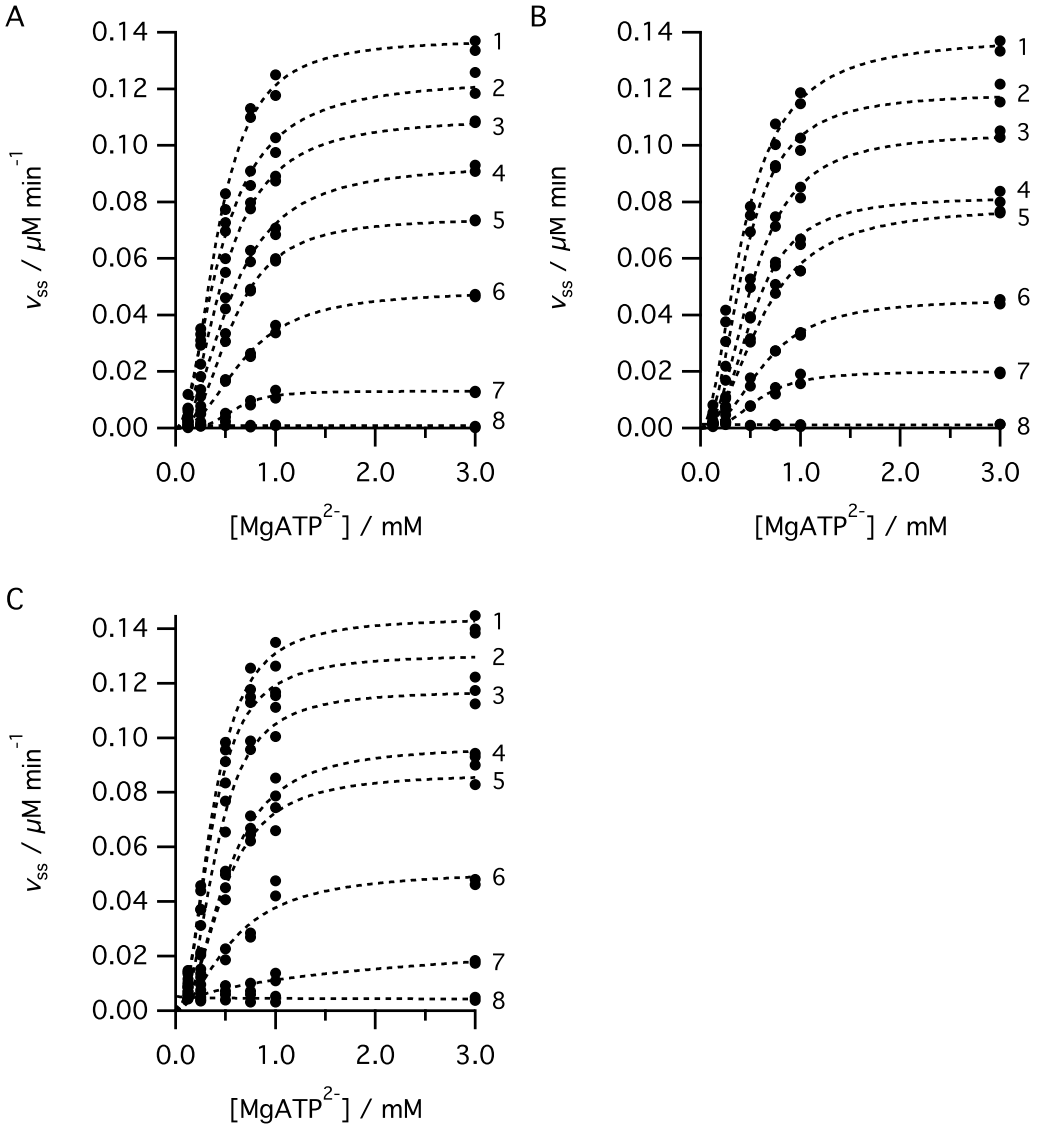

Figure 5.17: ChlI WT titrated against ATPase mutants at different concentrations of ATP - **A)** ChlI WT titrated against K53A at different concentrations of ATP; **B)** ChlI WT titrated against E154Q; **C)** ChlI WT titrated against R210A. Concentration of ChlH = 0.4 μM, ChlD = 0.1 μM, total concentration of ChlI WT and Mutant = 0.1 μM. Assay conditions 50 mM MOPS, 0.3 M glycerol, 1 mM DTT, pH 7.7, 34 °C. 1, 0% mutant; 2, 12.5% mutant; 3, 25% Mutant; 4, 37.5% Mutant; 5, 50% Mutant; 6, 62.5% mutant; 7, 75% mutant; 8, 100% mutant. Data fitted to equation 2.2.

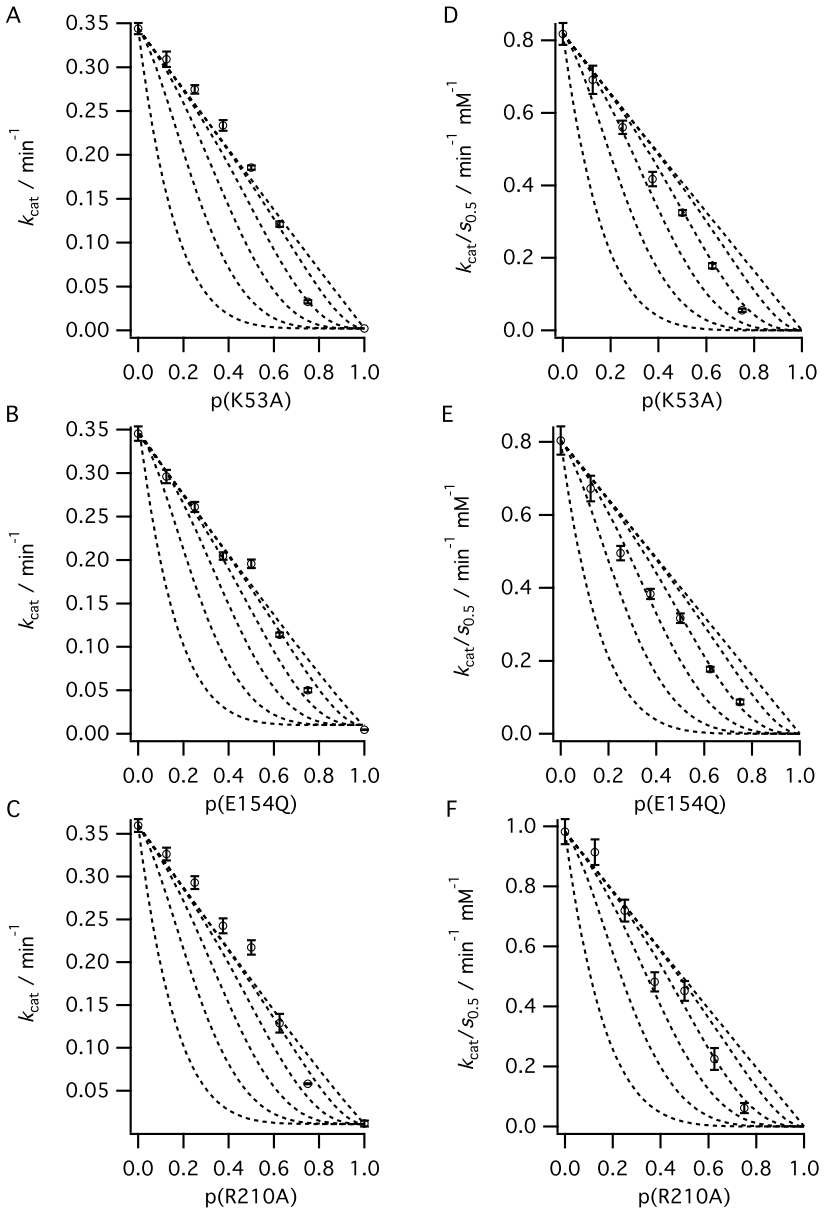

Figure 5.18: k_{cat} and $k_{cat}/s_{0.5}$ with respect to the mixing of mutant with wild type protein - Graphs A, B and C show plots of the 1st order rate constant, k_{cat} against the proportion of mutant. Graphs D, E, and F show plots of second order rate constant $k_{cat}/s_{0.5}$ against proportion of mutant. The lines plotted are theoretical plots of activity of mixes from equations 5.1 and 5.2).

Table 5.4: Comparing the variance of $k_{cat}/s_{0.5}$ experimental results to predicted results based on the models in figure 5.18D-F using the sum of squares of the difference between experimental and modelled results. *Modeled number of subunits that can be substituted before failure to power chelation.

Protein	Comparison Model*					
	independent	five	four	three	two	one
K53A	0.0537	0.0327	0.0053	0.0299	0.1764	0.5483
E154Q	0.0589	0.0414	0.0170	0.0313	0.1464	0.4689
R210A	0.0721	0.0437	0.0145	0.0731	0.3311	0.9510

It can be concluded that cooperative communication between subunits does not affect k_{cat}. At saturating nucleotide concentrations the rate determining step does not require coordinated action by ChlI and may not directly depend on hydrolysis of ATP in the active site of ChlI. Once nucleotide is bound, there is no communication between subunits to promote activity, suggesting probabilistic ATP hydrolysis.

The second order rate constant $k_{cat}/s_{0.5}$ (figure 5.18 D, E and F), reveals the enzyme efficiency at limiting substrate concentration. The mixing data show a non-linear drop in activity on increasing the proportion of mutant. Comparison of these data with the modelled curves suggest a model where two or three subunits are essential (table 5.4).

The simplest interpretation is that there is a change in behaviour between the k_{cat} and $k_{cat}/s_{0.5}$ conditions. An alternative explanation is at limiting nucleotide concentrations decreased activity may arise from a failure to assemble. The model proposed in figure 5.18 is too simple when hyperbolic behaviour is displayed for the no mutant control at limiting nucleotide concentrations (figure 5.16B). $k_{cat}/s_{0.5}$ of the mixed mutant species are consistently lower than the wild type control (figure 5.19). This observation suggest that mixed complexes of mutant and wild type are formed under these conditions and show less activity than the wild-type alone. Therefore interactions between wild type and mutant occur and disrupt metal ion chelation. This suggests cooperative

action between ChlI subunits is involved in binding nucleotide; binding of nucleotide on one subunit assists the binding of nucleotide to an adjacent subunit. It is unknown how substituted mutants are spatially distributed in the ChlI ring and there are a large number of potential substitution patterns (figure 5.20), which may affect nucleotide binding at $k_{\mathrm{cat}}/s_{0.5}$ conditions.

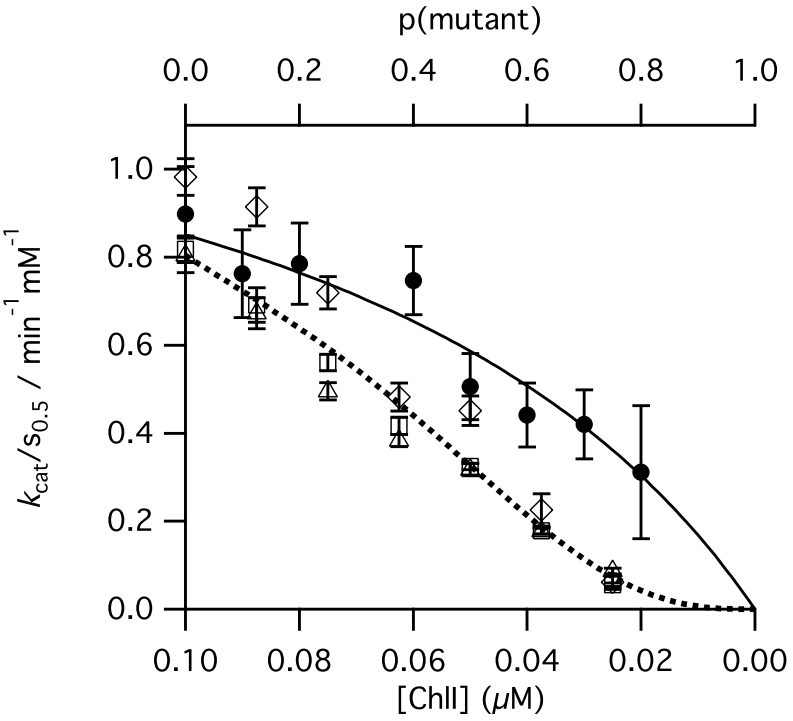

Figure 5.19: Comparing $k_{\mathbf{cat}}/s_{0.5}$ between control and mutant mixing - Filled circles, wild type control, decreasing the concentration (bottom x axis). Open squares, Walker A (K53A); Open Triangles, Walker B (E154Q); Open Diamonds, arginine finger (R210A) (proportion of mutant present top x axis). Solid line is binding equation 5.3 fitted to the wild type data. Dashed line is theoretical line for model where 3 substitution are acceptable, but on the 4th substitution activity is lost from equations 5.2 and 5.1.

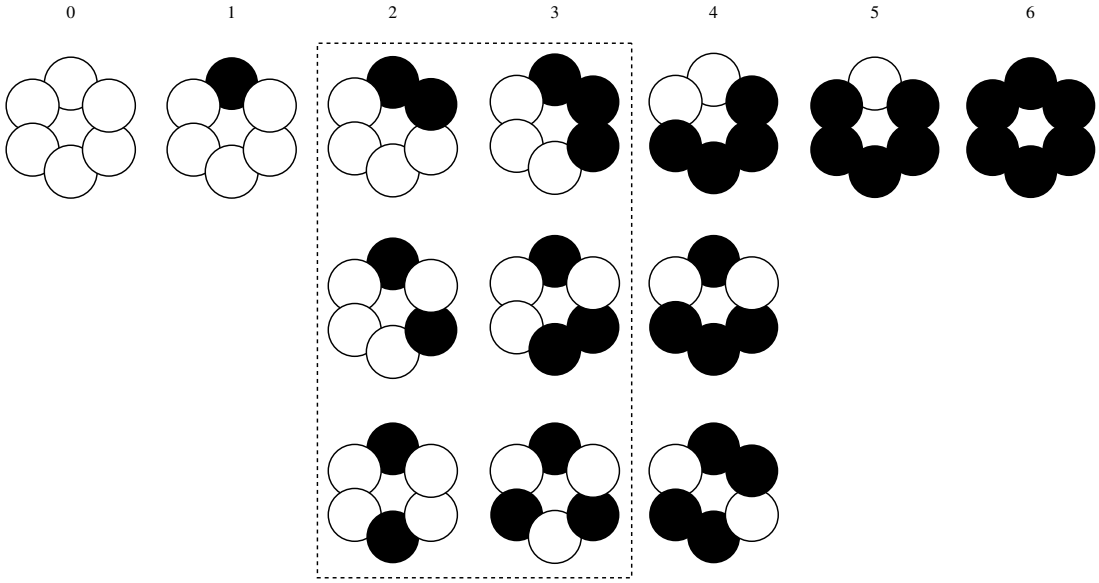

Figure 5.20: The distribution of isomers within the ring. - The dashed box indicates isomers of hexamers which may have either an increased or decreased catalytic power compared to that predicted by the model.

5.2.5 Additional global analysis of mutant mixing data

To perform a global fit on the steady state rate (ν_{ss}) data as reported in figure 5.17, a model was built (equation 5.4). This model has assumptions based on the analysis shown in figure 5.18 and assumes that the Hill equation describes the kinetic behaviour at any single concentration of mutant, showing cooperative behaviour with respect to the concentration of $MgATP^{2-}$.

$$\nu_{ss} = \sum_{i}^{n} \left(\left(\frac{v_{max,i} \cdot [\mathrm{ATP}]^{x,i}}{[\mathrm{ATP}]^{x,i} + s_{0.5,i}^{x,i}} \right) \cdot \left(\begin{bmatrix} n \\ i \end{bmatrix} p^i \left(1-p\right)^{n-i} \right) \right) \tag{5.4}$$

The global analysis appears to produce reasonable fits when compared to the raw data and the individual fits (figures 5.21, 5.22 and 5.23) with a good distribution of residuals. This model is more complex than those used earlier. The characterising parameters for each mixed species is unconstrained and under this condition they do

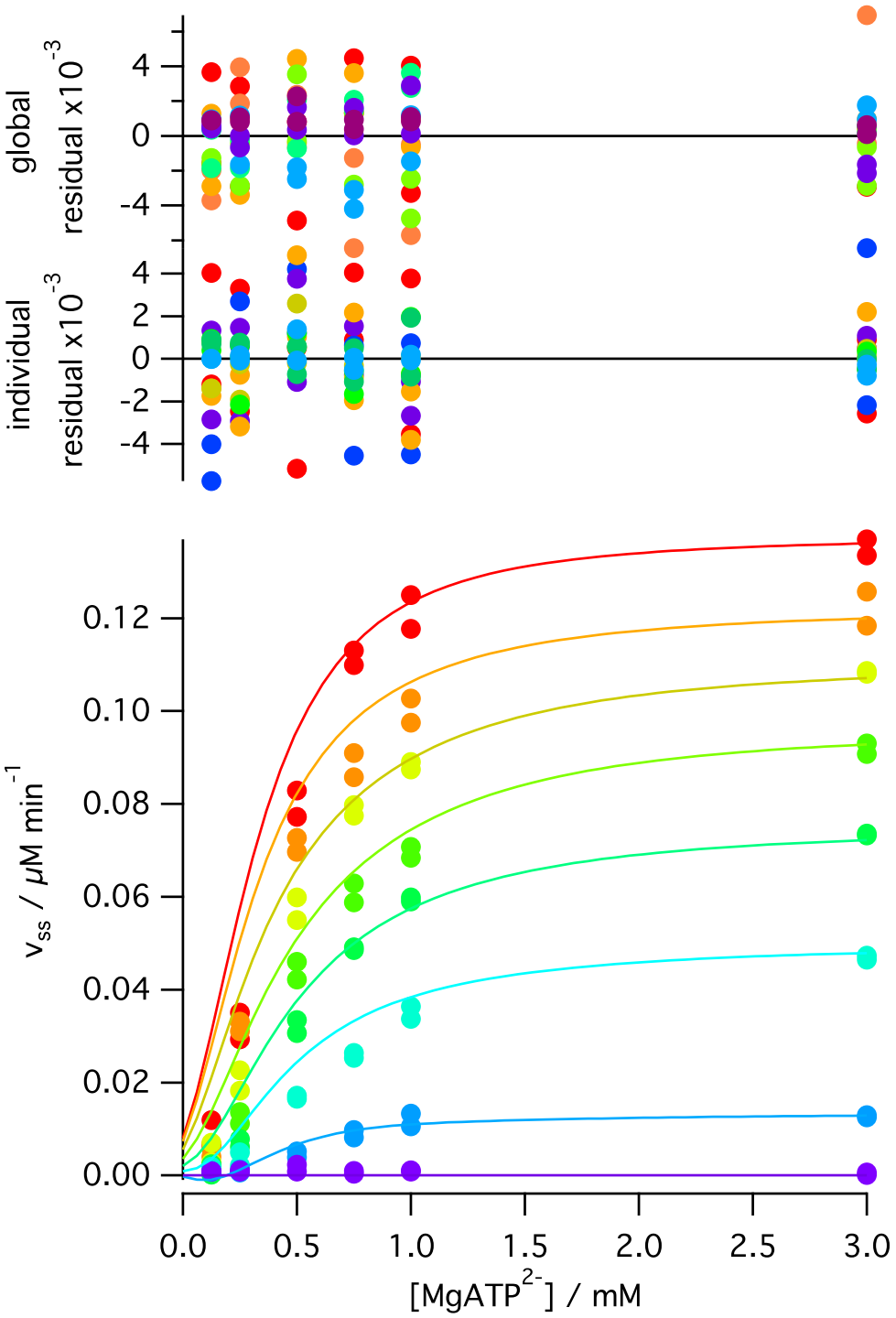

Figure 5.21: Comparison between global and individual mix fitting for Walker A mutant - K53A - Global fit in solid lines. Red, $p = 0$; orange, $p = 0.125$; yellow, $p = 0.250$; light green, $p = 0.375$; green, $p = 0.500$; light blue, $p = 0.625$; dark blue, $p = 0.750$; purple, $p = 1$.

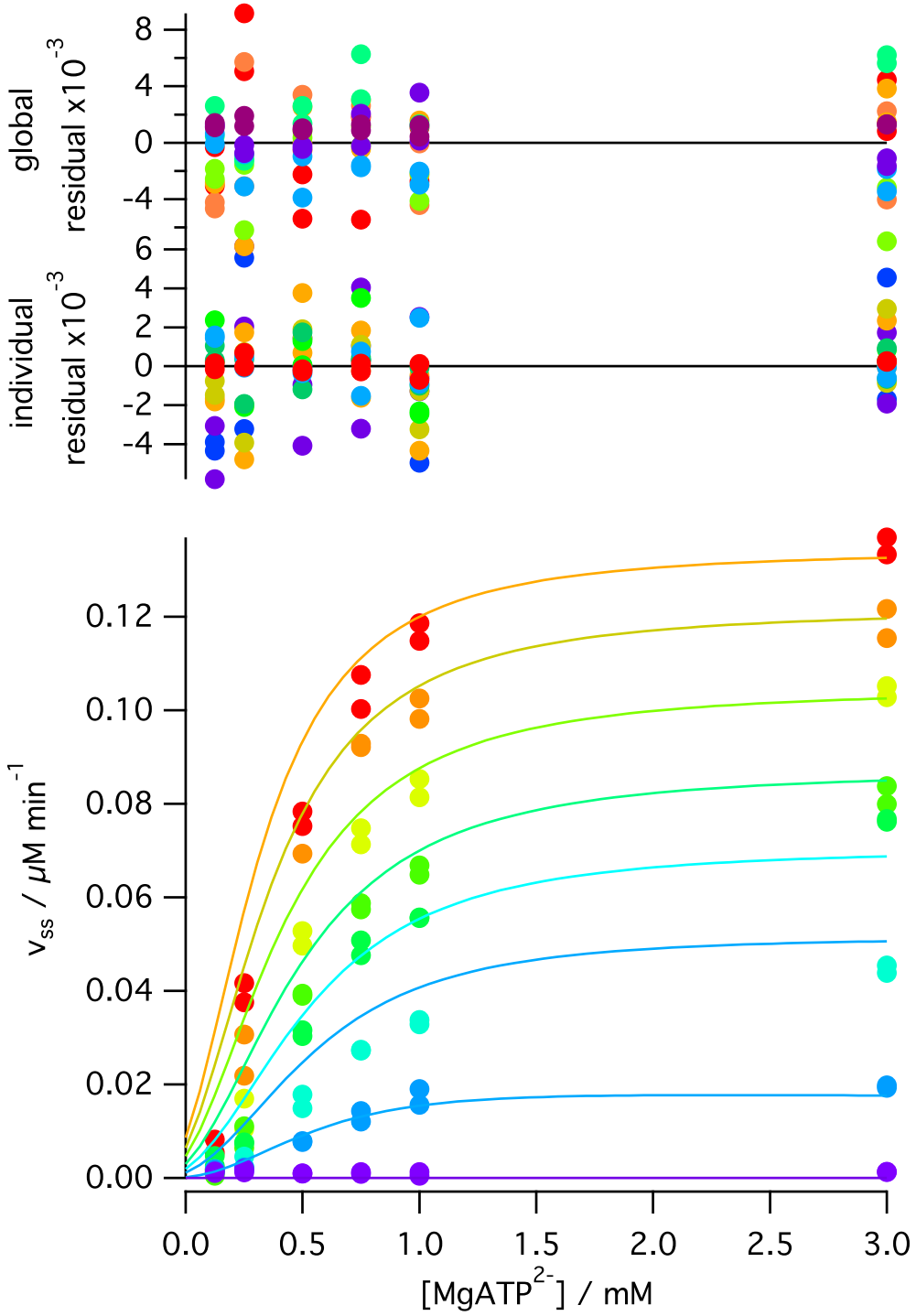

Figure 5.22: Comparison between global and individual mix fitting for Walker B mutant - E154Q - Global fit in solid lines. Red, $p = 0$; orange, $p = 0.125$; yellow, $p = 0.250$; light green, $p = 0.375$; green, $p = 0.500$; light blue, $p = 0.625$; dark blue, $p = 0.750$; purple, $p = 1$.

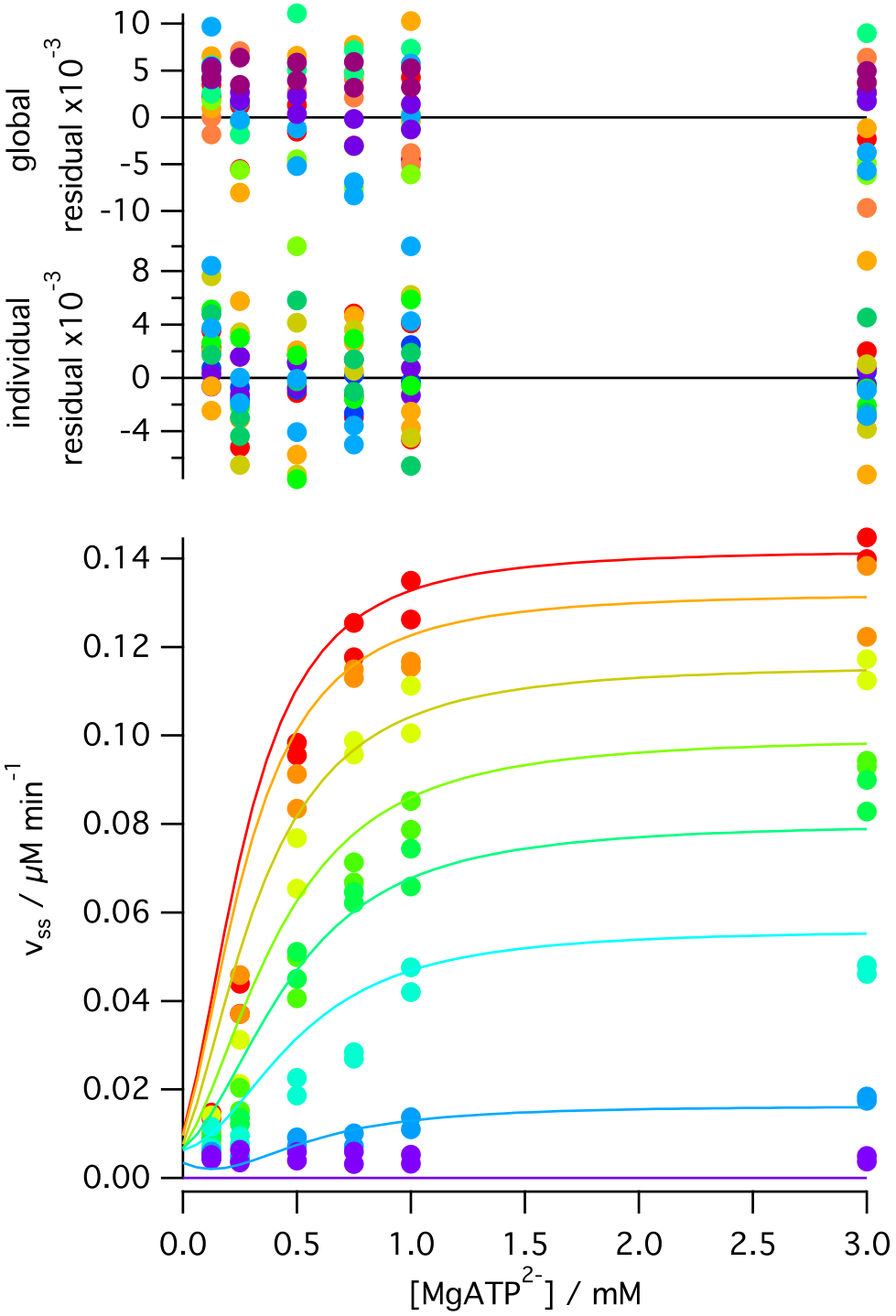

Figure 5.23: Comparison between global and individual mix fitting for Arginine Finger mutant - R210A - Global fit in solid lines. Red, $p = 0$; orange, $p = 0.125$; yellow, $p = 0.250$; light green, $p = 0.375$; green, $p = 0.500$; light blue, $p = 0.625$; dark blue, $p = 0.750$; purple, $p = 1$.

Table 5.5: Table of values of global fit coefficients from equation 5.4 fitted to the values of v_{ss} from the mutant mixing assays, where v_n is the maximal velocity of a ring with n substitutions, and s_n is the $s_{0.5}$ value of a ring with n substitutions.

Kinetic Parameter	Walker A (K53A)	Walker B (E154Q)	Arginine Finger (R210A)
v_0 / μM min^{-1}	0.138 ± 0.002	0.134 ± 0.002	0.142 ± 0.003
v_1 / μM min^{-1}	0.102 ± 0.007	0.135 ± 0.012	0.148 ± 0.014
v_2 / μM min^{-1}	0.126 ± 0.020	0.036 ± 0.027	0.047 ± 0.035
v_3 / μM min^{-1}	0.078 ± 0.026	0.156 ± 0.031	0.172 ± 0.039
v_4 / μM min^{-1}	0.062 ± 0.024	0.006 ± 0.028	0.020 ± 0.029
v_5 / μM min^{-1}	-0.051 ± 0.015	-0.006 ± 0.017	-0.037 ± 0.021
v_6 / μM min^{-1}	–	–	–
s_0 / mM	0.42 ± 0.01	0.42 ± 0.01	0.36 ± 0.02
s_1 / mM	0.34 ± 0.03	0.49 ± 0.07	0.34 ± 0.04
s_2 / mM	0.76 ± 0.10	0.64 ± 0.61	0.65 ± 0.50
s_3 / mM	0.72 ± 0.19	0.65 ± 0.13	0.57 ± 0.14
s_4 / mM	0.43 ± 0.21	0.43 ± 2.07e+03	0.001 ± 5.74
s_5 / mM	0.41 ± 0.28	0.49 ± 5.26	0.25 ± 0.24
s_6 / mM	–	–	–

not converge to give a physically realistic solution (table 5.5). We conclude that the simpler analysis given above (section 5.2.4.3) is more appropriate for this data set.

5.2.6 Developing methodology to assess the assembly model of magnesium chelatase

The data analysis in this chapter requires a robust model of the complex size. Many AAA^+ proteins form hexameric rings. Previously Reid *et al* (60) published a structure for ChlI which detailed a heptameric structure for ChlI. This now appears to be a minor species; ChlI preferentially adopts a hexameric structure (*pers com*, Pu Qian, University of Sheffield).

The bacterial BchID complex from *Rhodobactor capsulatus* shows dual homohexamers of ChlI and ChlD. This dual ring structure has a resemblance to members of the AAA^+ HslU/ClpX/Lon/ClpA/B-C clade (58) as some of these proteins also form dual hexameric rings. The structure (figure 5.24) deposited in the protein data bank (67) does not show all of BchD, instead it appears just the integrin domain has been modelled. Some monomers of BchI share a close resemblance to the published crystal structure of BchI (orange in figure 5.24). A very different structure is also observed, with the C-terminal domain apparently pushed to a different conformation by the helix in red (yellow in figure 5.24).

The *Synechocystis* ChlID complex has been far more elusive. Analysis using hydrodynamic (size exclusion chromatography coupled with multi-angled light scattering and analytical ultra centrifugation) and imaging techniques (electron microscopy) has not yet provided a conclusive model.

5.2.6.1 ChlI forms a hexamer

In the presence of nucleotide, ChlI forms hexamers based on data from electron microscopy and size exclusion chromatography. In contrast, the size and structure of the

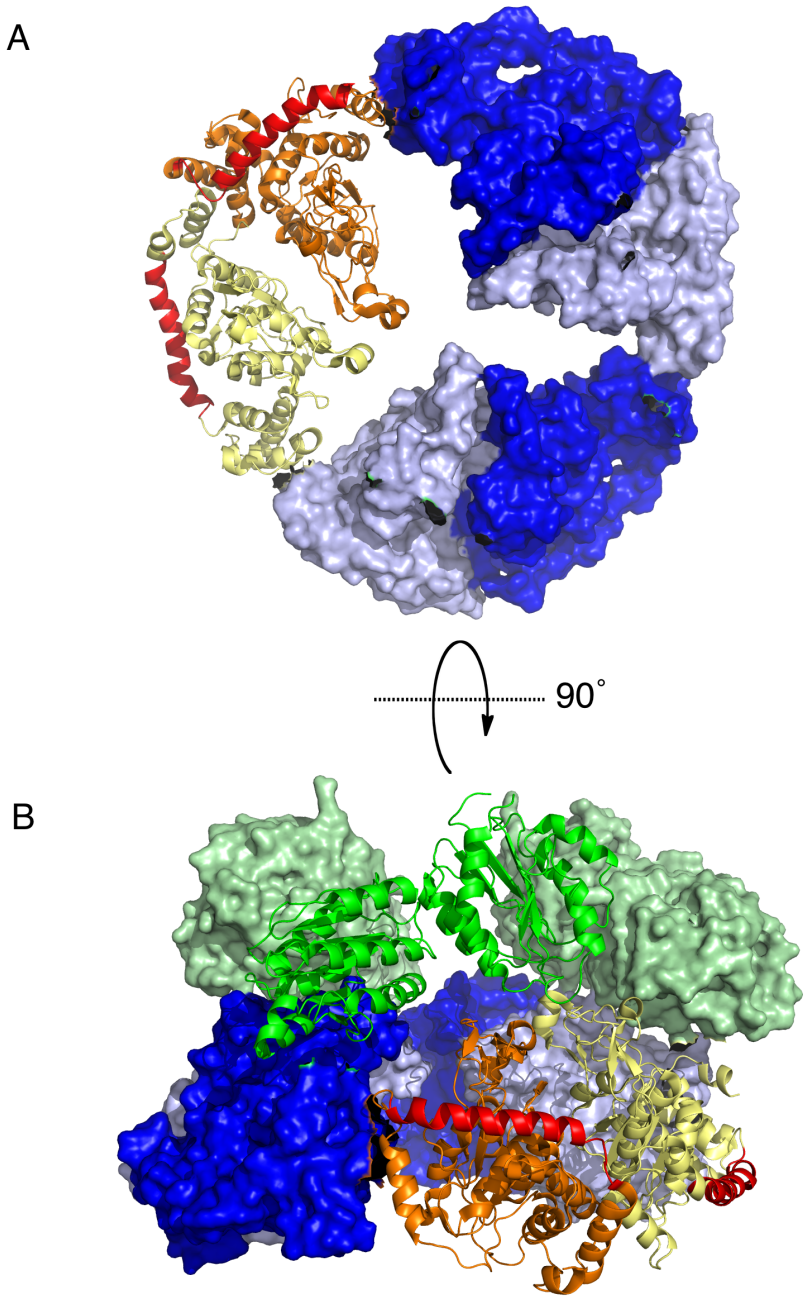

Figure 5.24: Cryo EM reconstruction of BchID - **A** a hexamer of BchI is shown, with a surface representation in light and dark blue of four monomers, in their dimer like state, with two monomers represented as cartoon in orange and yellow. The entire hexamer appears as a trimer of dimers. The red coloured helix appears to push the C terminal of BchI to different locations within the structure. **B** 90 ° rotation of **A** with the addition of the apparent BchD structure in green from homology modelling as both surface and cartoon representations. PDB Code: 2X31, structure rendered using PyMOL (41).

ChlID complex and the size and structure of the entire catalytically competent magnesium chelatase complex has yet to be determined.

Size exclusion chromatography of wild-type ChlID in the presence of saturating nucleotide (figure 5.25), shows the majority of the fluorescently labelled ChlI is in a complex of 226 kDa in size, which equates to 6 monomers. When this peak is analysed by electron microscopy (figure 5.28) a hexameric ring with C3 symmetry is the majority structure observed, and no ChlD is observed by SDS-PAGE. The peak at 16 minutes in figure 5.25 is likely monomeric ChlD mixed with non-assembly competent ChlI. SEC of ChlD in nucleotide appears to be a monomer which elutes at 16 minutes (figure 5.26). There is no peak in either the light scattering or absorbance elution profile attributable to a $ChlI_6CHlD_6$ (*ca.* 670 kDa) complex.

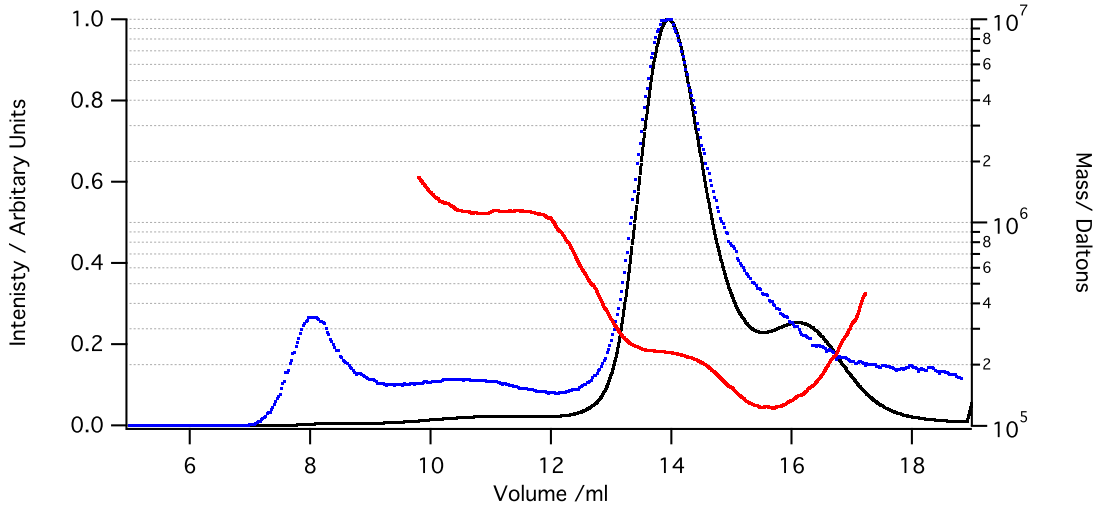

Figure 5.25: Size Exclusion Chromatography of ChlID complex - 12.5 μM ChlI labelled with fluorescein-5-maleimide, 7 μM ChlD; Black line is UV absorbance at 473 nm, blue line is light scattering and red line is absolute molecular weights. Chromatography was performed in 50 mM tricine/NaOH, 0.3 M glycerol, 1 mM DTT, 5 mM ADP, 15 mM $MgCl_2$, pH 7.9, 25 °C.

Analytical ultracentrifugation (AUC) monitoring the sedimentation of ChlI labelled with fluorescein-5-maleimide in the presence of nucleotide shows there are many differ-

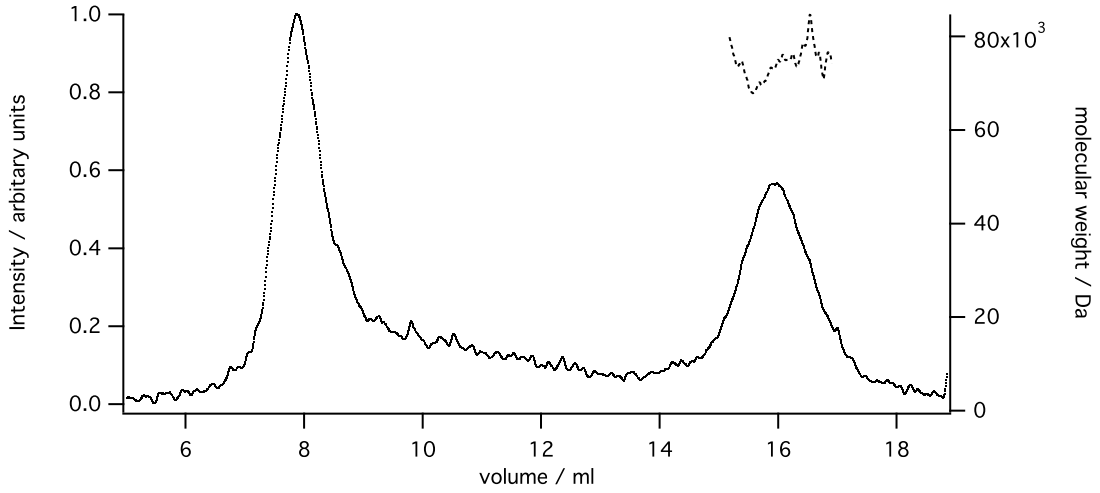

Figure 5.26: SEC of ChlD in the presence of ADP - ChlD in the presence of ADP showed one peak with a molecular weight of 75 kDa. Chromatography was performed in to 50 mM tricine/NaOH, 0.3 M glycerol, 1 mM DTT, 5 mM ADP, 15 mM $MgCl_2$, pH 7.9, 25 °C.

ent complexes present in solution (figure 5.27 bottom trace). When ChlD is mixed with ChlI in equimolar amounts, the broad spread of complexes seen with ChlI coalesces to a large peak of around 120 kDa is size. This does not correlate with the proposed $ChlI_6ChlD_6$ peak.

No complex has yet been detected which could be identified as a $ChlI_6ChlD_6$ complex, and subunit stoichiometry remains uncharacterised.

5.2.6.2 Capturing the ChlID complex on a surface

To understand how the magnesium chelatase complex is constructed, the active ChlID complex which binds to ChlH must be characterised.

A single molecule spectroscopy approach has been investigated. **F**luorescence **i**magining at **o**ne **n**anometre **a**ccuracy (FIONA) is an optical imaging technique which provides imaging resolutions far beyond the diffraction limit of light. Imaging of labelled protein can be achieved at the 1 – 10 nm range (136, 137). Using single molecule spectroscopy,

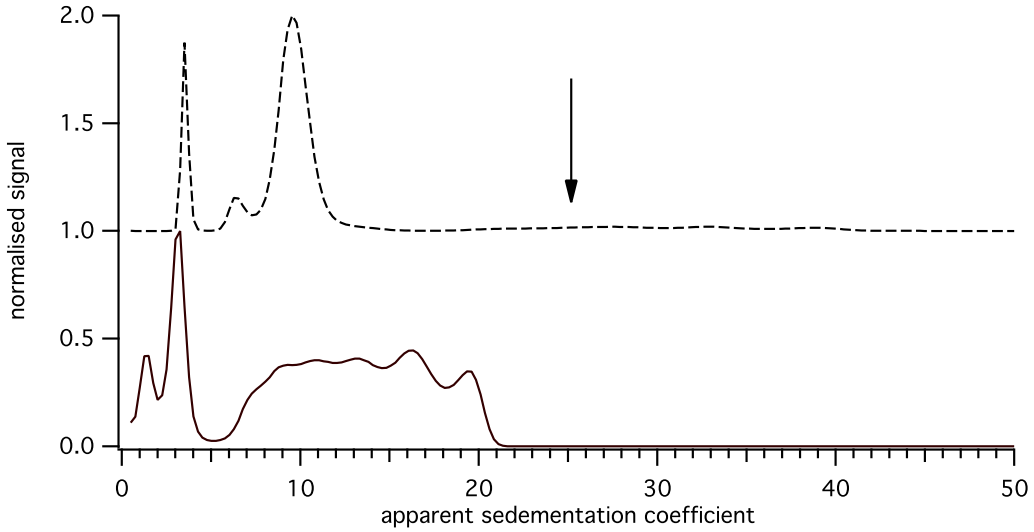

Figure 5.27: Analytical ultracentrifugation of ChlI and ChlID - Bottom trace, 8 μM ChlI labelled with fluorescein-5-maleimide (ChlI-f5m), top trace 8 μM ChlI-f5m and 8 μM ChlD. The arrow indicates the approximate location a $ChlI_6ChlD_6$ complex would appear on the trace. AUC was performed in 50 mM tricine/NaOH, 0.3 M glycerol, 1 mM DTT, 5 mM ADP, 15 mM $MgCl_2$, pH 7.9, 25 °C

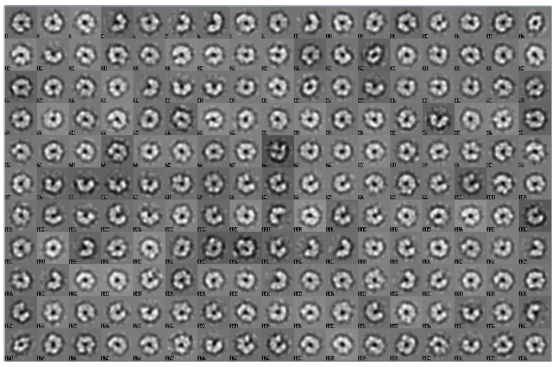

Figure 5.28: Electron micrograph of ChlI rings - Negative stain electron micrograph of ChlI in the presence of ADP. ChlI appears to form either hexamers, or partially constructed rings, such as trimers and dimers. Image courtesy of Amanda Brindley.

the stoichiometry of individual complexes can be determined. One approach monitors stepwise photobleaching of fluorophores within a complex, counting the number of bleaching events that occur. This provides a number of subunits present. More simply monitoring the fluorescence intensity of individual complexes allows a similar determination of stoichiometry. In mixed complexes of wild-type and mutant, it is expected that labelling wild-type and mutant with different fluorescent labels will allow calculation of the level of substitution within a ring.

These techniques require purified recombinant protein to be attached to a surface while still able to catalyse a reaction. The His_6 tag of ChlD was exploited to attach protein to a Ni-NTA functionalised glass cover slip (scheme 5.4), via the mechanism in scheme 5.5 (84).

Scheme 5.4: Schematic representation of surface modification. A clean glass substrate, **1**, is immersed in a solution of (3-Aminopropyl)triethoxysilane to produce the functionalised substrate **2**, which is coupled to glutaraldehyde and then a Ni-NTA amine conjugate, providing a chelating surface, **4**.

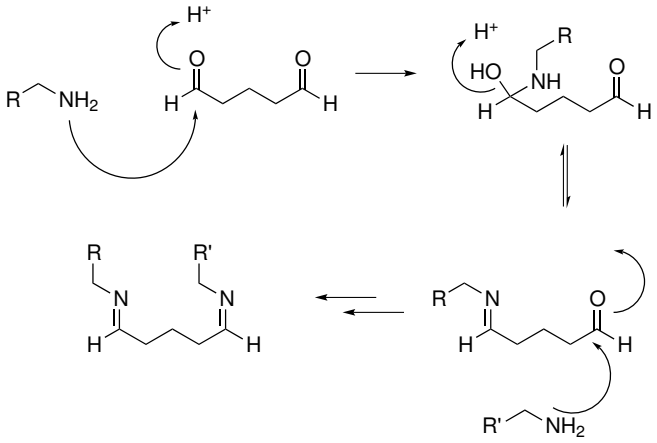

Scheme 5.5: The mechanism of amine – amine coupling via glutaraldehyde, reproduced from Ducker (84).

A patterned surface (138) with squares functionalized with Ni-NTA ligands was used to bind His_6-ChlD labelled with tetramethylrhodamine-5-maleimide and imaged using confocal microscopy (figure 5.29). The images clearly show regular squares of labelled ChlD bound to the surface.

Similarly a mixture of ChlI labelled with fluorescein-5-maleimide and ChlD labelled with tetramethylrhodamine-5-maleimide in the presence of ADP was bound to a patterned coverslip and the two different fluorophores imaged with confocal microscopy (figure 5.30). It was found that the two proteins were collocated in the same square pattern. This demonstrates that the two proteins were able to interact to form a complex. When non tagged ChlI was flowed on the surface without ChlD, no bound protein was observed.

5.2.7 Maintaining chelatase activity with labelled proteins.

On labelling ChlI with fluorescent tags, effectively all of the chelatase activity of the protein was abolished. Although the protein was still able to interact with ChlD (see figures 5.10 and 5.30) the loss of chelatase activity suggests that the full catalytic complex may not be formed. Previous modification of cysteines did not abolish activity but that study used the relatively small *N*-ethylmaleimide instead of larger fluorophores used here (59). Therefore the loss of activity is likely due to steric changes introduced

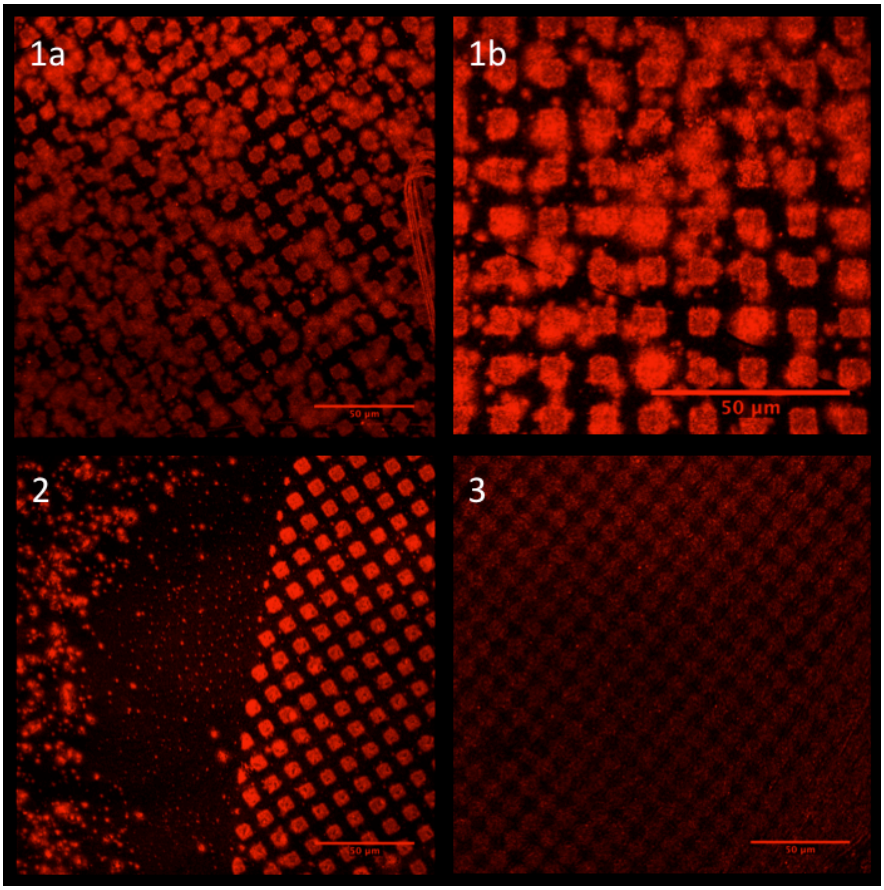

Figure 5.29: ChlD on a surface - Confocal microscopy of ChlD labelled with tetramethylrhodamine-5-maleimide. 1a) High concentration of ChlD (∼100 nM solution bound to surface in 20 μl for 30 seconds) Tetramethylrhodamine was excited using 543 nm (80% transmission) and emission detected between 565 and 615 nm. b) enlargement and rotation of section from image a highlighting regular 15 μm squares; 2)Edge image showing difference between patterned and unpatterned surface, 3)lower concentration of ChlD (∼10 nM) bound to surface. All slides were in a solution of 50 mM MOPS/KOH, 0.3 M glycerol, 5 mM ADP, 15 mM $MgCl_2$, pH 7.9. Scale bar 50 μm.

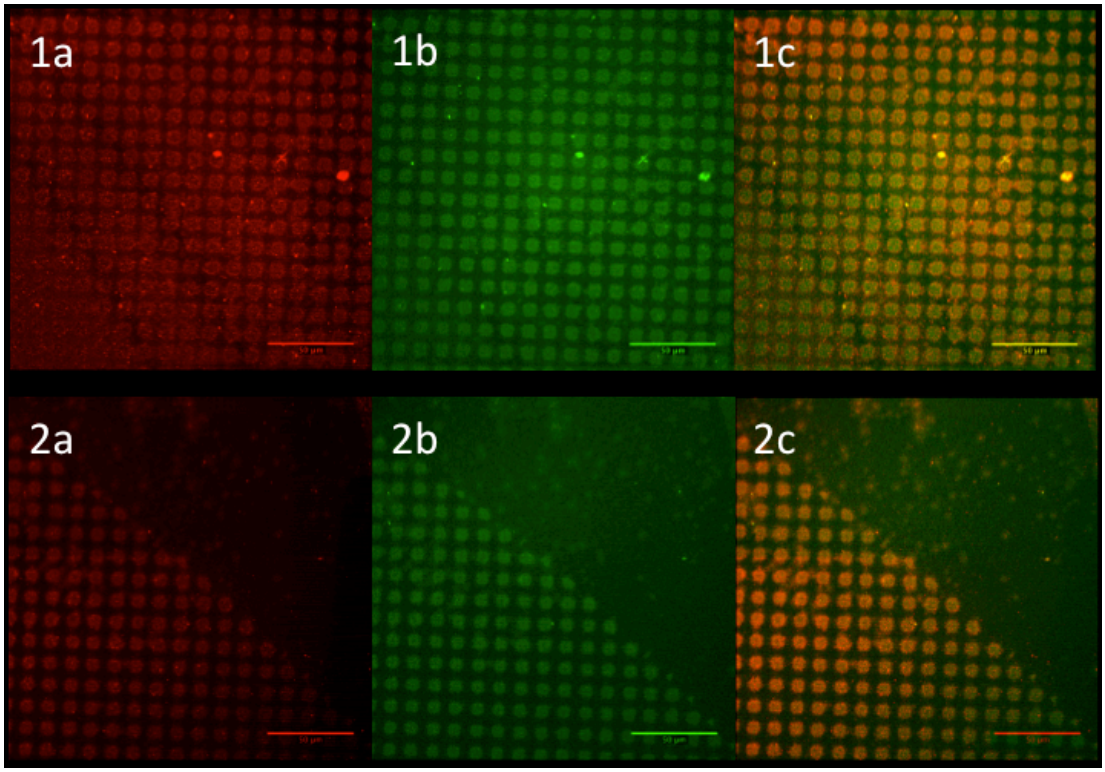

Figure 5.30: ChlID complex on surface - Confocal microscopy of ChlD labelled with tetramethylrhodamine-5-maleimide and ChlI labelled with fluorescein-5-maleidmide. 1) Section highlighting regular structure of square patten. 2) Edge section comparing morphology of labelled and unlabelled surface. a) Excitation at 543 nm (80% transmission) with emission monitored between 565 and 615 nm, showing the emission of labelled ChlD attached to surface through His_6, with the a square pattern Ni-(NTA) surface; b) excitation of ChlI at 488 nm (6% transmission) with emission monitored between 500 and 550 nm c) two channel combination of images a and b highlighting the co localisation of the protein on the surface. Approximately 20 nM of protein was washed onto surface for 30 seconds in 50 mM MOPS/KOH, 0.3 M glycerol, 5 mM ADP, 15 mM $MgCl_2$, pH 7.7. Scale bar 50 μm.

by the label. As the labelling protocol uses maleimide chemistry which modifies the cysteines, mutagenesis of these residues may allow production of active labelled protein.

A series of single cysteine mutants were produced. These proteins were monitored for activity before and after labelling with fluorescein. Two mutants (C244S and C324S) were active after labelling (table 5.6).

5.2.7.1 Stability of cysteine mutants and interactions with wild-type ChlD.

CD spectroscopy of the mutants (figure 5.31) revealed that the mutant C121S was not folded correctly, while the other three mutants (C244S, C282S and C324S) were folded. Pull down assays of the interaction between wild type His_6ChlD and ChlI cysteine mutants (figure 5.32) showed that C121S failed to form a complex with His_6ChlD. The other three mutants were able to form a complex in the presence of free magnesium and nucleotide.

5.2.7.2 ChlI cysteine mutants labelled with fluorescein-5-maleimide retain chelatase activity.

Purified cysteine mutants were labelled in the standard manner, with desalting in a spin column. The C244S mutant via inspection of the gel appears to label to a much lower degree compared to C282S and C324S (figure 5.33). The C282S protein was inactive after labelling. C244S maintained full or greater activity ($k_{\mathrm{rel}} = 1.4$) compared to unlabelled protein, while C324S activity lowers ($k_{\mathrm{rel}} = 0.36$) compared to unlabelled protein (figure 5.34).

Table 5.6: Summary of characterisation of ChlI cysteine mutants. *concentrations and therefore relative chelatase activity is based on column efficiencies as supplied by the manufacturer.

Mutant	DNA Sequenced	Transformed/Expressed	Purified	CD Spec	Melting Temperature / °C	Chelatase activity	Relative chelatase activity after labelling / Percentage*
C121S	✓	✓	✓	not folded	not folded	n.d.	–
C244S	✓	✓	✓	✓	52	✓	140
C282S	✓	✓	✓	✓	47	✓	< 0.01
C324S	✓	✓	✓	✓	38	✓	36

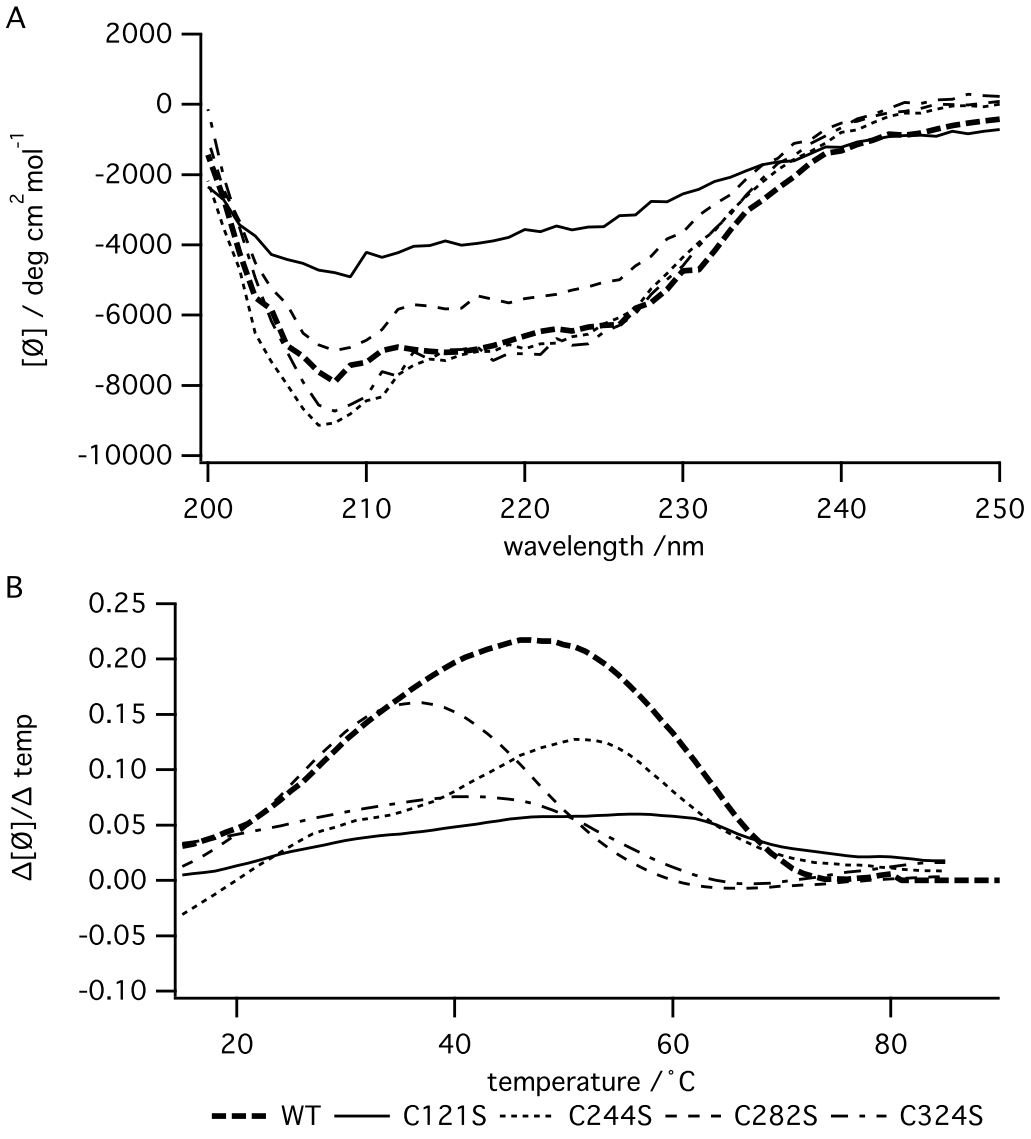

Figure 5.31: CD spectroscopy of ChlI cysteine mutants - **A** circular dichroism spectra of ChlI cysteine mutants, **B** Melting temperature of mutants. CD performed in 50 mM potassium phosphate buffer pH 7.4, spectra recorded at 25 °C, stepwise detection, 4 second response. Melting temperature determined by monitoring circular dichroism at 222 nm while increasing temperature at 1 °C per minute, and the first derivative of the graph taken. The major peak in the first derivative is taken as the melting temperature. For mutant C244S there appears to be two melting temperatures.

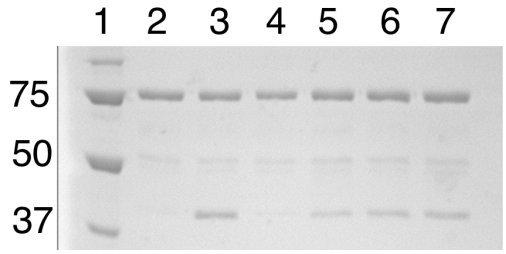

Figure 5.32: Pulldown Assay of ChlI Cysteine mutants with ChlD - 8% SDS-PAGE gel of cysteine mutants in the presence of $MgATP^{2+}$. Lane 1, Markers (units kDa); lane 2, WT ChlI no ATP; lane 3, WT and ATP; lane 4, C121S + ATP; lane 5, C244S + ATP; lane 6, C282S; lane 7, C324S + ATP.

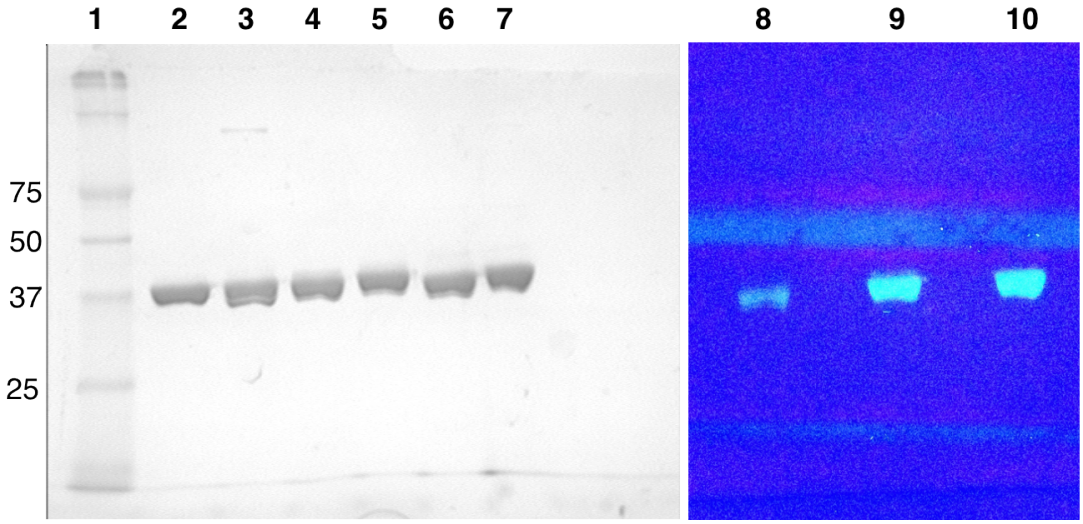

Figure 5.33: Labelling Cysteine mutants with fluorescein-5-maleimide - Cysteine mutants were labelled in the presence of ADP and $MgCl_2$. Lane 1, markers; lane 2, C244S pre label; lane 3, C244S post label; lane 4, C282S pre label; lane 5, C282S post label; lane 6, C324S pre label; Lane 7, C324S post label. Lane 8, C244S; lane 9, C282S and lane 10 C324S after maleimide labelling illuminated with a UV transilluminator.

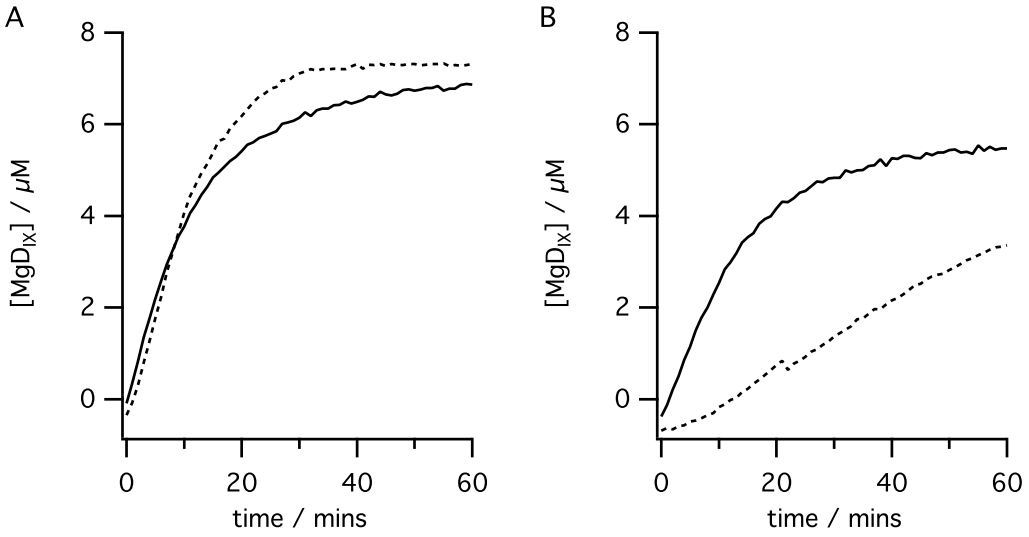

Figure 5.34: Chelatase assays showing activity of mutants after labelling - ChlI cysteine mutants were assayed before and after labelling. Solid traces before labelling and dashes after labelling with fluorescein-5-maleimide. A) C244S B) C324S. Assays were performed in 50 mM MOPS/KOH, 0.3 M glycerol, 1 mM DTT, 5 mM ATP, 15 mM $MgCl_2$, 8 μM D_{IX} pH 7.7 34 °C, with 0.1 μM ChlD, 0.2 μM ChlI and 0.4 μM ChlH. Protein concentrations after labelling was estimated based on column efficiency.

5.3 Conclusion

Introducing certain mutations into the conserved ATP binding motifs in the AAA^+ domain of ChlI severely impairs ATPase activity of this subunit, and prevents chelatase activity. Even though ATPase activity is severely impaired and chelatase activity abolished, formation of an ChlID complex with these mutants is still possible in the presence of nucleotide.

The chelatase inactive ATPase mutants of ChlI were used to probe for cooperative behaviour while monitoring chelatase activity. At saturating nucleotide conditions, there is no statistically significant reason to prefer any of the substitution models over the linear independent subunit model. A linear decrease in chelatase activity was observed with increasing substitution into the ring. At higher concentrations of mutant to wild-type, there is some deviation from the control, but this is not statistically significant. This observation suggests that when saturated with nucleotide the chelatase rate is linearly dependant on the number of ATPase units. This is not consistent with a concerted mechanism where multiple subunits hydrolyse ATP simultaneously to drive chelation. Similar impaired ATPase mutants of BchI (132) analysing a single eqimolar mix of mutant to wild type came to similar conclusions as this piece of work, with each subunit acting independently to power chelation.

At limiting nucleotide concentration non-linear loss of activity is seen on increasing the proportion of mutant. This is notably different from the dilution control. The conclusion is that when not bound to nucleotide (i.e. $k_{\mathrm{cat}}/s_{0.5}$ conditions) ChlI units in magnesium chelatase interact to promote productive binding of nucleotide. Substitution with three or four mutants prevents this interaction and poisons the complex.

This work has observed the effect of mutant substitution on the coupled activity of the enzyme. The logical next experiment would be to observe the effect of mutant substitution on ATPase activity, while the reaction is powering chelation. The experiment is difficult to perform as the presence of porphyrin swamps other spectral signals. Stopped assays, using a radioactive substrate are not ideal given the need to determine

both k_{cat} and $k_{cat}/s_{0.5}$ at every proportion of mutant.

ChlI is the subunit which provides the energy to power chelation. More information on the assembly model of ChlID with ChlH is required to understand how hydrolysis and conformational change powers chelation. Hydrolysis signals appear to be separate from any allosteric signals which ChlD provides (see chapter 6).

Similar statistical substitution experiments have been performed with other AAA^+ ATPases. Dual ring AAA^+ disaggregases, *E. coli* ClpB and the yeast homologue Hsp104 were both found to have a linear relationship between activity with mutant substitution when only one of the two nucleotide binding domains per protomer were mutated (116, 117). Although disaggregase activity was linearly dependant on subunit substitution, the ATPase activity was not. In the single ring AAA^+ protein ClpX which associates with chaperones to power protease activity, Martin *et al* (131) produced constructs where subunits were covalently linked so that the precise substitution pattern was known. The work found at saturating nucleotide concentrations the the linked protease activity was powered probabilistically. At limiting substrate conditions it was proposed that ATP binding was cooperative (131). Martin *et al* fully characterised protein activity with respect to nucleotide concentration, but the majority of other studies have only characterised effect of mutant substitution using reaction rates at arbitrary substrate concentrations. Fully characterising the activity of the chelatases revealed cooperative action at limiting nucleotide concentrations, it remains to be seen if this is a general feature of AAA^+ enzymes.

In this study, it was also found that both the Sensor II arginine 291 and cysteine 121 are both vital residues required for correct protein folding.

Ensemble measurements do not allow visualisation of what is occurring to individual complexes. Single molecule spectroscopy of individual ChlID complexes attached to a surface will provide an opportunity to dissect the nucleotide bound state and potentially visualise any concerted or coordinated ATP hydrolysis using fluorescently labelled nucleotides and proteins. Forming ID complexes on a surface will provide a

valuable platform for future work on complex assembly and nucleotide binding.

6

The nucleotide binding site in ChlD is required for magnesium chelation.

6.1 Introduction

ChlD is essential for magnesium chelatase activity. With the two other essential proteins (ChlI and ChlH) it forms a multisubunit protein complex which powers chelation. The precise role of ChlD within this complex is not understood, but has been generally assigned a structural role within the chelatase (1). A purely structural role appears unlikely as ChlD is large protein containing various domains each associated with specialised functions in other proteins.

ChlD is a member of the AAA^+ family of proteins via sequence alignment (figure 6.1). The AAA^+ domain of ChlD is located at the beginning of the N-terminal (up to approximately residue 330). This region in *Nicotiana tabacum* ChlD shares 46 % sequence identity with ChlI, indicating a shared heritage. The AAA^+ domain of BchD has 38 % identity with BchI from *R. sphaeroides*, and homology modelling predicts a high degree of similarity for this region (figure 6.2). Although they both share an ATPase domain, there is no evidence to suggest that ChlD can bind or hydrolyse ATP in the absence of ChlI. AAA^+ proteins function by forming oligomeric structures, so it is possible that ChlD interacts with ChlI through the N-terminal AAA^+ domain to act as a scaffold for complex construction.

The C-terminal region contains an integrin domain. Modelling studies (figures 6.2 and 6.3) indicate a typical von Willebrand like region, with a surface exposed metal ion dependant adhesion site (MIDAS) motif. Integrins have a general structure consisting of a central β sheet surrounded by seven α helices in a typical α/β Rossmann fold (142). The MIDAS motif is a cation dependant functional site, regulating multi-protein interactions.

Between the N-terminal AAA^+ domain and the C-terminal domain there is a large polyproline linker. This polyproline linker has been previously shown to be the only essential part of the tobacco protein required for chelatase activity. As yet this has not been rationalised (63). One explanation could be that the N-terminal AAA^+ domain has a purely regulatory role, and the C-terminal protein-protein interaction domain is involved with protein-protein interactions outside of the core chelatase subunits (e.g.

Figure 6.1: Sequence alignment of ChlI and ChlD N-terminus subunits from various species - Key: ChlD Syn - *Synechocystis PCC 6803*, ChlD Pea - Garden Pea *Pisum sativum*, ChlD Tobac - Common tobacco *Nicotiana tabacum*, BchD R p - *Rhodopseudomonas palustris*, BchD R s - *Rhodobacter sphaeroides*, BchD R c - *Rhodobacter capsulatus*, ChlI Syn - *Synechocystis PCC 6803* Subunit I. Conserved motifs: red, Walker A; yellow, Walker B; green, arginine finger; blue, sensor II arginine.Alignment performed on UniProt (65) using the Clustal Omega program (120).

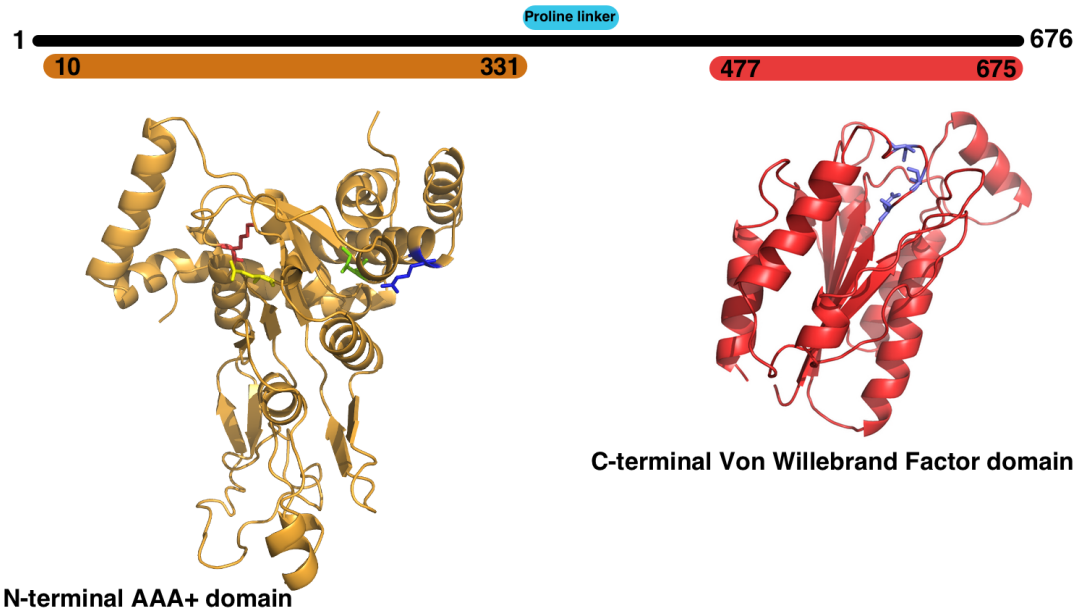

Figure 6.2: Structural features of ChlD by homology modelling - The ChlD amino acid sequence when parsed through Swiss Model (139) matches two areas to known structures and produced two models. The N-terminal (mustard colour) is matched to the structure of BhlI (38 % identity with in the region modelled) (PDB:1G8P) (56). The cartoon structure features stick representations of the conserved domains within the ATPase site: red, Walker A lysine; yellow, Walker B Glutamine; green , arginine finger; blue, sensor II arginine. The proline linker does not match any known structures. The C-terminal has 17% sequence identity with Tumour Endothelial Marker 8 (PDB: 3N2N) (56), which has the typical integrin fold found within von Willebrand domains. The MIDAS motif (DXSXS where X is any amino acid) is the functional part of the integrin, binding divalent cations is shown in blue sticks. Protein structures were rendered using PyMol (41).

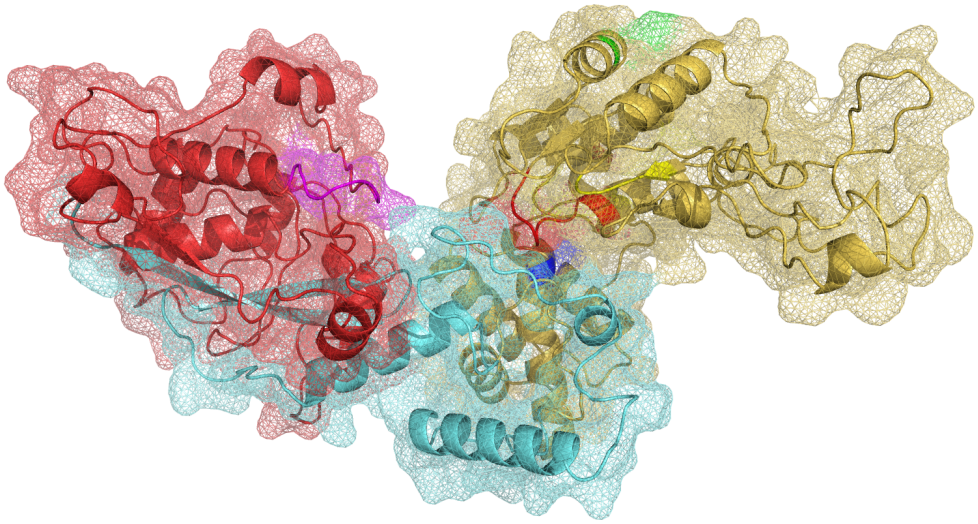

Figure 6.3: Homology model of ChlD - Whole structural model of ChlD produced by the I-TASSER server (140, 141). The model shows the AAA^+ domain in mustard, the proline and linker region in cyan and the c-terminal integrin domain in red. Structural features on the ribbon shown in the N terminal AAA^+ domain are red, Walker A domain; yellow, Walker B; green, arginine Finger; blue, sensor II arginine. In the von Willebrand domain purple highlights the MIDAS motif. The model predicts a surface accessible MIDAS domain, which would allow protein-protein interactions to occur at this interface. Protein structures rendered using PyMol (41).

with Gun4 or ChlM). Both ChlH and ChlI have the complementary motif to the MIDAS motif, so this is unlikely. It is likely that ChlD has a part to play in the intricate binding and regulatory process between ChlI and ChlH.

Despite the range of motifs present in the protein, no clear function has been assigned to ChlD. To address this lack of understanding, a series of mutants in the AAA^+ N-terminal domain were generated. These mutants were analysed to determine their assembly and catalytic properties. Functional analysis of these mutants reveal that this site is required for full activity.

6.2 Results and Discussion

6.2.1 Mutations in the AAA^+ domain of ChlD.

Point mutations of ChlD were introduced using the QuickChange method, sequencing confirmed insertion of the point mutation. Protein was expressed in Rosetta cells, and purified as wild type. Mutants expressed with similar yields as wild type. Table 6.1 summarises the mutations introduced and biophysical characterisation performed.

6.2.2 Biophysical Characterisation of ChlD mutants

Circular dichroism spectra were recorded for the four mutants of ChlD (figure 6.4) and were found to have no major changes of secondary structure or melting temperature (figure 6.5). It was deemed on this basis that the proteins were likely to have folded correctly.

6.2.3 Probing the interaction between ChlD and ChlI

ChlI and ChlD require the presence of nucleotide in order to interact, which can be monitored via a pull down assay via the His_6 tag on ChlD. In the previous chapter, it was shown that mutations in the ATP binding site of ChlI do not inhibit the formation

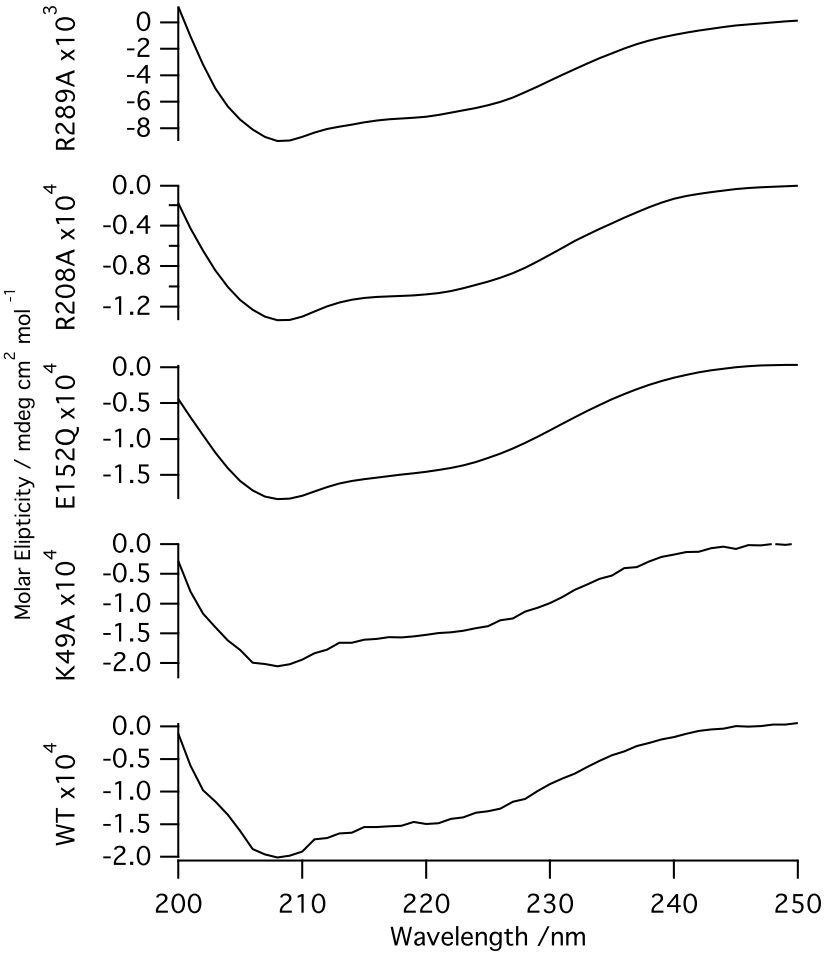

Figure 6.4: Circular Dichroism spectra of ChlD mutants from 250 – 200 nm - in 50 mM Potassium Phosphate buffer, pH 7.4, at 0.1 mg ml^{-1}, 25 °C. 0.2 mm pathlength, 4 second response

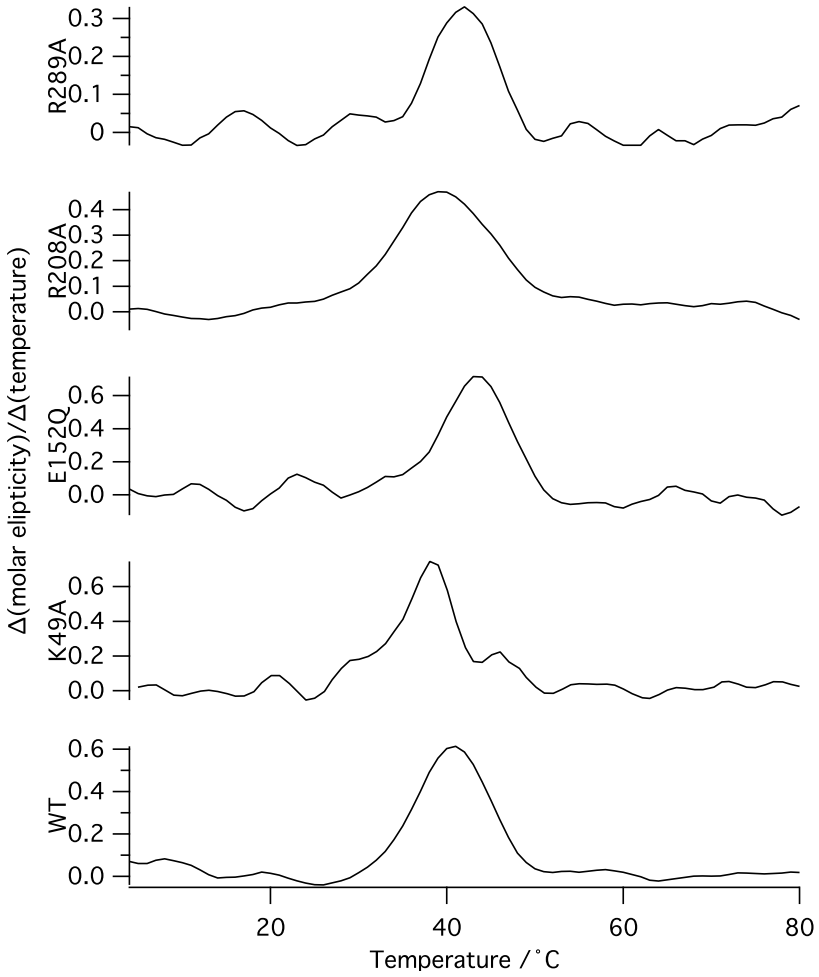

Figure 6.5: Circular Dichroism monitoring of 222 nm while increasing temperature at 1 °Cmin^{-1}, from 5 – 80 ° C - in 50 mM Potassium Phosphate buffer, pH 7.4, at ≈ 0.1 mg ml^{-1}, 25 °C. 0.2 mm pathlength, 4 second response.

Table 6.1: Table of mutants introduced into ChlD, with a summary biophysical characterisation.

Motif	Secondary Structure by CD	Melting Temperature / °C	Pulls down with ChlI	Chelatase Activity
Walker A K49A	✓	42	✓	✗
Walker B E152Q	✓	38	✓	✓
Arginine Finger R208A	✓	39	✓	✓
Sensor II R289A	✓	41	✗	✓

of a complex between ChlI and ChlD. ChlD when assayed individually has no intrinsic ATPase activity, and non-hydrolysable analogues of ATP do not inhibit the formation of an ChlID complex (78).

A pulldown between ChlI wild type and ChlD mutants (6.6) reveals that all mutants except for R289A (in the sensor II motif) are able to copurify ChlI in the presence of saturating nucleotide. Mutants in the Walker A motif are still able to interact.

6.2.4 Steady state characterisation of ChlD Mutants

The mutants were assayed for magnesium chelatase activity. The Walker A mutant was inactive. The three remaining active mutants were characterised with respect to concentration of $MgATP^{2-}$ (figure 6.7 and table 6.2), free Mg^{2+} concentration (figure 6.8 and table 6.3) and D_{IX} concentration (figure 6.9 and table 6.4).

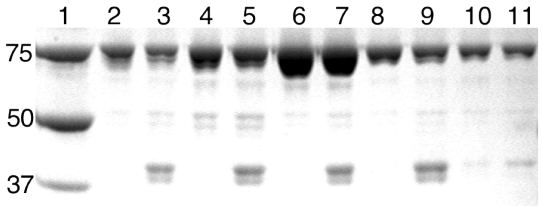

Figure 6.6: 8 %SDS Page gel photograph of pulldown between ChlI WT and ChlD ATPase mutants - Lane 1, Markers; 2, WT no ATP; 3, WT with ATP; 4, ChlD K49A no ATP; 5, ChlD K49A with ATP; 6, E152Q no ATP; 7, E152Q with ATP; 8, R208A no ATP; 9, R208A with ATP; 10, R289A no ATP; 11, R289A with ATP. Bands at $\approx$ 75 kDa are ChlD, $\approx$ 40 kDa are ChlI.

6.2.4.1 ChlD requires an intact nucleotide binding site for chelatase activity.

All mutants displayed activity except for the mutant K49A in the Walker A motif (figure 6.7). This mutation may prevent nucleotide binding to ChlD (54). The lack of activity indicates that this residue is important in the chelatase cycle, CD spectroscopy indicates the protein is folded, and the copurification with ChlI reveals the protein is still able to form a ChlID complex.

Other mutants of ChlD showed a decreased k_{cat} and an increased $s_{0.5}$ with respect to $MgATP^{2-}$ (table 6.2). These large changes in $k_{cat}/s_{0.5}$ are consistent with impaired nucleotide handling by the enzyme.

The Sensor II arginine mutant (R289A) displayed only minimal activity. In other AAA^+ systems this mutant is reported to be involved with inter-subunit interactions on ATP binding (54). On close inspection of the data (figure 6.7B) the protein appears to lose cooperative behaviour, and can be described equally well by the Michaelis-Menten or Hill model ($n_h = 0.9$). An initial hypothesis is that the sensor II arginine may be involved in a global conformational change in response to $MgATP^{2-}$. Preventing this conformational change by removing the arginine side chain stops the enzyme transitioning into a more active form. If the behaviour of the R289A mutant reflects the behaviour of the inactivated species, we can see that it shows substantially less activity

($k_{\text{cat}} \sim 12\%$ wild-type) than the wild-type protein.

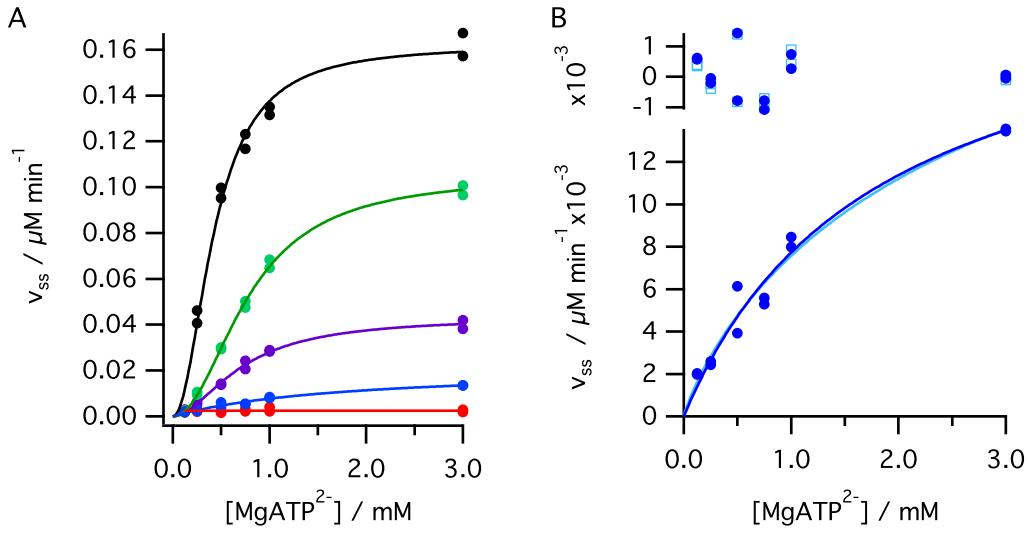

Figure 6.7: Magnesium chelatase steady state rates with respect to concentration of $\mathbf{MgATP^{2-}}$ - A) Black, Wild Type; Red, Walker A (K49A); Purple, Walker B (E152Q); Green, Arg Finger (R208A); Blue, Sensor II (R289A). **B)** Expansion of Sensor II data, lines described by Hill (light blue) and Michaelis-Menten equation (dark blue), with residuals above. Assays performed with 0.1 μM ChlD, 0.2 μM ChlI, 0.4 μM ChlD in 50 mM MOPS/KOH, 0.3 M glycerol,1 mM DTT 10 mM free Mg^{2+}, I = 0.1 with KCl, 8 μM D_{IX}, pH 7.7, 34 °C. The lines are theoretical, and described by the Hill equation with characterising parameters in table 6.2, except dark blue trace in panel B which is described by the Michaelis-Menten equation.

6.2.4.2 Mutations in the ATPase site affect enzyme handling of free Mg^{2+}.

The mutants of ChlD display a decreased ability to to utilise free magnesium (table 6.3), with comparable decrease in k_{cat} as above. Magnesium chelatase displays cooperative behaviour with respect to the concentration of free magnesium in solution (76). The Walker B and Arginine finger mutants continue to display cooperative behaviour with magnesium, with higher values for $s_{0.5}$, indicating a need for more magnesium for less overall activity. This change in kinetic parameters leads to a decrease in enzyme handling of free magnesium (from the overall 2nd order constant $k_{\text{cat}}/s_{0.5}$). There may

Table 6.2: Magnesium chelatase steady state catalytic coefficients with respect to concentration of $MgATP^{2-}$. Assays performed with 0.1 μM ChlD, 0.2 μM ChlI, 0.4 μM ChlD in 50 mM MOPS/KOH, 0.3 M glycerol,1 mM DTT, 10 mM free Mg^{2+}, $I = 0.1$ with KCl, 8 μM D_{IX}, pH 7.7, 34 °C. *The R289A Sensor II mutant did not show a cooperative response to $MgATP^{2-}$ ($n = 0.9$), K_m and k_{cat}/K_m are given.

Enzyme	k_{cat} / min^{-1}	$s_{0.5}$/ mM	$k_{cat}/s_{0.5}$ / $min^{-1}mM^{-1}$	n
Wild Type	0.41 ± 0.01	0.43 ± 0.03	0.94 ± 0.06	2
Walker A (K49A)	–	–	–	–
Walker B (E152Q)	0.11 ± 0.004	0.72 ± 0.044	0.15 ± 0.01	1.8
Arg Finger (R208A)	0.26 ± 0.005	0.79 ± 0.02	0.33 ± 0.01	2
Sensor II (R289A)*	0.05 ± 0.005	1.79 ± 0.32	0.02 ± 0.004	–

be slightly modified binding of magnesium to these mutants, but the small changes are difficult to interpret.

The Sensor II mutant (R289A) displays behaviour with respect to the concentration of free Magnesium (figure 6.8B) that does not fit to the Hill equation. These data have been fitted to the linear equation $v_{ss}/[\text{Enzyme}] = (k_{cat}/K_m)[Mg^{2+}]$. The mutation may abolish the cooperative behaviour with free magnesium concentration, much the same as with $MgATP^{2-}$. This linear response of ν_{ss} to $[Mg^{2+}]$ is consistent with both the Michaelis-Menten equation (where $[Mg^{2+}] \ll K_m$) and cooperative models (where $[Mg^{2+}] \ll s_{0.5}$). It cannot be concluded that this mutant has abolished the cooperative response to Mg^{2+}, but it can however be concluded that this mutant has a much poorer interaction with Mg^{2+} than wild-type. This altering of the behaviour may link the ATP binding site of ChlD and the MIDAS motif which is expected to bind to divalent cations (such as Mg^{2+}). Conformational changes on ATP binding transmitted through this arginine may lead to a change in the exposure of the MIDAS motifs. Future work should focus on mutations in the MIDAS motif to determine the effect on activity. If MIDAS mutants are active or partially active, double mutants in both the sensor II and the MIDAS motif should also be produced.

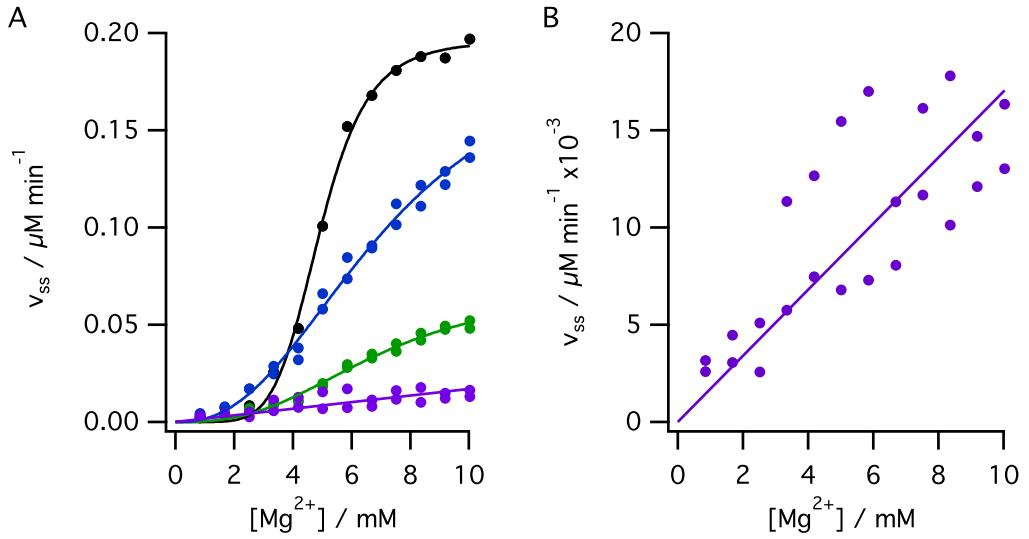

Figure 6.8: MgC steady state rates with respect to concentration of Mg^{2+} - **A)**Black, Wild Type; purple, Walker B (E152Q); green, Arg Finger (R208A); Blue, Sensor II (R289A). **B)** Expansion of Sensor II data, fitted to the linear equation $V_{max}/E = (k_{cat}/K_m)[Mg^{2+}]$. Assays performed with 0.1 μM ChlD, 0.2 μM ChlI, 0.4 μM ChlD in 50 mM MOPS/KOH, 0.3 M glycerol, 1 mM DTT , 5 mM ATP, I = 0.1 with KCl, 8 μM D_{IX}, pH 7.7, 34 °C. The lines plotted for WT, E152Q and R208A are theoretical, and described by the Hill equations, except R289A which is fitted to the linear equation $v_{ss}/[\text{Enzyme}] = (k_{cat}/K_m)[Mg^{2+}]$ with characterising parameters in table 6.3.

Table 6.3: Magnesium chelatase steady state catalytic coefficients with respect to concentration of Mg^{2+}. Assays performed with 0.1 μM ChlD, 0.2 μM ChlI, 0.4 μM ChlD in 50 mM MOPS/KOH, 0.3 M glycerol,1 mM DTT, 5 mM free ATP, I = 0.1 with KCl, 8 μM D_{IX}, pH 7.7, 34 °C. ‡ This value calculated from a linear fit to $v_{ss}/E = (k_{cat}/K_m)[Mg^{2+}]$.

Enzyme	k_{cat} / min^{-1}	$s_{0.5}$/ mM	$k_{cat}/s_{0.5}$ / $min^{-1}mM^{-1}$
Wild Type	0.49 ± 0.006	4.92 ± 0.04	0.10 ± 0.001
Walker A (K49A)	–	–	–
Walker B (E152Q)	0.17±0.02	6.97±0.67	0.03±0.004
Arg Finger (R208A)	0.50 ± 0.06	7.18 ± 0.74	0.07 ± 0.01
Sensor II (R289A)	–	–	0.0016 ± 0.0001‡

6.2.4.3 Mutations in the putative ATP binding site of ChlD do not affect enzyme handling of porphyrin

These mutants of ChlD show a range of behaviours in their response to porphyrin. With the mutation in the arginine finger motif (R208A), both k_{cat} and k_{cat}/K_m show little change from wild-type. In contrast the mutation in the Walker B motif (E152Q) shows a substantial drop in k_{cat} but no significant change in k_{cat}/K_m. The decrease in k_{cat} is comparable to that seen with the other substrates. As k_{cat}/K_m remains at around 75 % of wild-type in these mutants we can conclude that these mutations do not affect porphyrin handling by the chelatase. In contrast the mutant in the sensor II motif (R289A) has a lower k_{cat}/K_m at *ca.* 40 % wild type, which may be due to the enzyme being in the inactivated form.

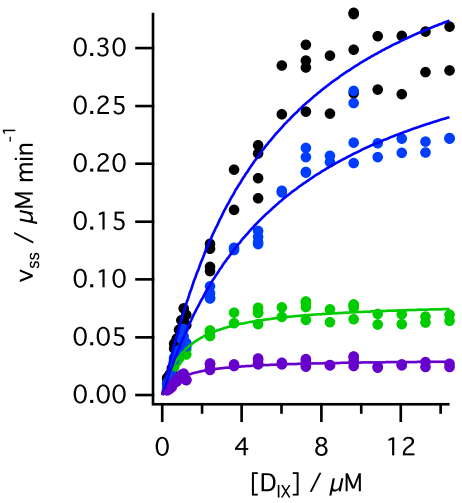

Figure 6.9: Magnesium chelatase steady state rates with respect to concentration of D_{IX} - Black, Wild Type; purple - Walker B (E152Q); green, Arg Finger (R208A); blue - Sensor II (R289A). Assays performed with 0.1 μM ChlD, 0.2 μM ChlI, 0.4 μM ChlD in 50 mM MOPS/KOH, 0.3 M glycerol, 1 mM DTT, 5 mM ATP, I = 0.1 with KCl, 8 μM D_{IX}, pH 7.7, 34 °C, in duplicate. Lines plotted are theoretical and described using the Michaelis-Menten equation with characterising parameters in table 6.4.

Table 6.4: Magnesium chelatase steady state catalytic coefficients with respect to concentration of D_{IX}. Assays performed with 0.1 μM ChlD, 0.2 μM ChlI, 0.4 μM ChlD in 50 mM MOPS/KOH, 5 mM ATP, 15 mM Mg^{2+}, I = 0.1 with KCl, pH 7.7, 34 °C.

Enzyme	k_{cat} / min^{-1}	K_m/ μM	k_{cat}/K_m / min^{-1} μM^{-1}
Wild Type	1.13 ± 0.06	5.74 ± 0.77	0.20 ± 0.03
Walker A (K49A)	–	–	–
Walker B (E152Q)	0.20±0.005	1.23±0.132	0.16±0.02
Arg Finger (R208A)	0.86 ± 0.046	6.31 ± 0.75	0.14 ± 0.02
Sensor II (R289A)	0.08 ± 0.002	1.00 ± 0.12	0.08 ± 0.01

6.3 Conclusion

The concentration of tetrapyrroles within cells is tightly regulated, as porphyrins are photolabile and toxic (143). Build-up of these products in any of the three main branches of porphyrin biosynthesis is rapidly contained via a number of signalling pathways, including microRNA and protein transcription inhibition (143, 144).

Magnesium chelatase stands at the branch point between heme and chlorophyll biosynthesis, and has a regulatory role on the level of chlorophyll biosynthesis. It has been shown the ChlH subunit in particular has a number of regulatory roles (34, 145).

These mutations of ChlD indicate there is extensive coordination between subunits within the magnesium chelatase complex. Unlike similar mutations in ChlI, removing highly conserved residues in the putative ATPase site does not stop chelation. The nucleotide binding site on ChlD is an allosteric regulator rather than one that directly drives chelation, although the interesting behaviour of the sensor II mutants indicates an involvement with productive binding of nucleotide, free magnesium and porphyrin.

At this stage it is unknown whether ChlD hydrolyses ATP, as that reaction is difficult to isolate from the ChlI ATPase activity. ChlD at high concentrations (*ca.* 10 μM) precipitates in the presence Mg^{2+}, leading to difficulties in determining low ATPase

activity. In future work ChlI could be chemically modified with a covalently bound ATP analogue, and then the ATPase activity of the protein could be monitored. But as the ChlI ATPase site is required for chelatase activity, this would not then be able to describe the contribution of the ChlD active site to chelation.

Previous work has shown that there is a high stoichiometry between number of ATP molecules hydrolysed compared to magnesium porphyrin products produced (76). The presence of a ATP binding site on ChlD may begin to explain this. Depending on the number of ChlD subunits in the complex there may be up to 12 binding sites for ATP on the magnesium chelatase complex. If ChlD hydrolyses ATP in a signalling role, this may explain the high stoichiometry. The free energy of ATP hydrolysis on ChlD may amplify allosteric signals between protein subunits.

7

Discussion

7.1 Summary of thesis

Magnesium chelatase is a complex multisubunit enzyme of unknown stoichiometry which inserts a magnesium ion into protoporphyrin IX. This is the first committed step in the synthesis of chlorophyll (1). All organisms that synthesise chlorophyll *a* have been found to contain magnesium chelatase.

Standing at the branch point of heme and chlorophyll synthesis, magnesium chelatase catalyses the first committed step in chlorophyll biosynthesis. Studying this enzymatic process allows us to understand the flux of pigment precursors. As well as a catalytic role inserting the metal ion, within higher plants and *Synechocystis*, the ChlH subunit has a role in regulating the levels of abscisic acid (48) and appears to be involved in plastid to nucleus signalling (145).

This thesis has focused mainly on the role of the two AAA^+ proteins of magnesium chelatase, ChlI and ChlD. The work presented provides insights into how the free energy released by the hydrolysis of ATP is coupled to metal ion insertion, and how that energy is related to the levels of products produced, and has begun the process of dissecting the allosteric signalling pathways within the complex.

7.1.1 Insights into the ATP hydrolysis pathway of Magnesium Chelatase.

AAA^+ proteins can be viewed as modular systems with conserved domains which interact with many biochemical systems and provide energy through the hydrolysis of ATP. The hydrolysis of ATP drives protein conformational changes which power reactions at spatially distinct active sites. This is in contrast to other ATPases that activate their products through phosphorylation.

Magnesium chelatase forms a non-covalent E.Pi complex within the reaction pathway. This intermediate is formed when the chelatase is catalysing metal ion insertion. The alternative E.ADP complex was not detected except in the ATPase reaction of isolated ChlI (scheme 7.1).

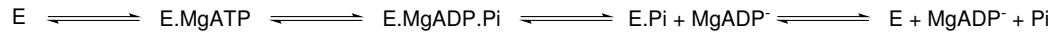

Scheme 7.1: The on enzyme pathway of ATP hydrolysis - an enzyme-phosphate complex was detected when magnesium chelatase is catalysing metal ion insertion.

Magnesium chelatase does bind ADP, however, as ADP stimulates the formation of ChlID complexes, and ADP inhibits magnesium chelation. BchI adopts different conformations in the presence of ADP and non-hydrolysable analogues of ATP suggesting nucleotide dependant conformation changes (60, 67). Based on this pathway information, structural studies (such as SAXS and EM) in the presence of phosphate and at high enough enzyme concentration for self-assembly would be of interest, as high concentration of phosphate does not inhibit chelatase activity. The E.Pi species is likely to reflect a biologically relevant complex.

7.1.2 How powerful an Enzyme is Magnesium Chelatase?

Understanding how an enzyme can temporarily shift the mass action ratio towards unfavourable products requires understanding of the fundamental thermodynamics of an enzyme mediated reaction. Magnesium chelatase shifts the mass action ratio, $[MgD_{IX}]/[Mg^{2+}][D_{IX}]$, from 10^{-6} to 150 at saturating conditions of porphyrin, MgATP and free magnesium by coupling the free energy of ATP hydrolysis with magnesium ion insertion. The free energy associated with this change in mass action ratio is +53 kJ mol^{-1}, well within the free energy of ATP hydrolysis at cytoplasmic concentrations. Potentially the fact that deuteroporphyrin is not the natural substrate for the protein may induce the super-stoichiometry (15 ATP to 1 MgD_{IX} - on the order of 840 kJ mol^{-1} free energy released per magnesium porphyrin produced), there is scope for investigating the ATP stoichiometry with the natural substrate, protoporphyrin IX. As there is super-stoichiometry of ATP to metal ion insertion process, something more subtle is occurring in energy linkage. It is possible magnesium chelatase titrates down the amount of free energy available via leak pathways (103) to decrease the amount of magnesium porphyrins produced, due to the photolabile and cytotoxic nature of these products.

Magnesium chelatase enhances the rate of reaction ($k_{\mathrm{cat}}/k_{\mathrm{uncat}}$) by 400×10^6 M^{-1}. Among enzymes studied, this is a value within the range of observed rate enhancements. The turnover of magnesium chelatase is not fast, but the large rate enhancement is accounted by the incredibly slow rate of spontaneous magnesium deuteroporphyrin production. Magnesium chelatase is also an effective catalyst ($\frac{k_{\mathrm{cat}}/(K_{\mathrm{M}}^{\mathrm{DIX}}s_{0.5}^{\mathrm{Mg}})}{k_{\mathrm{uncat}}} = 30 \times 10^{15}\mathrm{M}^{-1}$) with a catalytic proficiency corresponding to an attomolar transition state affinity. The putative transition state analogue, *N*-methylmesoporphyrin has only micromolar affinity for the magnesium chelatase, as opposed to nanomolar inhibition in ferrochelatase. The transition state affinity is likely altered along the ATP hydrolysis pathway. The amount of energy required for the magnesium chelatase reaction is likely due to the strong magnesium-water coordination bond which must be broken and replaced with a weaker magnesium-nitrogen bond.

7.1.3 The unconcerted ATP hydrolysis powering magnesium chelation.

Mutating the conserved AAA^+ binding motifs abolished chelatase activity and severely impairs ATPase activity. The ATPase activity of ChlI is required to power metal ion chelation.

These AAA^+ mutants were used to investigate if coordinated ATPase activity is required for chelatase activity. When these mutants are mixed with wild type, mixed heterohexamers are produced. When the proportion of mutant subunits is increased there is a linear decrease in k_{cat}. This linear loss of activity is consistent with the subunits acting independently. At saturating nucleotide the ATPase activity of one monomer contributes one sixth of the activity of a hexamer of ChlI, and the turnover of the chelatase reaction is stochastic rather than coordinated. In contrast at limiting MgATP^{2-} concentrations (i.e. following $k_{\mathrm{cat}}/s_{0.5}$) we observe a notably non-linear loss of activity on increasing the proportion of mutant. This arises as subunits interact to bind ATP.

7.1.4 A function for ChlD.

The AAA^+ domain in ChlD is an allosteric activator of magnesium chelatase activity. On mutating conserved residues in this domain, the activity of magnesium chelatase decreases. Removing the Walker A lysine deactivates the enzyme entirely, this is an essential residue. Other mutants (in the Walker B, arginine finger and sensor II motifs) decrease the activity. These results are not completely consistent with previous data where it was shown that only the linker between the N-terminal AAA^+ domain and the C-terminal integrin domain was required for activity (63).

The sensor II arginine appears to be directly involved in regulating cooperativity towards both magnesium and $MgATP^{2-}$. The mutant in this motif (R289A) shows a hyperbolic response to $MgATP^{2-}$ and a linear, albeit scattered, response to Mg^{2+}. This suggests a role in communicating between subunits of the protein (66, 67).

7.2 Towards an allosteric signalling pathway between ChlI and ChlD.

The interaction mechanism within the ID complex may be similar to the yeast AAA^+ chaperone Hsp104 (ClpB in *E. coli*). The Hsp100/Clp family of chaperones assist in proteolysis, genetic regulation and responses to environmental stress (146). Hsp104 and ClpB are homologous and respond to heat shock by deaggregating proteins.

Hsp104 and ClpB form hexameric rings containing 12 nucleotide binding sites, two per subunit, with a two tired ring structure resembling the published BchID complex (67, 147). In these heat shock proteins, there is allosteric communication both within and between subunits (117). The nucleotide binding sites in each ring of these deaggregases have different properties; one ring binds nucleotide tightly but with low activity while the other binds less tightly but readily hydrolyses nucleotide. These sites communicate; mutations in one ring affect the properties of the other (117, 147). Cooperative behaviour is displayed with ATP binding in one site inducing binding and turnover in the next (146, 147). This interplay between binding sites is required for the coordinated

procession of proteins through the hexamers central pore (147, 148).

The interplay between the two nucleotide binding domains is revealed when both binding sites within a protomer are mutated (116, 147, 149). A complicated signalling pathway between the binding sites within a protomer exists which then communicates with the adjacent subunit (117, 150), altering the affinity and turnover of ATP in a concerted manner.

The AAA^+ mutants of ChlD have shown the importance of this domain in controlling chelation. If similar domain–domain interactions exist between ChlI and ChlD then ring interactions models need to be considered. A plausible example is given in figure 7.1. Experimentally such models could be tested with the simultaneous use of mutants in ChlI and ChlD. It is possible that allosteric signals in either of the proteins are transduced by the MIDAS motif, as mutations in this domain abolish activity in BchD (66). To fully interpret these experiments, the catalytic ChlID species should be defined.

7.3 Different assembly complexes of ChlID which power chelation.

The definite stoichiometry of the ChlID complex has not been determined (figure 7.2), but it does appear different assembled species in solution are able to power chelation. When titrating ChlI into a constant concentration of ChlD and monitoring chelatase activity, the fastest turnover observed occurs at approximately equimolar concentrations of ChlI and ChlD, with a tight binding curve (figure 7.2A). Notably the hyperbolic change in the second order rate constant $k_{cat}/s_{0.5}$ (figure 5.16B), shows the kinetic consequences of nucleotide dependant complex formation.

The opposite titration, where ChlD is titrated into a constant concentration of ChlI, produces very different results (figure 7.2B). In this case, the chelatase system rapidly reaches a maximum in turnover number when the subunit ratio is 5 : 1 ChlI : ChlD.

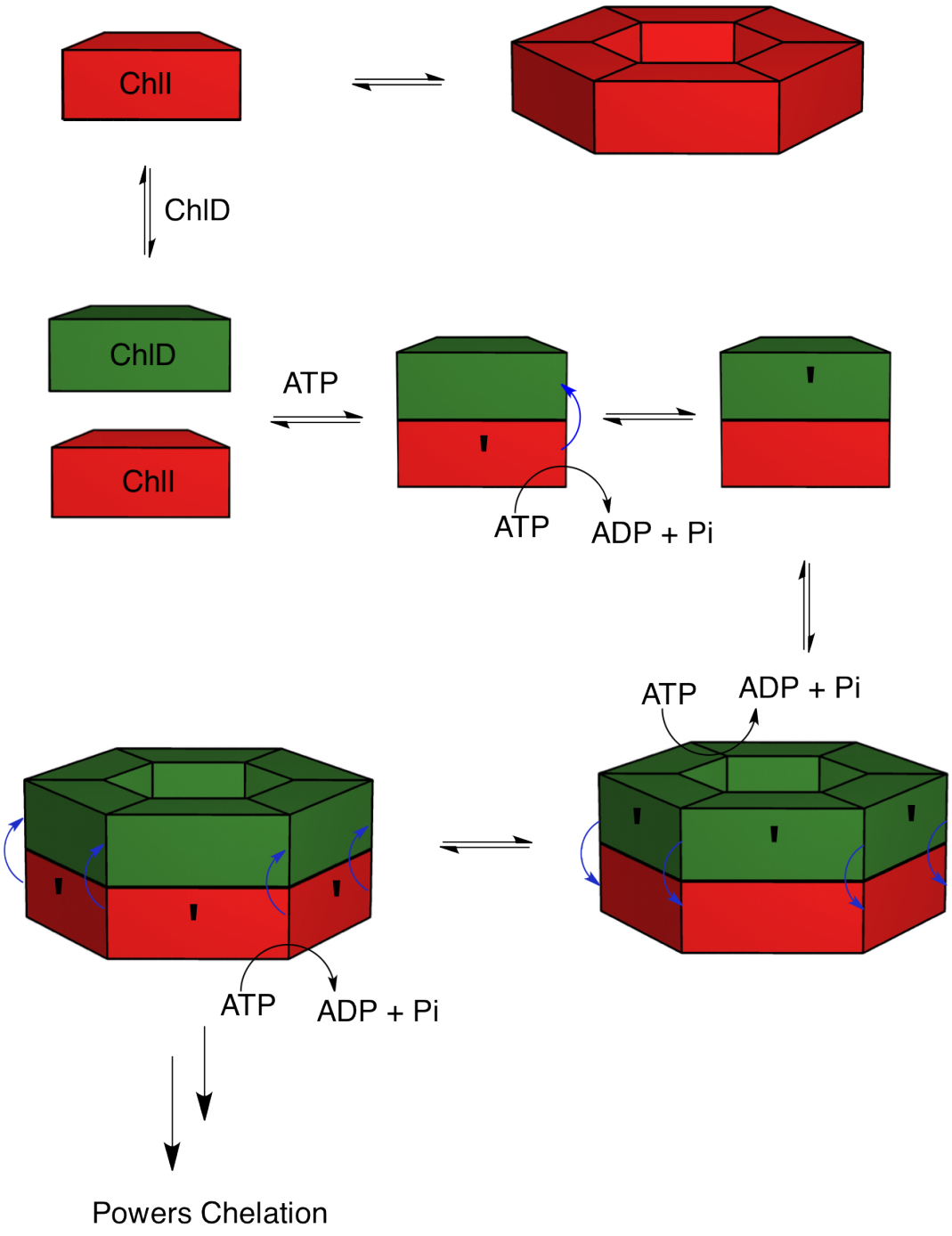

Figure 7.1: Proposed model of allosteric regulation of chelatase activity - ChlI in red is promoted into an ID complex. On the addition of nucleotide and possibly ChlH, a binding signal from ChlI allows the formation of the ChlID complex. This further assembles with ChlD in the ATP bound form. Once a competent complex is constructed (the proposed $ChlI_{6C}hlD_6$ ring), the ChlD ring sends signals to ChlI via ATP binding or hydrolysis to allow the ChlI ring to power chelation, the ' indicates a change in conformation.

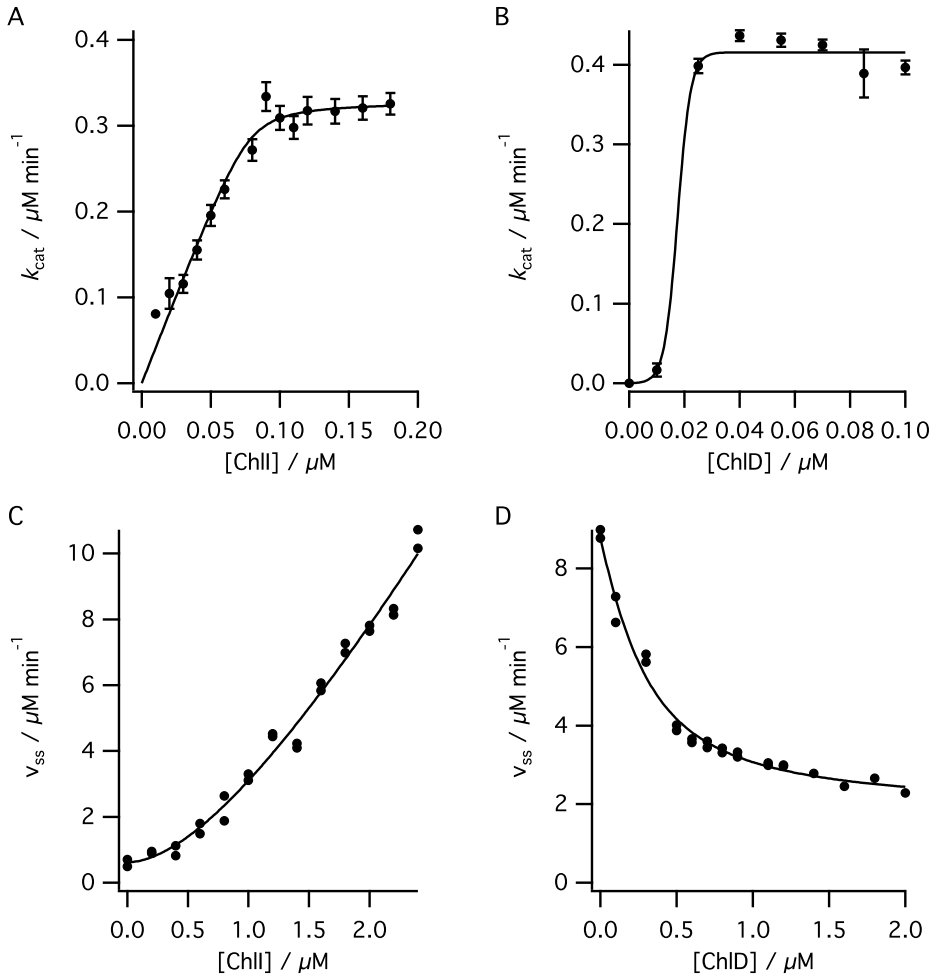

Figure 7.2: Binding titration at saturating nucleotide concentrations where either ChlD or ChlI is held constant while monitoring chelatase or ATPase activity - **A)**Turnover of chelatase assays where ChlI is titrated into constant [ChlD] (0.1 μM), line is theoretical, data fitted to the binding equation 5.3, where $E = 0.078 \pm 0.005$ μM, K_d 0.0017 $\pm$ 0.002 μM. **B)** $k_{\text{cat}}$of chelatase assays where ChlD is titrated into constant [ChlI] (0.1 μM), line is empirical and for guidance only. Values for k_{cat} obtained from the concentration of ChlH, panels **A** and **B** conditions: 50 mM MOPS/KOH, 0.3 M Glycerol, 0.125 – 3 mM ATP, 10 mM free $MgCl_2$, 8 μM D_{IX}, pH 7.7, 34 °C. **C)** Steady state ATPase rates where ChlI is titrated into constant [ChlD] (1 μM), line fitted is arbitrary and for guidance only. **D)** Steady state ATPase rates where ChlD is titrated into constant [ChlI] (1 μM), line is theoretical and described by the binding equation 5.3, where $E = 0.217 \pm 0.116$ μM, K_d 0.184 $\pm$ 0.068 μM. Panels **C** and **D** conditions: 50 mM MOPS/KOH, 0.3 M Glycerol, 5 mM ATP, 10 mM free $MgCl_2$, pH 7.7, 34 °C.

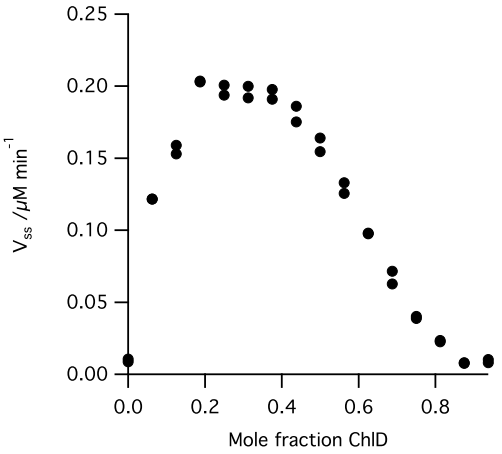

Figure 7.3: Job Plot of chelatase steady state rates - The molar ratio of ChlD to ChlI was altered while maintaining total concentration of the enzymes at 0.2 μM in the presence of 0.4 μM ChlH in 50 mM MOPS/KOH, 0.3 M glycerol, 1 mM DTT, pH 7.7, 34 °C, $I = 0.1$, 5 mM ATP 15 mM $MgCl_2$, 8 μM D_{IX}.

A Job plot (figure 7.3) confirms that the chelatase activity is maximal with a subunit ratio of 5 : 1 ChlI and ChlD.

The ATPase activity of ChlID reflects the stability of the complex in the absence of ChlH. Binding between the two subunits appears to be weak when monitoring ATPase activity, displaying hyperbolic behaviour (figure 7.2C and D). There is a two order of magnitude increase in the dissociation constant on removing ChlH and porphyrin (0.184 μM in the absence of ChlH compared to 1.7 nM in the presence of ChlH), with a much lower value when ChlH present (figure 7.2A). This may explain the difficulties in isolating the ChlID complex in the absence of ChlH.

The kinetics suggest multiple different forms of a catalytically competent magnesium chelatase in solution. Any one of these species may be the complex present *in vivo* powering chelation, and in some respects resembles the dynamic different sized homo-oligomers controlled by allosteric interactions recently reviewed by Selwood and Jaffe (151). It may be that more than one ratio of ChlI and ChlD in an ID complex is able to power chelation depending on the physiological conditions of the cell.

An alternative theory of the chelatase complex can be advanced based on the binding titration data shown in figure 7.2 and 7.3. The most active chelatase complex exists at 5:1 ratios of ChlI:ChlD. This may reflect a hexamer of five ChlI subunits and a single ChlD subunit interacting through the N-terminal AAA^+ domains (figure 7.4). This can be backed up with the fact analytical ultracentrifugation, size exclusion chromatography, static light scattering and electron microscopy has never conclusively detected a complex of the appropriate mass for the dual ring hexamer for the chlorophyll producing magnesium chelatases from *Synechocystis* and *Thermosynechococcus elongatus* (*pers com* Amanda Brindley and Pu Qian, The University of Sheffield). The dual ring hexamer model (67) and the BchI hexamer (56) has been the accepted theory within the magnesium chelatase community for some time. These complexes may be biochemical artefacts, unrelated to the true magnesium chelatase complex, particularly the chlorophyll producing magnesium chelatases.

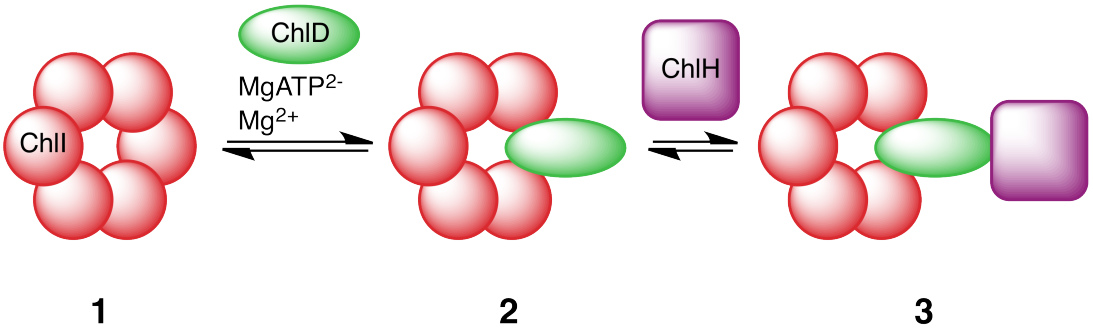

Figure 7.4: An alternative ChlID complex - A store of hexameric ChlI (**1**) on binding with ChlD may alter to a different hexamer of five ChlI subunits and one ChlD subunit interacting via the N-terminal AAA^+ domains (**2**). ChlH may then bind to the C-terminal of ChlD, perhaps via the intergrin domain (**3**). The chemomechanical result of ATP hydrolysis on ChlI may be directed to ChlD which can then power a conformational change on ChlH, allowing magnesium insertion to occur.

7.4 Future perspectives

How the coordinated ATPases of magnesium chelatase power chelation is of great interest. Mutant mixing in the presence of all three subunits and porphyrin should be conducted, but following ATP hydrolysis would be valuable. But as the extent of communication depends on the concentration of nucleotide substrate, these assays can only feasibly be performed in a high throughput assay system.

The stoichiometry of the ChlID complexes which power chelation needs to be determined before the allosteric signalling pathway between ChlI and ChlD can be fully dissected. There are a multitude of hydrodynamic techniques which could be of value, including multi-angled light scattering, analytical ultracentrifugation and small angle x-ray scattering.

As the labelling of protein becomes more robust, the possibility of using FRET to analyse complexes present in solution provides another ensemble binding titration measurement. Single molecule spectroscopy techniques will provide methods of observing individual complexes attached to surface (152, 153).

Ultimately, understanding the link between ATP hydrolysis and metal ion insertion will require both enzymology and structural techniques. As magnesium chelatase has a highly fluorescent substrate and product it is likely studying this system will provide insight into the action of other members of the AAA^+ super family. The most substantial obstacle remaining to understand the function of magnesium chelatase is the quaternary structure of the active enzyme.

References

[1] R. D. Willows and M. Hansson, *Mechanism, Structure, and Regulation of Magneisum Chelatase*, vol. 13 of *The Porphyrin Handbook*. Academic Press, 1 ed., 2002. xv, 12, 13, 14, 15, 25, 88, 153, 169

[2] M. Hansson and C. G. Kannangara, "ATPases and phosphate exchange activities in magnesium chelatase subunits of Rhodobacter sphaeroides.," *Proceedings of the National Academy of Sciences of the United States of America*, vol. 94, no. 24, pp. 13351–6, 1997. xv, 24, 25, 35, 36, 61

[3] D. Hall and K. Rao, *Photosynthesis (Studies in Biology)*. Cambridge University Press, 5 ed., 1994. 2, 3, 4, 5, 7

[4] D. Lawlor, *Photosynthesis: Molecular, Physiological and Environmental Processes*. Longman Pub Group, 3 ed., 2000. 2, 3, 4

[5] R. P. F. Gregory, *Biochemistry of Photosynthesis*. John Wiley and Sons, 1971. 2, 5

[6] L. Milgrom, *The Colours of Life: An Introduction to the Chemistry of Porphyrins and Related Compounds*. Oxford University Press, USA, 1997. 3, 4, 6, 8, 9, 12

[7] J. Falk, *Porphyrins and metalloporphyrins: Their general physical and coordination chemistry, and laboratory methods (Biochimica et Biophysica Acta library;vol.2)*. Elsevier, 1964. 3, 4, 49

[8] L. Pierson and H. Geurts, "Leaf Chloroplast," *http://www.vcbio.science.ru.nl/en/fesem/applets/chloroplast/*, October 2011. 5

[9] T. Masuda, "Recent overview of the Mg branch of the tetrapyrrole biosynthesis leading to chlorophylls.," *Photosynthesis research*, vol. 96, no. 2, pp. 121–43, 2008. 8, 12

[10] B. Frydman and R. Frydman, "Biosynthesis of uroporphyrinogens from porphobilinogen. Mechanism and nature of the process," *Acc. Chem. Res.*, vol. 8, no. 6, pp. 201–208, 1975. 8

[11] P. E. Jensen, L. C. Gibson, K. W. Henningsen, and C. N. Hunter, "Expression of the chlI, chlD, and chlH genes from the Cyanobacterium synechocystis PCC6803 in Escherichia coli and demonstration that the three cognate proteins are required for magnesium-protoporphyrin chelatase activity.," *The Journal of biological chemistry*, vol. 271, no. 28, pp. 16662–7, 1996. 9, 14, 41

[12] Y. Fujita and C. Bauer, "Reconstitution of Light-independent Protochlorophyllide Reductase from Purified Bchl and BchN-BchB Subunits," *Journal of Biological Chemistry*, vol. 275, no. 31, pp. 23583–23588, 2000. 12

[13] J. Nomata, L. Swem, C. Bauer, and Y. Fujita, "Overexpression and characterization of dark-operative protochlorophyllide reductase from Rhodobacter capsulatus," *Biochimica et Biophysica Acta (BBA) - Bioenergetics*, vol. 1708, no. 2, pp. 229–237, 2005. 12

[14] S. Reinbothe, C. Reinbothe, N. Lebedev, and K. Apel, "PORA and PORB, Two Light-Dependent Protochlorophyllide-Reducing Enzymes of Angiosperm Chlorophyll Biosynthesis.," *The Plant cell*, vol. 8, no. 5, pp. 763–769, 1996. 12

[15] T. Masuda, K. Inoue, M. Masuda, M. Nagayama, A. Tamaki, H. Ohta, H. Shimada, and K.-i. Takamiya, "Magnesium Insertion by Magnesium Chelatase in the Biosynthesis of Zinc Bacteriochlorophyll a in an Aerobic Acidophilic Bacterium Acidiphilium rubrum," *Journal of Biological Chemistry*, vol. 274, no. 47, pp. 33594–33600, 1999. 12

[16] Shelnutt, X.-Z. Song, J.-G. Ma, S.-L. Jia, W. Jentzen, Medforth, and Medforth, "Nonplanar porphyrins and their significance in proteins," *Chem. Soc. Rev.*, vol. 27, no. 1, pp. 31–42, 1998. 12

[17] H. Schubert, E. Raux, K. Wilson, and M. Warren, "Common Chelatase Design in the Branched Tetrapyrrole Pathways of Heme and Anaerobic Cobalamin Synthesis," *Biochemistry*, vol. 38, no. 33, pp. 10660–10669, 1999. 12

[18] L. Debussche, M. Couder, D. Thibaut, B. Cameron, J. Crouzet, and F. Blanche, "Assay, purification, and characterization of cobaltochelatase, a unique complex enzyme catalyzing cobalt insertion in hydrogenobyrinic acid a,c-diamide during coenzyme B12 biosynthesis in Pseudomonas denitrificans.," *Journal of Bacteriology*, vol. 174, no. 22, pp. 7445–7451, 1992. 12

[19] J. W. Buchler, *Porphyrins and Metalloporphyrins*, ch. 5, pp. 157 – 231. Amsterdam: Elsevier, 2 ed., 1975. 13, 32, 90

[20] P. Hambright and P. B. Chock, "Metal-porphyrin interactions. III. Dissociative-interchange mechanism for metal ion incorporation into porphyrin molecules," *J. Am. Chem. Soc.*, vol. 96, no. 10, pp. 3123–3131, 1974. 13, 34

[21] C. J. Walker and J. D. Weinstein, "The magnesium-insertion step of chlorophyll biosynthesis is a two-stage reaction.," *The Biochemical journal*, vol. 299, no. 1 994, pp. 277–84, 1994. 13, 32, 35, 36

[22] A. Gorchein, "Magnesium protoporphyrin chelatase activity in Rhodopseudomonas spheroides. Studies with whole cells.," *The Biochemical journal*, vol. 127, no. 1, pp. 97–106, 1972. 14

[23] A. Gorchein, "Control of magnesium-protoporphyrin chelatase activity in Rhodopseudomonas spheroides. Role of light, oxygen, and electron and energy transfer.," *The Biochemical journal*, vol. 134, no. 4, pp. 833–845, 1973. 14

[24] B. Smith and C. Rebeiz, "Chloroplast biogenesis: Detection of Mg-protoporphyrin chelatase in vitro," *Archives of Biochemistry and Biophysics*, vol. 180, no. 1, pp. 178–185, 1977. 14

[25] C. J. Walker and J. D. Weinstein, "Further characterization of the magnesium chelatase in isolated developing cucumber chloroplasts : substrate specificity, regulation, intactness, and ATP requirements.," *Plant physiology*, vol. 95, no. 4, pp. 1189–96, 1991. 14, 35

[26] R. Guo, M. Luo, and J. D. Weinstein, "Magnesium-Chelatase from Developing Pea Leaves," *Plant Physiology*, vol. 116, no. 2, pp. 605–615, 1998. 14, 34, 35, 36

[27] J. Papenbrock, S. Gräfe, E. Kruse, F. Hänel, and B. Grimm, "Mg-chelatase of tobacco: identification of a Chl D cDNA sequence encoding a third subunit, analysis of the interaction of the three subunits with the yeast two-hybrid system, and reconstitution of the enzyme activity by co-expression of recombinant CHL D,," *The Plant journal : for cell and molecular biology*, vol. 12, no. 5, pp. 981–90, 1997. 14, 15, 26

[28] P. E. Jensen, L. Petersen, B. Stummann, K. Henningsen, R. Willows, U. Vothknecht, C. Kannangara, and D. Wettstein, "Structural genes for Mg-chelatase subunits in barley Xantha-f, -g; and -h," *Molecular and General Genetics MGG*, vol. 250, no. 4, pp. 383–394, 1996. 14, 35

[29] L. C. Gibson, R. D. Willows, C. G. Kannangara, D. von Wettstein, and C. N. Hunter, "Magnesium-protoporphyrin chelatase of Rhodobacter sphaeroides: reconstitution of activity by combining the products of the bchH, -I, and -D genes expressed in Escherichia coli.," *Proceedings of the National Academy of Sciences of the United States of America*, vol. 92, no. 6, pp. 1941–4, 1995. 14

[30] D. W. Bollivar, J. Y. Suzuki, J. T. Beatty, J. M. Dobrowolski, and C. E. Bauer, "Directed mutational analysis of bacteriochlorophyll a biosynthesis in Rhodobacter capsulatus," *Journal of molecular biology*, vol. 237, no. 5, pp. 622–640, 1994. 14

[31] R. D. Willows, "Three separate proteins constitute the magnesium chelatase of Rhodobacter sphaeroides," *European Journal of Biochemistry*, vol. 235, no. 1-2, pp. 438–443, 1996. 14, 15

[32] B. Petersen, P. Jensen, L. Gibson, B. Stummann, C. N. Hunter, and K. Henningsen, "Reconstitution of an Active Magnesium Chelatase Enzyme Complex from the bchI, -D, and-H Gene Products of the Green Sulfur BacteriumChlorobium vibrioforme Expressed in Escherichia coli," *Journal of Bacteriology*, vol. 180, no. 3, pp. 699–704, 1998. 14

[33] P. Qian, C. Marklew, J. Viney, P. Davison, A. Brindley, C. Soderberg, S. Al-Karadaghi, P. Bullough, G. Grossmann, and N. Hunter, "Structure of the cyanobacterial magnesium chelatase H subunit determined by single particle reconstruction and small-angle X-ray scattering," *Journal of Biological Chemistry*, vol. 287, pp. 4946 – 4956, 2011. 14, 15, 16, 18, 19

[34] Y.-Y. Shen, X.-F. Wang, F.-Q. Wu, S.-Y. Du, Z. Cao, Y. Shang, X.-L. Wang, C.-C. Peng, X.-C. Yu, S.-Y. Zhu, R.-C. Fan, Y.-H. Xu, and D.-P. Zhang, "The Mg-chelatase H subunit is an abscisic acid receptor.," *Nature*, vol. 443, no. 7113, pp. 823–6, 2006. 15, 19, 166

[35] P. E. Jensen, L. C. Gibson, and C. N. Hunter, "Determinants of catalytic activity with the use of purified I, D and H subunits of the magnesium protoporphyrin IX chelatase from Synechocystis PCC6803.," *The Biochemical journal*, vol. 334 (Pt 2, pp. 335–44, 1998. 15, 24, 28, 35, 36, 122

[36] G. A. Karger, J. D. Reid, and C. N. Hunter, "Characterization of the binding of deuteroporphyrin IX to the magnesium chelatase H subunit and spectroscopic properties of the complex.," *Biochemistry*, vol. 40, no. 31, pp. 9291–9, 2001. 15

[37] N. Sirijovski, J. Lundqvist, M. Rosenbäck, H. Elmlund, S. Al-Karadaghi, R. D. Willows, and M. Hansson, "Substrate-binding model of the chlorophyll biosynthetic magnesium chelatase BchH subunit," *The Journal of biological chemistry*, vol. 283, no. 17, pp. 11652–60, 2008. 15, 16, 18, 35, 36

[38] J. Viney, *Characterisation of magnesium protoporphyrin IX chelatase from Synechocystis sp. PCC6803*. PhD thesis, Univerisity of Sheffield, Western Bank, Sheffield, South Yorkshire, 2006. 15

[39] D. Lecerof, M. Fodje, A. Hansson, M. Hansson, and S. Al-Karadaghi, "Structural and mechanistic basis of porphyrin metallation by ferrochelatase," *Journal of Molecular Biology*, vol. 297, no. 1, pp. 221–232, 2000. 15, 17, 34

[40] S. Al-Karadaghi, R. Franco, M. Hansson, J. a. Shelnutt, G. Isaya, and G. C. Ferreira, "Chelatases: distort to select?," *Trends in biochemical sciences*, vol. 31, no. 3, pp. 135–42, 2006. 16, 34

[41] Schrödinger, LLC, "The PyMOL molecular graphics system, version 1.3r1." 2010. 17, 21, 22, 62, 100, 135, 155, 156

[42] A. Sawicki and R. Willows, "BchJ and BchM interact in a 1 : 1 ratio with the magnesium chelatase BchH subunit of Rhodobacter capsulatus.," *The FEBS journal*, vol. 277, no. 22, pp. 4709–4721, 2010. 18, 91

[43] A. Alawady, R. Reski, E. Yaronskaya, and B. Grimm, "Cloning and expression of the tobacco CHLM sequence encoding Mg protoporphyrin IX methyltransferase and its interaction with Mg chelatase," *Plant Molecular Biology*, vol. 57, no. 5, pp. 679–691, 2005. 18, 19

[44] M. Shepherd and C. N. Hunter, "Transient kinetics of the reaction catalysed by magnesium protoporphyrin IX methyltransferase.," *The Biochemical journal*, vol. 382, no. Pt 3, pp. 1009–1013, 2004. 19, 110

[45] M. Shepherd, S. McLean, and C. N. Hunter, "Kinetic basis for linking the first two enzymes of chlorophyll biosynthesis.," *The FEBS journal*, vol. 272, no. 17, pp. 4532–9, 2005. 19

[46] M. Shepherd, J. D. Reid, and C. N. Hunter, "Purification and kinetic characterization of the magnesium protoporphyrin IX methyltransferase from Synechocystis PCC6803.," *The Biochemical journal*, vol. 371, no. Pt 2, pp. 351–360, 2003. 19

[47] T. Osanai, M. Imashimizu, A. Seki, S. Sato, S. Tabata, S. Imamura, M. Asayama, M. Ikeuchi, and K. Tanaka, "ChlH, the H subunit of the Mg-chelatase, is an anti-sigma factor for SigE in Synechocystis sp. PCC 6803," *Proceedings of the National Academy of Sciences*, vol. 106, no. 16, pp. 6860–6865, 2009. 19

[48] F.-Q. Wu, Q. Xin, Z. Cao, Z.-Q. Liu, S.-Y. Du, C. Mei, C.-X. Zhao, X.-F. Wang, Y. Shang, T. Jiang, X.-F. Zhang, L. Yan, R. Zhao, Z.-N. Cui, R. Liu, H.-L. Sun, X.-L. Yang, Z. Su, and D.-P. Zhang, "The Magnesium-Chelatase H Subunit Binds Abscisic Acid and Functions in Abscisic Acid Signaling: New Evidence in Arabidopsis," *Plant Physiology*, vol. 150, no. 4, pp. 1940–1954, 2009. 19, 169

[49] A. Müller and M. Hansson, "The Barley Magnesium Chelatase 150-kD Subunit Is Not an Abscisic Acid Receptor," *Plant Physiology*, vol. 150, no. 1, pp. 157–166, 2009. 19

[50] J. Risk, R. Macknight, and C. Day, "FCA does not bind abscisic acid," *Nature*, vol. 456, no. 7223, pp. E5–E6, 2008. 19

[51] T. Tsuzuki, K. Takahashi, S.-i. Inoue, Y. Okigaki, M. Tomiyama, M. Hossain, K.-i. Shimazaki, Y. Murata, and T. Kinoshita, "Mg-chelatase H subunit affects ABA signaling in stomatal guard cells, but is not an ABA receptor in Arabidopsis thaliana," *Journal of Plant Research*, vol. 124, no. 4, pp. 527–538, 2011. 19

[52] J. P. Erzberger and J. M. Berger, "Evolutionary relationships and structural mechanisms of AAA+ proteins.," *Annual review of biophysics and biomolecular structure*, vol. 35, pp. 93–114, 2006. 20, 21, 23

[53] S. Licht and I. Lee, "Resolving Individual Steps in the Operation of ATP-Dependent Proteolytic Molecular Machines: From Conformational Changes to Substrate Translocation and Processivity," *Biochemistry*, vol. 47, no. 12, pp. 3595–3605, 2008. 20

[54] P. I. Hanson and S. W. Whiteheart, "AAA+ proteins: have engine, will work.," *Nature reviews. Molecular cell biology*, vol. 6, no. 7, pp. 519–29, 2005. 20, 98, 99, 107, 161

[55] A. Neuwald, L. Aravind, J. Spouge, and E. Koonin, "AAA+: A Class of Chaperone-Like ATPases Associated with the Assembly, Operation, and Disassembly of Protein Complexes," *Genome Research*, vol. 9, no. 1, pp. 27–43, 1999. 20, 98

[56] M. N. Fodje, a. Hansson, M. Hansson, J. G. Olsen, S. Gough, R. D. Willows, and S. Al-Karadaghi, "Interplay between an AAA module and an integrin I domain may regulate the function of magnesium chelatase.," *Journal of molecular biology*, vol. 311, no. 1, pp. 111–22, 2001. 20, 21, 23, 24, 26, 28, 34, 98, 155, 177

[57] N. Guex and M. C. Peitsch, "SWISS-MODEL and the Swiss-PdbViewer: an environment for comparative protein modeling.," *Electrophoresis*, vol. 18, no. 15, pp. 2714–2723, 1997. 22

[58] L. M. Iyer, D. D. Leipe, E. V. Koonin, and L. Aravind, "Evolutionary history and higher order classification of AAA+ ATPases.," *Journal of structural biology*, vol. 146, no. 1-2, pp. 11–31, 2004. 23, 134

[59] P. E. Jensen, J. D. Reid, and C. N. Hunter, "Modification of cysteine residues in the ChlI and ChlH subunits of magnesium chelatase results in enzyme inactivation," *Biochemical Journal*, vol. 352, no. Pt 2, p. 435, 2000. 23, 26, 34, 35, 67, 108, 110, 141

[60] J. D. Reid, C. A. Siebert, P. a. Bullough, and C. N. Hunter, "The ATPase activity of the ChlI subunit of magnesium chelatase and formation of a heptameric AAA+ ring.," *Biochemistry*, vol. 42, no. 22, pp. 6912–20, 2003. 24, 71, 98, 134, 170

[61] B. L. Petersen, C. G. Kannangara, and K. W. Henningsen, "Distribution of ATPase and ATP-to-ADP phosphate exchange activities in magnesium chelatase subunits of Chlorobium vibrioforme and Synechocystis PCC6803.," *Archives of microbiology*, vol. 171, no. 3, pp. 146–50, 1999. 24, 26, 61, 122

[62] N. B. P. Adams and J. Reid, "Nonequilibrium Isotope Exchange Reveals a Catalytically Significant Enzyme–Phosphate Complex in the ATP Hydrolysis Pathway of the AAA+ ATPase Magnesium Chelatase," *Biochemistry*, vol. 51, no. 10, pp. 2029–2031, 2012. 24

[63] S. Gräfe, H.-P. Saluz, B. Grimm, and F. Hänel, "Mg-chelatase of tobacco: The role of the subunit CHL D in the chelation step of protoporphyrin IX," *Proceedings of the National Academy of Sciences*, vol. 96, no. 5, pp. 1941–1946, 1999. 26, 28, 153, 172

[64] A. Waterhouse, J. Procter, D. Martin, M. Clamp, and G. Barton, "Jalview Version 2—a multiple sequence alignment editor and analysis workbench," *Bioinformatics*, vol. 25, no. 9, pp. 1189–1191, 2009. 27

[65] T. U. Consortium, "Reorganizing the protein space at the Universal Protein Resource (UniProt)," *Nucleic Acids Research*, vol. 40, no. D1, pp. D71–D75, 2012. 27, 46, 99, 154

[66] E. Axelsson, J. Lundqvist, A. Sawicki, S. Nilsson, I. Schröder, S. Al-Karadaghi, R. D. Willows, and M. Hansson, "Recessiveness and dominance in barley mutants deficient in Mg-chelatase subunit D, an AAA protein involved in chlorophyll biosynthesis.," *The Plant cell*, vol. 18, no. 12, pp. 3606–16, 2006. 28, 29, 34, 172, 173

[67] J. Lundqvist, H. Elmlund, R. P. Wulff, L. Berglund, D. Elmlund, C. Emanuelsson, H. Hebert, R. D. Willows, M. Hansson, M. Lindahl, and S. Al-Karadaghi, "ATP-induced conformational dynamics in the AAA+ motor unit of magnesium chelatase.," *Structure (London, England : 1993)*, vol. 18, no. 3, pp. 354–65, 2010. 28, 29, 30, 31, 67, 71, 120, 122, 134, 170, 172, 177

[68] L. Gibson, P. Jensen, and C. Hunter, "Magnesium chelatase from Rhodobacter sphaeroides: initial characterization of the enzyme using purified subunits and evidence for a BchI-BchD complex.," *The Biochemical journal*, vol. 337 (Pt 2), pp. 243–251, 1999. 29

[69] J. Viney, P. A. Davison, C. N. Hunter, and J. D. Reid, "Direct measurement of metal-ion chelation in the active site of the AAA+ ATPase magnesium chelatase.," *Biochemistry*, vol. 46, no. 44, pp. 12788–94, 2007. 29, 94

[70] R. M. Larkin, J. M. Alonso, J. R. Ecker, and J. Chory, "GUN4, a regulator of chlorophyll synthesis and intracellular signaling.," *Science (New York, N.Y.)*, vol. 299, no. 5608, pp. 902–6, 2003. 31

[71] P. A. Davison, H. L. Schubert, J. D. Reid, C. D. Iorg, A. Heroux, C. P. Hill, and C. N. Hunter, "Structural and biochemical characterization of Gun4 suggests a mechanism for its role in chlorophyll biosynthesis.," *Biochemistry*, vol. 44, no. 21, pp. 7603–12, 2005. 31, 32, 91

[72] P. A. Davison and C. N. Hunter, "Abolition of magnesium chelatase activity by the gun5 mutation and reversal by Gun4," *FEBS Letters*, vol. 585, no. 1, pp. 183–186, 2011. 31

[73] S. Baum and R. Plane, "Kinetics of the Incorporation of Magnesium(II) into Porphyrin," *J. Am. Chem. Soc.*, vol. 88, no. 5, pp. 910–913, 1966. 32, 33, 89

[74] P. Hambright, *Porphyrins and Metalloporphyrins*, ch. 6, pp. 233 – 278. Amsterdam: Elsevier, 2 ed., 1975. 34

[75] Y. Shen and U. Ryde, "Reaction Mechanism of Porphyrin Metallation Studied by Theoretical Methods," *Chem. Eur. J.*, vol. 11, no. 5, pp. 1549–1564, 2005. 34, 88, 90

[76] J. D. Reid and C. N. Hunter, "Magnesium-dependent ATPase activity and cooperativity of magnesium chelatase from Synechocystis sp. PCC6803," *Journal of Biological Chemistry*, vol. 279, no. 26, p. 26893, 2004. 34, 36, 48, 60, 81, 87, 91, 94, 162, 167

[77] L. Gibson, P. E. E. Jensen, and C. N. Hunter, "Magnesium chelatase from Rhodobacter sphaeroides: initial characterization of the enzyme using purified subunits and evidence for a BchI-BchD complex.," *Biochemical Journal*, vol. 337, no. Pt 2, p. 243, 1999. 35

[78] P. E. Jensen, L. C. Gibson, and C. N. Hunter, "ATPase activity associated with the magnesium-protoporphyrin IX chelatase enzyme of Synechocystis PCC6803: evidence for ATP hydrolysis during Mg2+ insertion, and the MgATP-dependent interaction of the ChlI and ChlD subunits," *Biochemical Journal*, vol. 339, no. Pt 1, p. 127, 1999. 35, 36, 71, 98, 108, 160

[79] J. Sambrook, *Molecular Cloning: A Laboratory Manual, Third Edition (3 volume set)*. Cold Spring Harbor Laboratory Press, 3rd ed., 2001. 39, 47

[80] D. Hanahan, *DNA Cloning, a Practical Approach*, vol. 1, p. 109. London: IRL Press, LTD, 1985. 39

[81] W. Studier, "Protein production by auto-induction in high-density shaking cultures," *Protein Expression and Purification*, vol. 41, no. 1, pp. 207–234, 2005. 47

[82] U. K. Laemmli, "Cleavage of Structural Proteins during the Assembly of the Head of Bacteriophage T4," *Nature*, vol. 227, no. 5259, pp. 680–685, 1970. 47

[83] P. C. Engel, ed., *Enzymology LabFax*. Academic Press, 1996. 49

[84] R. E. Ducker, *Scanning Near-Field Photolithography: A Novel Route to Biological Nanostructures*. PhD thesis, University of Sheffield, 2007. 56, 139, 141

[85] D. L. Purich and R. Donald Allison, "Isotope exchange methods for elucidating enzymic catalysis," *Methods in Enzymology*, vol. 64, pp. 3–46, 1980. 59

[86] A. Cornish-Bowden, *Fundamentals of Enzyme Kinetics*. Portland Press Ltd, 3rev ed ed., 2004. 59

[87] L. F. Hass and W. L. Byrne, "The Mechanism of Glucose-6-phosphatase," *Journal of the American Chemical Society*, vol. 82, no. 3, p. 947, 1960. 60

[88] D. L. Nandi, "Studies on δ-Aminolevulinic Acid Synthase of Rhodopseudomonas spheroides," *Journal of Biological Chemistry*, vol. 253, no. 24, p. 8872, 1978. 60

[89] L. J. Zatman, N. O. Kaplan, and S. P. Colowick, "Inhibition of Spleen Diphosphopyridine Nucleotidase by Nicotinamide, an exchange reaction," *Journal of Biological Chemistry*, 1953. 60

[90] D. P. Kosow and I. A. Rose, "Product inhibition of the hexokinases," *The Journal of biological chemistry*, vol. 245, no. 1, pp. 198–204, 1970. 60

[91] J. Thomas, J. Fishovitz, and I. Lee, "Utilization of positional isotope exchange experiments to evaluate reversibility of ATP hydrolysis catalyzed by Escherichia coli Lon protease.," *Biochemistry and cell biology = Biochimie et biologie cellulaire*, vol. 88, no. 1, pp. 119–128, 2010. 61, 63

[92] A. N. Page, N. P. George, A. H. Marceau, M. M. Cox, and J. L. Keck, "Structure and biochemical activities of Escherichia coli MgsA," *Journal of Biological Chemistry*, no. 18, pp. 1–20, 2011. 61

[93] H. Schmidt, E. Gleave, and A. Carter, "Insights into dynein motor domain function from a 3.3-Åcrystal structure," *Nat Struct Mol Biol*, vol. 19, no. 5, pp. 492–497, 2012. 61

[94] H. Roobottom, Jenkins, J. Passmore, and L. Glasser, "Thermochemical Radii of Complex Ions," *J. Chem. Educ.*, vol. 76, no. 11, p. 1570, 1999. 61

[95] H. Krishnamurthy, H. Lou, A. Kimple, C. Vieille, and R. Cukier, "Associative mechanism for phosphoryl transfer: A molecular dynamics simulation of Escherichia coli adenylate kinase complexed with its substrates," *Proteins*, vol. 58, no. 1, pp. 88–100, 2005. 65

[96] L. Noda, *The Enzymes*, vol. 8, ch. 8. Academic Press, 3 ed., 1973. 65

[97] Y. Shyy, G. Tian, and M. Tsai, "Mechanism of adenylate kinase. Does adenosine 5'-triphosphate bind to the adenosine 5'-monophosphate site?," *Biochemistry*, vol. 26, no. 20, pp. 6411–6415, 1987. 65

[98] N. Price, G. Reed, and M. Cohn, "Magnetic resonance studies of substrate and inhibitor binding to porcine muscle adenylate kinase," *Biochemistry*, vol. 12, no. 17, pp. 3322–3327, 1973. 65

[99] M. Snider, B. Temple, and R. Wolfenden, "The path to the transition state in enzyme reactions: a survey of catalytic efficiencies," *J. Phys. Org. Chem.*, vol. 17, no. 6-7, pp. 586–591, 2004. 73

[100] R. Wolfenden, "Benchmark Reaction Rates, the Stability of Biological Molecules in Water, and the Evolution of Catalytic Power in Enzymes," *Annual Review of Biochemistry*, vol. 80, no. 1, pp. 645–667, 2011. 73, 76, 77

[101] R. Wolfenden and M. Snider, "The Depth of Chemical Time and the Power of Enzymes as Catalysts," *Acc. Chem. Res.*, vol. 34, no. 12, pp. 938–945, 2001. 73, 93, 94

[102] A. Radzicka and R. Wolfenden, "A proficient enzyme," *Science*, vol. 267, no. 5194, pp. 90–93, 1995. 76, 77

[103] C. T. Grubmeyer, J. W. Gross, and M. Rajavel, "Energy coupling through molecular discrimination: Nicotinate phosphoribosyltransferase," *Methods in Enzymology*, vol. 308, 1999. 79, 81, 92, 170

[104] T. S. Leyh, "On the advantages of imperfect energetic linkage," *Methods in Enzymology*, vol. 308, 1999. 80, 81

[105] M. Hansson, T. Karlberg, M. Rahardja, S. Al-Karadaghi, and M. Hansson, "Amino Acid Residues His183 and Glu264 in Bacillus subtilis Ferrochelatase Direct and Facilitate the Insertion of Metal Ion into Protoporphyrin IX," *Biochemistry*, vol. 46, no. 1, pp. 87–94, 2006. 89

[106] S. J. Ferguson and D. G. Nicholls, *Bioenergetics*. GB: Academic Press, 07 2002. 91

[107] A. Sawicki and R. D. Willows, "Kinetic analyses of the magnesium chelatase provide insights into the mechanism, structure, and formation of the complex.," *The Journal of biological chemistry*, vol. 283, no. 46, pp. 31294–302, 2008. 91

[108] R. Goody and W. Hofmann-Goody, "Exchange factors, effectors, GAPs and motor proteins: common thermodynamic and kinetic principles for different functions," *European Biophysics Journal*, vol. 31, no. 4, pp. 268–274, 2002. 91

[109] R. Goody, "The significance of the free energy of hydrolysis of GTP for signal-transducing and regulatory GTPases," *Biophysical Chemistry*, vol. 100, no. 1-3, pp. 535–544, 2003. 91

[110] W. P. Jencks, "How does a calcium pump pump calcium?," *The Journal of biological chemistry*, vol. 264, no. 32, pp. 18855–18858, 1989. 92

[111] M. A. Hoggins, H. A. Dailey, C. N. Hunter, and J. D. Reid, "Direct Measurement of Metal Ion Chelation in the Active Site of Human Ferrochelatase," *Biochemistry*, vol. 46, no. 27, pp. 8121–8127, 2007. 93

[112] H. A. Dailey and T. A. Dailey, *The Porphyrin Handbook, Volume 12*, vol. 12. Academic Press, 2003. 93

[113] A. G. Cochran and P. G. Schultz, "Antibody-catalyzed porphyrin metallation," *Science*, vol. 249, no. 4970, pp. 781–783, 1990. 93

[114] P. Matias, S. Gorynia, P. Donner, and M. Carrondo, "Crystal Structure of the Human AAA+ Protein RuvBL1," *Journal of Biological Chemistry*, vol. 281, no. 50, pp. 38918–38929, 2006. 98

[115] M. Babst, B. Wendland, E. J. Estepa, and S. D. Emr, "The Vps4p AAA ATPase regulates membrane association of a Vps protein complex required for normal endosome function.," *The EMBO journal*, vol. 17, no. 11, pp. 2982–93, 1998. 98

[116] N. D. Werbeck, S. Schlee, and J. Reinstein, "Coupling and dynamics of subunits in the hexameric AAA+ chaperone ClpB.," *Journal of molecular biology*, vol. 378, no. 1, pp. 178–90, 2008. 98, 110, 120, 150, 173

[117] T. M. Franzmann, A. Czekalla, and S. G. Walter, "The regulatory circuits of the AAA+ disaggregase HSP104.," *The Journal of biological chemistry*, vol. 286, no. 20, pp. 17992–18001, 2011. 98, 101, 110, 150, 172, 173

[118] E. A. Matveeva, P. He, and S. W. Whiteheart, "N-Ethylmaleimide-sensitive fusion protein contains high and low affinity ATP-binding sites that are functionally distinct.," *The Journal of biological chemistry*, vol. 272, no. 42, pp. 26413–8, 1997. 98

[119] J. Weibezahn, C. Schlieker, B. Bukau, and A. Mogk, "Characterization of a trap mutant of the AAA+ chaperone ClpB.," *The Journal of biological chemistry*, vol. 278, no. 35, pp. 32608–17, 2003. 98, 101

[120] F. Sievers, A. Wilm, D. Dineen, T. Gibson, K. Karplus, W. Li, R. Lopez, H. McWilliam, M. Remmert, J. Soding, J. Thompson, and D. Higgins, "Fast, scalable generation of high-quality protein multiple sequence alignments using Clustal Omega," *Molecular Systems Biology*, vol. 7, no. 1, 2011. 99, 154

[121] K. Arnold, L. Bordoli, J. Kopp, and T. Schwede, "The SWISS-MODEL workspace: a web-based environment for protein structure homology modelling," *Bioinformatics*, vol. 22, no. 2, pp. 195–201, 2006. 100

[122] A. Mogk, C. Schlieker, C. Strub, W. Rist, J. Weibezahn, and B. Bukau, "Roles of individual domains and conserved motifs of the AAA+ chaperone ClpB in oligomerization, ATP hydrolysis, and chaperone activity.," *The Journal of biological chemistry*, vol. 278, no. 20, pp. 17615–24, 2003. 101

[123] Y.-h. Watanabe, K. Motohashi, and M. Yoshida, "Roles of the two ATP binding sites of ClpB from Thermus thermophilus.," *The Journal of Biological Chemistry*, vol. 277, no. 8, pp. 5804–9, 2002. 101

[124] J. J. Hartman and R. D. Vale, "Microtubule Disassembly by ATP-Dependent Oligomerization of the AAA Enzyme Katanin," *Science*, vol. 286, no. 5440, pp. 782–785, 1999. 101

[125] S. W. Whiteheart, K. Rossnagel, S. A. Buhrow, M. Brunner, R. Jaenicke, and J. E. Rothman, "N-ethylmaleimide-sensitive fusion protein: a trimeric ATPase whose hydrolysis of ATP is required for membrane fusion.," *The Journal of cell biology*, vol. 126, no. 4, pp. 945–54, 1994. 101

[126] S. Dalal, M. F. Rosser, D. M. Cyr, and P. I. Hanson, "Distinct roles for the AAA ATPases NSF and p97 in the secretory pathway," *Molecular biology of the cell*, vol. 15, no. 2, p. 637, 2004. 101

[127] T. Ogura, S. W. Whiteheart, and A. J. Wilkinson, "Conserved arginine residues implicated in ATP hydrolysis, nucleotide-sensing, and inter-subunit interactions in AAA and AAA+ ATPases," *Journal of Structural Biology*, vol. 146, no. 1-2, pp. 106–112, 2004. 101

[128] I. Rombel, P. Peters-Wendisch, A. Mesecar, T. Thorgeirsson, Y.-K. Shin, and S. Kustu, "MgATP Binding and Hydrolysis Determinants of NtrC, a Bacterial Enhancer-Binding Protein," *Journal of Bacteriology*, vol. 181, no. 15, pp. 4628–4638, 1999. 101

[129] K. Karata, T. Inagawa, A. Wilkinson, T. Tatsuta, and T. Ogura, "Dissecting the Role of a Conserved Motif (the Second Region of Homology) in the AAA Family of ATPases," *Journal of Biological Chemistry*, vol. 274, no. 37, pp. 26225–26232, 1999. 101

[130] M. Bochtler, C. Hartmann, H. Song, G. Bourenkov, H. Bartunik, and R. Huber, "The structures of HslU and the ATP-dependent protease HslU-HslV," *Nature*, vol. 403, no. 6771, pp. 800–805, 2000. 101

[131] A. Martin, T. a. Baker, and R. T. Sauer, "Rebuilt AAA + motors reveal operating principles for ATP-fuelled machines.," *Nature*, vol. 437, no. 7062, pp. 1115–20, 2005. 101, 110, 150

[132] A. Hansson, R. Willows, T. Roberts, and M. Hansson, "Three semidominant barley mutants with single amino acid substitutions in the smallest magnesium chelatase subunit form defective aaa+ hexamers," *Proceedings of the National Academy of Sciences*, vol. 99, no. 21, pp. 13944–13949, 2002. 101, 149

[133] G. Hermanson, *Bioconjugate Techniques*. Academic Press, 2 ed., 2008. 110, 111

[134] I. Johnson and M. T. Z. Spence, eds., *Molecular Probes Handbook, A Guide to Fluorescent Probes and Labeling Technologies*. Invitrogen, 11th ed., 2010. 114

[135] H. Elmlund, J. Lundqvist, S. Al-Karadaghi, M. Hansson, H. Hebert, and M. Lindahl, "A new cryo-EM single-particle ab initio reconstruction method visualizes secondary structure elements in an ATP-fueled AAA+ motor.," *Journal of molecular biology*, vol. 375, no. 4, pp. 934–47, 2008. 120

[136] B. Huang, H. Babcock, and X. Zhuang, "Breaking the diffraction barrier: super-resolution imaging of cells.," *Cell*, vol. 143, no. 7, pp. 1047–58, 2010. 137

[137] S. W. Hell, "Far-field optical nanoscopy.," *Science (New York, N.Y.)*, vol. 316, no. 5828, pp. 1153–8, 2007. 137

[138] N. Reynolds, J. Tucker, P. Davison, J. Timney, C. N. Hunter, and G. Leggett, "Site-Specific Immobilization and Micrometer and Nanometer Scale Photopatterning of Yellow Fluorescent Protein on Glass Surfaces," *J. Am. Chem. Soc.*, vol. 131, no. 3, pp. 896–897, 2009. 141

[139] T. Schwede, J. Kopp, N. Guex, and M. Peitsch, "SWISS-MODEL: an automated protein homology-modeling server," *Nucleic Acids Research*, vol. 31, no. 13, pp. 3381–3385, 2003. 155

[140] A. Roy, A. Kucukuai, and Y. Zhang, "I-TASSER: a unified platform for automated protein structure and function prediction," *Nature Protocols*, vol. 5, pp. 725 – 738, 2010. 156

[141] Y. Zhang, "I-TASSER server for protein 3D structure prediction," *BMC Bioinformatics*, vol. 9, p. 40, 2008. 156

[142] J. M. Bergelson and M. E. Hemler, "Integrin-ligand binding. do integrins use a 'midas touch' to grasp an asp?," *Curr Biol*, vol. 5, no. 6, pp. 615–617, 1995. 153

[143] R. Tanaka and A. Tanaka, "Tetrapyrrole Biosynthesis in Higher Plants," *Annual Review of Plant Biology*, vol. 58, no. 1, pp. 321–346, 2007. 166

[144] M. Faller, M. Matsunaga, S. Yin, J. Loo, and F. Guo, "Heme is involved in microRNA processing," *Nature Structural and Molecular Biology*, vol. 14, no. 1, pp. 23–29, 2006. 166

[145] N. Mochizuki, J. A. Brusslan, R. Larkin, A. Nagatani, and J. Chory, "Arabidopsis genomes uncoupled 5 (GUN5) mutant reveals the involvement of Mg-chelatase H subunit in plastid-to-nucleus signal transduction.," *Proceedings of the National Academy of Sciences of the United States of America*, vol. 98, no. 4, pp. 2053–8, 2001. 166, 169

[146] E. Schirmer, D. Ware, C. Queitsch, A. Kowal, and S. Lindquist, "Subunit interactions influence the biochemical and biological properties of Hsp104," *Proceedings of the National Academy of Sciences*, vol. 98, no. 3, pp. 914–919, 2001. 172

[147] J. Fernández-Higuero, S. Acebrón, S. Taneva, U. Castillo, F. Moro, and A. Muga, "Allosteric Communication between the Nucleotide Binding Domains of Caseinolytic Peptidase B," *Journal of Biological Chemistry*, vol. 286, no. 29, pp. 25547–25555, 2011. 172, 173

[148] A. Biter, S. Lee, N. Sung, and F. Tsai, "Structural basis for intersubunit signaling in a protein disaggregating machine," *Proceedings of the National Academy of Sciences*, vol. 109, no. 31, pp. 12515–12520, 2012. 173

[149] U. Castillo, J. Fernández-Higuero, S. Pérez-Acebrón, F. Moro, and A. Muga, "Nucleotide utilization requirements that render ClpB active as a chaperone," *FEBS Letters*, vol. 584, no. 5, pp. 929–934, 2010. 173

[150] S. Hodson, J. Marshall, and S. Burston, "Mapping the road to recovery: The ClpB/Hsp104 molecular chaperone," *Journal of Structural Biology*, vol. 179, no. 2, pp. 161–171, 2012. 173

[151] T. Selwood and E. Jaffe, "Dynamic dissociating homo-oligomers and the control of protein function," *Archives of Biochemistry and Biophysics*, vol. 519, no. 2, pp. 131–143, 2012. 176

[152] Y. Jiang, N. R. Douglas, N. R. Conley, E. J. Miller, J. Frydman, and W. E. Moerner, "Sensing cooperativity in ATP hydrolysis for single multisubunit enzymes in solution.," *Proceedings of the National Academy of Sciences of the United States of America*, vol. 108, no. 41, 2011. 178

[153] L. J. Friedman, J. Chung, and J. Gelles, "Viewing dynamic assembly of molecular complexes by multi-wavelength single-molecule fluorescence.," *Biophysical journal*, vol. 91, no. 3, pp. 1023–31, 2006. 178

8

Appendix

8.1 Published works

BIOCHEMISTRY
including biophysical chemistry & molecular biology

Rapid Report

pubs.acs.org/biochemistry

Nonequilibrium Isotope Exchange Reveals a Catalytically Significant Enzyme−Phosphate Complex in the ATP Hydrolysis Pathway of the AAA$^+$ ATPase Magnesium Chelatase

Nathan B. P. Adams and James D. Reid*

Department of Chemistry, University of Sheffield, Sheffield S3 7HF, U.K.

Supporting Information

ABSTRACT: Magnesium chelatase is an AAA$^+$ ATPase that catalyzes the first committed step in chlorophyll biosynthesis. Using nonequilibrium isotope exchange, we show that the ATP hydrolysis reaction proceeds via an enzyme−phosphate complex. Exchange from radiolabeled phosphate to ATP was not observed, offering no support for an enzyme−ADP complex.

The AAA$^+$ superfamily of enzymes couple ATP hydrolysis to an exceptionally broad range of biological activities.[1−4] These enzymes hydrolyze ATP, driving a series of conformational changes that then modify biological activity. Consistent with this view, many enzymes in the superfamily adopt different structures with ATP bound, ADP bound, and nucleotide free.[5−8] These structures are often interpreted as reflecting the different conformations adopted during an ATP hydrolysis cycle.

With two products, ADP and phosphate (P_i), enzyme-catalyzed hydrolysis of ATP could conceivably involve enzyme−ADP (EADP) or enzyme−phosphate (EP_i) complexes (Scheme 1). AAA$^+$ ATPases could prefer either pathway.

Scheme 1. Random Release of Products from Enzyme-Catalyzed ATP Hydrolysis[a]

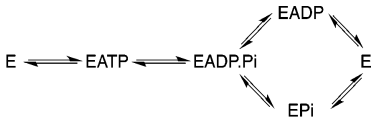

[a]Mg^{2+} and H^+ omitted for the sake of clarity.

We present evidence that a reactive enzyme−phosphate complex is formed by the AAA$^+$ ATPase magnesium chelatase.

Structural and biochemical evidence demonstrates that members of the AAA$^+$ superfamily can form both EADP and EP_i complexes.[5−9] While it is tempting to conclude that a structurally characterized enzyme−product complex is on the reaction pathway, the same species could arise as a dead-end inhibitor complex (Scheme 2). Additional approaches are needed to demonstrate that a species is catalytically relevant. We have used a simple, effective, and well-established method to show that magnesium chelatase, a member of the AAA$^+$ superfamily, has a kinetic mechanism that involves an enzyme−phosphate complex.

Scheme 2. Ordered Release of Products from an Enzyme-Catalyzed ATP Hydrolysis Proceeding via an Enzyme−Phosphate Complex[a]

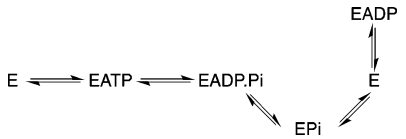

[a]ADP acts as a dead-end inhibitor. Mg^{2+} and H^+ omitted for the sake of clarity.

Magnesium chelatase is a well-characterized member of the family that catalyzes the first committed step in chlorophyll biosynthesis.[10−16] The chelatase contains a porphyrin binding subunit (ChlH) and two types of AAA$^+$ ATPase subunits, the active ChlI and the inactive ChlD.[13,14] ChlI and ChlD form a complex with reduced ATPase activity (ChlID).[14] All three subunits (ChlIDH) are needed to couple ATP hydrolysis to metalloporphyrin synthesis. We demonstrate that magnesium chelatase produces an EP_i complex on the ATP hydrolysis pathway by observing nonequilibrium isotope exchange between radiolabeled ADP and substrate.

In these experiments, a small amount of radiolabeled product ([α-^{32}P]ADP or [^{32}P]P_i) was added to conventional magnesium chelatase reaction mixtures with the substrates required for ATP hydrolysis and metal ion chelation (ATP, $MgCl_2$, and porphyrin). All reaction mixtures also included coupling enzymes to remove the nonradiolabeled product of ATP hydrolysis (pyruvate kinase for ADP and purine nucleoside phosphorylase for P_i). The rate of synthesis of radiolabeled ATP was then followed. Under these conditions, radiolabeled ATP can appear only if an enzyme−product complex reacts with the radiolabeled species (Scheme 3). Therefore, exchange of [α-^{32}P]ADP with ATP would be evidence of the existence of an EP_i complex, and exchange of [^{32}P]P_i with ATP would be evidence of an EADP complex.

Received: February 2, 2012
Revised: February 28, 2012
Published: February 28, 2012

dx.doi.org/10.1021/bi300149z | *Biochemistry* 2012, 51, 2029−2031